ADVANCED RESERVOIR CHARACTERIZATION IN THE ANTELOPE SHALE TO ESTABLISH THE VIABILITY OF CO_2 ENHANCED OIL RECOVERY IN CALIFORNIA'S MONTEREY FORMATION SILICEOUS SHALES

Final Progress Report

Reporting Period: February 7, 2002 - February 6, 2003

Contract Number: DE-FC22-95BC14938

Chevron USA Production Company
9525 Camino Media
Bakersfield, California 93311

Date of Report: May 15, 2003
Contract Date: February 7, 1996
Official Completion Date: July 1, 2003

Program Manager: Gary D. Walker, NPTO
Principal Investigator: Pasquale R. Perri, ChevronTexaco

DISCLAIMER

TABLE OF CONTENTS

TABLE OF CONTENTS (cont.)

LIST OF FIGURES

LIST OF FIGURES (cont.)

LIST OF FIGURES (cont.)

LIST OF FIGURES (cont.)

LIST OF FIGURES (cont.)

LIST OF TABLES

ABSTRACT

This report describes the evaluation, design, and implementation of a DOE funded CO_2 pilot project in the Lost Hills Field, Kern County, California. The pilot consists of four inverted (injector-centered) 5-spot patterns covering approximately 10 acres, and is located in a portion of the field, which has been under waterflood since early 1992. The target reservoir for the CO_2 pilot is the Belridge Diatomite. The pilot location was selected based on geologic considerations, reservoir quality and reservoir performance during the waterflood. A CO_2 pilot was chosen, rather than full-field implementation, to investigate uncertainties associated with CO_2 utilization rate and premature CO_2 breakthrough, and overall uncertainty in the unproven CO_2 flood process in the San Joaquin Valley.

A summary of the design and objectives of the CO_2 pilot are included along with an overview of the Lost Hills geology, discussion of pilot injection and production facilities, and discussion of new wells drilled and remedial work completed prior to commencing injection.

Actual CO_2 injection began on August 31, 2000 and a comprehensive pilot monitoring and surveillance program has been implemented. Since the initiation of CO_2 injection, the pilot has been hampered by excessive sand production in the pilot producers due to casing damage related to subsidence and exacerbated by the injected CO_2. Therefore CO_2 injection was very sporadic in 2001 and 2002 and we experienced long periods of time with no CO_2 injection. As a result of the continued mechanical problems, the pilot project was terminated on January 30, 2003.

This report summarizes the injection and production performance and the monitoring results through December 31, 2002 including oil geochemistry, CO_2 injection tracers, crosswell electromagnetic surveys, crosswell seismic, CO_2 injection profiling, cased hole resistivity, tiltmetering results, and corrosion monitoring results. Although the Lost Hills CO_2 pilot was not successful, the results and lessons learned presented in this report may be applicable to evaluate and design other potential San Joaquin Valley CO_2 floods.

ACKNOWLEDGMENTS

I would like to thank the following individuals for their help and participation on this project: John Cooney, William Fong, Wendy Guo, Dale Julander, Gregg Molesworth, Michael Morea and Bradley Wiest of ChevronTexaco Exploration and Production Company; Irene Gullapalli and Dengen Zhou of ChevronTexaco Exploration and Production Technology Company; Rong Hwang of ChevronTexaco Energy Research and Technology Company; Michael Wilt of Electromagnetic Instruments, Incorporated; Barry Kirkendall and Jeffery Roberts of Lawrence Livermore National Laboratory; G. Michael Hoversten, Roland Gritto, and Tom Daley of Lawrence Berkeley National Laboratory; John Washbourne of TomoSeis Incorporated; David R. Cole, Oak Ridge National Laboratory; and Earuch Broacha of ProTechnics, Incorporated.

EXECUTIVE SUMMARY

Introduction:
The primary objective of our project was to conduct advanced reservoir characterization and modeling studies in the Antelope Shale of the Buena Vista Hills Field. Work was subdivided into two phases or budget periods. The first phase of the project would focus on a variety of advanced reservoir characterization techniques to determine the production characteristics of the Antelope Shale reservoir. Simulation models based on the results of the characterization work would then be used to evaluate how the reservoir would respond to enhanced oil recovery (EOR) processes such as of CO_2 flooding. The second phase of the project would be to implement and evaluate a CO_2 flood in the Buena Vista Hills Field. A successful project would demonstrate the economic viability and widespread applicability of CO_2 flooding in siliceous shale reservoirs of the San Joaquin Valley.

However, it was decided not to proceed with a Phase II field trial in Buena Vista Hills because of its very low oil saturation, lithologic heterogeneity and relatively few natural fractures in the siliceous shale reservoirs. Although Buena Vista Hills turned out to be a poor CO_2 EOR candidate, our reservoir characterization has demonstrated that under the right conditions, CO_2 is a viable enhanced recovery process for other siliceous shales. Therefore, the Phase II CO_2 pilot was moved to Lost Hills Field, about 30 miles north of Buena Vista Hills with the DOE's concurrence.

Lost Hills Field:
The target reservoir at Lost Hills is the Belridge Diatomite of the Monterey Formation. The Belridge Diatomite is a diatomaceous mudstone and is not present at Buena Vista Hills. The diatomite has high oil saturation (50%) and high porosity (45 - 70%), but its low permeability (<1 millidarcy) has led to low primary oil recovery (3 - 4% of OOIP). Due to the low primary recovery and large amount of remaining oil in place, Lost Hills presents an attractive target for EOR. In addition to the large resource base, there is technical and economic justification for CO_2 flooding that was developed through our reservoir characterization and simulation efforts. CO_2 flood production forecasts were generated using Chevron's proprietary reservoir simulation software. The simulation results indicate a tremendous oil response associated with CO_2 flooding. This is mainly due to the improved injectivity with CO_2. CO_2 injectivity is at least two to three times greater than that of water or steam. Two other favorable mechanisms associated with CO_2 injection are reservoir oil viscosity reduction and increased fluid expansion.

Preliminary economics for full-scale implementation of a CO_2 Flood in Lost Hills has identified several key uncertainties, which will be evaluated as part of the pilot demonstration. The main economic uncertainties that can only be further evaluated by the pilot are oil response, and the corresponding CO_2 utilization required for such a response. The pilot has been designed and implemented to significantly reduce the range of uncertainty for these two key items.
Funding is also included in this project to further evaluate the feasibility and cost of local long-term CO_2 supplies. Since it is very unlikely that a CO_2 pipeline to California will be

built anytime soon, success of a full-scale CO_2 flood will depend on utilization of CO_2 entrained in local produced gas and flue gas. Global warming and future world emission trading of CO_2 credits may drastically increase the availability and lower the cost of CO_2 in California. As part of project scoping, the CO_2 Team will continue to track developments for global warming.

Background & Present Situation:
The Lost Hills Field, located 45 miles northwest of Bakersfield, California, was discovered in 1910. Reserves in the shallow sands, diatomite, and chert pools were developed using slotted liner completion techniques until the late 1970's. From the late 1970's to 1987, small volume hydrofracture completions were performed covering the entire Belridge Diatomite.

Advances in hydraulic fracturing technology in the late 1980's resulted in increased oil recovery that led to a more aggressive development program by Chevron. From 1987 to the present, high volume hydrofracture completions have been performed across the entire Belridge Diatomite and the Upper Brown Shale resulting in significant production increases. The Lost Hills Field is developed on a 5 acre (siliceous shale) to 1.25 acre (diatomite) well spacing. There are over 2.2 billion barrels of oil in place in the Belridge Diatomite in Lost Hills. To date only 112 million barrels have been produced, or approximately 5% of the original oil in place (OOIP).

Chevron initiated a pilot diatomite waterflood project in December 1990 and began full-project development in April 1992. Since 1992, two hundred and eight 2-1/2 acre patterns have been put on water injection spanning parts of four sections (Sections 4, 5, 32 Fee, and 33). Since the initiation of first project water injection in April 1992, production has increased approximately 4,000 BOPD from 6,400 BOPD to the current rate of 10,400 BOPD.

CO_2 Pilot Installation:
During the year 2000, Chevron installed a four-pattern, 2.5 acre pilot on Section 32 Fee to evaluate the potential of CO_2 flooding the Lost Hills Diatomite. The pilot installation included remedial work to evaluate and upgrade the tubing and packers in the existing injectors. Two existing injection wells were successfully repaired. Three observation wells and two replacement injection wells were drilled and completed. In 2000, the CO_2 facility construction was completed for the well gauging and the liquid CO_2 injection facilities. The pilot construction and all associated well work were completed and CO_2 injection commenced on August 31, 2000. A comprehensive CO_2 monitoring program has been put in place and baseline surveys taken prior to the injection of CO_2.

Objectives:
A CO_2 a pilot was installed in Section 32 Fee of the Lost Hills field to test the technical and economic viability of CO_2 flooding the low permeability diatomite resource. A full-scale CO_2 project is economically justified by an incremental analysis and comparison to the

current base case waterflood. Incremental tertiary reserves are estimated to be 80 MMBOEG and are technically supported by reservoir simulation. However, the project is only marginally economic and considerable uncertainty exists in the magnitude of predicted CO_2 recoveries. Installing a pilot will provide us with an opportunity to gather and analyze the pertinent geologic, reservoir, and production data and gather facilities design information necessary to commit to a full-field project. In addition, the pilot capital and operating costs will take advantage of available DOE funding of nearly 2.7 million dollars. The following are the main objectives of the recently installed CO_2 pilot:

- Gain information that could benefit other drive mechanisms in Diatomite such as steamflooding and fireflooding.
- Learn how injecting a gas (very low viscosity fluid) differs from injecting water into the diatomite in terms of fracture azimuth, injectivity, and areal and vertical sweep.
- Mitigation measures for CO_2 breakthrough problems can be applied to other IOR operations.
- Learn how much of the diatomite pay zone can effectively be processed. This knowledge can be applied to other IOR process designs.
- Learn how to mitigate and/or control hydrofracture growth (vertically and areally).
- Potential Federal Regulations may make CO_2 a "free" commodity 5 to 10 years down the road. Injecting CO_2 may be used to offset emissions from other nearby Chevron facilities.

Pilot Operation:

CO_2 injection commenced on August 31, 2000. CO_2 injection began slowly at 50 MCF/D per injector as we de-bugged and became acquainted with the new facilities. We continued to increase CO_2 injection rates slowly to the target rate of 500 MSCF/D per injector to prevent any premature CO_2 breakthrough. Through December 31, 2002, 375,113 MCF of CO_2 has been injected into the Diatomite or 0.05 HCPVS's. An initial oil response was observed in one well (11-8E) as a result of the CO_2 injection. However, the initial oil response in well 11-8E was curtailed due to sanding problems with it and five other pilot producers. During 2001, re-occurring sanding problems continuously hampered the CO_2 pilot. At first, it was assumed that most of the problems were due to subsidence related casing damage. Remediation programs were developed to correct these problems and CO_2 injection was resumed in early May 2002. Sanding problems continued to be an issue in 2002 and when the tubing in well 11-8E was severely damaged, CO_2 injection was permanently suspended. It was concluded that CO_2 injection played a major role in the sanding problems. The project was officially terminated by ChevronTexaco management on January 30, 2003.

Pilot Conclusions:

The following conclusions have been arrived at after operating and monitoring the CO_2 pilot for two years, including both pre-pilot and post-pilot simulation studies:

1. The tracer and salinity survey data suggest the producers are highly connected with the injectors.
2. Simulations show that the existence of higher flow channels in the reservoir play an adverse role on the performance of Lost Hills CO_2 pilot. Most of injected CO_2 flows through the high flow channels and only a small portion of the injected CO_2 invades the reservoir formation. Because of low viscosity, CO_2 prefers the high permeability zones, which has been waterflooded before the WAG started. The combination of the high flow channels and the poor sweep efficiency contributes to the poor performance observed in the pilot.
3. It appears CO_2 is capable of increasing oil recovery from the diatomite.
4. CO_2 is very good at finding the proverbial "path of least resistance" and by-passing matrix oil.
5. CO_2 predominantly flows through the induced hydraulic fractures, connects with the natural fractures, faults, and channels through a very small portion of the reservoir carrying high-velocity sand. The sand-laden CO_2 finds holes already in place due to subsidence-related well failures and exacerbates the sanding problems and can even lead to catastrophic tubing failure.

Pilot Monitoring and Surveillance:

Although the CO_2 pilot was not an economic and technical success, the pilot monitoring and surveillance program was a huge success. An extensive program was carried out to monitor the CO_2 pilot using a combination of routine and new, experimental methods. In fact, some new experimental monitoring methods were developed that could be applied to other siliceous shale reservoirs. Some of the monitoring results are highlighted below:

- Image log data showed that the natural fracture network had fracture azimuths that differed from the typical induced hydraulic azimuth direction. These observations are consistent with other image log data in the field. Natural fractures, while not prevalent, do play a role in distributing injection fluid through the reservoir.
- CO_2 injection tracers showed that a small amount of tracer traveled quickly through the natural fractures, faults and induced hydraulic fractures. This phenomenon has also been observed in water injection tracer tests in the 1.25 and 0.625 acre pilots in other areas of the field.
- Produced water salinity studies in the CO_2 pilot area also show that injection fluids move quickly through a natural fracture network (Zhou et al., 2002).
- Oil geochemistry surveys showed no increase in sulfur or asphaltenes due to CO_2 injection.
- Corrosion was not an issue during the life of the project.
- Injection rate was not an issue during the life of the project.
- Pressure could not be monitored due to an error during perforating the long and short strings of the pressure observation well (OB-C3).
- CO_2 injection profiles showed both good and poor vertical coverage, with the poor coverage mainly going out the top perforations. Similar variability can also be seen in water injection profiles through the waterflood.

- Cased hole, fiberglass observation well logging showed that minor changes in resistivity occurred in the J-L (clean diatomite), GG-BH (mixed) and D-FF (sandy and mixed) intervals. However the largest change occurred in the C (sandy) interval which is over 200 ft. above the injection interval.
- Baseline EM data (pre-CO_2) showed water injection to have mainly been confined to the GG-BH and J-K intervals. Post CO_2 injection EM surveys could not detect any additional change unfortunately due to the low volume of CO_2 injected during the pilot.
- Combined crosswell seismic and EM interpretation indicated that CO_2 moved above and out of zone along a fault/hydraulic fracture plane.
- Even though numerous remedial attempts were made, the sanding of producers was a major problem that could not reasonably be overcome. The sanding problem was the result of CO_2 finding its way through the natural and hydraulic fracture network and causing "frac" sand to enter the wellbores of most of the producers in the pilot.
- CO_2 did manage to adversely effect (spike in gas production/sanding) other wells outside the 10-acre pilot.

Overall, the monitoring program was very effective except for measuring pressure. Through the life of the pilot, CO_2 behaved similarly to injected water (waterflood) in that a larger portion of CO_2 traveled through the fracture network and only a small portion entered into the low permeability diatomite.

Lessons Learned:
The following is a summary of *Lessons Learned* that other siliceous shale reservoir pilots or projects may benefit from. They include *"Things That Went Well"* and *"What Could Have Been Improved"*.

Things That Went Well:

- **Safety:**
  There were zero incidents associated with the Pilot. Some elements of the safety plan that contributed to this success were: Detailed traffic plan for CO_2 deliveries, Awareness of the hazards of CO_2 and training by supplier (BOC) on handling, CO_2 evacuation drill conducted by Operations, An operator from Rangely CO_2 Operations (Reed Chernenko) was assigned to the pilot, and Facilities designed and operated with CO_2 hazards in mind.

- **Partnerships and Technology**:
  Strong partnerships formed and fostered with the DOE and National Labs resulted in shared pilot risk and advancement of monitoring technologies.

- **Commitment by Operations to the Pilot:**
  Operations supported and implemented the effort 100%. Operations attributed this to the fact that they understood the significant potential of CO_2 flooding, if the pilot

were successful. Frequent problem solving (i.e. producer sanding problems) meetings between the Project Team and Operations was also cited as a contributor.

- **Networking and Applying Best Practices:** The pilot was operated very successfully in spite of the fact that engineers and operators at Lost Hills are very unfamiliar with the process of CO_2 flooding. This success was attributed to the fact that the Project Team made several visits to CO_2 flood operations and established a network of contacts. Lessons learned from CO_2 floods/pilots in West Texas and Rangely Colorado were captured and applied.

What Could Have Been Improved?

- **Facility Design:**
  The CO_2 tank level telemetry system that communicated the amount of product onsite, to BOC (in Pennsylvania) was problematic. Power surges and inadequate phone lines were identified as the root causes. Infrastructure upgrades or alternative communication methods (wireless) were discussed as possible solutions.

- **Schedule Contingency**:
  Inadequate contingency was built into the schedule. Two elements of the project contributed to the start-up delay. These elements could easily be part of other pilots and should be taken into consideration:

  1. Allow sufficient time to establish reliable/accurate baseline information (i.e. oil/water/gas production rate from producers). This is especially true if you are relying on new, pilot dedicated equipment (new CO_2 gauging facilities), to establish the baseline.

  2. Build in extra contingency for processes that involve new technology or are new to the personnel that will be designing and operating the process. The need for new technology/processes schedule contingency is well known, but seldom applied as it should be.

SECTION 1

GEOLOGY

1.1 GEOLOGIC OVERVIEW OF LOST HILLS

Michael F. Morea
ChevronTexaco Exploration and Production Company

Structure:
Lost Hills Field was discovered in 1910 and is located 45 miles northwest of Bakersfield, CA (Figures 1.1-1 and 2). Productive intervals include Middle to Upper Miocene chert, porcelanite, siliceous shale, and diatomite, and Plio-Pleistocene sands. The field is situated along a northwest-southeast trending series of structural highs that begins with the Coalinga Anticline to the northwest and culminates with the Lost Hills Anticline to the southeast. This series of highs roughly parallels folds of similar age on the westside of the San Joaquin Valley. These folds are oriented nearly parallel to the trend of the San Andreas Fault to the west and approximately perpendicular to the direction of regional compression.

Lost Hills oil is trapped at the crest and along the southeast plunge of the anticline (Figures 1.1-3 and 4). In this portion of the field where the pilot is located, the structural plunge varies from 2 to 6º toward the southeast. Dips along the northeast flank average 30º while those on the southwest flank average 15 to 20º. This asymmetry in dips in the NE-SW direction is consistent with a fault-bend fold model (Medwedeff, 1989). Evidence from onlapping sediments shows the Lost Hills Anticline began to grow during the deposition of the Etchegoin Formation and continued into the Holocene. The resulting anticline is perched above a ramp thrust that is located around 13,000 feet below the surface. Numerous northeast-southwest trending normal faults with throws rarely exceeding 40 feet cut the Lost Hills structure. These faults do not appear to have a major impact on oil production. However the faults and fractures do appear to influence water and CO_2 injection (Zhou et al., 2002).

Stratigraphy and Sedimentation:
The stratigraphy at Lost Hills is shown in Figures 1.1-5 and 6. The Monterey Formation is comprised of the Devilwater/Gould Shale, McLure Shale and Reef Ridge members. The Devilwater/Gould consists of clay shales and siliceous shales. It is slightly phosphatic. The McLure is subdivided into the McDonald Shale and the Antelope Shale. The McDonald consists of interbedded porcelanites and siliceous shales. It is also slightly phosphatic. The Antelope is comprised of finely laminated cherts and porcelanites. The uppermost member of the Monterey Formation is the Reef Ridge and it is subdivided into the Brown Shale and Belridge Diatomite. The Brown Shale is made up of interbedded siliceous shale, shale, and silt. The Belridge Diatomite consists of interbedded diatomaceous mudstone, fine-grained, argillaceous sands/silts, and porcelanite.

Based on regional studies of late Miocene paleogeography and paleobathymetry, the rocks of the Monterey Formation were mainly deposited in a deep marine environment (Graham and Williams, 1985). In the San Joaquin Basin, the late Miocene environment was such that: water depths were bathyal (between 600 and 3,000 feet), cool water temperatures and upwelling in the upper 200 feet supported large diatom populations, and the deeper basin waters were oxygen poor. Two primary sedimentation processes were active in the basin at

that time. First, hemipelagic sedimentation: the settling of diatom frustules and clay-sized particles onto the basin floor from the overlying water column. And second, turbidite sedimentation: the deposition of sand, silt, and clay-sized particles carried into the basin by density currents (usually originating along the basin margins).

This combination of environmental conditions and sedimentation processes led to the accumulation of thick deposits of organic-rich, laminated, diatomaceous sediments which occasionally are interrupted by thin-bedded, clastic-rich turbidite deposits. However, compared to the southwestern San Joaquin Basin, sandy turbidites at Lost Hills are not common. The Monterey Formation in the San Joaquin Basin differs from the coastal and offshore Monterey in that it is much more clastic rich.

The composition of the Monterey can be described in terms of three primary components: biogenic silica, clay, and silt/sand. As shown in Table 1.1-1, there is a fair amount of vertical compositional variation within the stratigraphic column at Lost Hills. The Devilwater contains 27% biogenic silica, 50% clay, and 23% silt/sand. The McDonald is slightly richer in biogenic silica, roughly comparable in clay, and slightly lower in silt/sand. The Antelope is very rich in biogenic silica, poor in clay, and poor in silt/sand. The Brown Shale is clay rich. The Belridge Diatomite has roughly equal amounts of biogenic silica, clay and silt/sand. The overlying Etchegoin Formation is rich in silt/sand and clay, and almost totally lacking in biogenic silica.

Table 1.1-1. Average rock compositions from Well 166, Section 32, T26S/R21E.

Rock Unit	Average. % Biogenic Silica	Average % Clay	Average % Silt/Sand	Number of Samples
Etchegoin	4	38	58	8
Belridge Diatomite	33	36	31	19
Brown Shale	26	47	27	28
Antelope Shale	61	18	21	14
McDonald Shale	34	47	19	24
Devilwater/Gould Shale	27	50	23	8

Diagenesis:

As hemipelagic and occasional turbidite deposits in the Lost Hills area were buried by the overlying Etchegoin and Tulare sediments, the diatomaceous sediments of the Monterey Formation gradually lithified into the highly porous (50-60% or more) but low permeability (0.1-10.0 millidarcy) rock termed diatomite. As discussed above, anywhere from 26% to 61% of this diatomite was composed of diatom frustules. Diatom frustules consist of a form of silica called opal-A, which is an unstructured mineral (essentially a solidified gel) usually containing 3-10% water. As this diatomite is buried deeper and reaches greater temperatures (~ 45º C), the opal-A material in the diatom frustule becomes unstable and undergoes a phase transition (Keller and Issacs, 1985) to opal-CT (Figures 1.1-7 and 8). This form of silica is more structured than opal-A and has released much of its water. Porosity is reduced to about 40%. At still greater depths and higher temperatures (~ 80º C), the opal-CT undergoes a final phase transition to a form of quartz with only a trace of water left. The Monterey Formation at Lost Hills is presently comprised of opal-A rocks at shallow depths ($\pm$ 2,300 feet or shallower), opal-CT rocks at intermediate depths ($\pm$2,300 to $\pm$ 4,300 feet), and quartz phase rocks below $\pm$ 4300 feet.

The exact temperatures at which the opal-A to opal-CT and opal-CT to quartz phase changes occur is governed by the amount of biogenic silica (diatoms) in the rock. Opal-A rocks rich in biogenic silica convert to opal-CT at lower temperatures (and therefore shallower depths) than those poor in biogenic silica. Conversely, opal-CT rocks rich in biogenic silica convert to quartz phase at higher temperatures (and greater depths) than those poor in biogenic silica (higher clay content). For this reason, an interval of rocks whose laminations vary in their biogenic silica content create a transition zone (~ 100') of alternating phase changes near the phase transition temperature. These alternating beds of opal-A and opal-CT or opal-CT and quartz (particularly where the beds are thin) may be especially susceptible to natural fracturing, thereby enhancing system permeability. Volume reduction and water expulsion associated with the phase changes probably adds to the fracturing in these zones. In general, hydrocarbons are found in all three (opal-A, opal-CT, and quartz) phases. Also production is enhanced in the opal-A to opal-CT and, in particular, the opal-CT to quartz phase transition zones.

Petroleum Geochemistry:
Geochemical analyses have demonstrated that Monterey Formation rocks in Lost Hills are typically composed of 1% to 6% total organics, making them fair to good hydrocarbon source rocks. Studies of kerogen maturation have shown that the Monterey rocks are immature (i.e., they have not been buried deep enough to generate oil) within the confines of the Lost Hills Field. However, studies of samples taken from down-flank wells indicate that these rocks are mostly mature in the syncline to the east of Lost Hills and possibly below the ramp thrust immediately beneath the Lost Hills Anticline. Because the Monterey Formation kerogens and the produced oils at Lost Hills have similar isotopic compositions, and because they contain similar concentrations of sulfur, it is believed that Lost Hills oil was sourced from the Monterey Formation itself.

Hydrocarbons migrated into the low permeability Monterey rocks at Lost Hills by way of faults, fractures and thin sands. Also the opal-A to opal-CT and opal-CT to quartz phase transition zones with their higher fracture density probably served as pathways for hydrocarbons to migrate from source beds down-structure to their ultimate resting place in the crest of the anticline.

In the McDonald Shale and Lower Brown Shale/Antelope Shale pools, hydrocarbons are confined fairly well within or immediately below the fractured opal-CT to quartz phase transition rocks. In the Upper Brown Shale, fracturing also helps to make it productive. Because the McDonald, Antelope, and Brown shales have such low matrix permeability, most of the oil produced from these rocks comes out of the fractures. In the Belridge Diatomite with its relatively higher matrix permeability, hydrocarbons have saturated the uppermost opal-CT, the opal-A to opal-CT transition, and most of the opal-A rocks. Most of the oil produced from the diatomite comes from the matrix. Lastly, oil has also migrated into the overlying Etchegoin and Tulare Formations.

Belridge Diatomite at Lost Hills:
The Belridge Diatomite is comprised of varying amounts of biogenic silica, clay, and silt/sand, and ranges in depth from 800 to 3,000 feet (Figure 1.1-9). The diatomite has high porosity (40 - 65%) and low permeability (<1 – 10 millidarcies). Oil saturation ranges from 40% to 65% in opal-A, and from 10% to 30% in opal-CT (Table 1.1-2). Oil gravity ranges from 28 to 18º API.

Table 1.1-2. Comparison of rock types at the pilot location (Lost Hills) and at the original location in Buena Vista Hills.

Parameter	Lost Hills Pilot	Buena Vista Hills Pilot
Rock Unit	Belridge Diatomite	Upper Antelope Shale
Age	Uppermost Miocene	Upper Miocene
Depositional Environment	Hemipelagic; Progradational Slope	Hemipelagic-Turbidite; Basin
Rock Type	Diatomaceous Mudstone	Siliceous Shale
Silica Phase	Opal-A	Opal-CT
Percent Sand Beds	30%	5%
Sand Description	5-60 feet thick, fine-grained, argillaceous, bioturbated	<1 inch thick, fine-grained, non-bioturbated
Depth to Top of Unit	1,400 feet	4,200 feet
Thickness	700 feet	600 feet
Porosity	50%	29%
Permeability	0.1 – 10.0 millidarcies	<0.1 millidarcies
Oil Saturation	50%	14%

At Lost Hills, the Belridge Diatomite (opal-A) is informally subdivided into three lithology types: clean, sandy, and clayey diatomite (Fast et al., 1993). These designations are based on bulk density log cutoffs and are supported by core and rock geochemistry. Clean diatomite has bulk density values 1.6 gm/cc or less. Sandy diatomite has bulk density values greater than 1.75 gm/cc. Clayey diatomite has bulk density values between 1.6 and 1.75 gm/cc.

The clean and clayey portions of the Belridge Diatomite are finely laminated. In general these laminations alternate between a more detritus-rich lamina and a more diatomaceous-rich lamina. The laminations reflect cyclic variations in yearly runoff (detritus-rich) and upwelling (diatomaceous-rich).

The clean and clayey diatomites were deposited under oxygen poor to anoxic conditions that could sustain only a limited sediment-dwelling fauna. Thus laminations are preserved in the diatomites (Figures 1.1-10 and 11). Sandy diatomites, on the other hand, were deposited under oxygen poor to oxygenated conditions. Sandy diatomites were originally deposited as interlaminated sands and clays but shortly after deposition were heavily bioturbated.

Superimposed on the yearly depositional cycling was the deposition of sedimentary packages that reflect changes in relative sea level. During the Late Miocene, diatomaceous sediments were deposited from the outer shelf to the basin floor in the San Joaquin Basin. At Lost Hills, diatom frustules and clay particles settled onto the upper slope environment from the overlying water column. As sea level rose, diatomaceous rich deposits were deposited further up on the slope. As sea level fell, sandy diatomite deposits prograded down the slope.

(In the northern half of Lost Hills Field, the Belridge Diatomite grades into the shallow water clastics of the Etchegoin Formation.) These fluctuations in sea level caused the larger scale deposition of sedimentary units of clean diatomite, clayey diatomite, and sandy diatomite. Lastly, superimposed on these relative sea level changes was the overall progradation and coarsening upward of the Belridge Diatomite and the eventual filling in of the basin in the Pliocene.

The fluctuations in relative sea level led to the deposition of a series of parasequences (Perri et al., 2000). Lithologic and trace fossil evidence from cores indicates that at least four sequence boundaries, or their equivalents, can be recognized in the Belridge Diatomite (Figure 1.1-12): L Pt. (base Belridge Diatomite), BH Pt., EE Pt. and D Pt. (top Belridge Diatomite).

Fractures and Thief Zones:

There are two types of fractures in Lost Hills: natural and man-made. In general, all diatomite wells are hydraulically propped-fractured in order to increase production from the low permeability, diatomite reservoir. To efficiently develop the field, surface tiltmeters have been used to determine hydraulic fracture azimuths. The average fracture azimuth is N50ºE and ideally, wells are placed along a grid pattern that is aligned to that azimuth. Occasionally hydraulic fracturing of a new producer causes an existing producer to sand-up or there is an increase in water production if an injection well communicates with a producer. Hydraulic fractures intersecting existing wells can be the result of many factors. These include: 1) wells closely spaced and in fracture alignment; 2) presence of existing faults/fractures; and 3) localized areas of depletion due to production, or localized areas of re-pressurization from injection that cause the hydraulic fracture to propagate at an azimuth that is not aligned with the natural stress field.

Recent analysis of natural fractures by D. Julander using Electrical Micro Imaging (EMI) logs from the OB-7 and 12-8D wells allowed for observations to be made regarding their abundance and distribution (Figures 1.1-13 - 14). The EMI from the CO_2 injectivity test well 12-8D is fairly representative of this part of the Lost Hills Field. It shows a fracture frequency between 1 and 3 fractures per 10 feet of vertical interval. This fracture frequency includes all observable fractures: open, closed (clay-filled), and fractures of undeterminable type (due to being poorly imaged). This data indicates that the diatomite is not highly fractured in this part of the field.

With regards to thief zones, i.e., high permeability sands interbedded within the diatomite, there does not appear to be much evidence to support this idea. Recent data from the nearby OB-7 well (1,160 feet SW of 12-8D) clearly exemplifies this. OB-7 was drilled and cored only 20 feet (perpendicular to fracture azimuth) from a water injection well (10-9W) that was drilled in 1994. Core PKS data clearly showed that the sandy diatomites from OB-7 do not have highly reduced oil saturations as compared to the original nearby injector. This would be expected from a sand bed that was close to an injector and highly permeable. As stated above and illustrated in Figures 1.1-12 and 13, the sandy diatomites are clay rich and bioturbated. These features make it very difficult to behave as a thief zone. Also, the CO_2

injection profiles from wells 12-8D (injectivity test) and 12-7W also showed that CO_2 does not have a strong preference for the sandy diatomites.

In summary, while there are fractures and faults present in the diatomite, the reservoir should not be considered a highly fractured reservoir. However it should also be said that based on CO_2 and waterflood tracers, it appears that fractures and faults do play a role in the unpredictable distribution of low viscosity fluids at low injection rates.

Overview of Field Development:
Development of the Lost Hills Field has evolved over the years. From 1910 to the late 1970's, slotted liner completions were used in the upper Belridge Diatomite. From the late 1970's to 1987, small volume, hydrofrac completions were performed covering the entire Belridge Diatomite. From 1987 to the present, high volume hydrofrac completions have been performed across the entire Belridge Diatomite and the Upper Brown Shale. Since 1992 a portion of the diatomite has been under waterflood. The field is developed on a 5 acre (siliceous shale) to 0.625-acre (diatomite) well spacing. There are over 2 billion barrels of oil in place in the Belridge Diatomite in Lost Hills. Due to the reservoir's low permeability less than 7% of this oil has been produced.

Subsidence:
Due to the high compressibility of diatomite, the removal of fluids, and the de-pressurizing of the reservoir, Lost Hills has experienced subsidence over a portion of the field. Figure 1.1-15 is a map showing cumulative subsidence between 1989 and 2000. Based on ground positioning satellite (GPS) data, the field has subsided over 8 feet in 12 years. In order to mitigate the subsidence and reduce related wells failures, waterflooding was initiated in the diatomite in the early 1990's. This has greatly reduced the rate of subsidence in the field.

CO_2 Pilot Location:
The pilot was located in Section 32 T26S/R21E. The target reservoir was the FF – L interval of the Belridge Diatomite (Figures 1.1-16 - 18). The choosing of the CO_2 pilot location was based on the following criteria:

- The CO_2 pilot needed to be located in an area of the field that was isolated from other field testing that was taking place at that time.
- Existing wells needed to be in good mechanical condition.
- The area needed to be representative of the oil production in the field.
- The area needed to be representative of the reservoir and structural conditions in the field.

In the pilot area, the diatomite is in opal-A phase. A fault zone runs NE-SW through the center of the 10-acre pilot. The pilot is divided into four 2.5 acre patterns with four injector and ten producers. Three observation wells were drilled to monitor the pilot. Two were cased with fiberglass in order to perform cased hole logging crosswell seismic and crosswell EM. These were located very close to, and on either side of, one of the injector wells. The third well was drilled and located in the center on the pilot to measure pressure changes.

References:

Fast, R. E., Murer, A. S., and Zambrano, L. G., 1993, Lost Hills Diatomite Simulation Study: Predicting Waterflood Performance in a Low Permeability, Compacting Reservoir, SPE 26627.

Graham, S. A., and Williams, L. A., 1985, Tectonic, depositional, and Diagenetic History of Monterey Formation (Miocene), Central San Joaquin Basin, California, AAPG Bulletin, v. 69, n. 3, p. 385-411.

Keller, M. A., and Issacs, C. M., 1985, An Evaluation of Temperature Scales for Silica Diagenesis in Diatomaceous Sequences Including a New Approach Based on the Miocene Monterey Formation, California, Geo-Marine Letters, v. 5, p. 31-35.

Medwedeff, D. A., 1989, Growth Fault-Bend Folding at Southeast Lost Hills, San Joaquin Valley, California, AAPG Bulletin, v. 73, n. 1, p. 54-67.

Perri, P. R., Emanuele, M. A., Fong, W. S., and Morea, M. F., 2000, Lost Hills CO_2 Pilot: Evaluation, Design, Injectivity Test Results, and Implementation, SPE 62526.

Zhou, D., Kamath, J., Friedmann, F., and Morea, M., 2002, Identifying Key Recovery Mechanisms in a Diatomite Waterflood, SPE 75142.

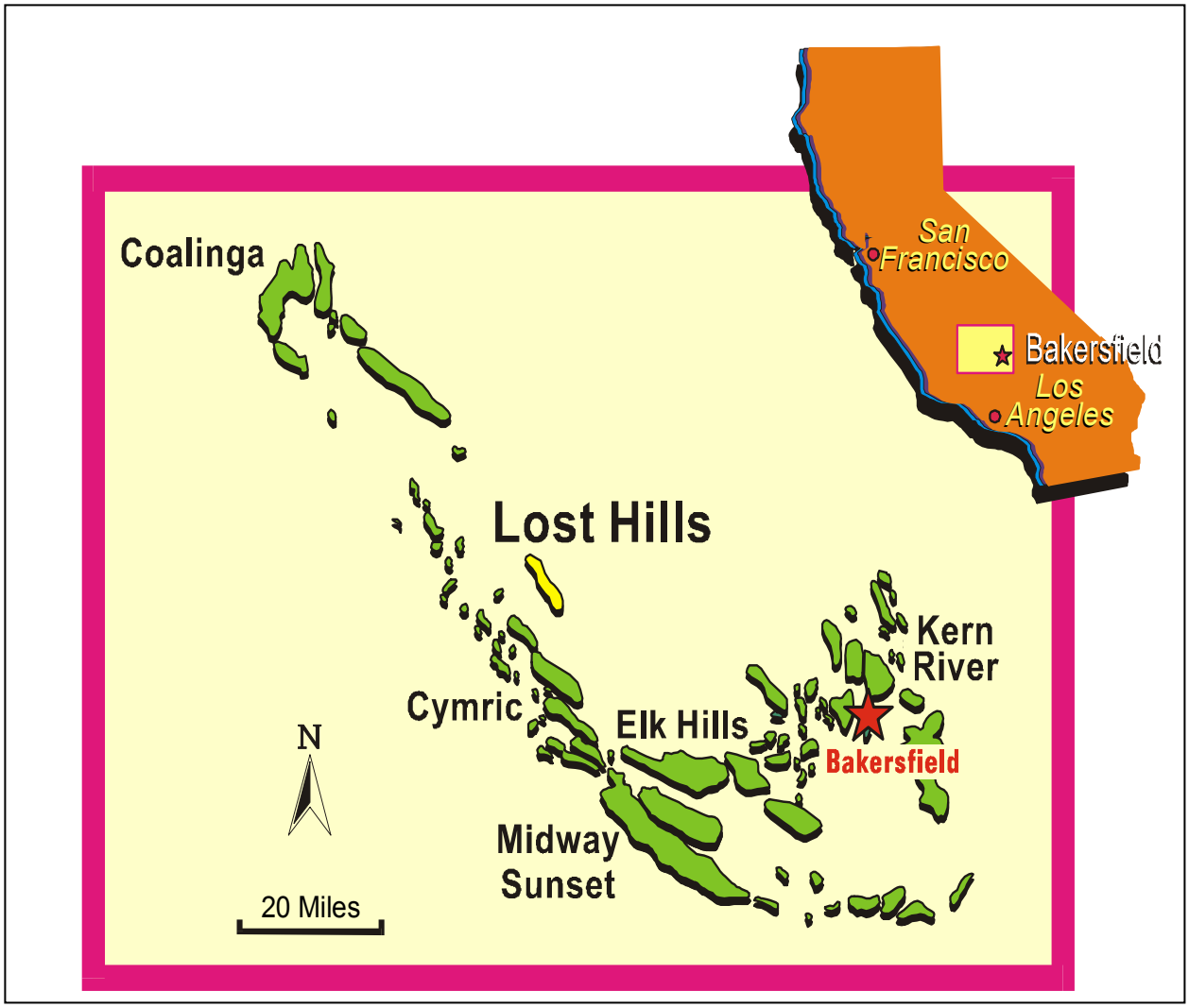

Figure 1.1-1. Location map of major oil fields in the southern San Joaquin Valley. Lost Hills Field is highlighted.

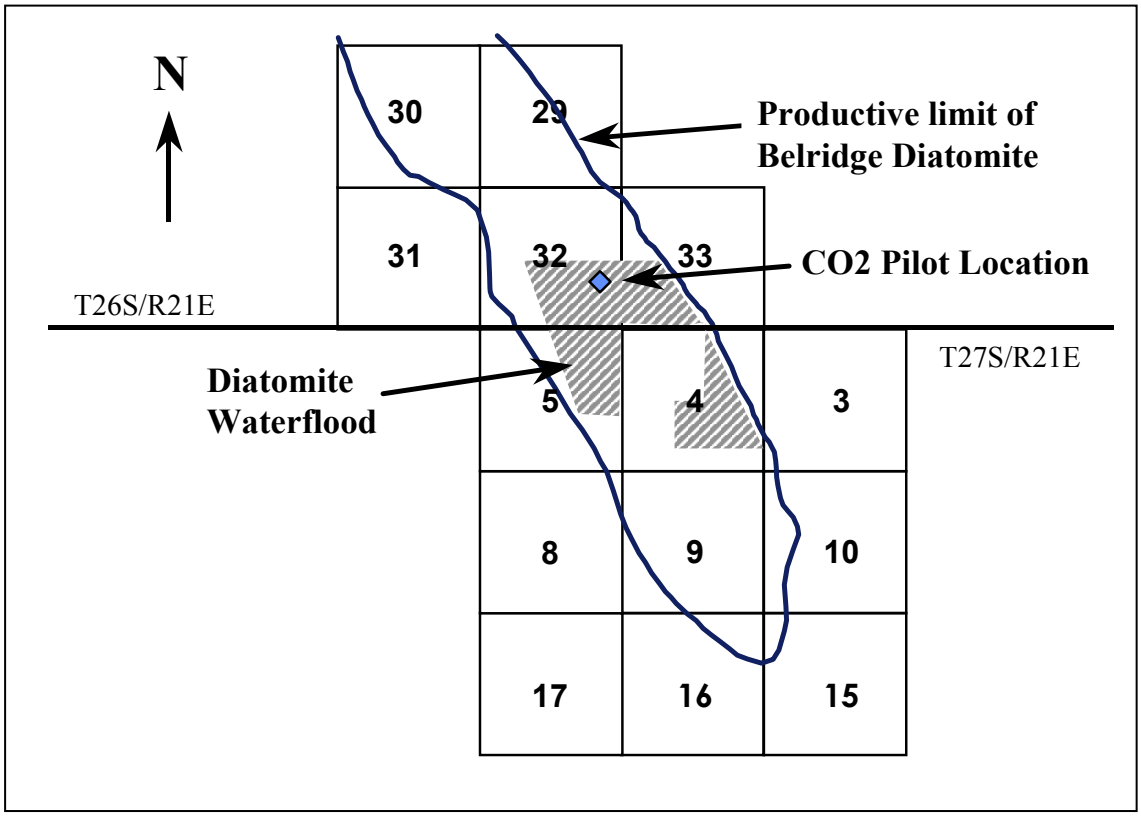

Figure 1.1-2. Productive limits of Belridge Diatomite follows trend of southeast plunge of the Lost Hills Anticline. Chevron diatomite waterflood and CO_2 pilot are also illustrated.

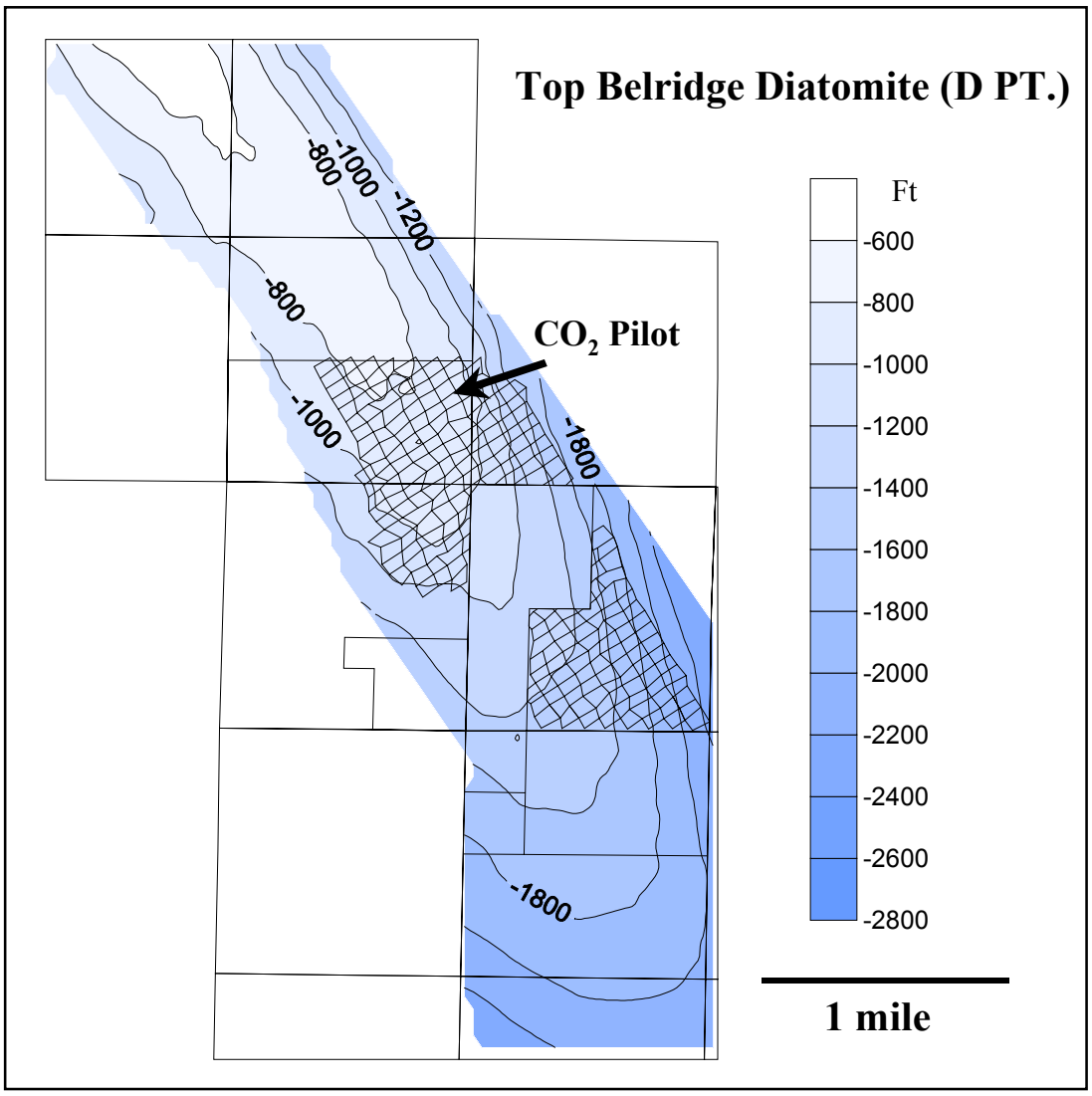

Figure 1.1-3. Lost Hills top Belridge Diatomite (D Point) structure map. Contour interval 200 feet.

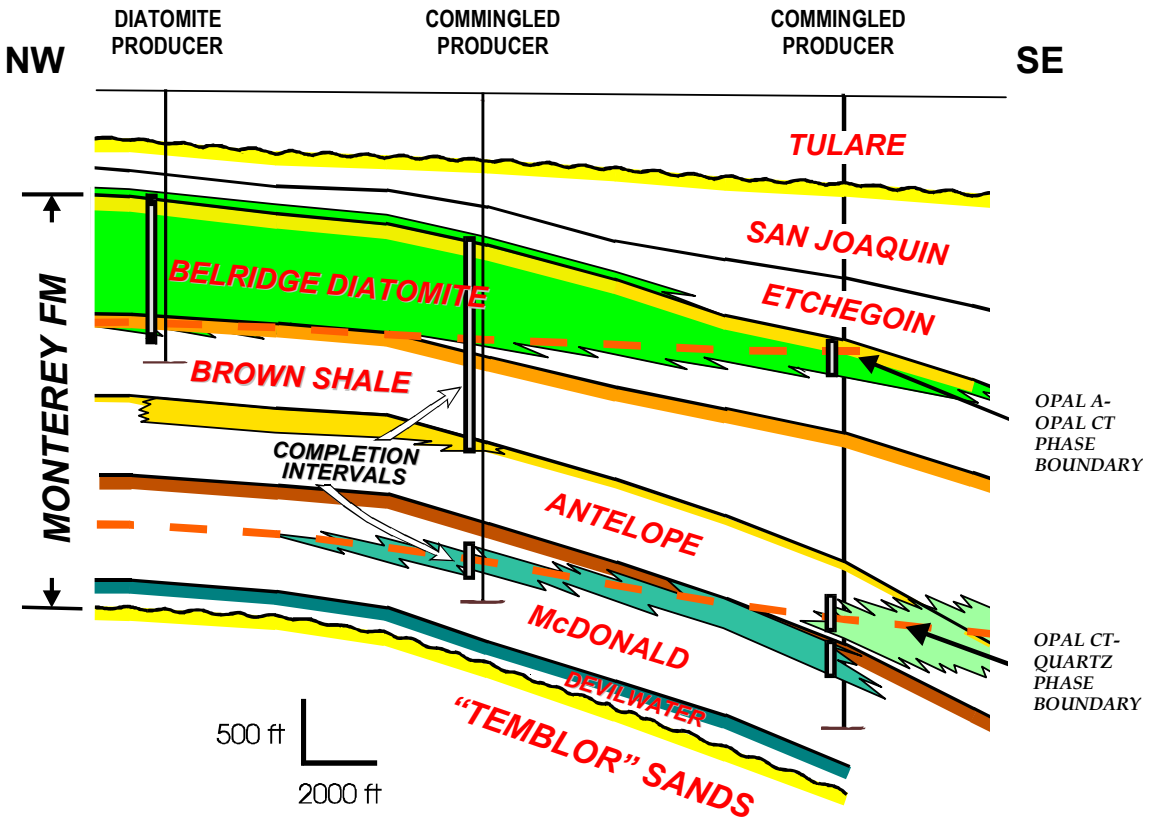

Figure 1.1-4. Generalized cross section along the crest of the southeast plunge of Lost Hills. The Belridge Diatomite is the objective of the CO_2 pilot project.

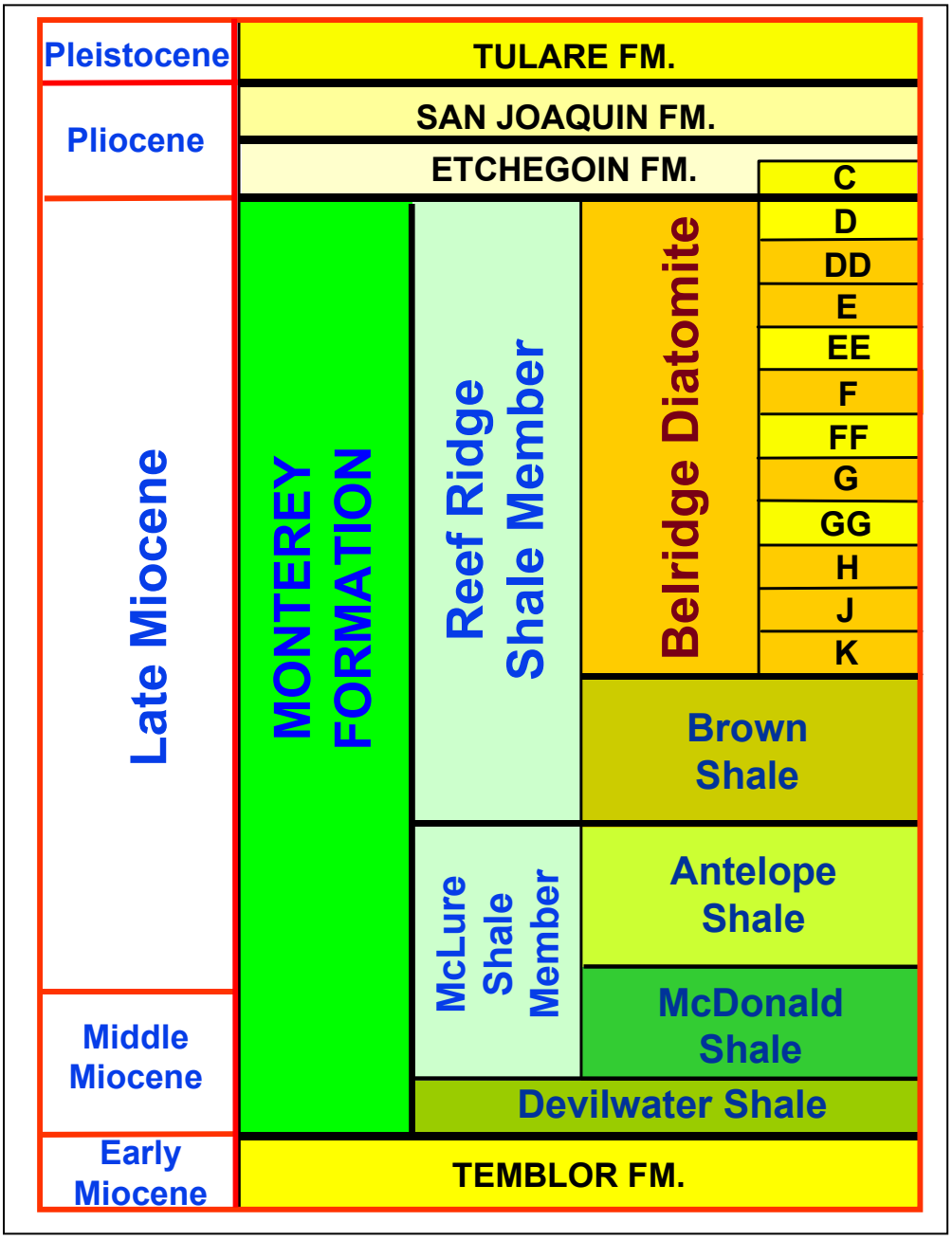

Figure 1.1-5. Monterey Formation stratigraphic column. In the Lost Hills area, the Devilwater and Gould members are undifferentiated and the Reef Ridge is subdivided into the Brown Shale and the Belridge Diatomite. The CO_2 pilot is in the Belridge Diatomite.

Lost Hills Type Log
166 Sec 32 26S/21E

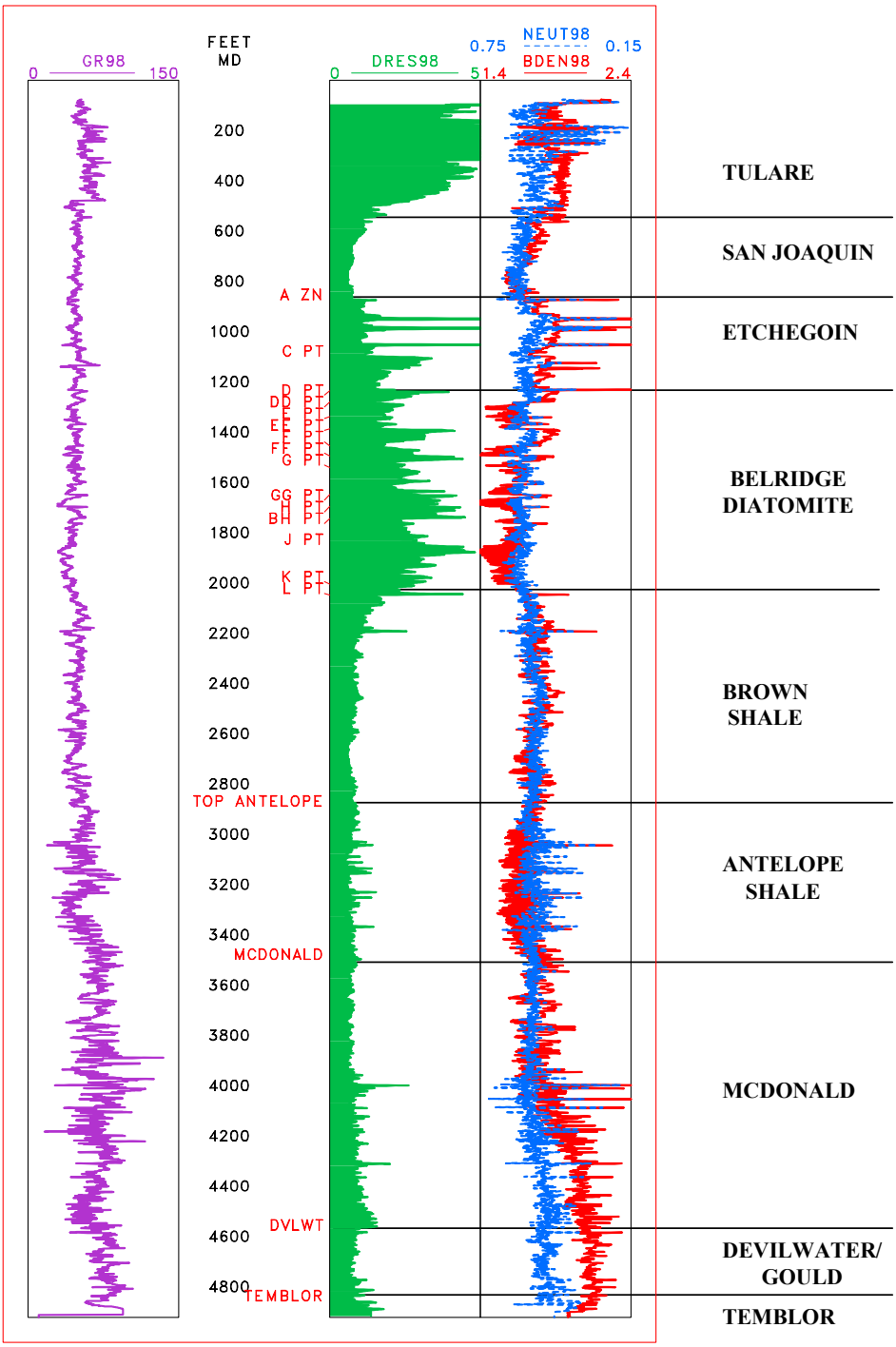

Figure 1.1-6. Lost Hills Type Log. Log tracks, from left to right, are: gamma ray; measured depth; geologic markers; deep resistivity; neutron, and bulk density.

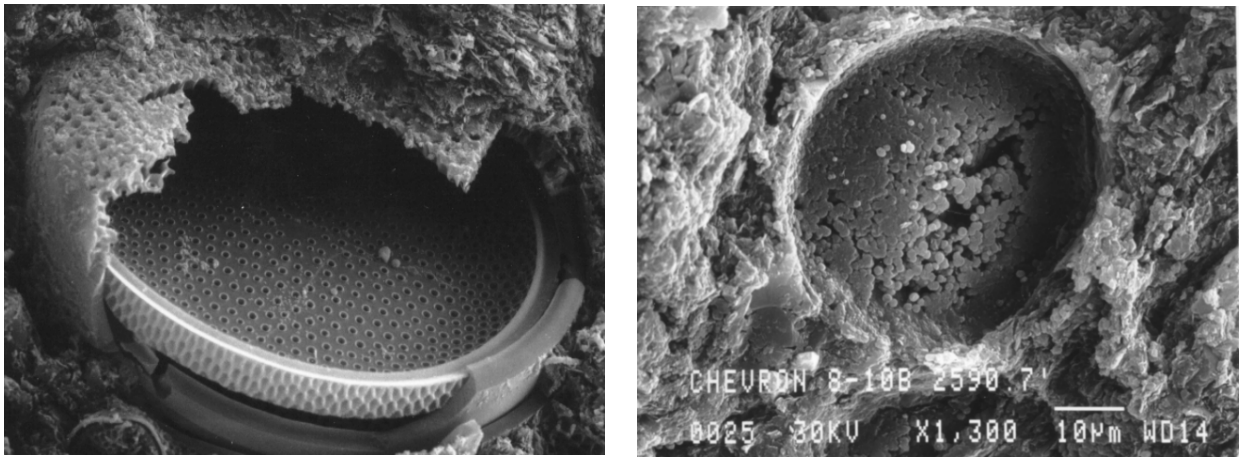

Figure 1.1-7. SEM photomicrographs of opal-A frustule starting to convert to opal-CT (left), and frustule converted to opal-CT (right). 1,300X magnification.

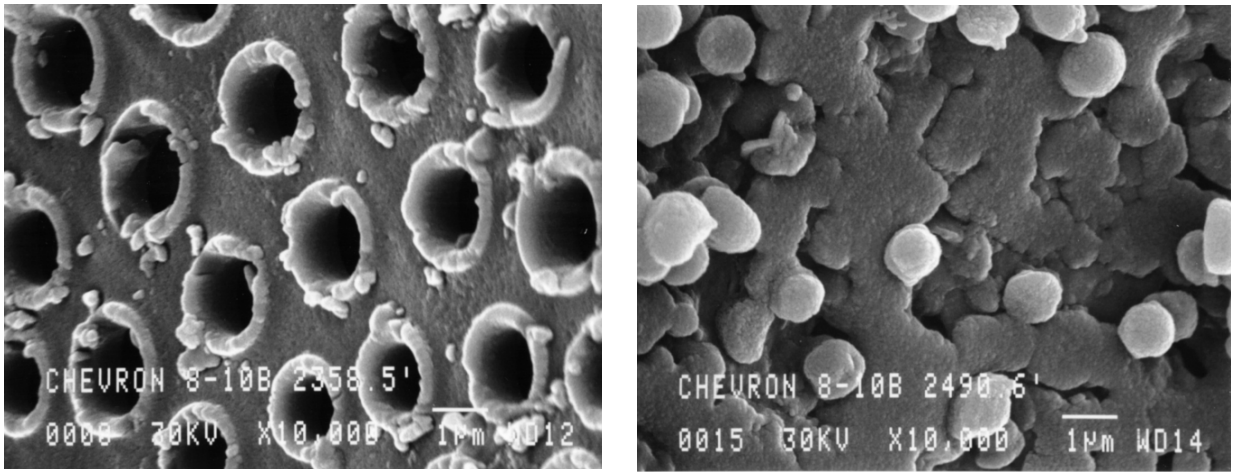

Figure 1.1-8. Opal-A frustule initiating conversion to opal-CT (left), and a frustule after its conversion to opal-CT. SEM photomicrographs, 10,000X magnification.

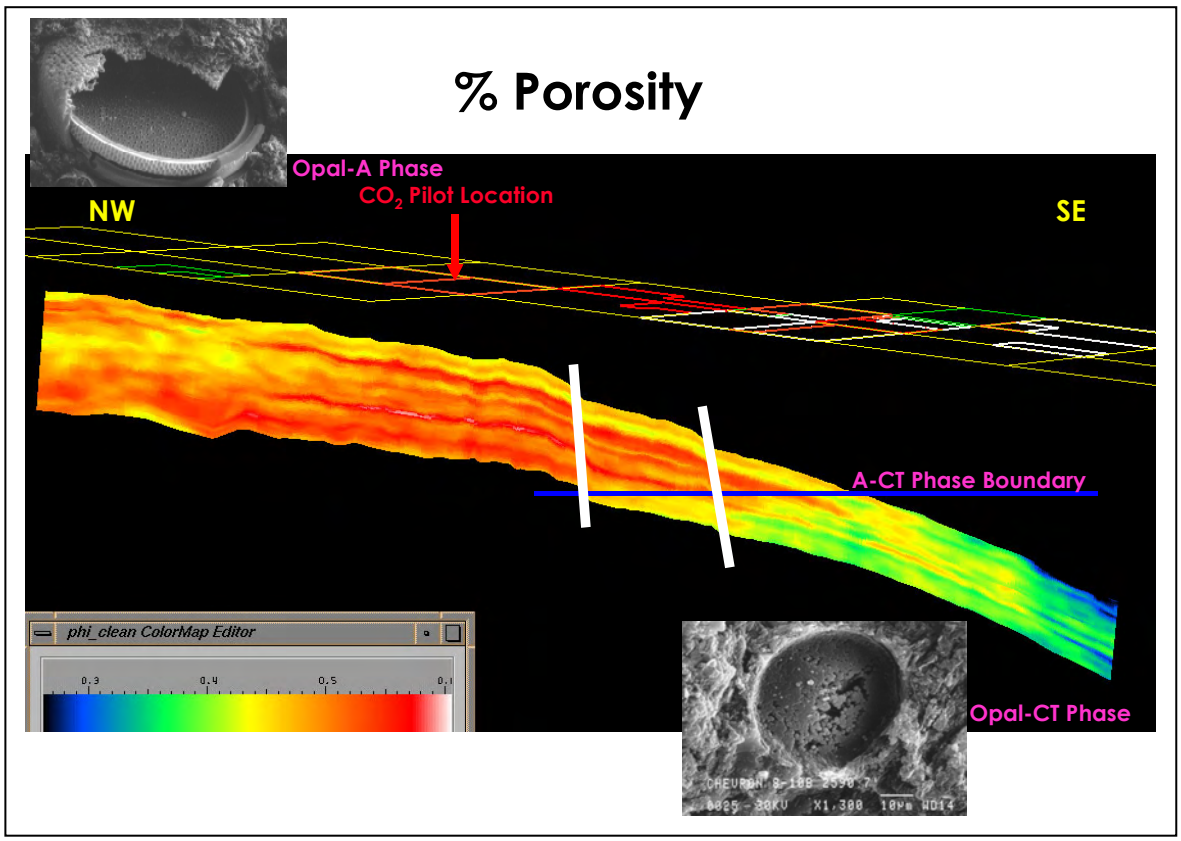

Figure 1.1-9. Cross section showing Belridge Diatomite geostatistical porosity distribution across the southern axis of Lost Hills Field. The overlying map shows the location of the CO_2 pilot in relation to the field. High porosity (red) represents opal-A. The lower porosity (green/yellow on the left, northwest) represents silt/sand. The lower porosity (green/yellow on the right, southeast) represents the conversion from opal-A to opal-CT. Scale: 0.27 to 0.6.

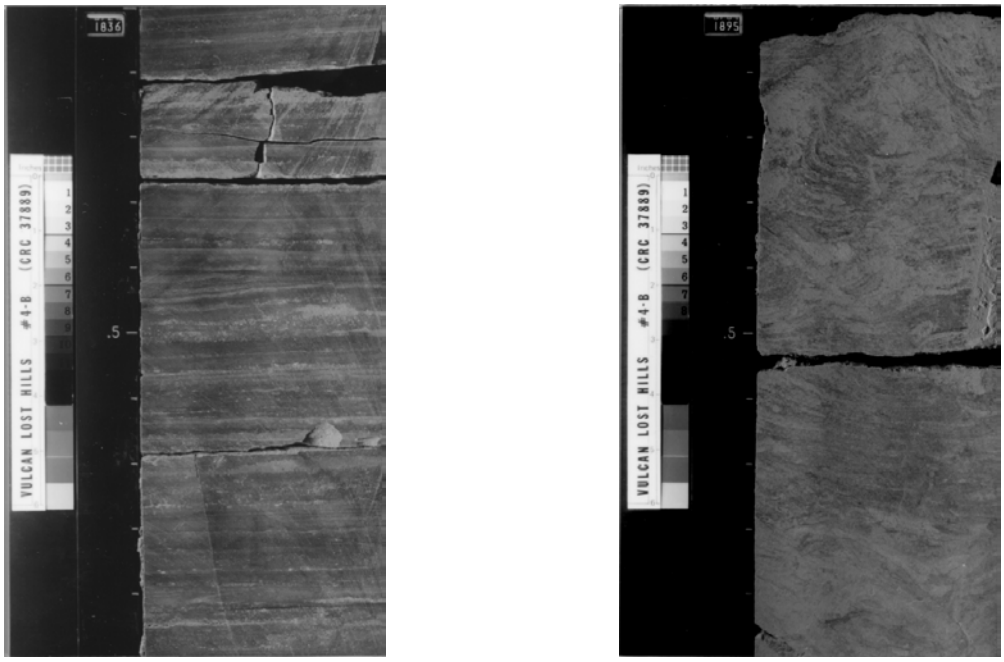

Figure 1.1-10. Slabbed core of laminated diatomite (left), and bioturbated sandy diatomite (right).

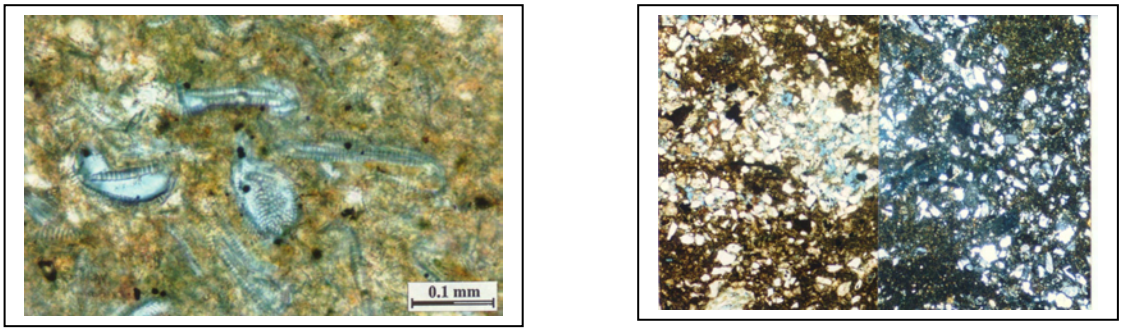

Figure 1.1-11. Thin section photomicrographs of a clean diatomite from the J Unit (left; 200X) and a sandy diatomite from the GG Unit (right; 40X, unpolarized and polarized light). The J unit thin section shows diatoms and porosity in blue. The GG Unit shows "blotchy" sand and porosity due to bioturbation.

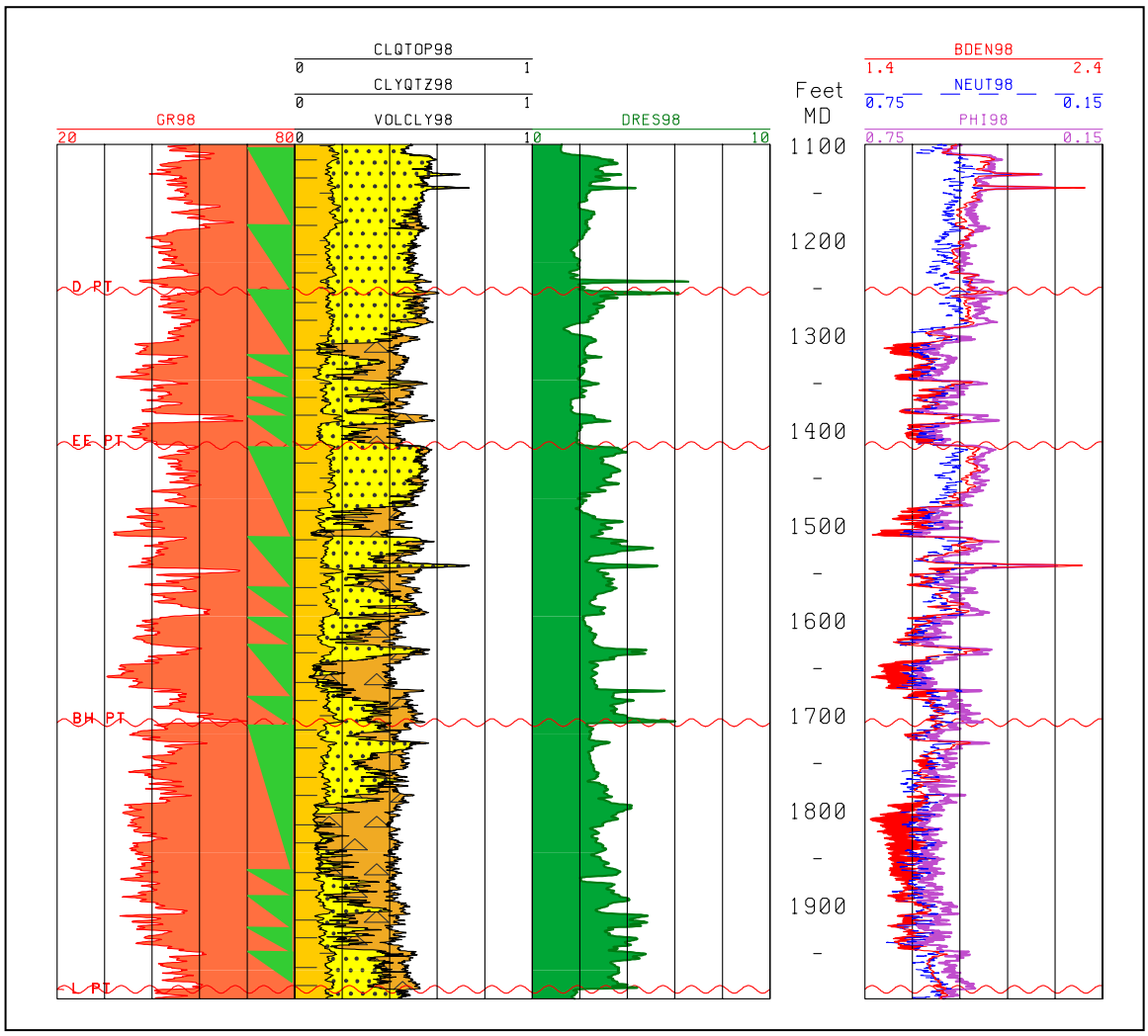

Figure 1.1-12. Representative well log of CO_2 pilot area illustrating parasequences (green triangles) and sequence boundaries (wavy red lines) of the Belridge Diatomite in Lost Hills. Log tracks from left to right are: gamma ray; % lithology (clay, silt/sand, and biogenic silica); gamma ray; deep resistivity, and bulk density.

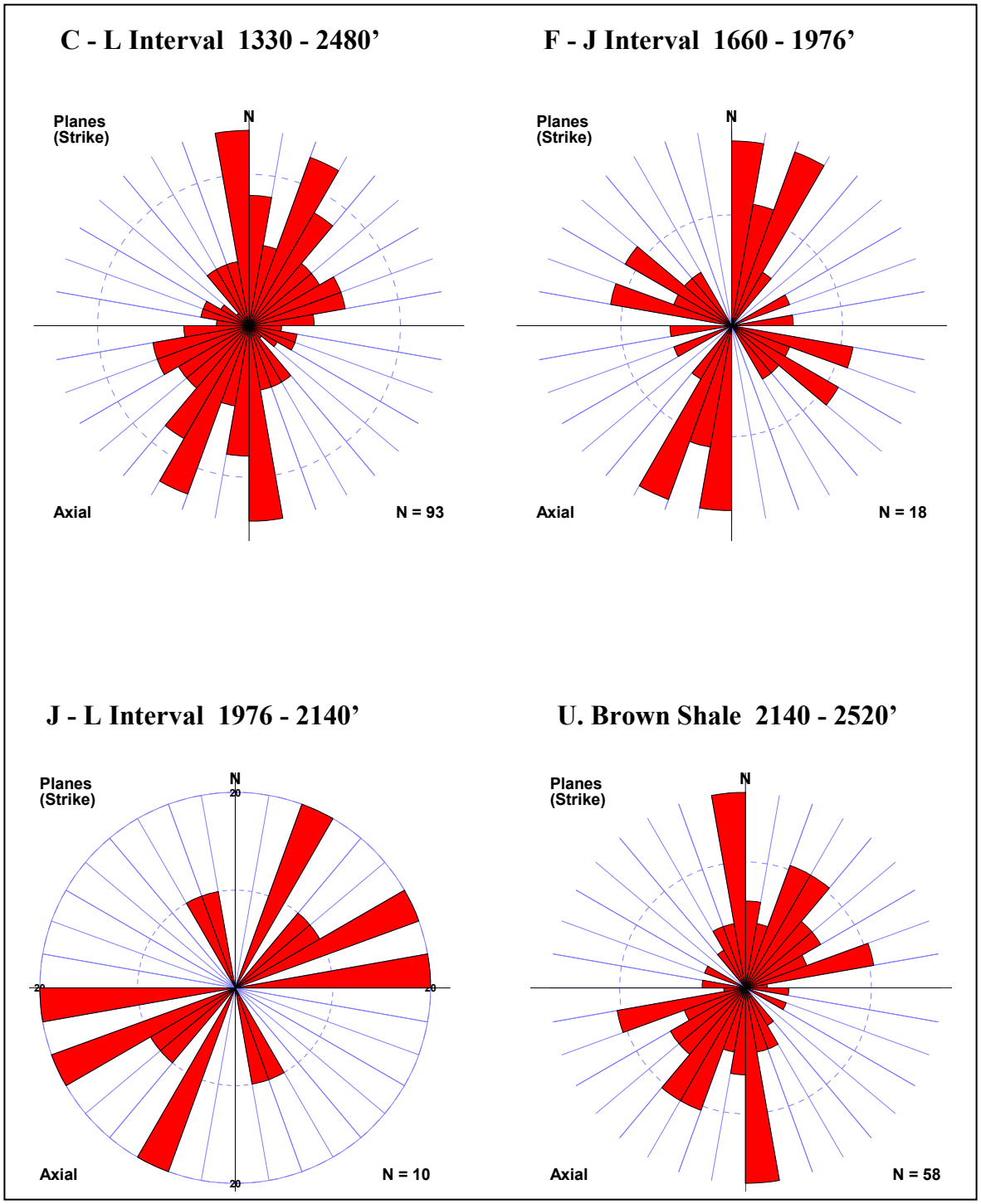

Figure 1.1-13. Azimuths of natural fractures as measured from the 12-8D EMI log. The CO_2 pilot will target the F-L interval. Note the increase in fractures and change in fracture azimuth in the Upper Brown Shale versus the F-J and J-L intervals. Data is from D. Julander and H. Wu.

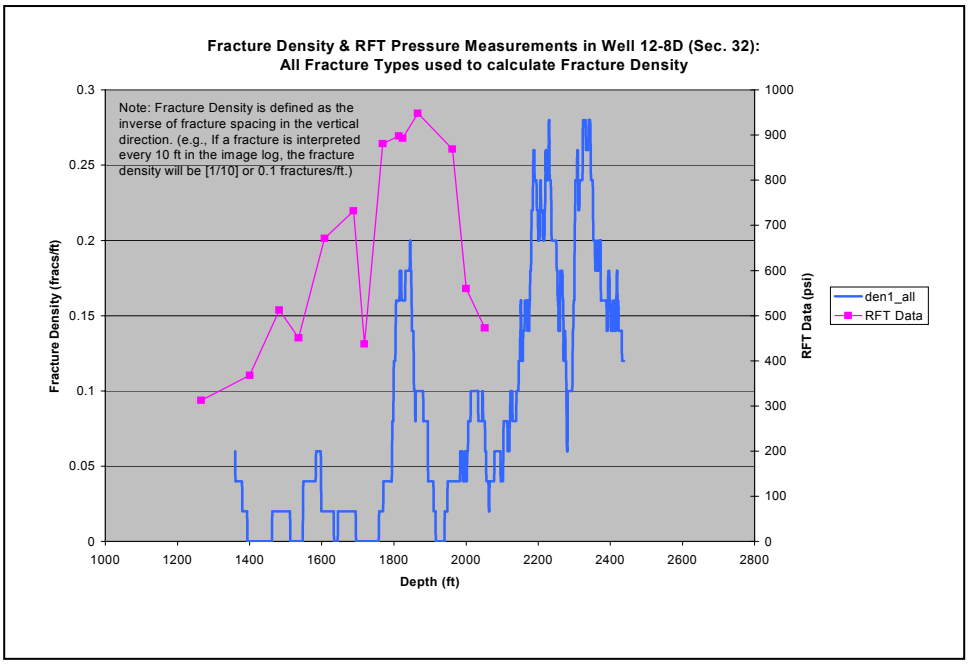

Figure 1.1-14. Halliburton Formation Tester measurements (upper curve) and fracture densities calculated from well 12-8D EMI log. Fracture data is from D. Julander.

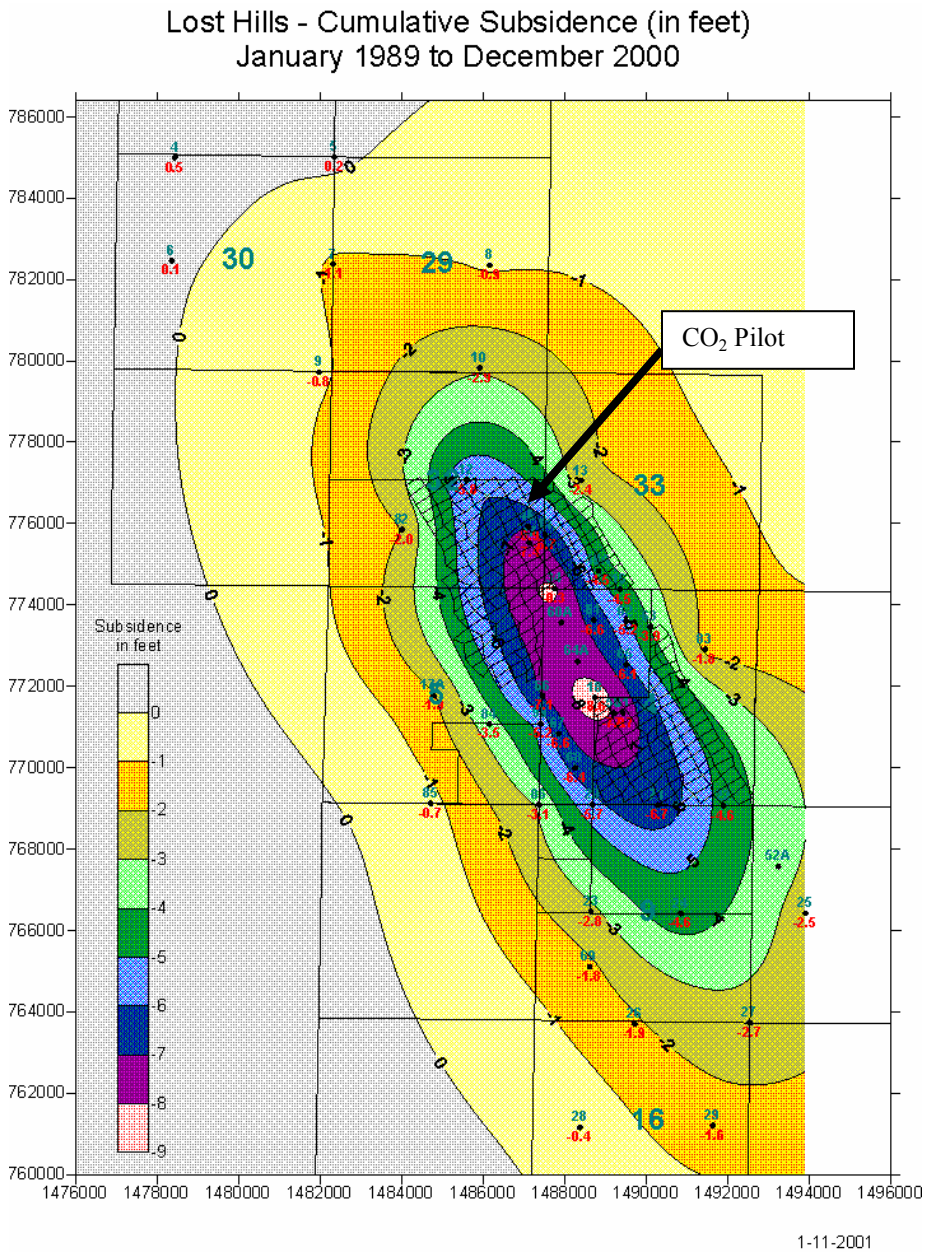

Figure 1.1-15. Map of cumulative subsidence (personal comm., N. Wildman). Lost Hills has subsided over 8 feet in 12 years. Waterflooding has greatly helped in reducing the subsidence rate and in reducing well failures due to subsidence.

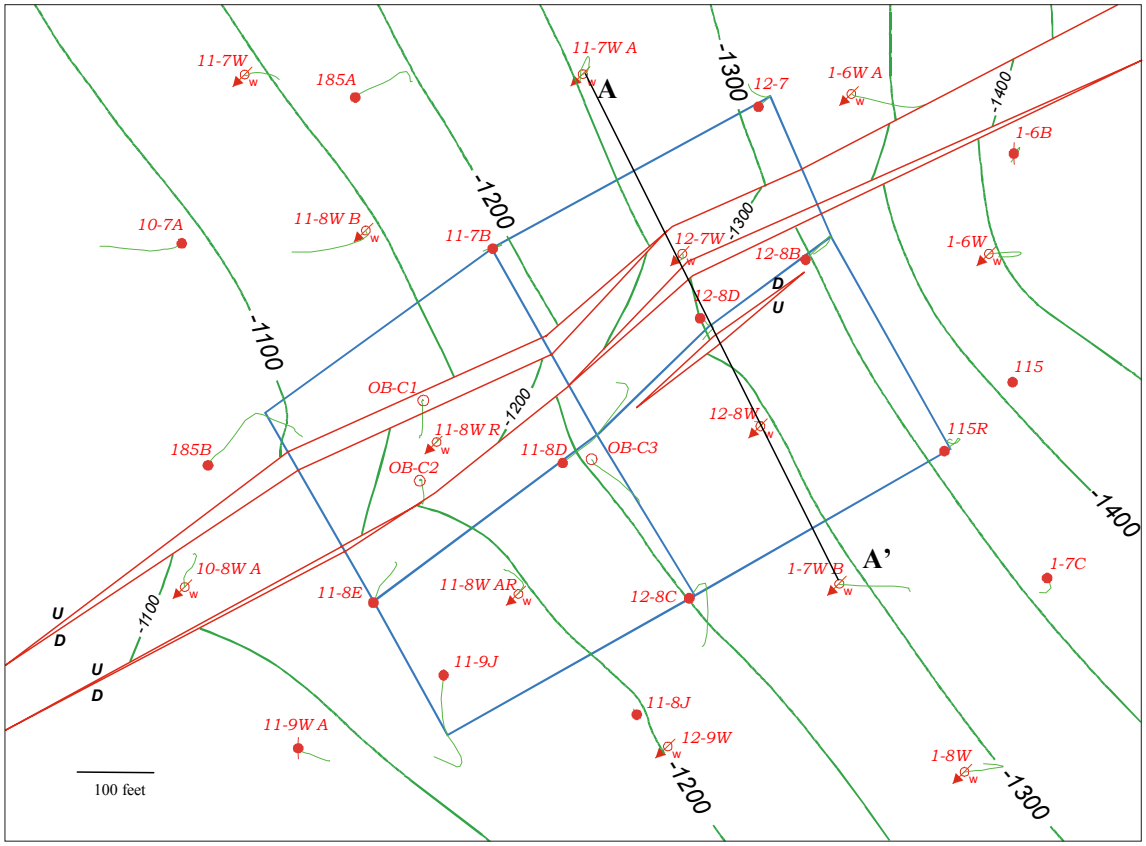

Figure 1.1-16. Lost Hills CO_2 pilot base map. Structure contours on FF Point (top of injection interval).

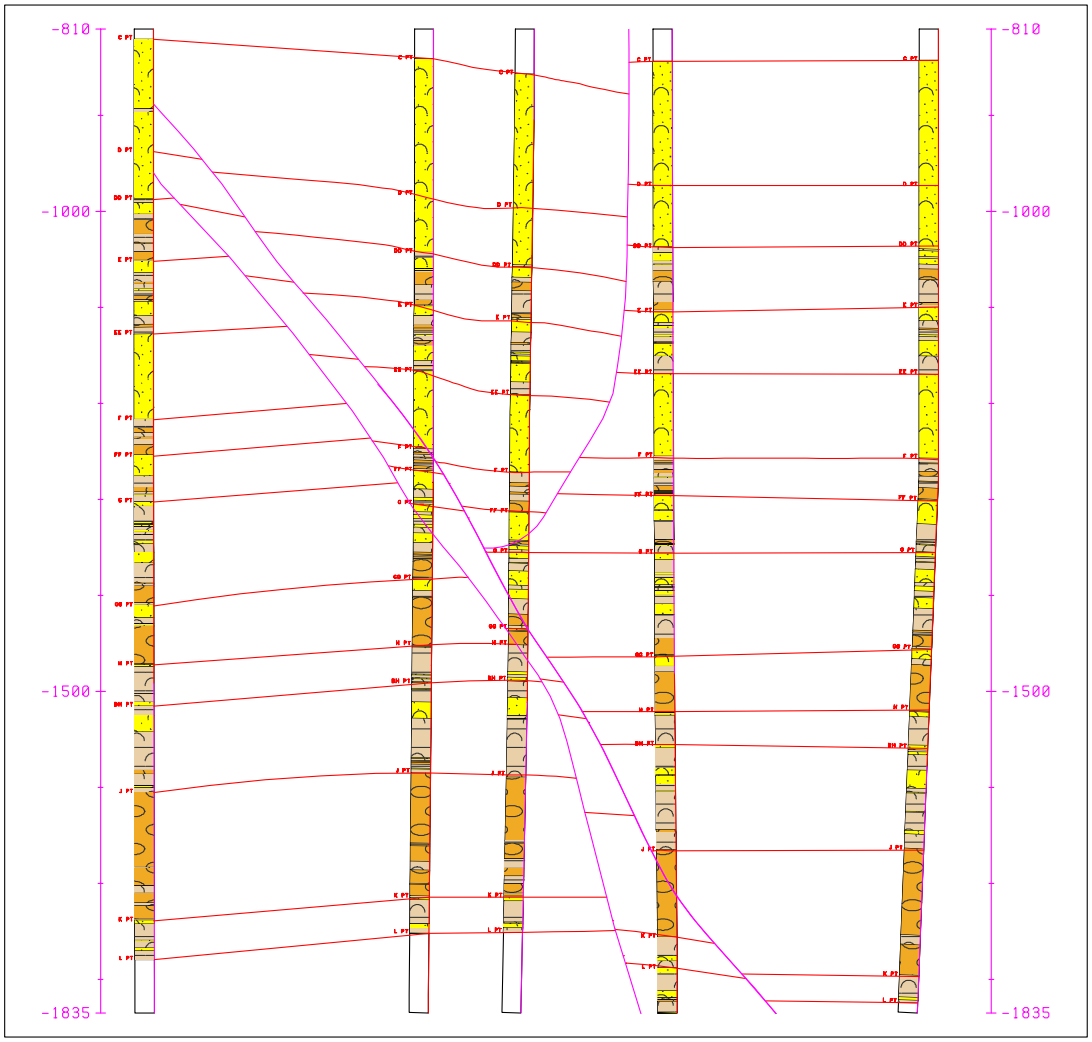

Figure 1.1-17. Cross Section A – A' through pilot area showing fault zone. The wells are from left to right are 11-7WA, 12-7W, 12-8D, 12-8W, and 1-7WB. Predominant lithologies (end members) shown: sandy diatomite (half circles and dots), clean diatomite (ovals), and clayey diatomite (half circles). CO_2 injection was in the FF through L interval which is predominantly clean and clayey diatomite.

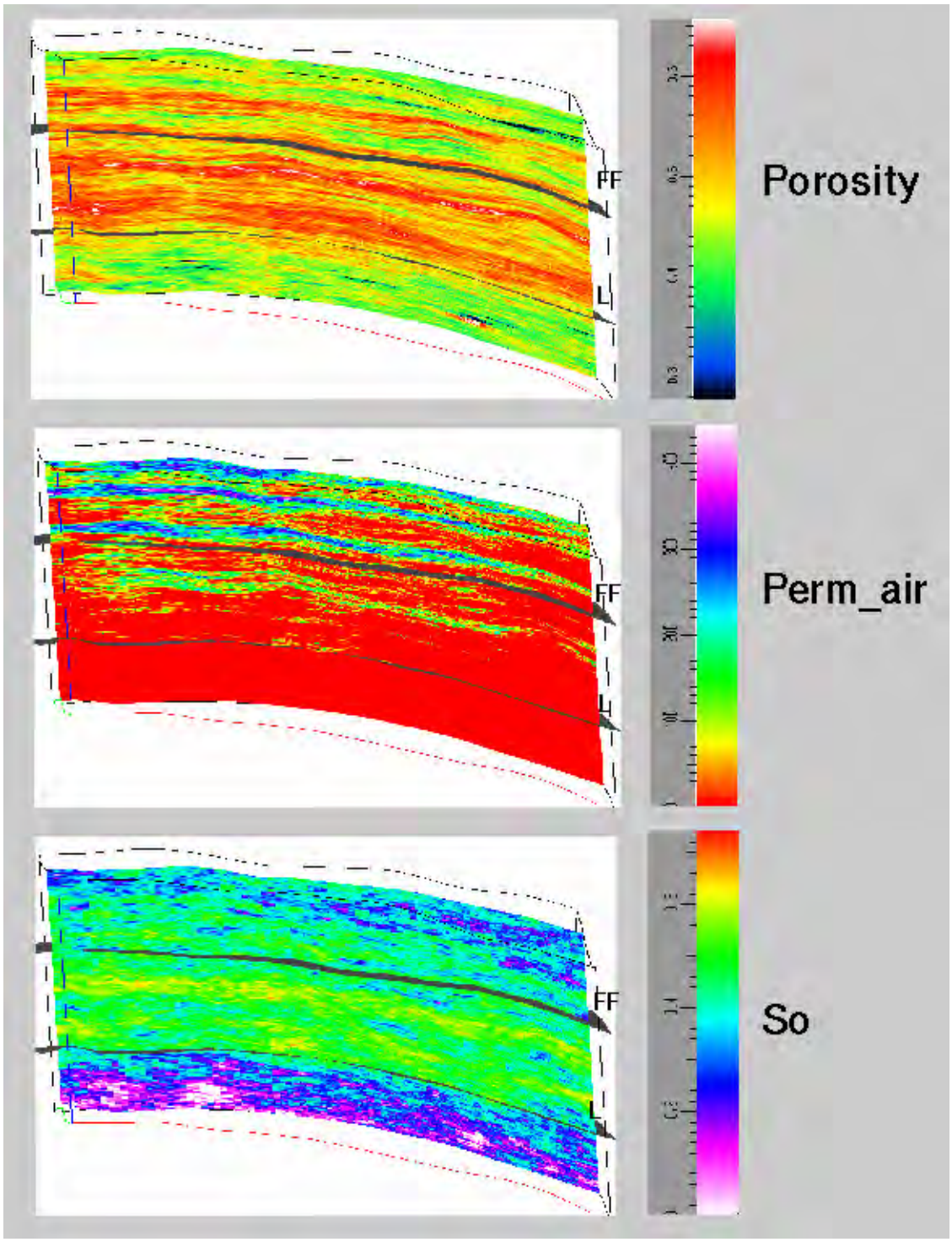

Figure 1.1-18. Cross-sections of porosity, air permeability, and oil saturation of the C Point to Upper Brown Shale interval from W. Fong's 3D Earth Model. The view is SW-NE and the length extends across 4 patterns (one on either side of the pilot). The CO_2 injection interval, FF - L, is highlighted. This is the same interval as the current waterflood.

1.2 FRACTURE INTERPRETATION OF WELL 12-8D FROM HALLIBURTON EMI LOG, CO_2 PILOT AREA

Dale R. Julander and Michael F. Morea
ChevronTexaco Exploration and Production Company

In December 1998, a Halliburton Electrical Micro Image (EMI) log was acquired in well 12-8D (Sec 32, T26S, R21E) in the Lost Hills Field. The logged interval extended from 1100' to 2510' MD and covered the bottom 284' of the Pliocene Etchegoin Formation, the entire Belridge Diatomite, and the upper 360' of the Upper Brown Shale. The log also covered the entire opal-A section and the uppermost 219' of opal-CT (the base of the opal-A is estimated to be at 2291').

Unfortunately, quality of the EMI data was degraded to some extent by excessive tool rotation during logging (greater than 4 rotations per 100 feet). The Halliburton logging engineers attempted multiple logging passes in the lower portion of the well in order to reduce the tool rotation but were unsuccessful. They eventually concluded that the rotation must be due to hole conditions and proceeded to log the rest of the well. High rates of tool rotation occurred sporadically throughout the entire logged interval. Fortunately, except for occasional thin zones (1 to 2 feet) where the tool rotation is extreme, the log was interpretable.

Z&S Recall software was used to interpret the EMI data. Bed boundaries were picked every 10 to 20 feet on average, and all recognizable fractures were picked in the interpretation. Each pick contains information about location, strike, dip, and type of event. Five fracture types with the following characteristics were interpreted from the image log data:

(1) *Open and clay-filled fractures:* high confidence picks which are resistive (usually black colored) compared to background image.
(2) *Faults:* high confidence picks with apparent offset.
(3) *Mineralized fractures:* high confidence picks which are conductive (usually yellow colored) compared to background image.
(4) *Poor fractures:* medium confidence picks which are predominantly open or clay-filled.
(5) *? Fractures:* lowest confidence picks which may be open, clay-filled, or mineralized.

Figures 1.2-1 through 4 show examples of EMI data from different intervals in the 12-8D well. In each figure, the left half shows the raw, uninterpreted data, while the right half shows the same data with its corresponding interpretation. In these examples, open and clay-filled fractures, faults, and bed boundaries have been interpreted from the image logs. Figure 1.2-1 shows an example of a fault in the H – BH interval. Figure 1.2-2 shows a fault-bound interval in the J – K interval (approximately 2028' to 2037') in which bedding is dipping at a significantly higher rate (~45^o in the N50^o-55^o direction) than the beds above and below (~15^o in the N50^o to 55^o direction). The lower bounding fault in Figure 1.2-2 appears to be a bedding-plane fault. Figure 1.2-3 shows a pair of faults in the Upper Brown Shale that have similar strikes (approximately east – west) but dip in opposite directions (the upper one 36^o

to the south and the lower one 54^{o} to the north). Figure 1.2-4 shows another pair of faults in the Upper Brown Shale with orientations of N2^{o}E/49^{o}ESE and S35^{o}E/42^{o}SW, respectively.

The fractures interpreted from the EMI data were used to calculate fracture density curves for the 12-8D well. Note that fracture density has units of fractures/ft, and is defined as the inverse of fracture spacing. Thus, as an example, if a fracture were interpreted every 10 feet from an image log, the fracture density in fractures/ft would be the inverse of 10 - - or 0.1. Two fracture density curves were calculated for 12-8D: one in which all of the above listed fracture types were included (blue curve in Figure 1.2-5), and one in which only fracture types 1 and 3 were used (magenta curve in Figure 1.2-5). A 50-foot averaging window was used to convert the irregularly sampled fracture picks to regularly sampled fracture density curves.

Figure 1.2-5 shows a fracture density trend that is similar to others observed in the Section 32 area of Lost Hills. Fracture densities calculated for all fracture types generally fall in the 0 to 0.1 fractures/ft range for the lower Etchegoin and Belridge Diatomite (1100' - 2140' interval). This is equivalent to fracture spacing in the vertical direction of roughly 10 feet or greater. For the Upper Brown Shale (2140' – 2510' interval), the fracture densities for all fracture types are in the 0.2 to 0.3 range. (Fracture densities of this magnitude correspond to vertical fracture spacings of roughly 3 to 5 ft.) The only significant anomaly in the data for the 12-8D well is the interval around 1800' – 1850' (Figure 1.2-5) where fracture densities are unusually high due to a concentration of fractures and faults between 1816' and 1836'. (See Figure 1.2-6 which shows both the uninterpreted [left] and interpreted [right] EMI data for the 1816' – 1836' interval.) This concentration of fractures and faults may coincide with an interval that appears to be anomalously thin based on correlations of the 12-8D open-hole logs to surrounding wells (M.F. Morea, personal communication). Table 1.2-1 provides a summary of orientation data for the faults in the 1816' – 1836' interval which may prove useful in the structural interpretation of the CO_2 pilot area.

The rapid increase in fracture density around the top of the Brown Shale is consistent with other fracture density trends in the Section 32 area. This increase is primarily a diagenetic opal phase change effect (due to the fact that the opal-A/CT transition usually occurs near the top of the Brown Shale in this part of the field).

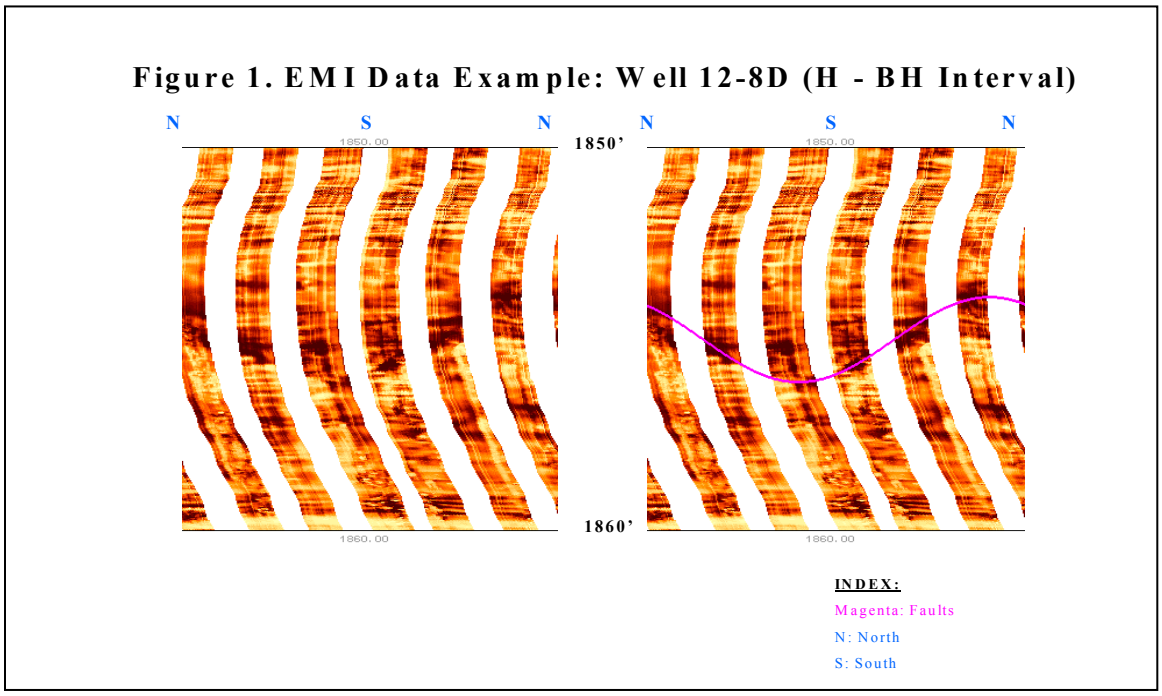

Figure 1.2-1. EMI data example from the H – BH interval inWell 12-8D.

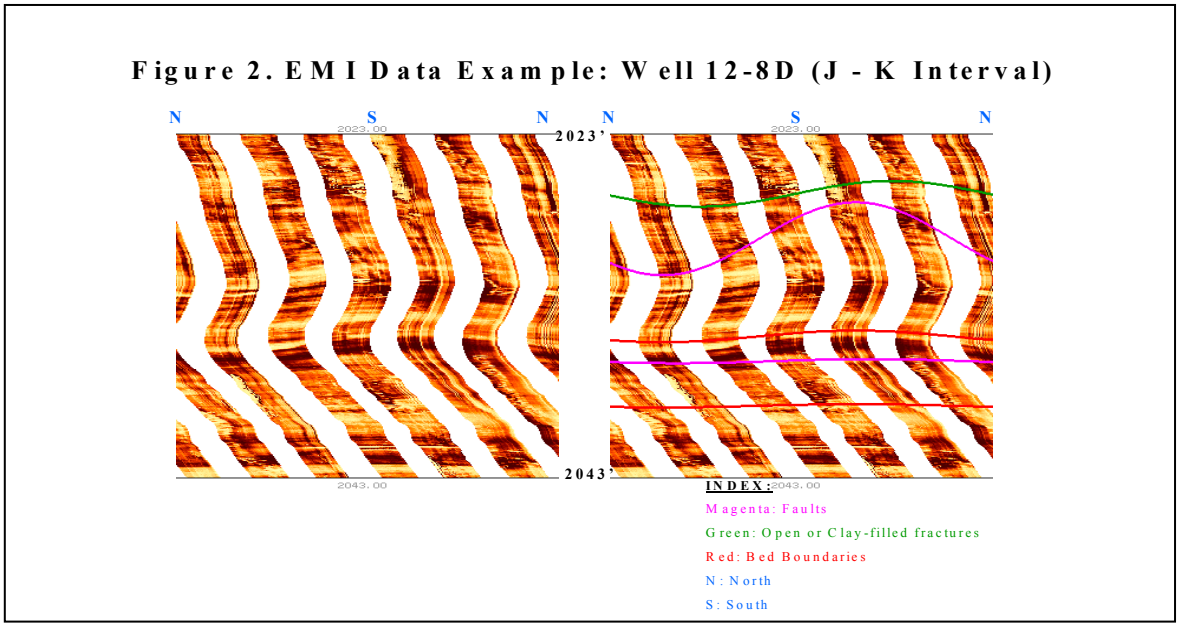

Figure 1.2-2. EMI data example from the J – K interval in Well 12-8D.

Figure 3. EMI Data Example: Well 12-8D (U. Brown Shale)

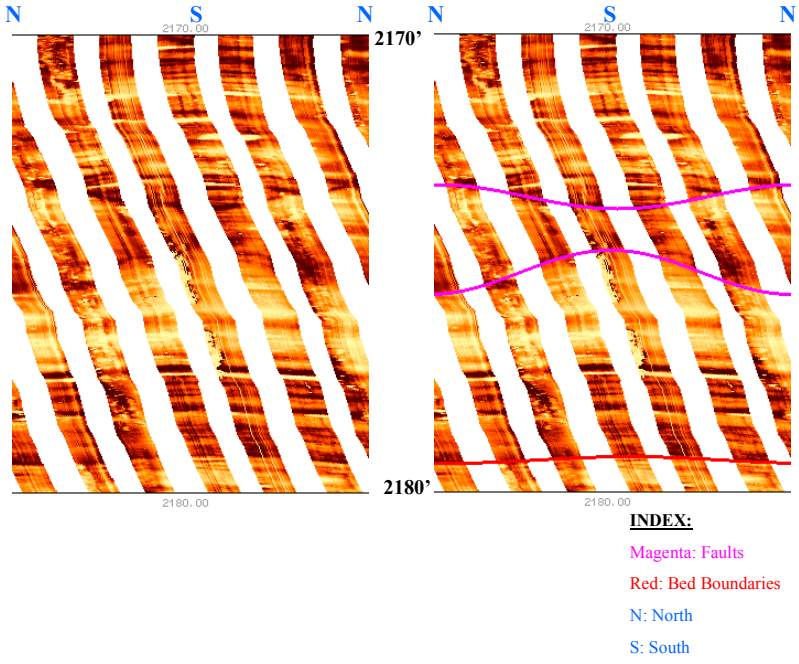

Figure 1.2-3. EMI data example 1 from the Upper Brown Shale interval in Well 12-8D.

Figure 4. EMI Data Example: Well 12-8D (U. Brown Shale)

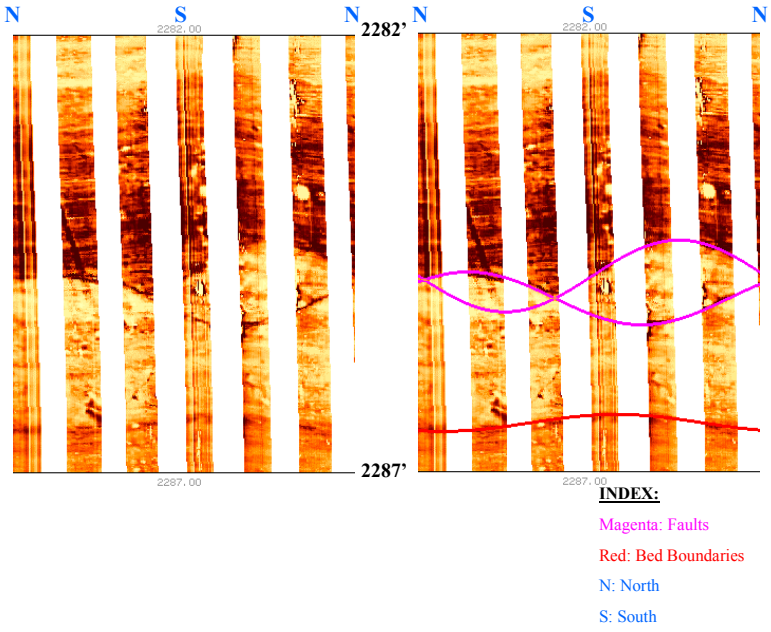

Figure 1.2-4. EMI data example 2 from the Upper Brown Shale interval in Well 12-8D.

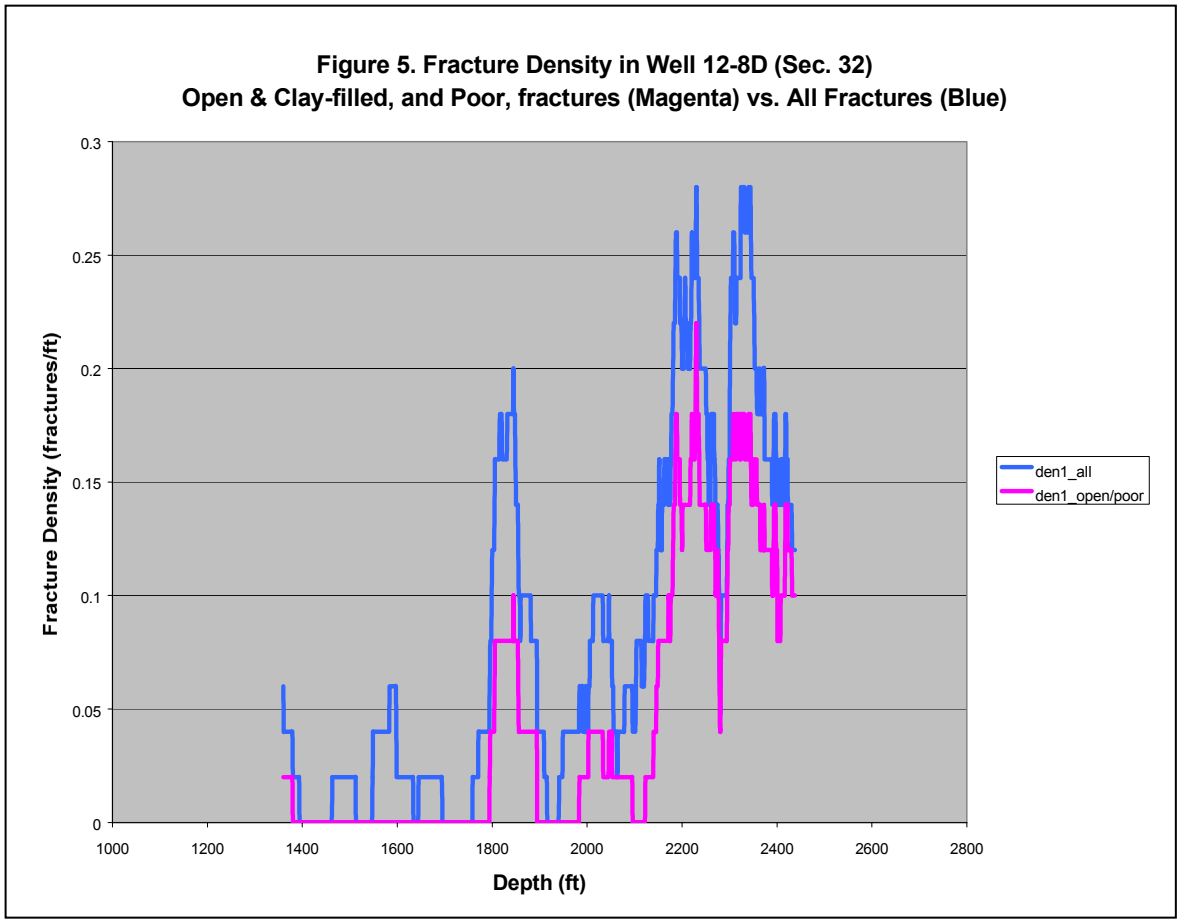

Figure 1.2-5. Fracture density in well 12-8D. The increase in fracture density at 1800-1900 ft is due to the presence of a fault zone. The increase at 2100 ft. is probably due to the diagenetic opal phase change that coincides at this depth in the Brown Shale.

Figure 6. EMI Data Example: Well 12-8D (G - H Interval)

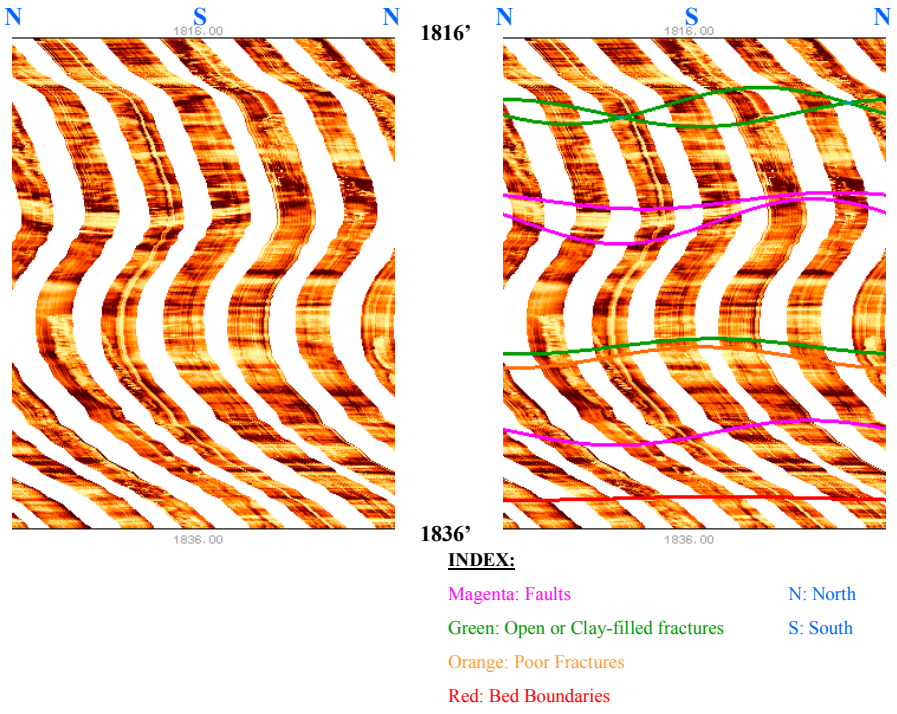

Figure 1.2-6. EMI data example from the G – H interval in well 12-8D.

Table 1.2-1. Fault data in the 1818 – 1832 ft interval in well 12-8D.

Table 1. Fault Data in the 1818' - 1832' Interval			
Depth	Strike	Dip (degrees)	Dip Direction
1822'	N41E	43	SE
1823'	N20E	69	SE
1832'	N16E	56	SE

SECTION 2

CO_2 PILOT INSTALLATION

2. CO_2 PILOT INSTALLATION

John F. Cooney, Pasquale R. Perri , and Bradley Wiest
ChevronTexaco Exploration and Production Company

2.1 CURRENT DEVELOMENT

Lost Hills Primary Development:
The Lost Hills Field, located 45 miles northwest of Bakersfield, California, (see Figure 2.1-1) was discovered in 1910. Reserves in the shallow sands, diatomite, and chert pools (Figure 2.1-2) were developed using slotted liner completion techniques until the late 1970's. From the late 1970's to 1987, small volume hydrofracture completions were performed covering the entire Belridge Diatomite.

Figure 2.1-1. Lost Hills Field Location Map.

Advances in hydraulic fracturing technology in the late 1980's resulted in increased oil recovery that led to a more aggressive development program by Chevron. From 1987 to the present, high volume hydrofracture completions have been performed across the entire Belridge Diatomite and the Upper Brown Shale resulting in significant production increases as shown in Figure 2.1-3.

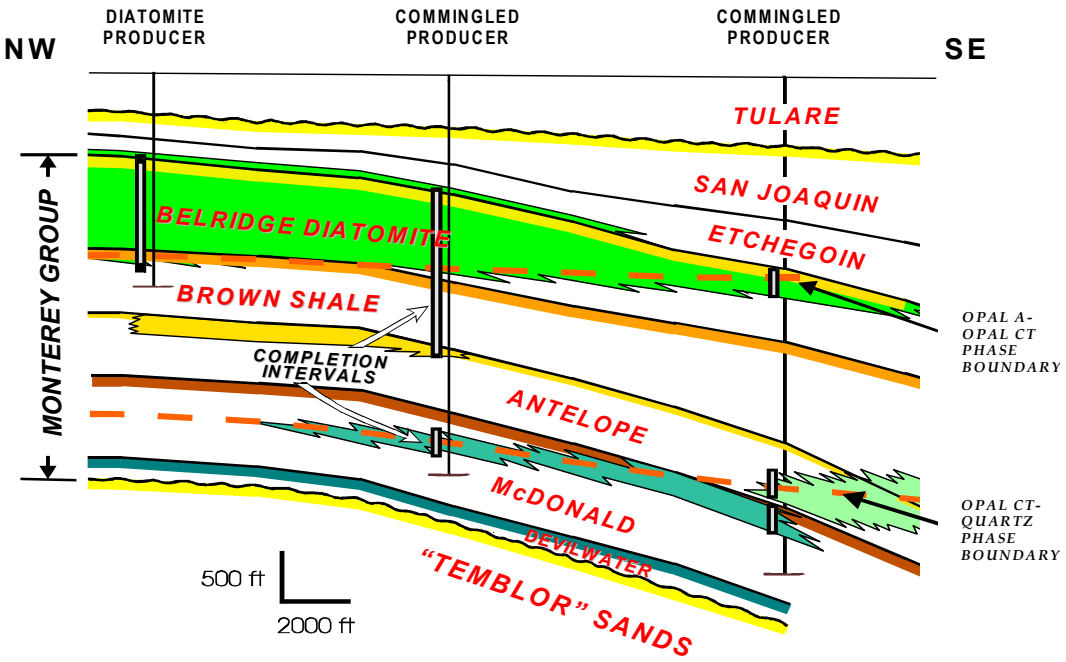

Figure 2.1-2. Lost Hills Field Regional Cross-Section.

The Lost Hills Field is developed on a 5 acre (siliceous shale) to 1.25 acre (diatomite) well spacing. There are over 2.2 billion barrels of oil in place in the Belridge Diatomite in Lost Hills. To date only 112 million barrels have been produced, or approximately 5% of the original oil in place (OOIP).

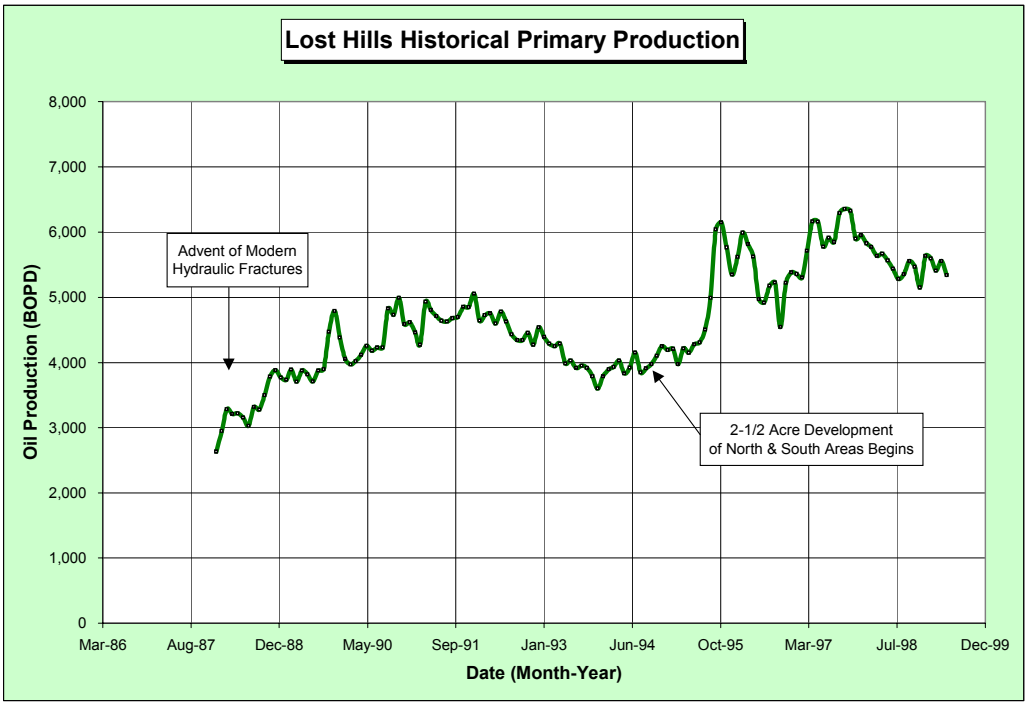

Figure 2.1-3. Lost Hills Historical Primary Production.

Diatomite Waterflood Development:

Chevron initiated a pilot diatomite waterflood project in December 1990 and began full-project development in April 1992. Since 1992, two hundred and eight 2-1/2 acre patterns have been put on water injection spanning parts of four sections (Sections 4, 5, 32 Fee, and 33) as shown in Figure 2.1-4. The historical performance of the Lost Hills waterflood performance can be seen in Figure 2.1-5. Since the initiation of first project water injection in April 1992, production has increased approximately 4,000 BOPD from 6,400 BOPD to the current rate of 10,400 BOPD.

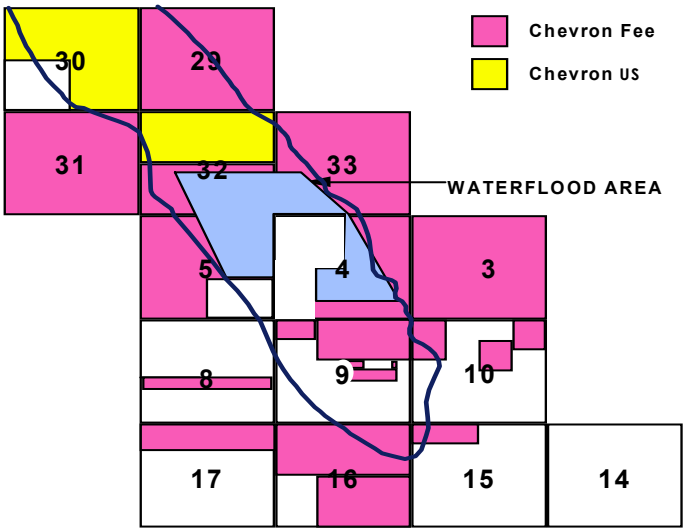

Figure 2.1-4. Lost Hills Waterflood Project Location Map.

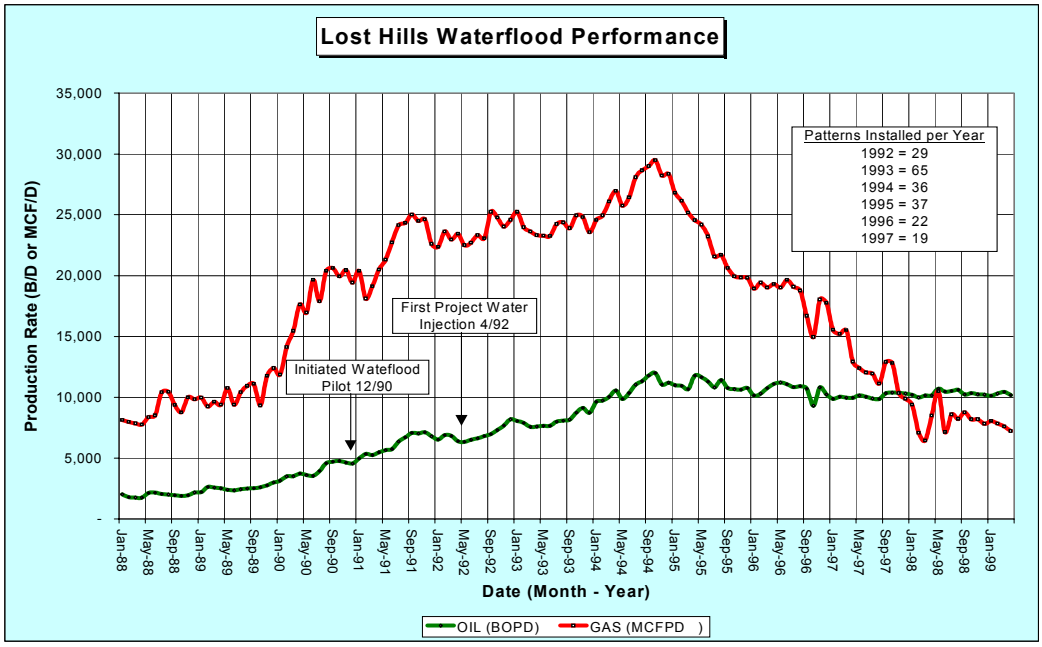

Figure 2.1-5. Lost Hills Waterflood Performance.

In terms of recovery efficiency, Figure 2.1-6 compares the estimated primary and secondary (waterflood) recoveries for each of the 4 sections under waterflood to the original Lost Hills waterflood project estimate (GO-36) on a per pattern basis. The height of the bars in Figure 2.1-6 represent the average pattern OOIP. Estimated ultimate waterflood recovery from the Lost Hills diatomite is 8.1% of OOIP, which is considerably less than the original project estimate of 19.6% of OOIP.

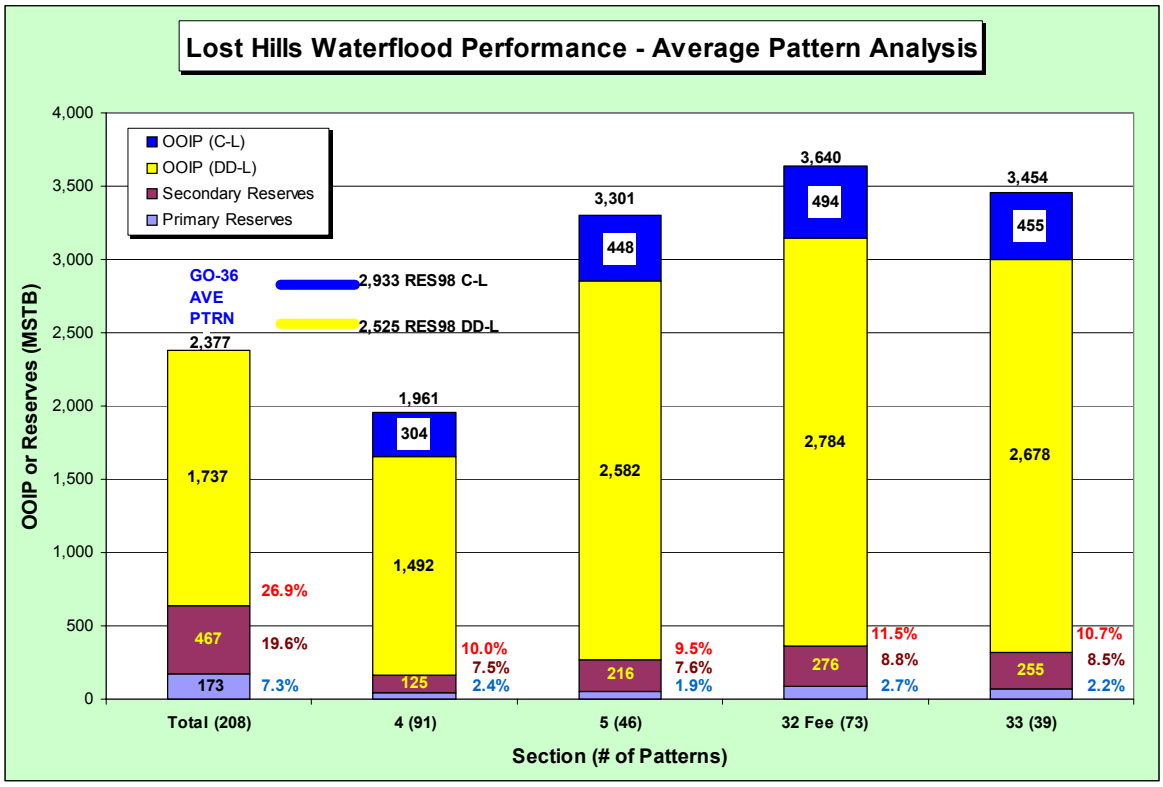

Figure 2.1-6. Lost Hills Estimated Waterflood Reserves and Recovery Factors.

Infill Primary Pilot:

An infill primary pilot was initiated by Chevron in Section 32 U.S. in 1998 to test the economic viability of improving primary recovery (3 – 4 % of OOIP to date) by infill drilling from the current 2-1/2 acre development down to 1-1/4 acre spacing. A total of 11 infill producers have been drilled and completed as part of the pilot test to date. The results have been disappointing and keeping the wells on production due to excessive sanding continues to be a problem.

Infill Waterflood Pilot:

Installation of an infill waterflood pilot began in late 1998 by Chevron in Section 32 Fee to test the potential of waterflooding with 1-1/4 acre "direct line-drive" patterns compared to the current 2-1/2 acre "staggered" patterns. To date, 28 wells (9 injectors and 19 producers) have been drilled on 1-1/4 acre spacing to determine if the current waterflood recovery can be accelerated, or better yet, if incremental waterflood reserves can be obtained by infill drilling.

Diatomite Steamflood Pilot:
Chevron initiated a diatomite steamflood/cyclic steam pilot in the southern portion of Section 29 in October 1998. The steamflood pilot consists of 7 injectors targeting the J – L "clean" diatomite intervals. A single pattern cyclic steam pilot consisting of 4 producers targeting the more permeable EE – F "sandy" diatomite was initiated concurrently. Both pilots are still under evaluation.

Horizontal Wells:
In 1997 Chevron began experimenting with horizontal wells to try to exploit the flanks of the field where vertical wells could not be economically justified due to the reduced oil column. Through December 2000, four horizontal wells have been drilled with mixed results. Figure 2.1-7 is a summary of the Lost Hills horizontal well performance to date.

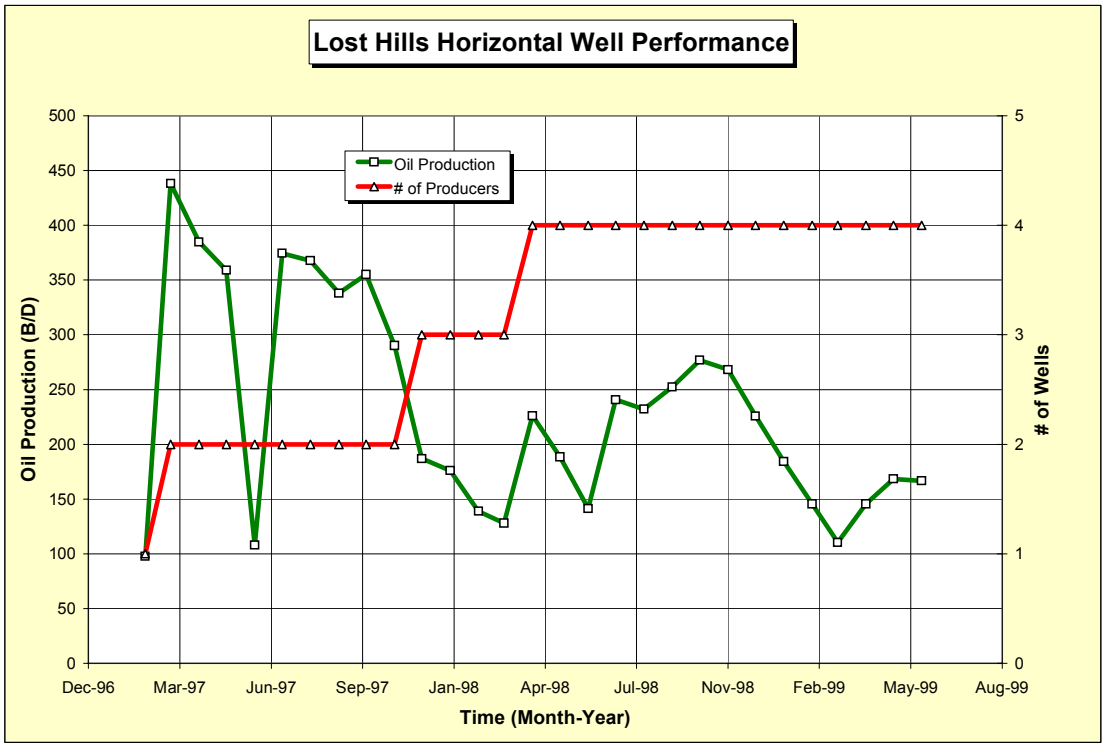

Figure 2.1-7. Lost Hills Horizontal Well Performance.

2.2 CO_2 PILOT LOCATION

The CO_2 Pilot is located in the southeast quarter-section of Section 32, T.26S., R.21E. of the Lost Hills Field as shown in Figure 2.2-1. A four-pattern pilot has been installed. The pilot area is enlarged in Figure 2.2-2 showing the four existing waterflood patterns (10-8WA, 11-8WA, 12-7W, and 12-8W) which were converted to CO_2 injection.

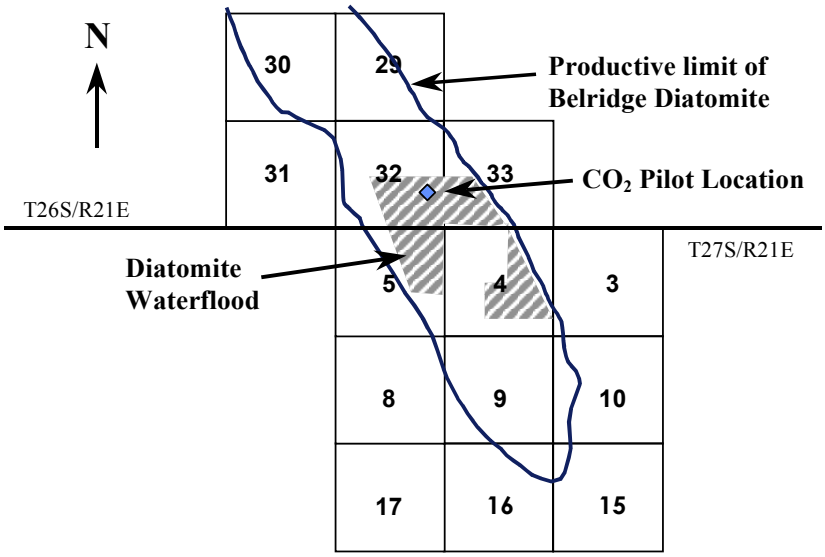

Figure 2.2-1. Lost Hills CO_2 Pilot Location Map.

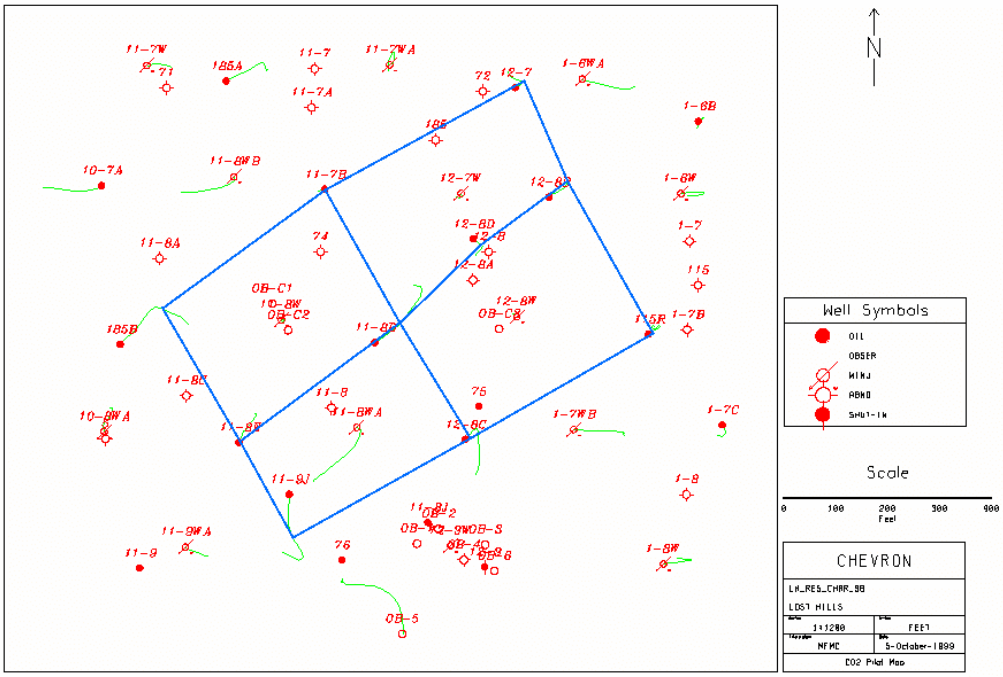

Figure 2.2-2. Lost Hills CO_2 Pilot Pattern Map.

Two of the existing injectors (10-8WA and 11-8WA) had to be replaced due to poor mechanical conditions of the wellbore. The two new injectors are 10-8WAR and 11-8WAR.

2.3 CO_2 PILOT DESIGN AND OBJECTIVES

Objectives:
The Lost Hills CO_2 Pilot was designed with the following goals and objectives in mind:

- Test the technical and economic viability of CO_2 flooding the low permeability Diatomite resource, which is one member of California's siliceous shale reservoirs of the Monterey Formation.
- Test the technical and economic viability of CO_2 flooding the Diatomite resource in a timely manner (3 years or less).
- Install a configuration that enhances the chance of process success (oil response).
- Install a configuration that minimizes the likelihood of premature CO_2 breakthrough.
- Provide an opportunity to gather and analyze reservoir, geologic, and production data and gather facilities design information necessary to commit to a full-field project.
- Install a CO_2 Pilot in Lost Hills safely, without incident, and in accordance with all county, state, and federal environmental rules and regulations.

With the foregoing objectives in mind, a four pattern (2.5 acre each) CO_2 pilot configuration was chosen as shown in Figure 2.3-1. This configuration confines one producer (11-8D) and reduces the risk of premature breakthrough that a 5/8 acre pilot configuration would likely incur.

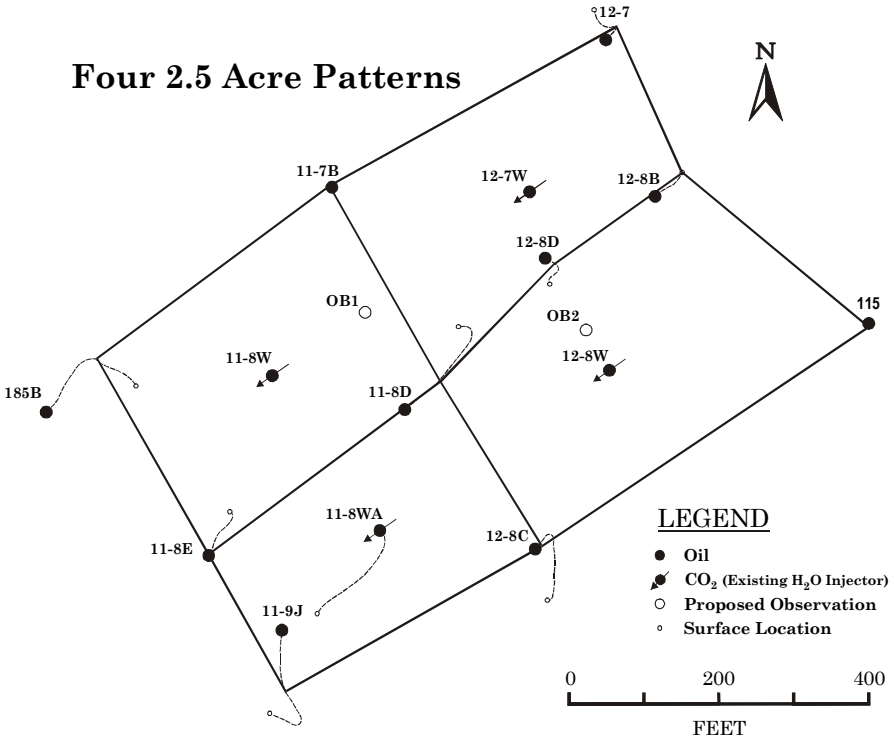

Figure 2.3-1. Four 2.5 Acre Patterns Pilot Configuration.

2.4 Pilot Facilities

Summary:
The facilities consisted of three main scopes:

1. CO_2 injection equipment
2. CO_2 distribution lines
3. Production handling facilities

BOC Gases Inc. procured and installed the injection CO_2 injection equipment. This equipment consisted of two 50 ton storage tanks, booster pumps, injection pumps, pressure building vaporizers, and a hot water bath heater. CO_2 liquid was stored at 0 ^{o} F and 300 psig. For injection it was boosted to roughly 1,000 psig and vaporized.

WAG (Water-Alternating-Gas) injection headers were installed to allow for quick switching between water and CO_2 injection. The headers also included flow and pressure monitoring devices that supplied information to a central data collection point at our Central Lost Hills Plant.

Dedicated well gauging facilities were installed. The intent was to establish reliable baseline well gauging information and to eliminate production "noise" from wells outside of the pilot area. The new gauging facilities were started in May 2000 in order to establish good baseline data prior to the start of injection in late August 2000. The new *CASE Services* software to assist with production and injection tracking was also installed in June 2000.

The following section goes into more detail on the facilities design basis and includes some actual photos of the gauging and injection equipment.

Design Basis:
The facilities were designed to support four 2.5 acre patterns with the following objectives or constraints:

- Four injection wells (existing water injectors) requiring a maximum pressure of 1200 psig.
- The equipment will be able to deliver a CO_2 rate as low as 100 MSCF/D per well, and as high as 500 MSCF/D per well. This range is based on the results of the March 1999 injectivity test.
- Ten producing wells. A phased approach is being taken to establish early baseline data from the existing producing wells in the CO_2 pilot.

Phase 1 – New Gauging Facilities:
The new gauging facilities started operating in early May 2000 in order to establish good baseline production data prior to starting injection. A picture of the new gauging facilities is shown in Figure 2.4-1. It should be noted that the new gauge setting can handle and monitor the production associated with the pilot. However, if the pilot period is extended it would be

advantageous to install the new gauge setting to improve metering accuracy and to minimize corrosion damage to existing facilities.

They are designed to handle and monitor the increased CO_2 production associated with the CO_2 pilot. The key objective of these facilities will be to isolate and handle the wet gases high in CO_2 to prevent excessive corrosion of the existing gathering system. The time lag between phase 1 and 2 facilities will be minimal (2 to 4 months). Since these gauging facilities will have salvage value to Chevron, regardless of the outcome of the pilot, the DOE is paying only 25% for this portion.

Figure 2.4-1. CO_2 pilot gauging facilities.

Some of the existing flow lines were utilized for the producers, while others were replaced with cement lined piping. Funding was included in the AFE to tie additional wells into the pilot dedicated gauge setting should they also experience CO_2 breakthrough outside the immediate pilot patterns. The facilities also include monitoring equipment, such as density meters and online corrosion monitors, to help detect CO_2 breakthrough.

Phase 2 - Injection Facilities:
The injection equipment is being leased and consists of; storage tanks, injection pumps, heaters, monitoring equipment, and injection lines. It will be very similar to the equipment utilized for the March 1999 injectivity test but with a greater capacity. SCADA equipment was installed to enable the existing infrastructure to gather and compile the data from the pilot.

Figure 2.4-2 is a picture of the CO_2 injection header and CO_2 storage vessel. Figure 2.4-3 is a picture of the CO_2 storage tanks. Figure 2.4-4 is a picture of the CO_2 injection pumps and heater.

Figure 2.4-2. CO_2 Pilot Injection Header.

All major components of the pilot facilities have been operational since August 31, 2000. We have been getting excellent run time out of the injection equipment. However, due to the power availability situation in California we have been required to shut down injection pumps when a stage 2 alert occurs. Cold weather spells result in several shut downs each week, that affect the entire Lost Hills Field, and last several hours.

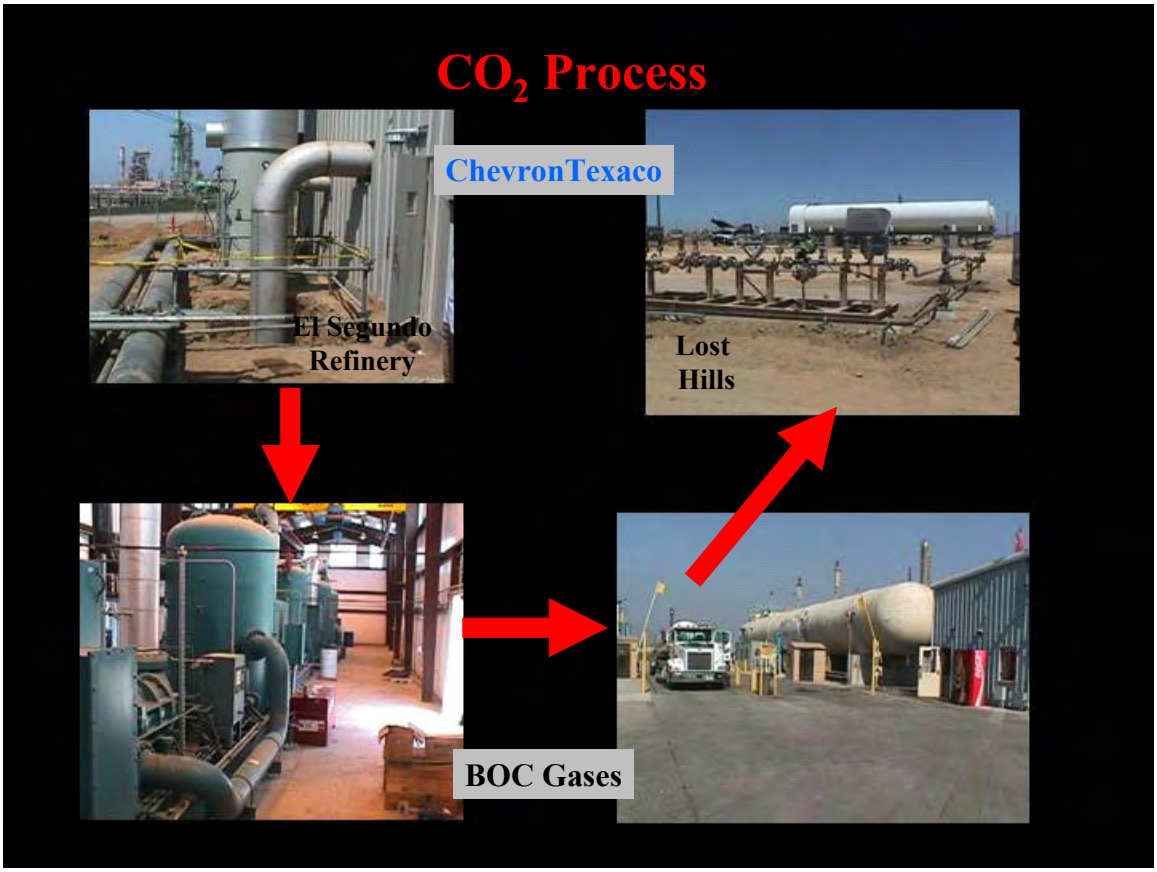

Figure 2.4-3. Process of Trucking CO_2 from El Segundo Refinery to Lost Hills.

As injection proceeds we continue to monitor and control all critical process parameters. Due to higher produced gas rates from well 11-8E, we had trouble gauging oil production for approximately one month. In early November 2000, we saw oil from this well increase from roughly 80 BOPD to over 100 BOPD. Unfortunately, the higher gas rates that occurred simultaneously prevented us from verifying the encouraging gauge. The gas-metering bottleneck has been eliminated but the well has been down due to sanding problems ever since. The next describes the remedial action that will be taken to return this well (11-8E) to production.

Figure 2.4-3. CO_2 storage facilities.

Figure 2.4-4. CO_2 injection pumps with heater in the background.

2.5 Remedial Work

Figure 2.5-1 is a map of the CO_2 pilot area showing the six pilot producers that have experienced sanding problems (11-8D, 11-8E, 12-8B, 12-8C, 12-8D, and 185B) or some kind of subsidence-related casing problems. The following is a brief discussion of the remedial work performed on the six pilot producers.

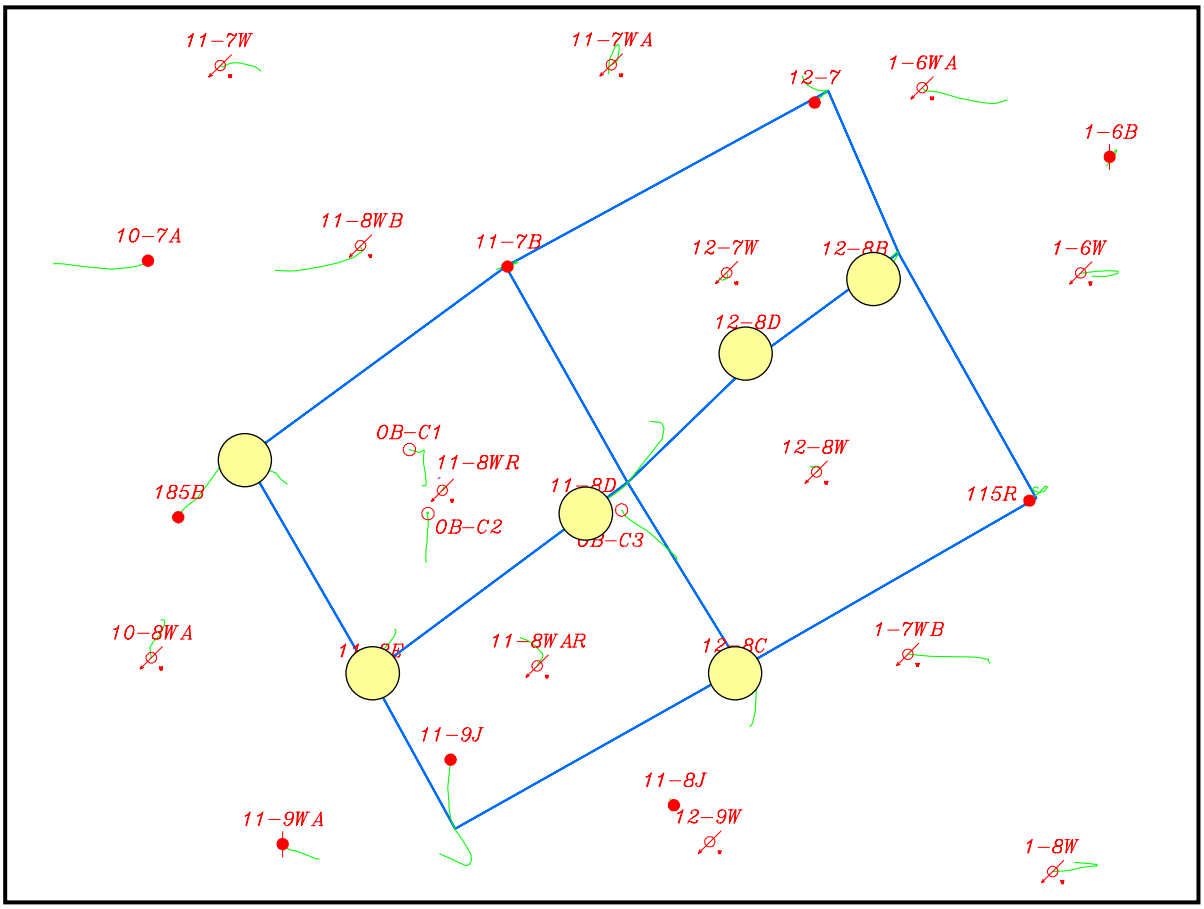

Figure 2.5-1. CO_2 pilot map-showing producers with sanding problems.

Well Work:

Well 11-8E developed severe sanding problems, apparently as a response to the CO_2 injection as indicated by increased production levels of oil and gas immediately prior to well failure. Attempts to return the well to production failed as sand continued to enter the wellbore and foul the pump. The pump would fail after only a few hours or days after repeated pulls. To address the problem, a sand consolidation treatment was designed for the well. A coiled tubing / jet tool HCl acid treatment was administered to address scale in the lower portion of the well as precursor to the Halliburton Sandwedge® sand consolidation treatment. The sand control treatment was administered with a proppant slurry to the well in 6 stages to correspond with the fracture intervals. A packer assembly was utilized to isolate zones, progressing up the hole. After the treatment, the well was returned to production and immediately sanded again. The pump was pulled and the well cleaned again. The well has not failed since and production has increased steadily to near pre-job levels.

The pumps were raised 300 – 400 feet above their previous levels on four pilot producers (wells 11-8D, 12-8B, 12-8C, and 12-8D) to help alleviate the sanding problems. However, the sanding problems re-occurred in April 2001 with the re-establishment CO_2 injection earlier that same month. Pump failures and sand-packed flowlines were problematic for wells 11-8D, 11-8E, 12-8B, 12-8C, and 12-8D. Failure of all the wells occurred abruptly such that all the wells failed within a week's time. Even well 11-8E, which had been treated for sand control with Halliburton Sandwedge®, failed due to excessive sand production.

The majority of the wells have been cleaned out and the pumps have been placed higher in the wellbore to facilitate a longer runtime. The Halliburton Sandwedge® treatment was determined to be ineffective for well 11-8E, leading to the trial of alternative treatments. Halliburton treated wells 11-8E and 11-8D with their Prop-Tak® treatment. This treatment is administered with a proppant slurry to the well in stages, which correspond with the fracture intervals. A packer assembly is utilized to isolate stages, progressing up the hole. Schlumberger treated wells 12-8B, 12-8C, and 12-8D with their Sandlock V® treatment. This treatment is a chemical squeeze into the fracture stages, administered without proppant utilizing a similar packer assembly for placement.

Casing damage was discovered in well 12-8B during a casing inspection log. Well 12-8C was returned to production in early August 2001 but experienced problems again and remains shut-in. Well 185B failed in August 2001 and it has been determined that it needs to be replaced. Well 11-8E failed again in November 2001 due to sand entry. Well 11-8E was returned to production in February 2002 after some remedial work to isolate the upper frac stage and appears to have been successful. As of March 1, 2002, three pilot producers are shut-in (12-8B, 12-8C, and 185B).

SECTION 3
PILOT PERFORMANCE

3. PILOT PERFORMANCE

Pasquale R. Perri
ChevronTexaco Exploration and Production Company

3.1 Injection Performance:

CO_2 injection commenced on August 31, 2000 into the four pilot injectors. CO_2 injection began slowly at 50 MCF/D per injector as we de-bugged and became acquainted with the new facilities. CO_2 injection was slowly ramped up from 50 MCF/D per injector to approximately 475 MSCF/D per injector prior to experiencing sanding problems in five producers. Sanding problems developed in CO_2 pilot producers 11-8D, 11-8E, 12-8B, 12-8C, and 12-8D in mid-December 2000. CO_2 injection was intermittent in 2001 as we had re-occurring producer sanding problems. We injected CO_2 from February 2001 until May 2001 when sanding problems surfaced again. CO_2 injection was discontinued until August 2001. We injected from August 2001 through November 2001 before terminating injection for a third time in December 2001. CO_2 injection remained shut-in while all the problem producers were remediated. CO_2 injection resumed in early May 2002 and we continued to inject until late August 2002 when the tubing in well 11-8E was severely damaged. CO_2 injection was suspended the rest of 2002. It was concluded that CO_2 injection played a major role in the sanding problems. The project was officially terminated by ChevronTexaco management on January 30, 2003.

Figures 3.1-1 through 3.1-4 are the individual water/CO_2 injection plots for the four pilot injectors. Figure 3.1-5 is the composite or total CO_2 injection for the pilot. Table 3.1-1 summarizes the cumulative CO_2 injected for the pilot through December 31, 2002. Since August 31, 2000, we have injected 375,113 MCF of CO_2 at the average rate of 239 MCF/D per injector. This equates to only 0.0499 HCPV's of CO_2 injected.

Table 3.1-1. Cumulative Pilot CO_2 Injection through December 31, 2002.

Injector	MCF	HCPV
11-8WR	94,412	0.0472
11-8WAR	93,172	0.0608
12-7W	95,773	0.0529
12-8W	91,756	0.0421
Total	**375,113**	**0.0499**

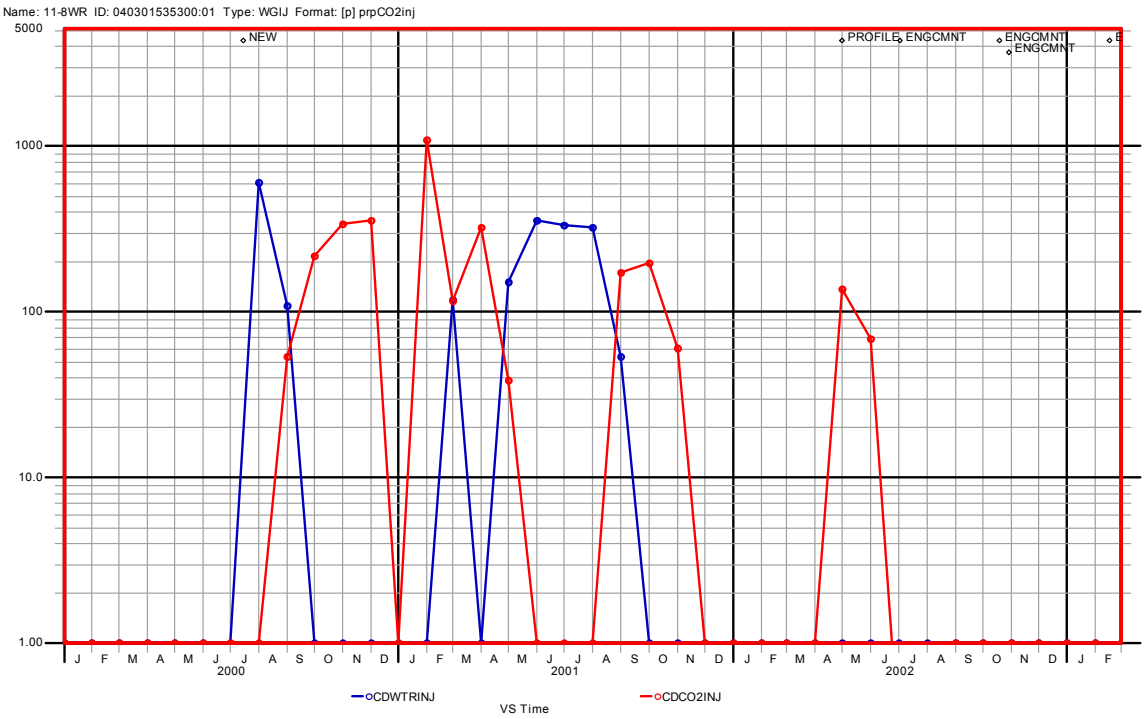

Figure 3.1-1. Injection Plot for CO_2 Injector 11-8WR.

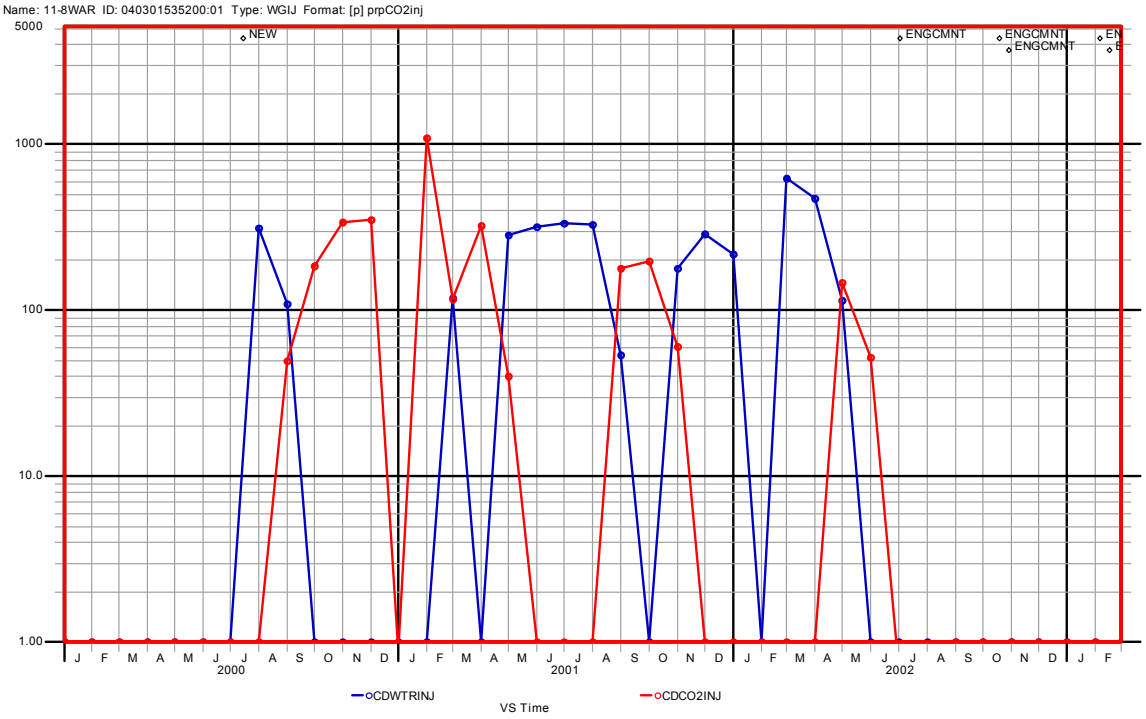

Figure 3.1-2. Injection Plot for CO_2 Injector 11-8WAR.

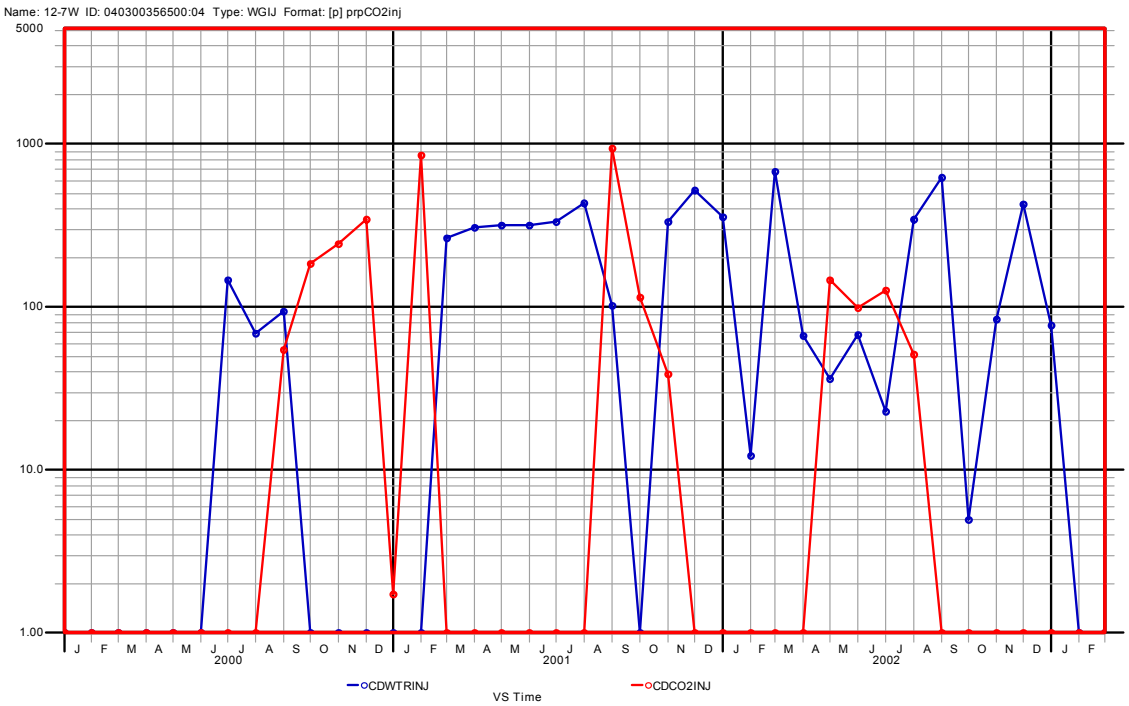

Figure 3.1-3. Injection Plot for CO_2 Injector 12-7W.

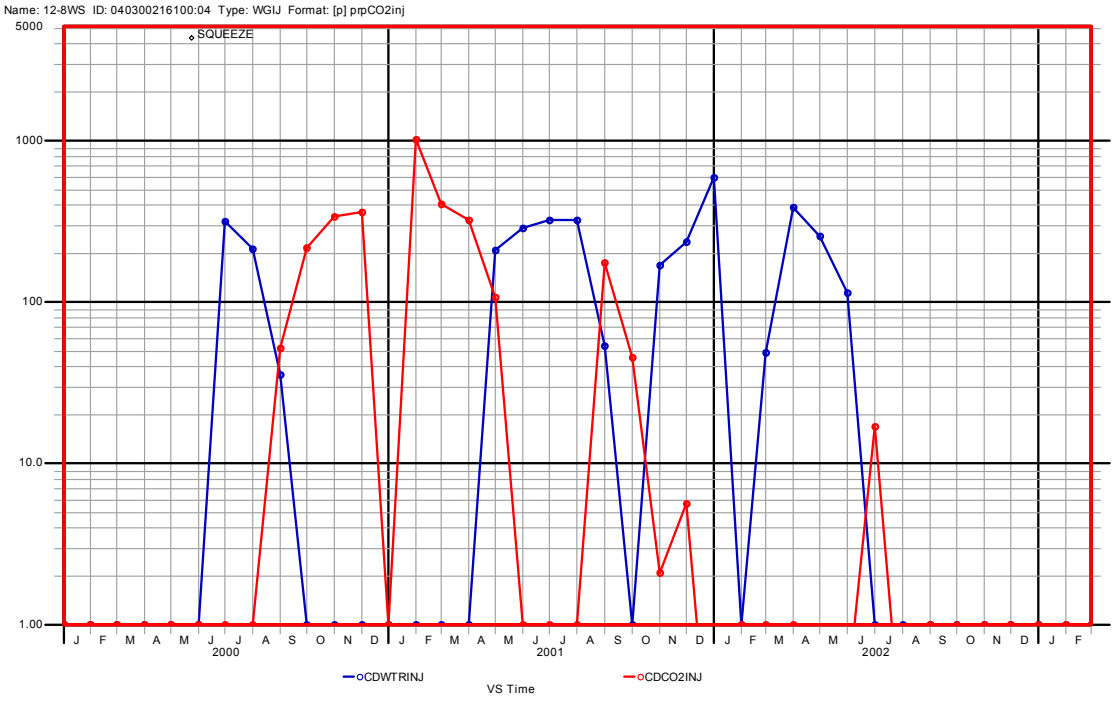

Figure 3.1-4. Injection Plot for CO_2 Injector 12-8W.

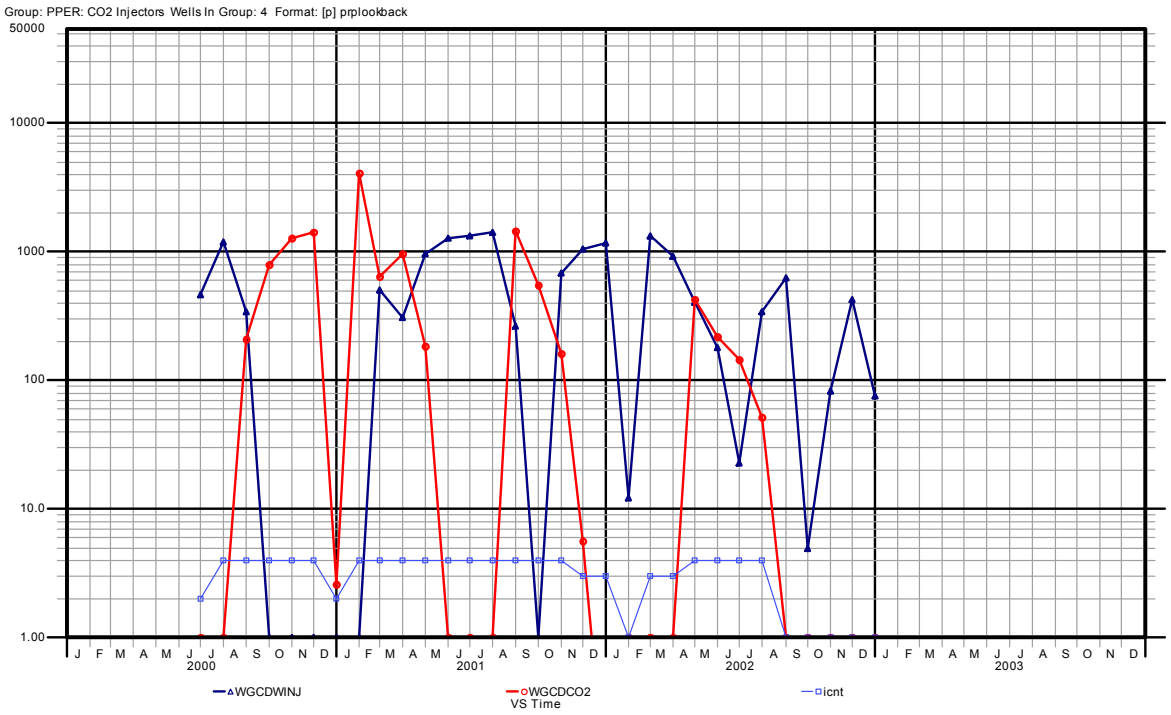

Figure 3.1-5. Total Injection Plot for CO_2 Pilot.

3.2 Production Performance:

CO_2 injection commenced on August 31, 2000. CO_2 injection began at 50 MCF/D and was slowly ramped up to the target rate of 500 MSCF/D per injector to prevent any premature CO_2 breakthrough. For several months nothing significant was observed until we started to see an oil response in mid-November 2000 in well 11-8E (see Figure 3.2-1). Unfortunately, at approximately the same time we began experiencing sanding problems and pilot production subsequently declined. Eventually four producers had to be shut-in due to extensive sanding. Figure 3.2-2 shows the five problem producers. Note that 4 out of the 5 wells are in hydraulic fracture azimuth alignment.

At first, it was assumed that most of the problems were due to subsidence related casing damage. Remediation programs were developed to correct these problems and CO_2 injection was resumed in early February 2001. Sanding problems continued to be an issue the remainder of 2001 and for most of 2002. In August 2002 the tubing in well 11-8E was severely damaged as shown in Figure 3.2-3. A hole in tubing was apparently created by high velocity sand entering the wellbore through a hole in the casing at 1499 feet. As a result of this tubing failure, CO_2 injection was suspended in all pilot injectors for the rest of the year.

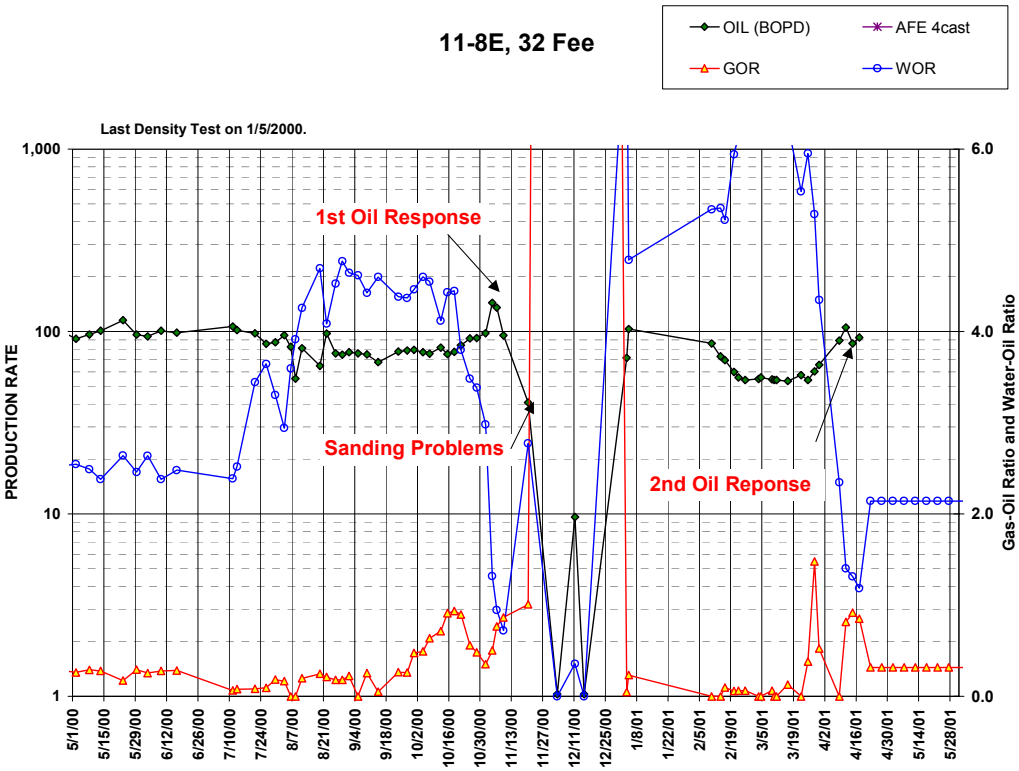

Figure 3.2-1. Production Plot for CO_2 Producer 11-8E, Section 32 Fee.

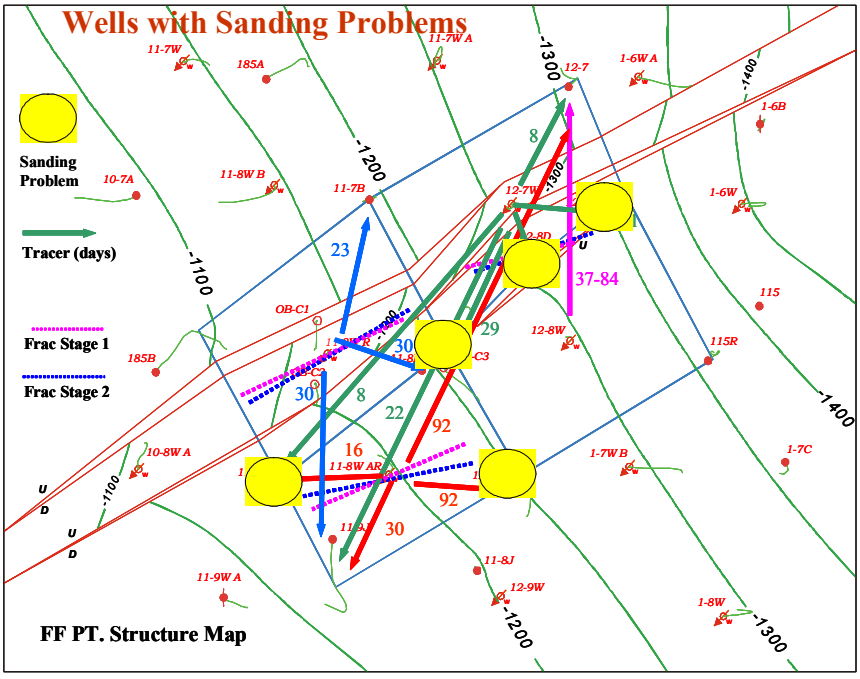

Figure 3.2-2 Map showing pilot producers that have experienced sanding problems. Four of the five problem producers are in hydraulic fracture azimuth alignment.

Table 3.2-1 shows the chronological periods of CO_2 injection and subsequent sanding problems for the project. The pilot project originally contained ten producers in addition to the four pilot injectors. Figures 3.2-1 through 3.2-10 are the individual production plot for the ten pilot producers. Figure 3.2-11 is the production plot for well 12-8E, which replaced pilot producer 12-8B. Well 12-8B had to be abandoned due to excessive sand damage.

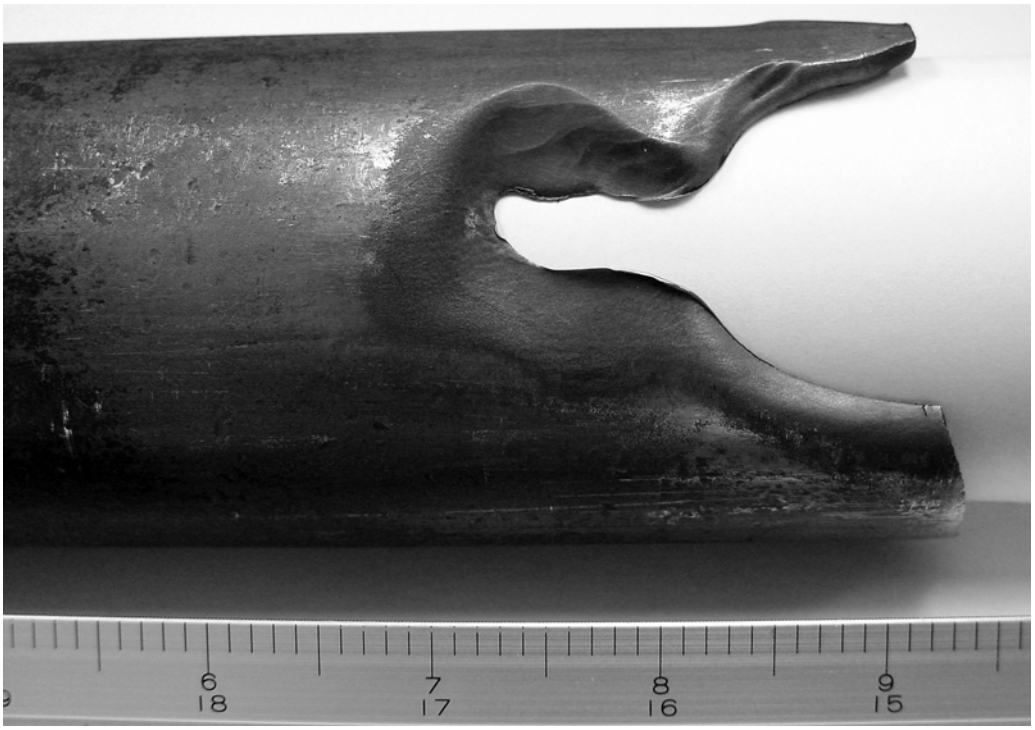

Figure 3.2-3 Tubing retrieved from pilot producer 11-8E. Hole in tubing was apparently created by high velocity sand entering the wellbore through a hole in the casing at 1499 feet.

Table 3.2-1. Chronological Periods of Lost Hills CO_2 Injection.

Chronology of Lost Hills CO_2 Pilot Injection			
Period	**Description**	**Time Period**	**Comments**
1	CO_2 Injection	8/31/00 - 12/26/00	
1A	CO_2 Injection Suspended	12/27/00 - 2/26/00	Sanding Problems
2	CO_2 Injection	2/27/01 - 5/7/01	
2A	CO_2 Injection Suspended	5/8/01 - 9/6/01	Sanding Problems
3	CO_2 Injection	9/7/01 - 11/5/01	
3A	CO_2 Injection Suspended	11/6/01 - 5/6/02	Sanding Problems
4	CO_2 Injection	5/7/02 - 7/31/02	
4A	CO_2 Injection Suspended	8/1/02 - Current	Sanding Problems, Cut Tubing

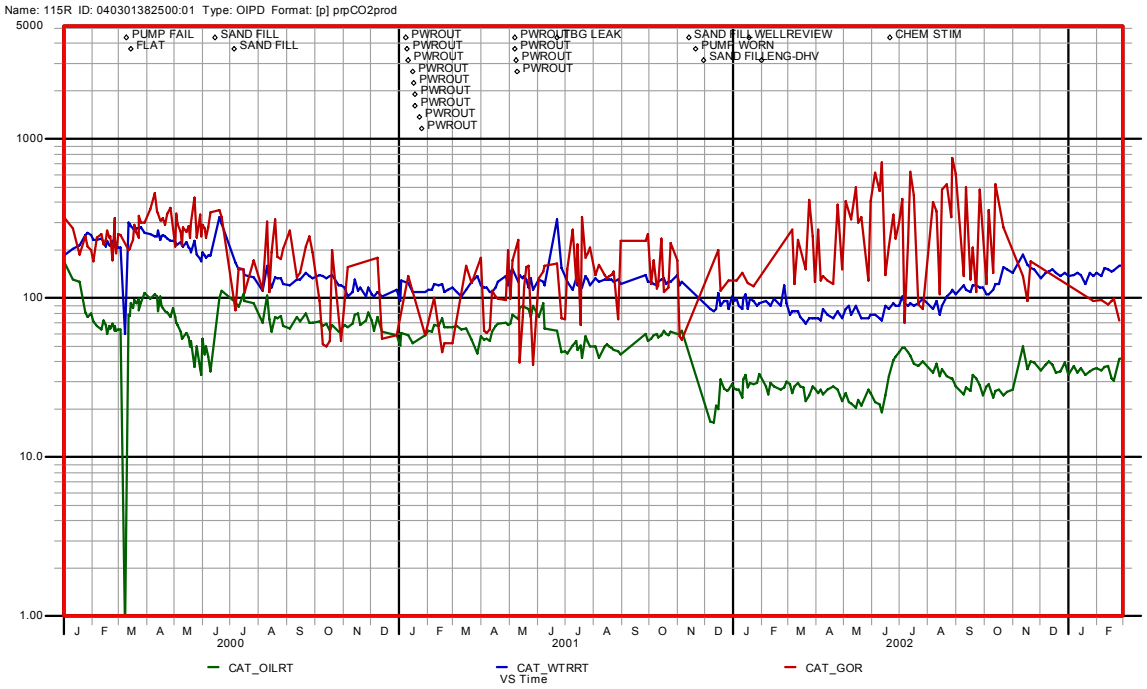

Figure 3.2-4. Production Plot for CO_2 Producer 115R, Section 33.

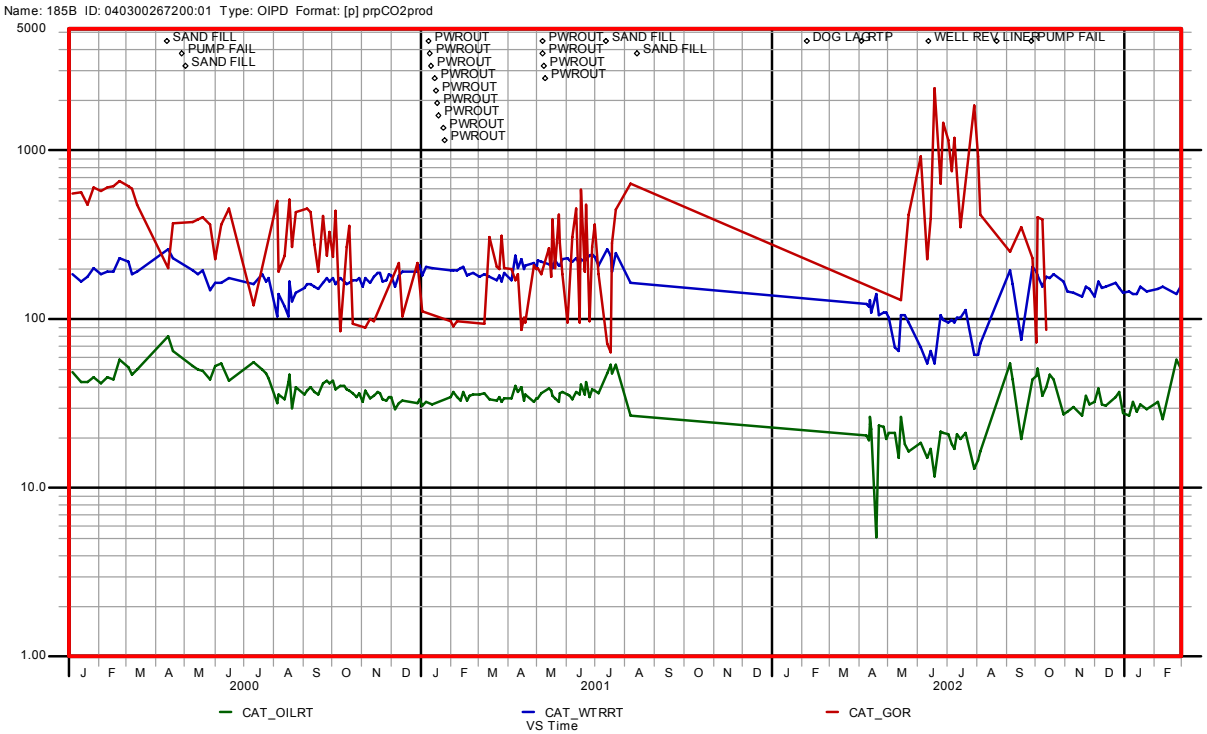

Figure 3.2-5. Production Plot for CO_2 Producer 185B, Section 32 Fee.

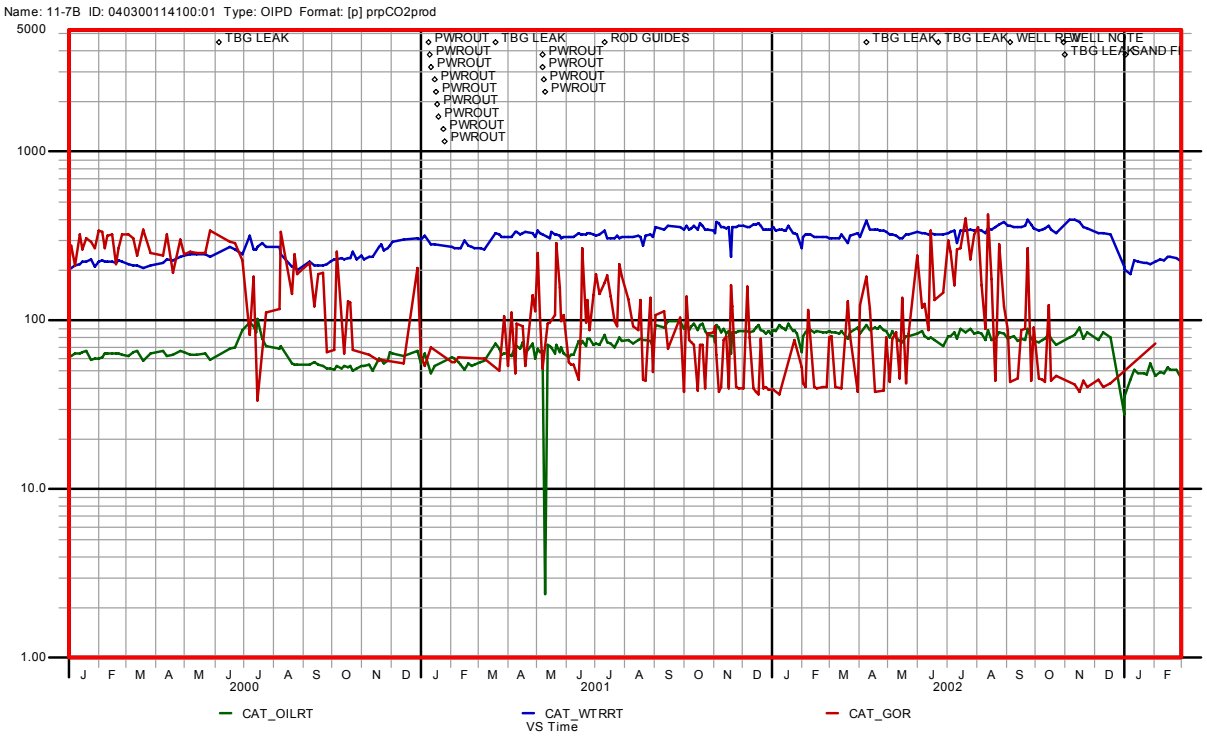

Figure 3.2-6. Production Plot for CO_2 Producer 11-7B, Section 32 Fee.

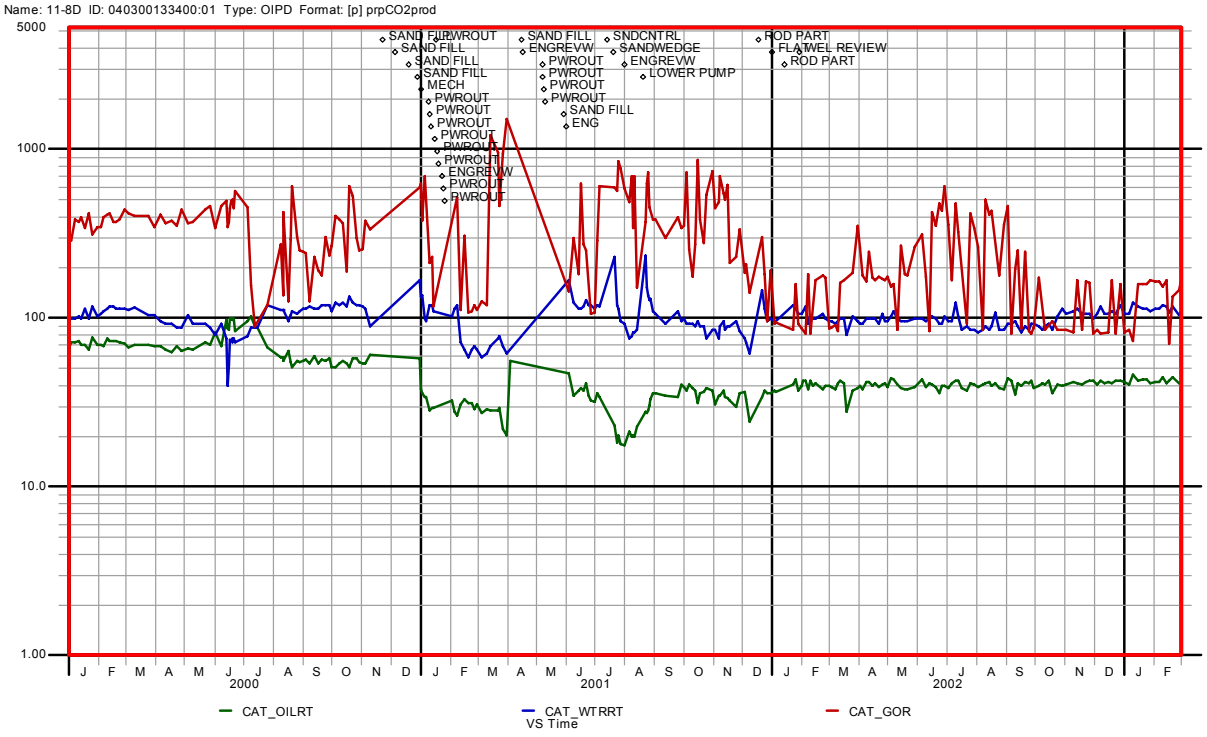

Figure 3.2-7. Production Plot for CO_2 Producer 11-8D, Section 32 Fee.

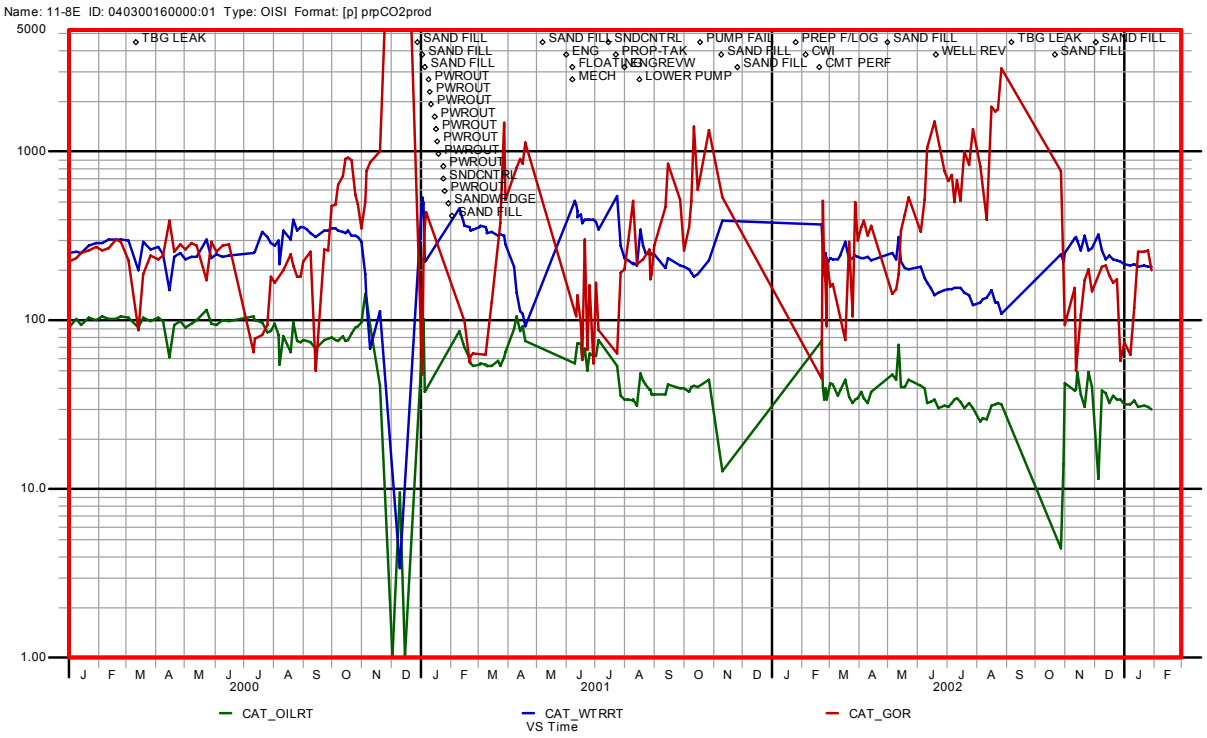

Figure 3.2-8. Production Plot for CO_2 Producer 11-8E, Section 32 Fee.

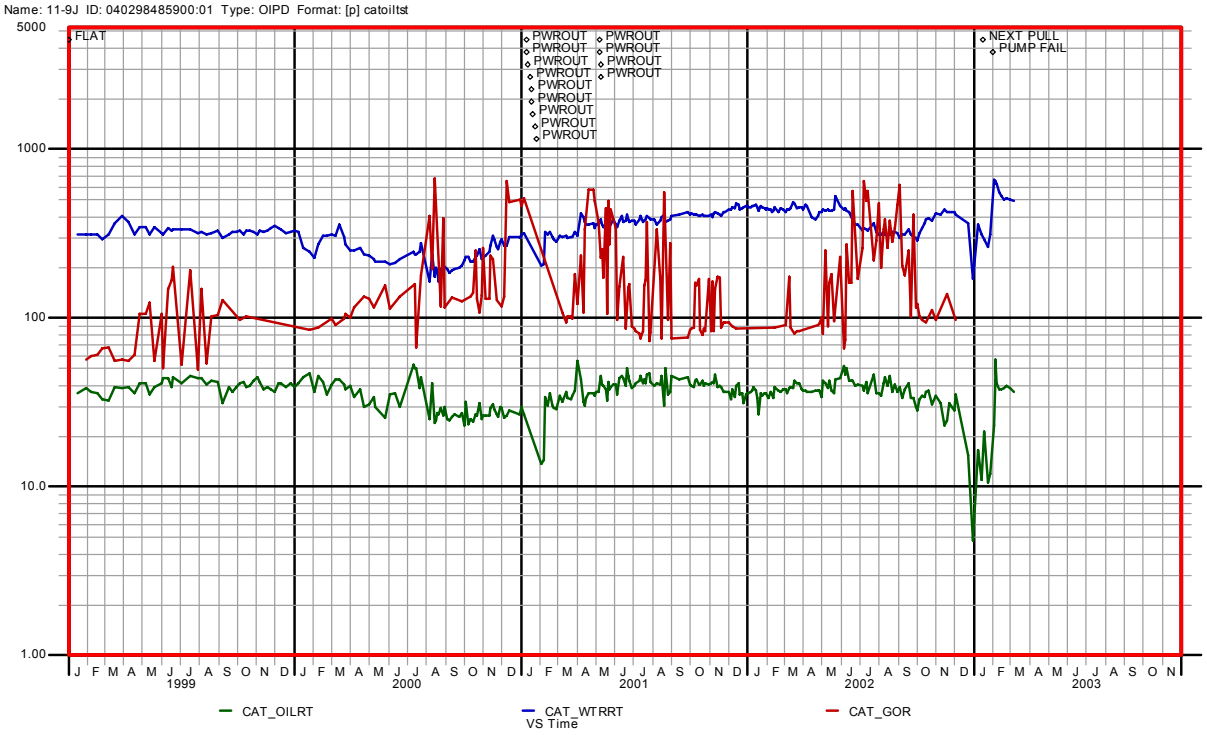

Figure 3.2-9. Production Plot for CO_2 Producer 11-9J, Section 32 Fee.

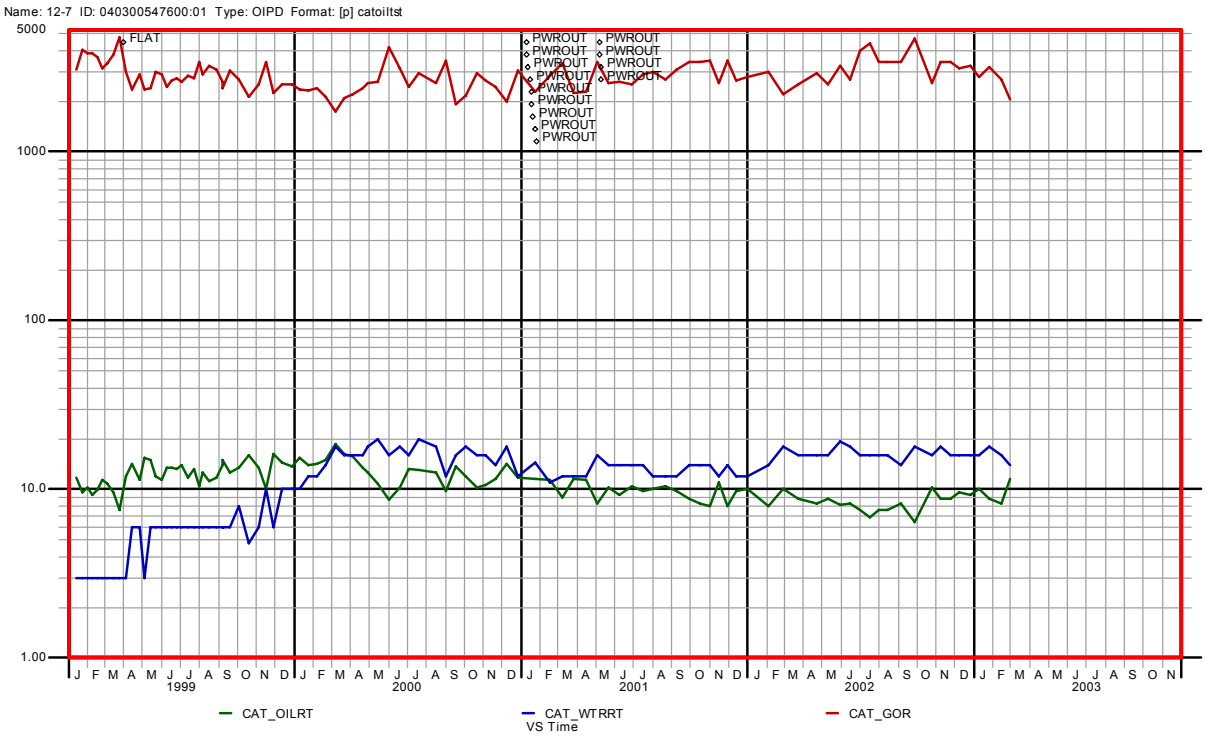

Figure 3.2-10. Production Plot for CO_2 Producer 12-7, Section 32 Fee.

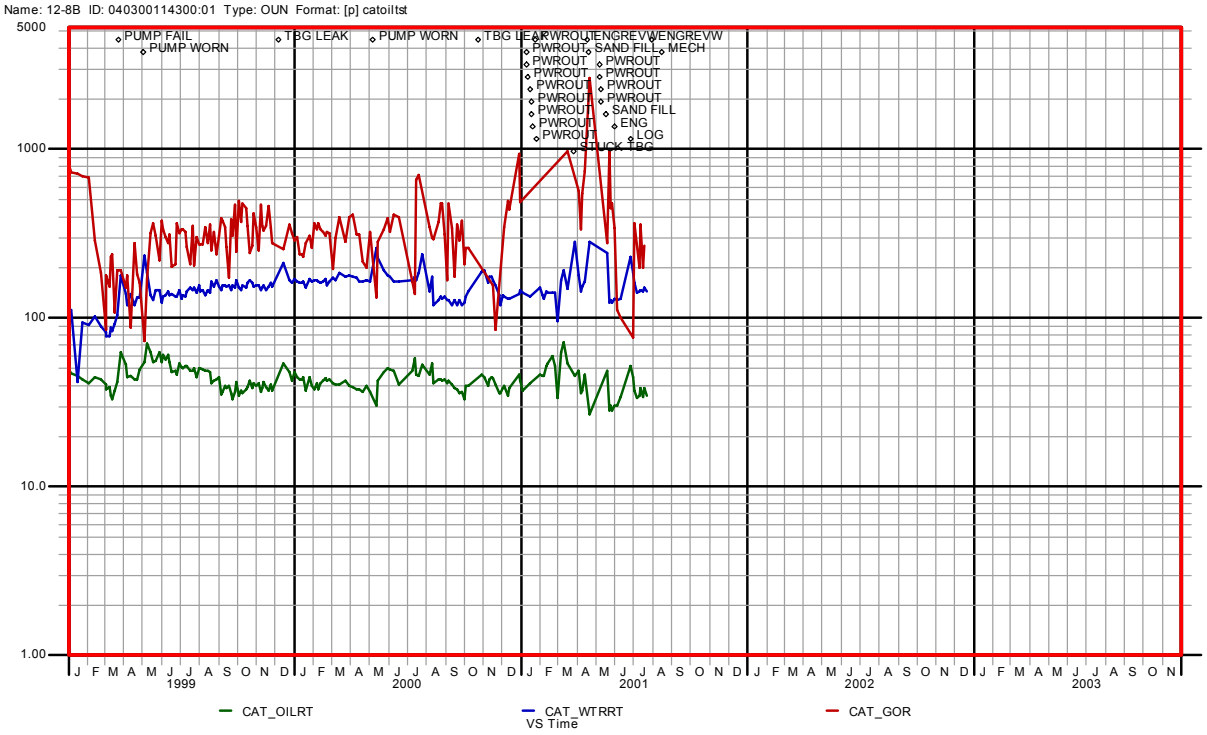

Figure 3.2-11. Production Plot for CO_2 Producer 12-8B, Section 32 Fee.

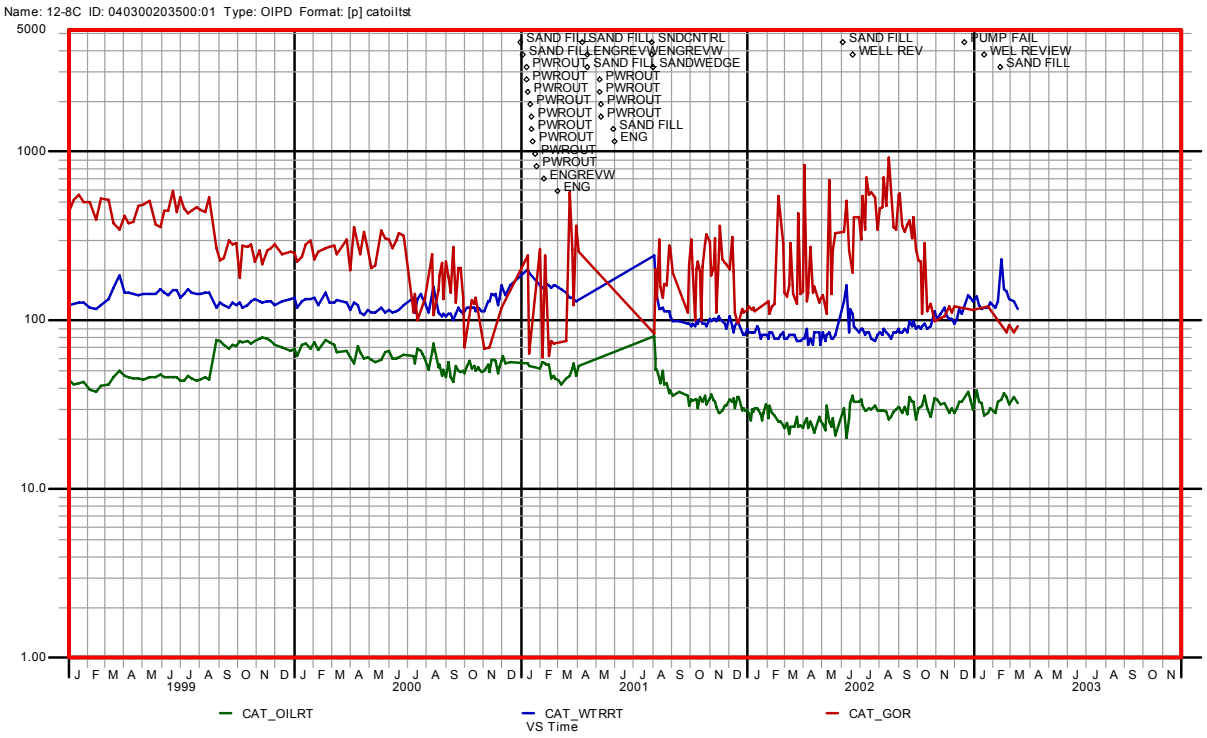

Figure 3.2-12. Production Plot for CO_2 Producer 12-8C, Section 32 Fee.

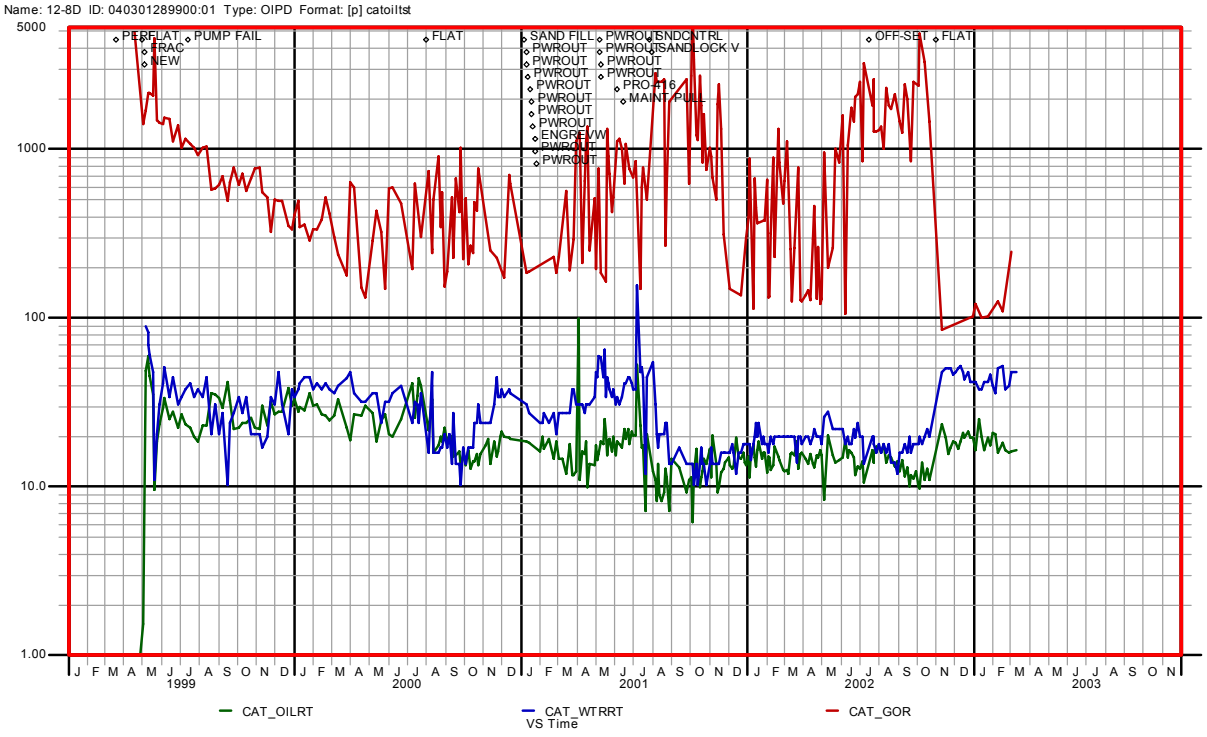

Figure 3.2-13. CO_2 Producer 12-8D, Section 32 Fee.

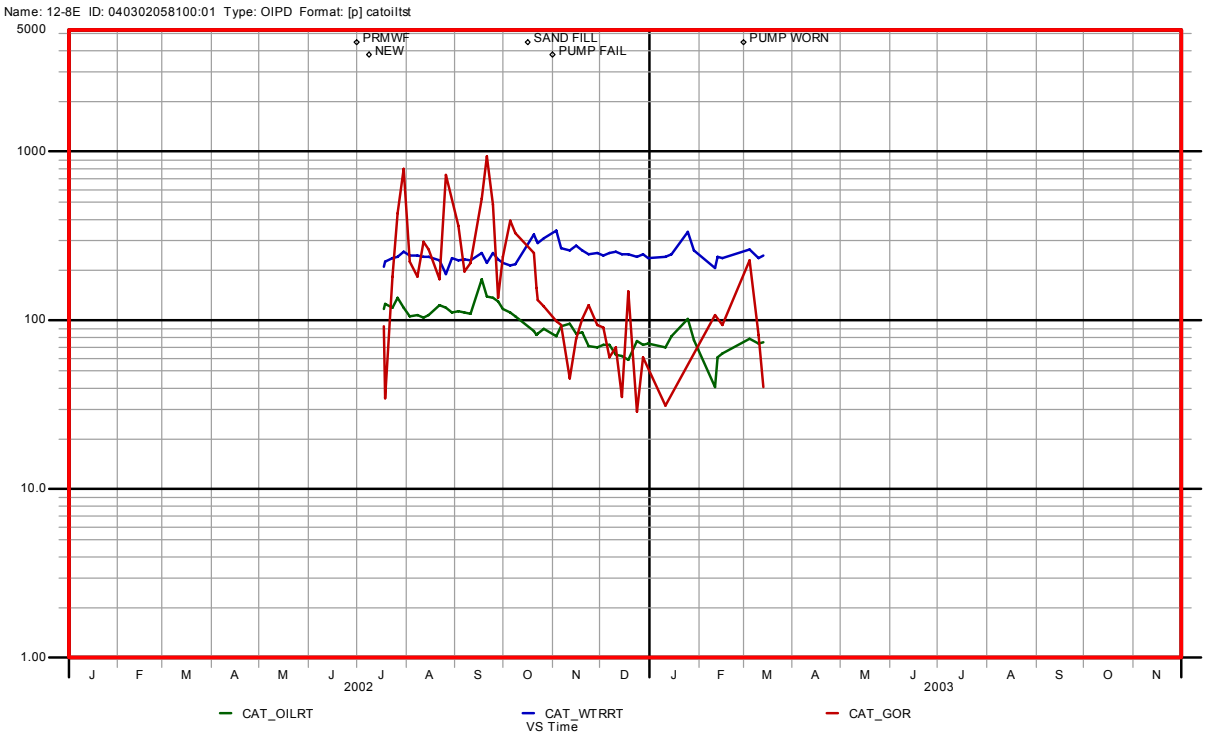

Figure 3.2-14. CO_2 Producer 12-8E, Section 32 Fee (replaces 12-8B).

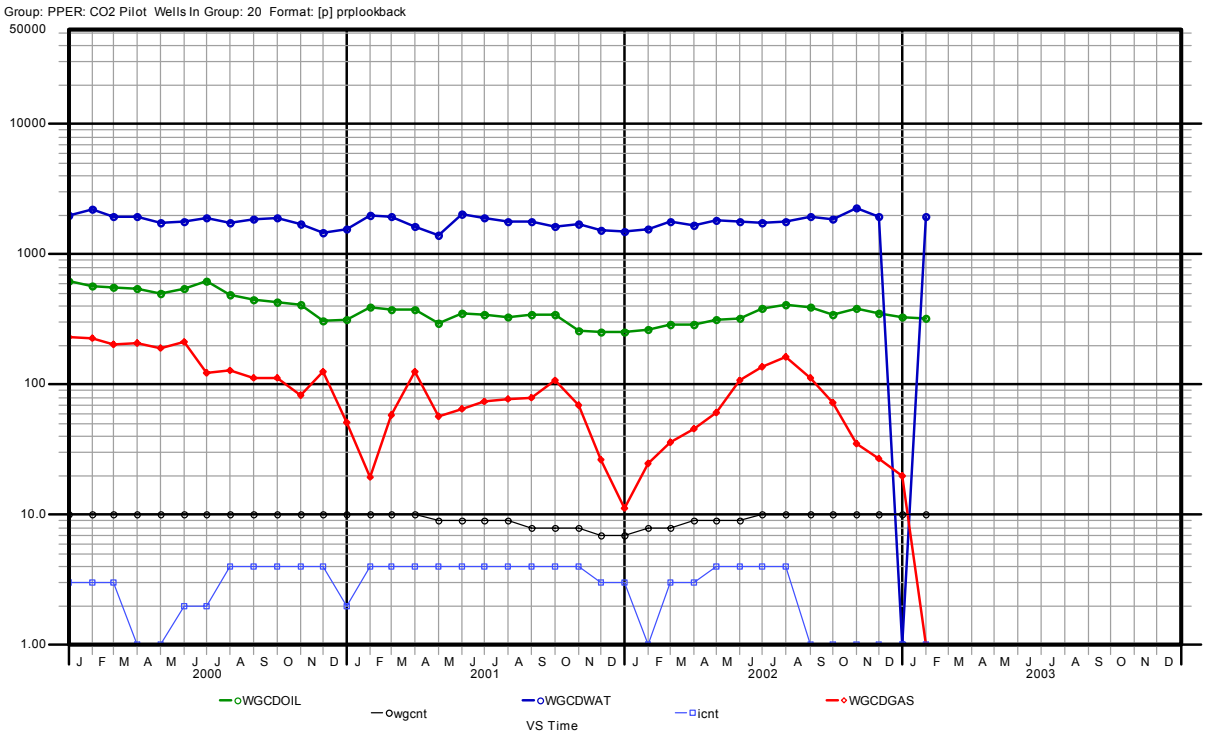

Figure 3.2-15. Total Production Plot for CO_2 Pilot.

Figure 3.2-15 is the total production performance plot for the ten producers since the initiation of CO_2 injection on August 31, 2000. Throughout 2001 and 2002, pilot production was up and down as we struggled to cope with the continuing sand problems. As you can see from the Figure 3.2-15, the CO_2 pilot has not been a technical success. Since initiating CO_2 injection on September 1, 2000, oil production has dropped from approximately 500 B/D to the current rate of 300 B/D. Realize that in September 2000 we had 10 pilot producers and from mid-2001 to mid-2002 we had only 7 wells producing.

Three pilot producers (185B, 12-8B, and 12-8C) had extensive subsidence-related casing damage and had to be repaired or replaced. Since the pilot has been hampered by excessive sanding problems and other subsidence related operational problems, we have not been able to truly evaluate the full potential for CO_2 flooding the Lost Hills diatomite. As it turned out, these operational problems could not be overcome. It was concluded that CO_2 injection played a major role in the sanding problems and that CO_2 flooding was not feasible for the Lost Hills Diatomite. ChevronTexaco management concurred with these conclusions and the pilot was officially terminated on January 30, 2003.

3.3 PILOT OPERATING STRATEGY

John F. Cooney, Pasquale R. Perri
ChevronTexaco Exploration and Production Company

WAG Optimization:
Based on the industry experience with West Texas CO_2 floods, we anticipate having to deal with CO_2 breakthrough. Therefore the operating strategy for the pilot centers around the need to control breakthrough individually for each pattern, on a moments notice.

The following table depicts the planned strategy for dealing with breakthrough:

Table 3.3-1. CO_2 Pilot WAG Operating Strategy.

Injectants	CO_2 / Water Injection Rate	CO_2 Injection Duration	Water Injection Duration	WAG Cycle Times	Synchronize Patterns ? (i.e. same injectant at all times?)
CO_2 Alt. With Water	Start with low of 100 mscfd per well and work up to 500 mscfd max.	Inject until breakthrough is detected (breakthrough defined by detection of tracer gases in one producer)	Either: • Inject until desired HCPVSI is achieved. or • If there is a production kick, "ride it out".	Continue with cycles until desired cumulative HCPVSI is achieved.	Control patterns individually. Some may be under CO_2 injection while others under water injection

By applying the above strategies, we hope to arrive at the optimal process for controlling CO_2 breakthrough while monitoring for an oil kick. As noted before, the above strategies will be tested before facilities to handle high CO_2 are installed. We are risking shutting down injection for a while but it reduces the capital investment risked up-front. If the cumulative CO_2 percentage for the area of the pilot stays low enough to avoid corrosion, injection will not be stopped to wait on facilities.

We eventually went to two week WAG cycles but this did not prevent the sanding problems.

SECTION 4
PILOT SIMULATION

4.1 PRE-PILOT RESERVOIR SIMULATION

William S. Fong
ChevronTexaco Exploration and Production Company

Simulation Model – History Match:
This section discusses the results of history matching the past 50 years of production in the CO_2 pilot area. Wells that started producing in the 1950's were non-hydraulically fractured wells. These wells produced until the late 1980's. From 1989 to present day, new hydraulically fractured wells, each year, have been put on production. Water injection also was initiated in the early 1990's. The history match was therefore made in two stages:

1. **Primary production match** with no hydraulic fractures in the model from 1949 - 1991.
2. **Waterflood match** in which all new wells are hydraulically fractured from 1991 - 1999.

To model hydraulic fractures, thin planes of cells were added to the simulation grid as shown in Figure 4.1-1.

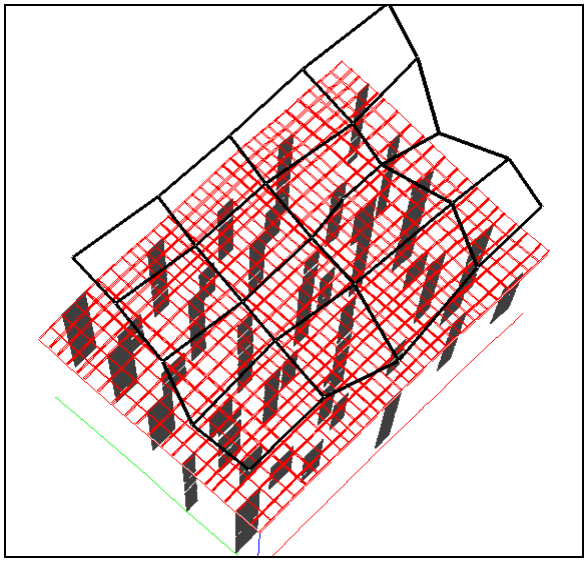

Figure 4.1-1. 16 pattern model showing hydraulic fractures. The CO_2 Pilot is encompassed by the center 4 patterns.

Primary Production History Match:
The result of the primary, or non-hydraulic fracturing, stage history match is considered satisfactory. Figures 4.1-2 and 4.1-3 are comparison plots of oil production and GOR history (lines) compared to simulation results (squares). By 1992, some water injection has already taken place, resulting in a decrease in GOR.

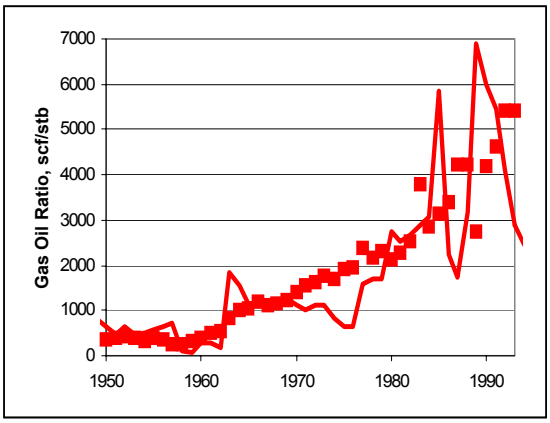

Figure 4.1-2. Cumulative oil match–primary.

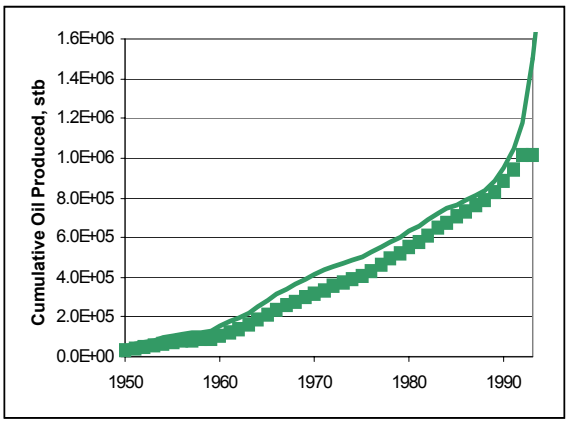

Figure 4.1-3. Gas-oil ratio match–primary.

Waterflood History Match:

The pressure, oil bubble point and saturations of the primary, or non-hydraulic fracturing, model at timestep 1991 was output to construct a model with hydraulic fractures at the newer wells for the waterflood history match. All the adjustments in the primary model were carried over to this model. We assumed all the wells that were put on production after 1991 are all hydraulically fractured at 1991 in the model. The history match was then continued.

Initially, due to the numerous hydraulic fractures in the model, the model ran very slow. A few adjustments were made, including (a) a reduction in fracture permeability from 1000 md to 250 md, and (b) a test a case in which the hydraulic fractures in the outer boundary of the 16-pattern model were inactive. The results were very satisfactory. Simulation run time was reduced to less than 1.5 cpu days. When the hydraulic fractures on the outer boundary were taken out, the model ran in 14 cpu hours.

Results from the following two cases are discussed here:

1. All the hydraulic fractures are retained (all_t6 case).
2. Hydraulic fractures in the outer boundary of the 16-pattern model are inactive (fhm5 case).

Figure 3.4-4 shows the oil production match for both cases. For both of the above models, the predicted oil matches historical production until later times (1996 – 2000) when the predicted oil is lower than actual oil production. This is because the model boundary patterns do not get enough pressure support, especially in the "fhm5" case, where the hydraulic fractures are inactive. The water-oil ratio (WOR) and gas-oil ratio (GOR) matches are shown in Figures 4.1-5 and 4.1-6, respectively, and are reasonably close.

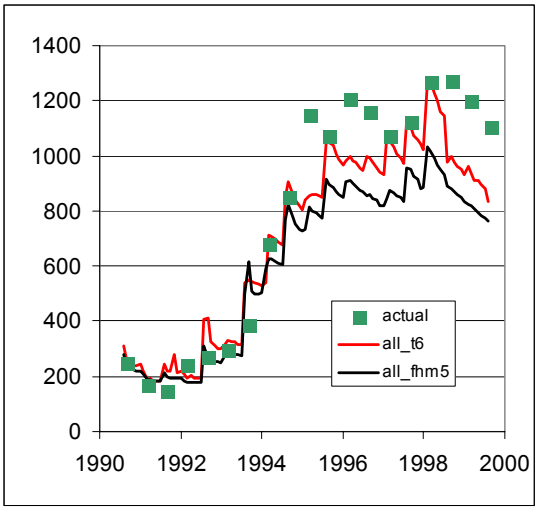

Fig. 4.1-4. Oil rate (bbl/d) match–waterflood.

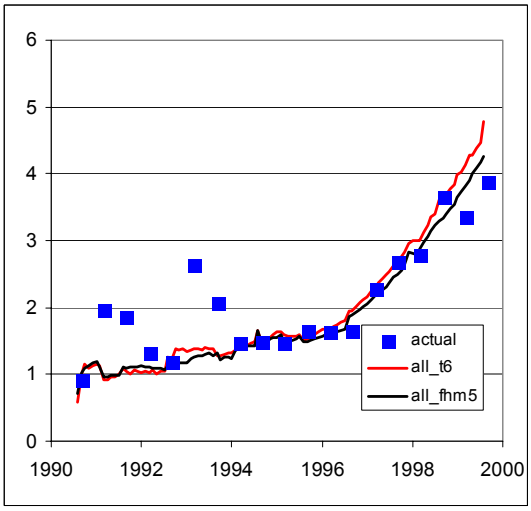

Figure 4.1-5. WOR (bbl/bbl) ratio match–waterflood.

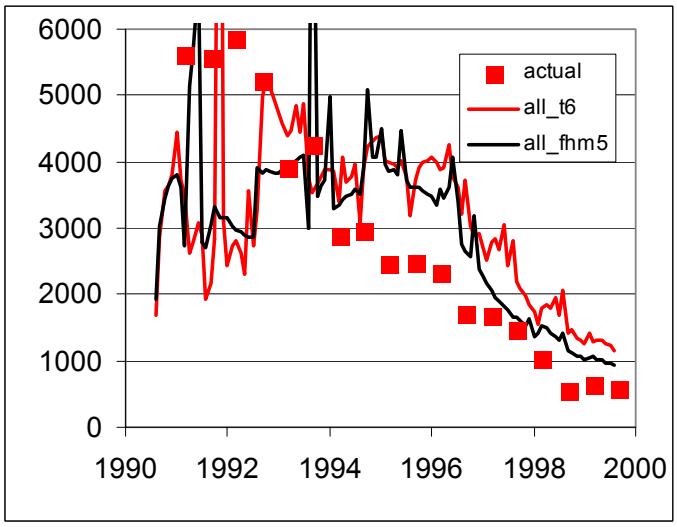

Figure 4.1-6. GOR (scf/stb) ratio match–waterflood.

The purpose of modeling sixteen patterns is to make sure the center four patterns (CO_2 pilot area) have accurate boundary conditions for the CO_2 simulation predictive runs. If we just plot the history match for the center four patterns only, then the quality of match improves, as shown in Figures 4.1-7 to 4.1-9. The oil history match (Figure 4.1-7) and the water production history match (Figure 4.1-8) are very good. However, the simulated GOR (Figure 4.1-9) still does not decrease as fast as the actual GOR. This could be due to the fact that all hydraulic fractures were turned on at the beginning of simulation in 1991, while in actuality, a number of new wells are added and fractured through 1994.

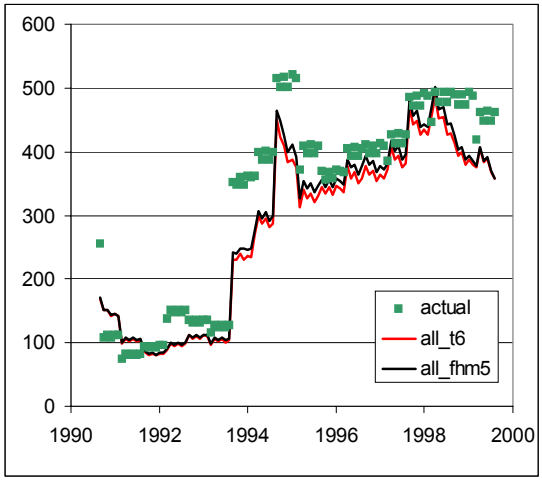

Fig. 4.1-7. Oil rate (bbl/d) match – center 4 patterns waterflood.

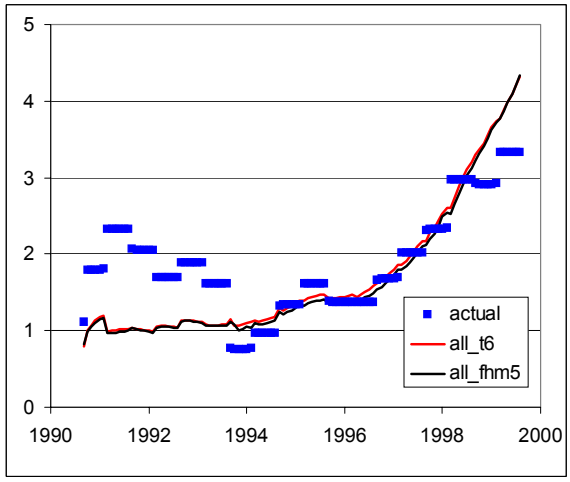

Figure 4.1-8. WOR (bbl/bbl) ratio - center 4 patterns waterflood.

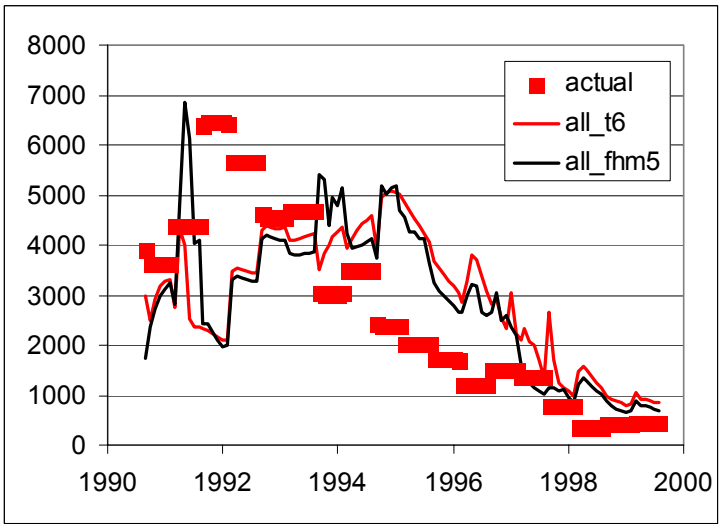

Figure 4.1-9. GOR (scf/stb) ratio match – center 4 patterns waterflood.

Figure 4.1-10 shows the changes in water saturation since initiating the waterflood in 1991. Figure 4.1-11 shows current pressure support due to waterflooding. The diamond symbols are cumulative water injection into each pattern. Figure 4.1-12 shows swept oil ellipsoids from each injector. Our next simulation step is to output pressure and saturation information from the waterflood run to a compositional version of the same model for subsequent CO_2 pilot history matching and CO_2 injection prediction runs.

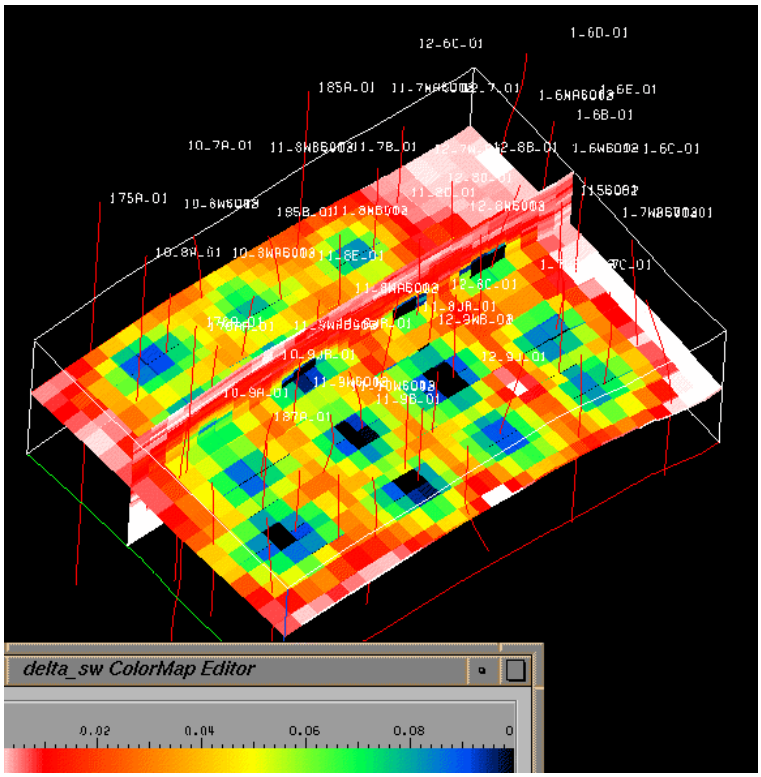

Figure 4.1-10. Change in water saturation from 1991 to 2000.

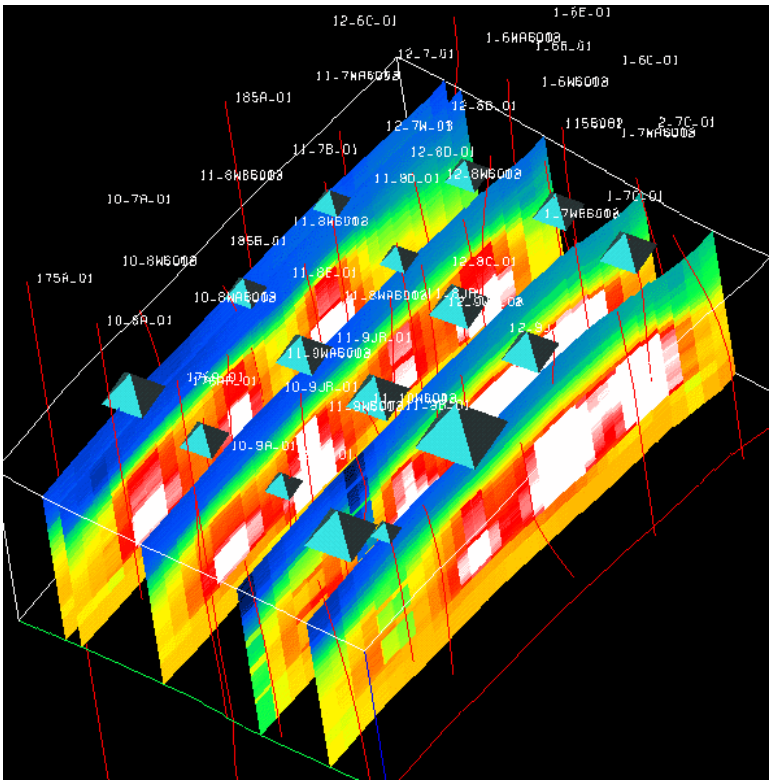

Figure 4.1-11. Current reservoir pressure showing waterflood support.

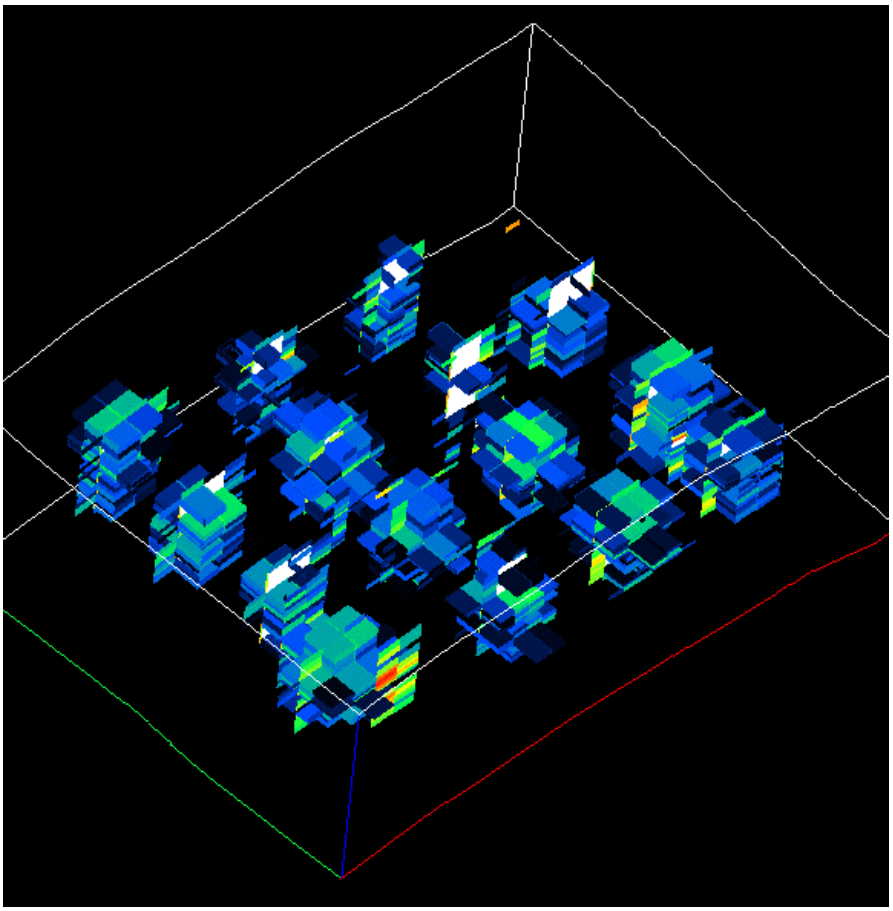

Figure 4.1-12. Decrease in oil saturation from 1991 to 2000. Showing sells with changes from 0.07 – 0.15.

4.2 POST-PILOT RESERVOIR SIMULATION

Dengen Zhou and Irene Gullapalli
ChevronTexaco Exploration and Production Technology Company

Summary:
Compositional simulations were conducted on a ¼ 5-spot sector model for understanding the performance of Lost Hills CO_2 pilot. The sector model was first calibrated by matching the average waterflood behavior in the pilot area and by honoring the tracer test and produced water salinity data. The tracer and salinity survey data suggest the producers are highly connected with the injectors. We employ high flow channels between injector and producer in our model. Simulations show that the existence of higher flow channels in the reservoir play an adverse role on the performance of Lost Hills CO_2 pilot. Most of injected CO_2 flows through the high flow channels and only a small portion of the injected CO_2 invades the reservoir formation. Because of low viscosity, CO_2 prefers the high permeability zones, which has been waterflooded before the WAG started. The combination of the high flow channels and the poor sweep efficiency contributes to the poor performance observed in the pilot.

Introduction:
Lost Hills field, located in the southern San Joaquin basin in California was discovered in 1910. There are over 2.6 billion barrels of oil at relatively shallow levels of an average depth of 2000 ft (Perri, et al. 2000). Early production was developed using slotted liner completion until the late 70's. From the late 70's to present hydro-fracture completions have been performed. By the end of 1999, only 135 million barrels (~5% of OOIP) have been produced. In 1992, Chevron began a waterflood project, which result in a significant production increase, and it is anticipated that an addition of 50-100 million barrels can be recovered by waterflooding. However, even including the potential waterflood reserves, the recovery efficiency only approaches 7 to 9% of the OOIP.

The low recovery of the Lost Hills field is mainly due to its unique reservoir properties: high porosity (>50%) and low matrix permeability (<1 mD). The large amount of remaining oil in place makes Lost Hills a large resource for enhanced oil recovery. Immiscible CO_2 injection could be the key to unlock this vast reserve because of higher injectivity and relative high solubility of CO_2 in oil.

Fong et al. (1992) conducted a number of coreflood experiments and numerical simulations to show the feasibility of CO_2 injection in lost Hills. They found that substantial amount of oil can be recovered by immiscible CO_2 with improved injectivity comparing with waterflood. In 1999 a CO_2 injection pilot project was implemented in Lost Hills (Perri et al. 2000). However, the observed CO_2 pilot performance is significantly different from the original design. What has caused the large discrepancy between the original design and the observed performance? Two possibilities exist: (1) the original simulations were not representative of the reservoir; and (2) the implementation of the pilot was not optimized. In this study, we re-examined the

simulation parameters and the reservoir model to identify the causes for the observed field performance. The relative permeability data were determined from unsteady state coreflood experiments. We then present more details of the reservoir model to be used in this study. The major difference of the reservoir model used in this study from previous ones is that the current geological model honors the tracer and salinity data, which were not available in previous studies. Finally we present the compositional simulation results. Our simulations suggest that there are directly linkages between the injectors and the producers in Lost Hills diatomite. The direct linkages channel CO_2 from producers to injectors, resulting poor CO_2 sweep efficiency in the matrix.

CO_2 Pilot Performance:

The CO_2 pilot consists of four inverted 5-spot patterns covering approximately 10 acres, and is located in a portion of the field, which has been under waterflood since 1992. A CO_2 pilot was chosen, rather than full field implementation, to investigate uncertainties associated with CO_2 utilization rates, CO_2 breakthrough and other operational issues. Actual CO_2 injection began on August 31, 2000.

CO_2 injection began at 50 MCF/D per injector and was slowly increased to the target rate of 500 MCF/D per injector. An initial oil response was observed in well 11-8E (see Figure 4.2-1). However, the initial response in well 11-8E was curtailed due to sanding problems. The breakthrough time for well 11-8E is about two months. The gas production rate jumped from about 20 mcf/D to 80 mcf/D. The sanding problem forced us to shut down the production. WAG was started (2 weeks of CO_2 and 2 weeks of water) to medicate the sanding problem. Although WAG somehow slowed down the sanding, the producers were shut in periodically for cleaning up.

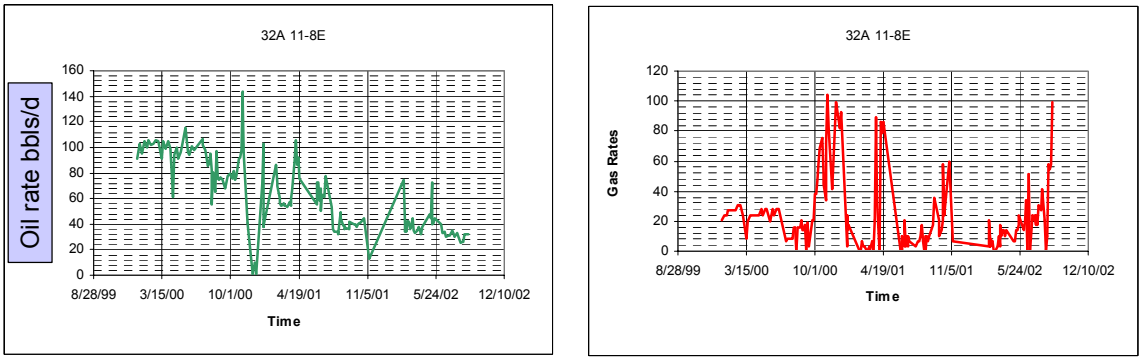

Figure 4.2-1. Oil and Gas response from well 11-8E to CO_2 injection. CO_2 injection began on August 31, 2000. The breakthrough time is about 2 months.

Oil response was also observed in well 11-9J, to a smaller degree, as shown in Figure 4.2-2. The oil rates from most of the wells in the pilot area, like 11-9J, were either insensitive or slightly decrease as CO_2 WAG proceeded. Because of the complex operation resulted from the sanding problem, it would not be very meaningful to history

match individual wells. In our simulation we aimed at reproducing the average behavior of the pilot.

As we will shown through simulations, CO_2 tends to flow through high permeability fracture networks. Only limited amount of CO_2 invades the reservoir formation (the upper part of the formation).

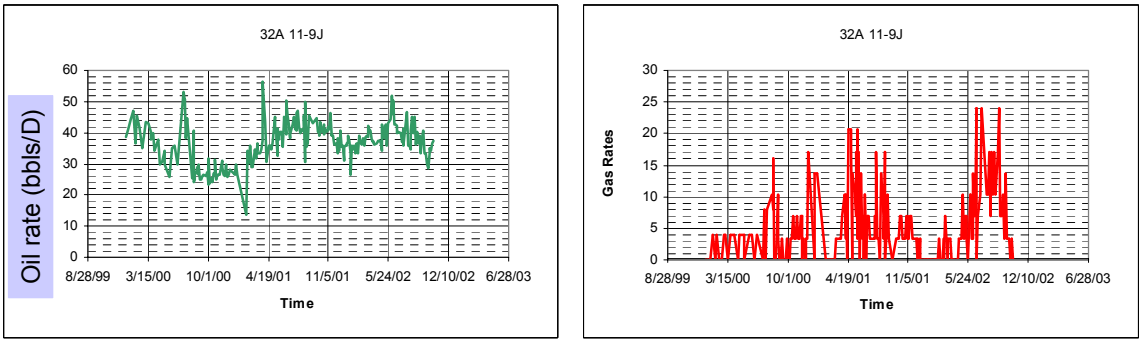

Figure 4.2-2. Oil and gas response of well 11-9J to CO_2. injection. The oil response lasts for very short period of time. The overall oil rate does not response to CO_2 injection.

Rock Properties:

For the last ten years, there have been a number of studies for determining waterflood parameters for simulation purposes. We conducted a series of coreflood experiments to check the consistence of the previous measurements and to generate new data sets. We conducted water, methane and CO_2 floods on the same set of cores to benchmark the relative displacement efficiencies of waterflood and CO_2 injection. Comparison of methane and CO_2 performance can help us identify the relative contributions of different recovery mechanisms involved in CO_2 injection. History match simulations were conducted to examine the consistence of water/oil and gas/oil relative permeability curves. Using the same set of water/oil and gas/oil relative permeability, we matched all three (water, methane and CO_2) flood experiments.

Water/Oil Relative Permeabilities:

In Figure 4.2-3 are the resulted water/oil relative permeability and the corresponding fractional flow curves. The water/oil relative permeability curves indicate that the reservoir is water-wet, with low water relative permeability end-point. The oil relative permeability decreases quickly as water saturation increases. CT-scanning suggests that diatomite is highly laminated at core scale (see Figure 4.2-4). Because of the core-scale lamination, water flows into the higher permeability layers first, which leads to quick reduction in oil permeability.

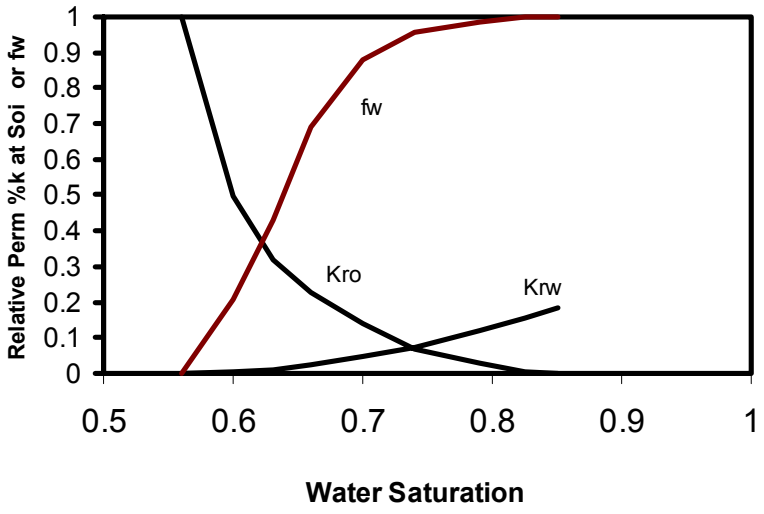

Figure 4.2-3. The calculated relative permeability curves and the corresponding water fractional flow curve at reservoir conditions. The oil relative permeability decreases dramatically as water saturation increases, while water relative permeability is almost linearly increasing as water saturation increases.

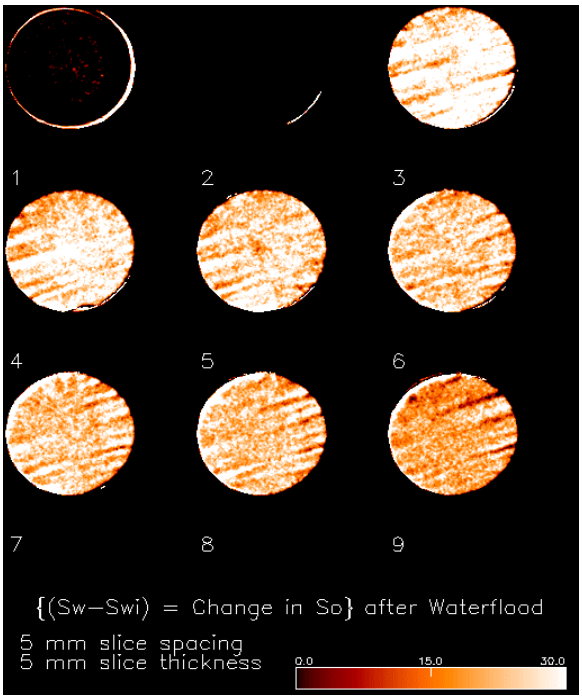

Figure 4.2-4. Examples of water saturation changes at the end of the waterflood. It is clear that the core is heterogeneous (mostly fine scale lamination). Water preferentially flows through some layers, resulting in low displacement efficiency.

Oil/Gas relative Permeabilities:

We performed water, methane and CO_2 floods on the same set of cores. The displacement data were then history-matched by conducting detailed compositional simulations. Both oil production and pressure history data were matched all experiments with one set of water/oil and gas/oil relative permeability curves, suggesting the compositional model used here is representative of the oil recovery mechanisms occurred in the cores.

The gas relative permeability is well defined, because we can determine the end-points of the gas relative permeability curve using the pressure drops and injection rates at the end of the experiments. The resulted gas/oil relative permeability curves are shown in Figure 4.2-5.

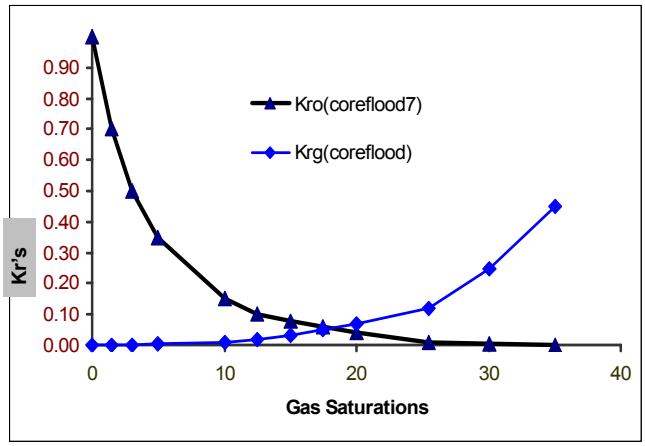

Figure 4.2-5. The gas/oil relative permeability curves determined from coreflood experiments. Oil relative permeability decreases quickly as gas saturation increases, which is consistent with data from laminated systems.

Reservoir Model:
Because of the close well-spacing in Lost Hills, extensive data are available for characterizing Lost Hills diatomite formation. A full field geological was built in 1997 to integrate geological information, well and SCAL data. We cut a ¼ of five-spot sector model from the full-field model for simulating the CO_2 injection process. Before simulating the CO_2 pilot, we first calibrate the geological model to reflect the average behavior of the waterflood performance and to honor other field observations.

Major Field Observations:
Significant effort has been made to characterize the fluid transport in the reservoir, including tracer tests, produced water salinity monitoring, and cross-well electromagnetic (EM) imaging. Principal observations are:

1. Water production rate responds very quickly to changes in water injection rate;
2. Oil production rates are relatively constant (on an average of 50 bbls/day/well) even after 0.3 HCPV water injected;

3. Oil production rates are independent of the water production rates;
4. Tracer tests show that an injector can have "short-circuits" with several producers, and that the most direct connections can be with wells farther away from the injector;
5. Salinity monitoring indicates that these "short-circuits" are a common feature in the waterflood area;
6. Cross-well EM images shows water invades the formation slowly with diffusive fronts.

To accurately represent what happens in the reservoir, we need to develop a reservoir model that can reproduce these observations. Thus, we need to calibrate the reservoir model with the field observations.

Calibrating the Reservoir Model:

We cut a sector model, which is slightly larger than a ¼ well pattern in the center of the waterflood area as show in Figure 4.2-6. The model dimensions are 204 x 204 x 500 ft with 32 x 34 x 41 grids. The diatomite formation has very small vertical permeability and long horizontal correlation lengths. In the field both injectors and producers are hydraulically fractured to obtain reasonable production/injection rates. However the dimensions of the fractures are not well defined because of the complex stress field. Thus, we need to consider the injection and production fracture lengths (Hp and Hi) as sensitivity parameters (see Figure 4.2-3)

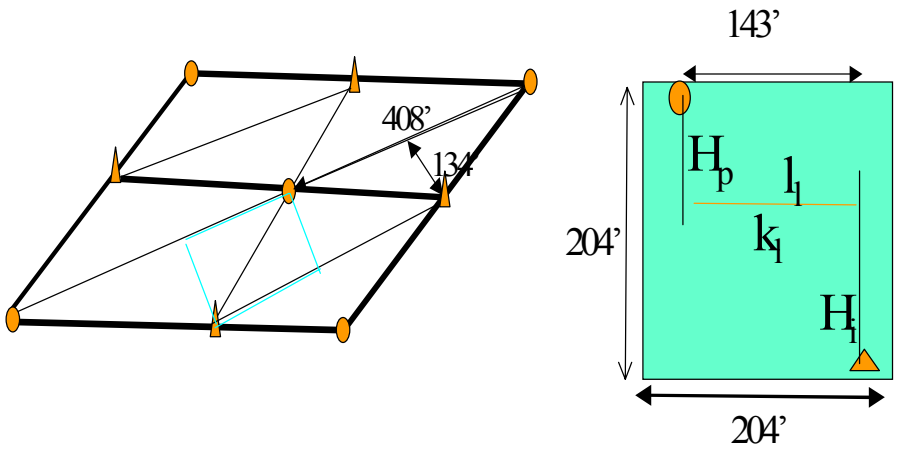

Figure 4.2-6. Lost Hills waterflood well patterns and the sector model dimensions.

Tracer tests and salinity survey data suggests that the producers and injectors are highly connected. In order to build this mechanism in the reservoir model we employ linkages (high permeability grids connecting the producer and injector) between the injection and production fractures. The length and the conductivity of the high permeability linkages are considered as sensitivity parameters. In Table 1 we listed the sensitivity parameters

and their ranges for calibrating the reservoir model. The bold numbers are values that can reproduce the field observations. It is clear that direct linkages are necessary to honor all field observations. Figure 4.2-7 compares the field average oil production rates with simulations. The same model also matches the tracer breakthrough time (Figure 4.2-8).

Table 4.2-1. Sensitivity parameters and their ranges.

H_p (ft)	0	**51**	**102**	153	204
H_i (ft)	0	51	**102**	**153**	**204**
L_l (ft)	0	36	72	107	**143**
K_l (mD)	10	25	**50**	**100**	200

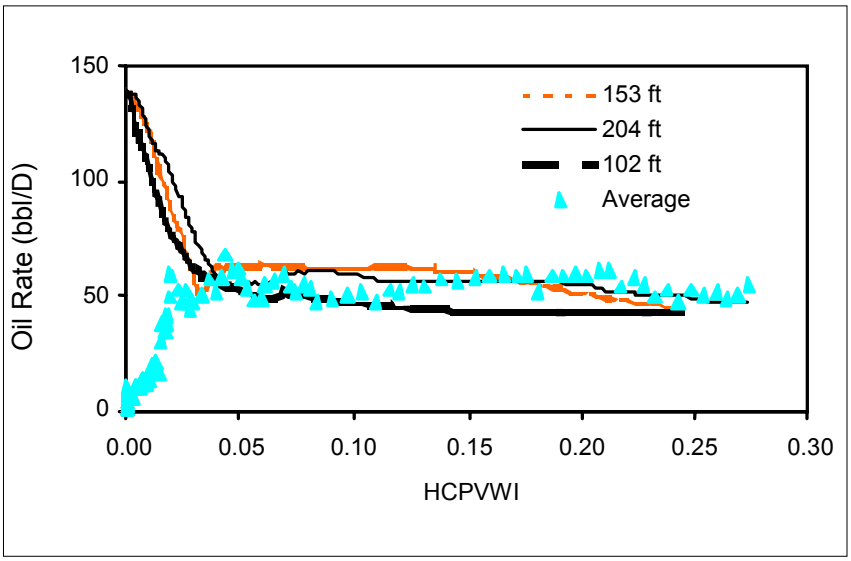

Figure 4.2-7. Simulated oil production rates with different injection fracture lengths (102, 153 and 204 feet).

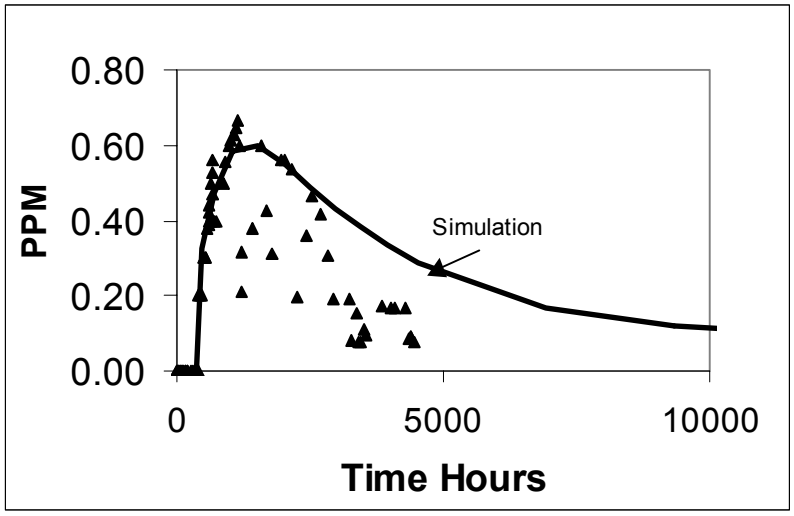

Figure 4.2-8. A comparison of the simulated and measured tracer breakthrough curves.

It is important to point out that the direct linkage between the injector and the producer is necessary for reproducing the tracer and salinity data, which was not included in previous simulation.

CO_2 Flood Simulations:
Once we developed a reservoir model, we try to simulate the CO_2 pilot. In this section, we report the simulation procedures and results.

Simulation Procedures:
The main objective of the simulation study is to understand the CO_2 pilot performance. Because of the complicated operations resulted from sanding problem, it would not be useful to history match the individual well's performance, rather to reproduce the typical behavior of the CO_2 injection process. At beginning CO_2 was injected continuously before sanding occurred. WAG was then implemented to medicate the sanding problem. In our simulations, we used average CO_2 and water rates of all the injectors.

The CO_2 pilot area has been waterflooded since early 1992. To generate similar water/oil saturation and pressure distributions, we first run the model with waterflood for 8 years and then CO_2 and WAG processes.

We employ a 5-component compositional model for simulating the pilot. The compositional model is developed based on live oil PVT measurement and slim tube data. The same characterization was used for the original CO_2 pilot design. Figure 4.2-9 lists the key characterization parameters used in our simulator (*CHEARS*).

```
COMPONENTS
*      NAME      MOL WT
       METHANE     16.0430
       CO2         44.0100
       HYP1        44.7000
       HYP2       151.0710
       HYP3       545.0000
*
OILVISC   LBC5   0.1023000   0.0233640   0.0585330  -0.0410290   0.0082010
GASVISC   LBC5   0.1023000   0.0233640   0.0585330  -0.0407580   0.0093324
*
PARACHOR
       71.0   81.1  121.8  505.2 1634.9
*
EOSPARMS
*      NAME      PC(PSIA)     TC(F)    VC(CUFT/LBMOL)    W          SC        OMEGAA      OMEGAB
       METHANE   667.8010  -116.6260      1.5899      0.0108    -0.1540   0.457240   0.077800
       CO2      1070.6000    87.8720      1.1560      0.2276    -0.2942   0.457240   0.077800
       HYP1      900.0890   130.3530      2.2024      0.1984    -0.2688   0.457240   0.077800
       HYP2      377.8950   711.4500     12.0000      0.4384    -0.0215   0.457240   0.077800
       HYP3      159.1817  1279.0028     40.0000      1.1801     0.0664   0.457240   0.077800
*
BININTCOEF
 0.1000
 0.0800  0.1000
 0.0350  0.1100  0.0800
 0.0500  0.1100  0.0800  0.0000
*
KVALUES  PREOS    200.000   2000.000
```

Figure 4.2-9. Gas/Oil property characterization used for the CO_2 pilot simulations. The same characterization was used for the original design simulations.

Simulation Results:

In order to better understand the simulation results, it is helpful to have a general idea of the permeability and oil saturation distributions in the reservoir. As Figure 3 shows, the reservoir has higher permeability in the upper part of the reservoir (sandy diatomite). We also observe relatively high permeability in the middle of the reservoir, in which oil saturation is also high. Cross-well EM imaging indicates that most of oil saturation changes from waterflood occurred in these zones.

Sensitivity simulations show that about 50% of injected water flows through the high permeability channels and rest of water invades the formation slowly. Figure 4.2-10 illustrates the water distribution after 5 years of water injection. After five years of water injection, water floods most of the upper sandy zones and a small portion of the higher permeability zones with high oil saturation in the middle of the formation. The saturation changes in these zones are relatively higher than that in other zones because of high initial oil saturation. This observation is consistent with what detected by the cross-well EM imaging. The cross-well EM techniques show that oil saturation changes slowly near the injection fracture in these zones. Although simulations indicate water floods the upper sandy zones, cross-well EM may not be able to detect it, because of relatively lower saturation changes.

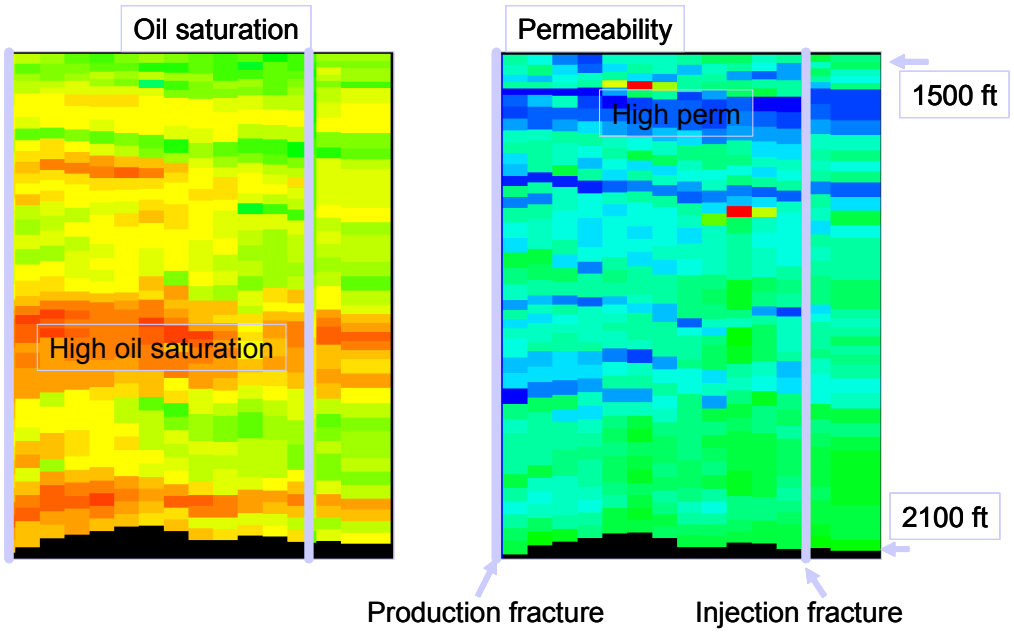

Figure 4.2-9. Vertical permeability and oil saturation distributions in the simulation model. The high oil saturation (red) is located in the lower middle zones, which is also corresponding relatively higher permeability. The top part of the reservoir has high permeability, but relatively low oil saturation because of earlier depletion.

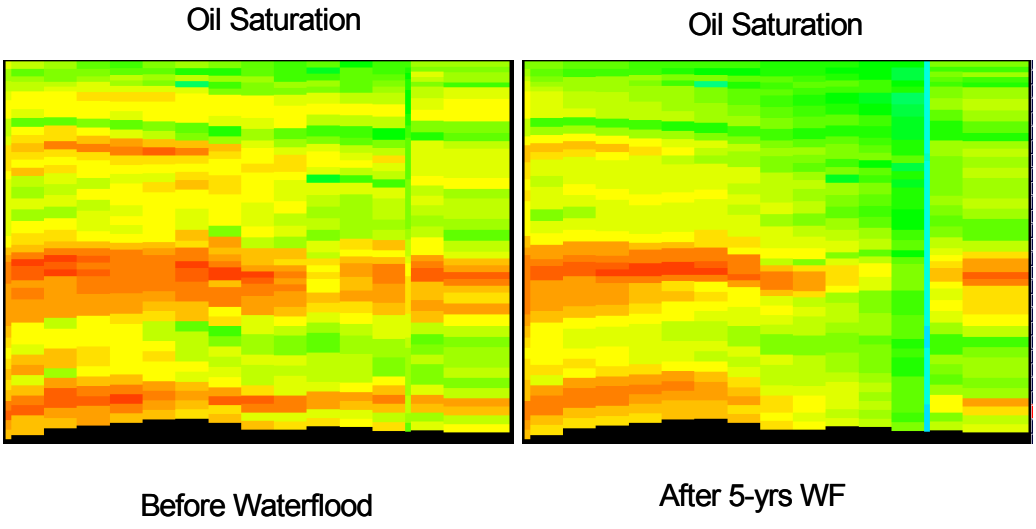

Figure 4.2-10. Oil Saturation changes before and after 5 years waterfloods. Water invades the formation slowly.

Figure 4.2-11 plots the simulated oil response from waterflood and CO_2 WAG processes. The overall response of WAG and water are similar. It is clear that the oil response to the

CO_2 WAG is very quick and lasts a very short period of time, which is consistent with what well 11-8E. Because CO_2 has substantially lower viscosity than water, most of CO_2 flow through the high flow channels. Only a small amount of CO_2 invades the formation. Figure 4.2-12 shows the simulated CO_2 distribution after 15 years of WAG injection. CO_2 invades only the upper part of the reservoir. It is important to notice that the upper part of the reservoir has been waterflooded during earlier water injection. Thus, although some CO_2 invades the formation, CO_2 mostly chases water in the upper part of the reservoir, resulting in low recovery efficiency.

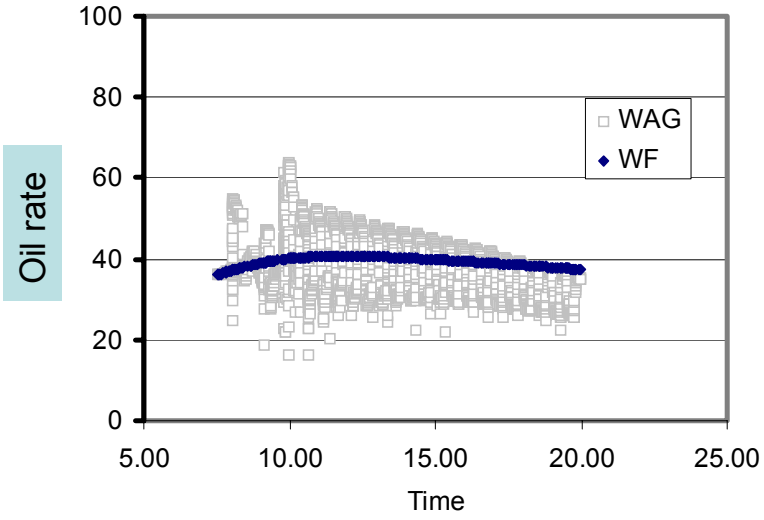

Figure 4.2- 11. Simulated oil production rates for waterflood and CO_2 WAG. We used the average field operation parameters (injection rates and bottom hole pressure) in the simulations for both water and CO_2 WAG.

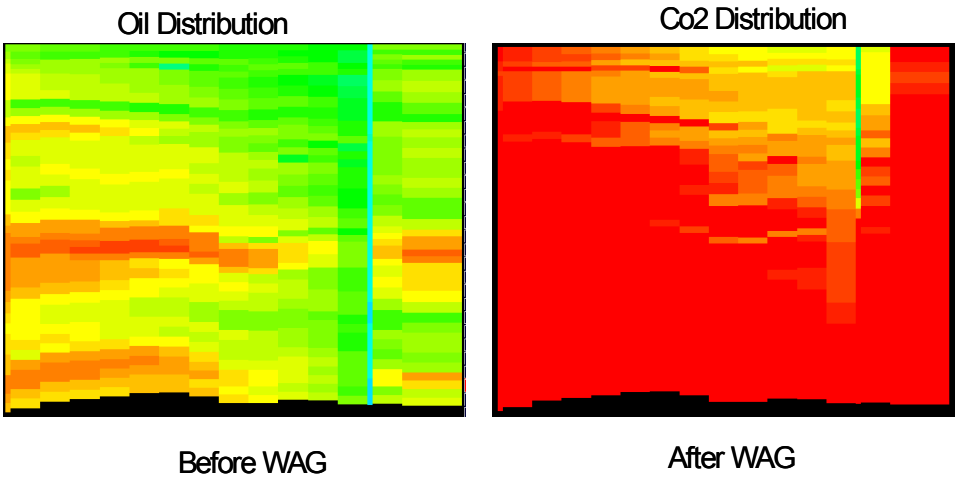

Figure 4.2-12. Simulated oil distribution before WAG and CO_2 distribution after WAG. For the CO_2 distribution color red indicates zero CO_2 in the reservoir. CO_2 invades the top part of the reservoir, which was waterflooded before CO_2 WAG started.

The results discussed above are consistent with what we observed in the field. However, we have not shown why the original design gave significantly favorable predictions. The major difference between the current reservoir model and that used in the original design is the inclusion of the high flow channels between the injector and producer. We conducted similar simulations on current geological model without the high flow channels. Without the high flow channels, all injected CO_2 is forced to flow through the reservoir formation, resulting in substantially higher oil rates as shown in Figure 4.2-13.

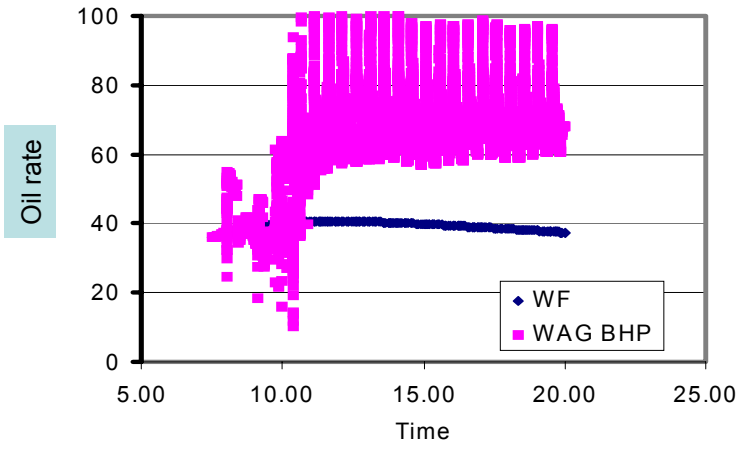

Figure 4.2-13. Simulated oil production rates for waterflood and CO_2 WAG with the high flow channels. It is clear that without the high flow channels, CO_2 WAG would lead to higher oil rate.

Summary:

Compositional simulations were conducted on a ¼ 5-spot sector model for understanding the performance of Lost Hills CO_2 pilot. The sector model was first calibrated by matching the average waterflood behavior in the pilot area and by honoring the tracer test and produced water salinity data. The tracer and salinity survey data suggest the producers are highly connected with the injectors. We employ high flow channels between injector and producer in our model. Simulations show that the existence of higher flow channels in the reservoir play an adverse role on the performance of Lost Hills CO_2 pilot. Most of injected CO_2 flows through the high flow channels and only a small portion of the injected CO_2 invades the reservoir formation. Because of low viscosity, CO_2 prefers the high permeability zones, which has been waterflooded before the WAG started. The combination of the high flow channels and the poor sweep efficiency contributes to the poor performance observed in the pilot.

References

1. Wallace, N.J. and Pugh, E. D.: "An Improved Recovery and Subsidence Mitigation Plan for the Lost Hills Field' California," SPE 26626 presented at 1993 SPE Annual Technical Conference and Exhibition, Houston, TX, Oct. 3-6.
2. Ross, C. M., and Kovseck, A. R.: "Microstructure and Fluid Distribution in a Diatomaceous Reservoir," SPE 75190 presented at SPE/DOE Thirteenth Symposium on Improved Oil Recovery held in Tulsa, Oklahoma, 13–17 April 2002.
3. Perri, P. R., Emanuele, M.A., Fong , W. S., and Morea, M. F.: "Lost Hills CO2 pilot: Evaluation, Design. Injectivity Test Results, and Implementation." SPE 62526 presented at the SPE/AAPG West Regional Meeting held in Long Beach, California, 19-23 June 2000.
4. Fast, R. E., Murer, A. S., and Zambrano, L. G.: "Lost Hills Diatomite Simulation Study: Predicting Waterflood Performance in a Low-Permeability, Compacting Reservoir." SPE 26627 presented at 1993 SPE Annual Technical Conference and Exhibition, Houston, TX. Oct. 3-6.
5. Zhou, D., Friedmann F., Kamath, J. and Morea M.: "Understanding Waterflood in Lost Hills Diatomite," SPE 75142 presented at the 13th SPE/DOR Improved Oil Recovery Symposium, Tulsa, OK, April 15-17, 2002.
6. Wilt, M., Zhang P., Morea M., Julander, D. and Mock P.: "Using Crosswell Electomagnetics to Map Water Saturation and Formation Structure at Lost Hills," SPE 68802 presented at the SPE Western Regional Meeting held in Bakersfield, CA. March 26-30, 2001.
7. Kamath J., de Zabala, E.F., and Boyer, R.E.: "Water/oil Relative Permeability Endpoints of Mixed-Wet, Low-Permeability Rocks," SPEFE (Mar. 1995) 4-10.
8. Zhou, D., Jia, L., Kamath, J. and Kovscek, A. R.: "Scaling of Counter-current Imbibition Processes in Low Permeability Porous Media," *Journal of Petroleum Science and Engineering* (2002) **33**, 61-74.
9. Johnson, E.F., Bossler, D.P. and Naumann, V.O.: "Calculation of Relative Permeability From Displacement Experiments," *Trans.* AIME (1959) **216**, 370.
10. Ilderton, D.C., Patzek, T.W., Rector, J.W., Vineger, H.J.: "Passive Imaging of Hydrofractures in South Belridge Diatomite." SPEFE (Nov. 1996) 46-54.

SECTION 5
PILOT MONITORING AND SURVEILLANCE

5.1 RESULTS of CO_2 INTERWELL TRACER PROGRAM

Earuch F. Broacha
ProTechnics
Michael F. Morea and Gregg Molesworth
ChevronTexaco Exploration and Production Company

An interwell tracer program was carried out by ProTechnics in the pilot area. Four gas phase interwell tracers (Perfluoromethylcyclopentane, Perfluorodimethyl-cyclohexane, Perfluoroethylcyclohexane, and Perfluorodimethylcyclobutane) were injected into four CO_2 injection wells per the following schedule (5.1-Table 1):

Table 5.1-1. Interwell Tracer Program.

Injection Well	Tracer Material	**Date of Injection**	**Injection** Time	**Amount** Tracer
11-8WR	PMCP	9-12-00	4 hrs.	0.50 kg
11-8WAR	PDMCH	9-12-00	4 hrs.	0.50 kg
12-8W	PMCH	9-13-00	5 hrs.	0.50 kg
12-7W	PDMCB	9-13-00	5 hrs.	0.50 kg

A review of the analyses performed on the collected produced gas samples from the thirteen producing wells in the Lost Hills CO_2 pilot area program indicates that tracer has arrived at six of these wells (Figure 5.1-1). Tracer breakthrough is being observed in wells 11-7B, 11-8D, 11-8E, 11-9J, 12-7 and 12-8D. The time required for initial tracer breakthrough to occur ranged from as little as 8 days to as long as 36 days following tracer injection. Seven of the producing wells being sampled in the program have shown no tracer breakthrough as of the last sample date analyzed (10-19-00). In the wells where tracer breakthrough is being observed, none of the tracer material introduced into injection well 12-8W has been detected.

Tracer mass balance calculations were performed on five of the six wells where breakthrough is currently occurring. The results of these calculations are summarized in Tables 5.1-2 and 3. As may be observed in these tables, very little of the injected tracers have been recovered as of the last sample analyzed.

These low tracer recoveries for the first 38 days of the program tend to indicate that no direct, large scale channeling of the injected CO_2 is occurring in the pilot area. This is assuming that all the injected CO_2 remained in the study area as defined by the thirteen producing wells currently being sampled. The small amount of tracer breakthrough that was observed was insignificant in comparison to the volume of CO_2 that was injected into the pilot area. However, significant CO_2 breakthrough did occur a few months later.

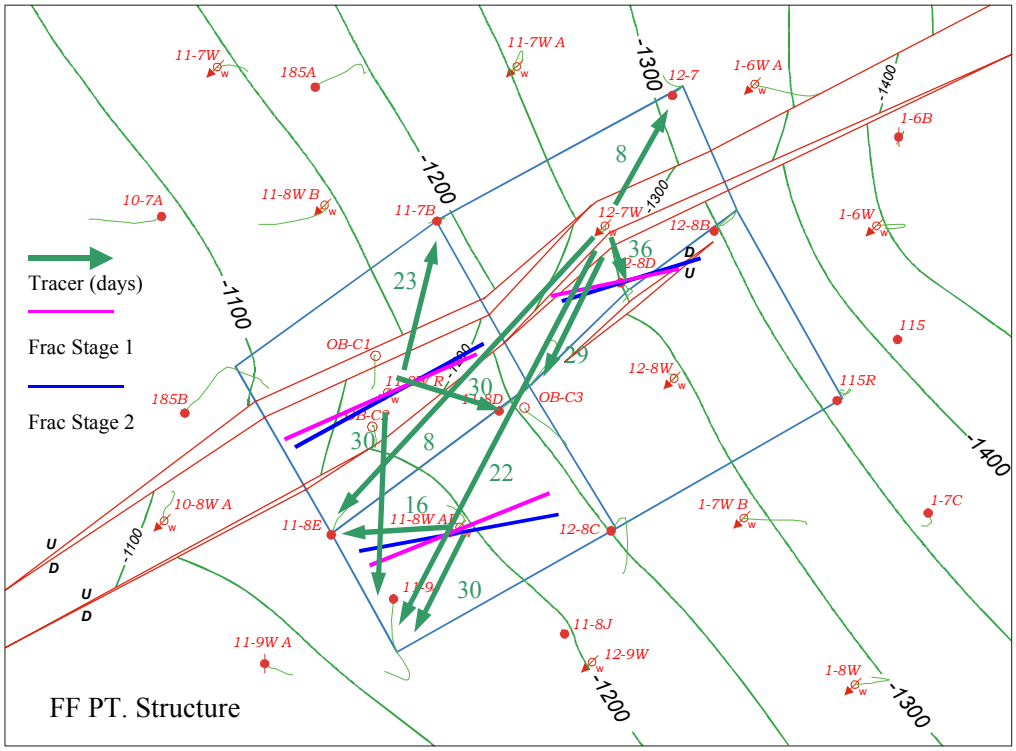

Figure 5.1-1. Structure map with faults (red) of the pilot area. The green arrows show the interwell connectivity between injectors and producers, as of 10/09/00, as determined from the tracers. The numbers next to the arrows represent the number of days it took the injection tracer to reach the producer. Tracer from 12-8W has not been observed in any of the 13 sampled producers. The pink and blue lines represent hydraulic propped fracture azimuths in 3 wells (the length of the line only represents azimuth, not fracture length).

Table 5.1-2. Tracer Mass Balance Calculations for Lost Hills Diatomite CO_2 Pilot Area.

Well Name	Amount of Injected Tracer Material Recovered (grams)			
	PMCP	PDMCB	PMCH	PDMCH
11-7B	0.425	0	0	0
11-8D	0.607	0.109	0	0
11-8E	0	12.430	0	8.488
11-9J	0.225	1.249	0	0.155
12-7	0	4.562	0	0
Total	1.257	18.350	0	8.643

Table 5.1-3. Percent Recovery of Injected Tracers for Lost Hills Diatomite CO_2 Pilot Area.

Well Name	Percent Recovery of Injected Tracer Material			
	PMCP	PDMCB	PMCH	PDMCH
11-7B	0.085%	0%	0%	0%
11-8D	0.121%	0.022%	0%	0%
11-8E	0%	2.49%	0%	1.70%
11-9J	0.045%	0.25%	0%	0.031%
12-7	0%	0.912%	0%	0%
Total	0.25%	3.67%	0%	1.73%

5.2 Electromagnetic Studies at the CO_2 Pilot

Mike Wilt
Electromagnetic Instruments, Incorporated

Data Interpretation

We collected crosswell and Geo-BILT data prior to CO2 start-up. Both data sets were interpreted utilizing automatic inverse computer codes. We assume a starting model based on the induction resistivity logs. In the crosswell case we interpolate the logs between the wells for a 2D-starting model; for the Geo-BILT data we use the logs to construct a 1D layered section.

Crosswell data were fit with the 2D inversion code (SINV2D) developed by Sandia Laboratories (Alumbaugh and Newmann, 1996). This code has been used for more than 3 years in crosswell data interpretation (Wilt and others, 2000).

Geo-BILT data were fit with a 3D inverse code, INV3D, also developed by Sandia Laboratories (Alumbaugh and Newmann, 1996). Although this code has been used in crosshole and surface data, these are the first single well data used for 3D inversion. 3D inversion is very computationally intensive, and for that reason it is impractical to use this tool on the entire data set. For these data, we focused attention on the depth interval from 1400-1800 ft, where the largest 3D effects were observed in the data and where there is strong evidence of waterflooding at the injection well.

Crosswell EM Results

In Figure 5.2-1 we show the resistivity cross-section derived from the crosswell EM data between wells OB-C1 and OB-C2. Included at the sides of the section are color-coded induction logs, for OB-C1 and OB-C2, for reference. The figure shows a roughly flat lying multilayered section throughout much of the image, although there is a clear lateral boundary near well OB-C1 in the deeper parts of the section.

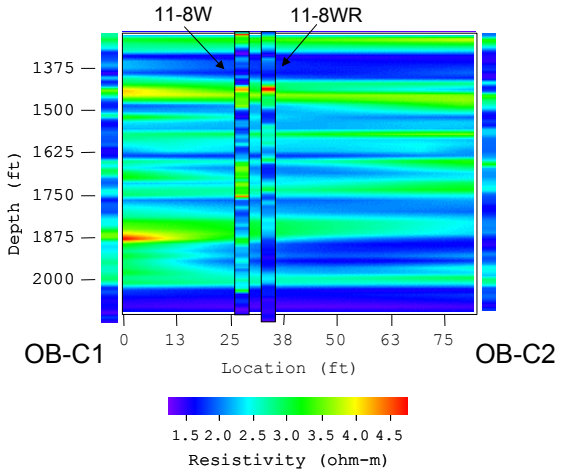

Figure. 5.2-1. Resistivity section from crosswell EM data.

The induction logs from well 11-8W and 11-8WR are color-coded and superimposed on the section. It is encouraging to note that the cross-section closely matches the resistivity from well 11-8WR, although this information was not used to constrain the inversion. Note the difference in resistivity between the borehole induction logs on either side of the image. Well OB-C1 is considerably higher in resistivity than OB-C2, especially at the basal section below 1650 ft.

Focusing on the section near OB-C1, we can see a clear lateral boundary at a depth of 1900 ft, about 15 ft south of well OB-C1 and a much more diffuse boundary at a depth of 1700 ft. The implication from this image is that the existing waterflood has mainly penetrated into the deeper, diatomite rich layers in the section. In these layers, it has reduced the resistivity by up to 50 percent. It also suggests that the edge of the water flood in some of these layers has reached well OB-C1, but in other layers it is still short of the well.

Geo-BILT Interpretation

Geo-BILT results are interpreted in two ways. First, the apparent resistivity logs are examined qualitatively by matching them to the geologic sections. This allows for some average determination of saturation. The cross-coupled logs are then examined for near well anomalous zones that may be related to fractures or in this case waterflooded horizons. A more rigorous interpretation is the application of these data in a 3D inversion. Here we wish to reconstruct a 3D-resistivity distribution around the borehole that honors both the data as well as being consistent with the known geology.

We applied the 3D inversion to the 6 kHz Geo-BILT data in the depth interval from 1400-1800 ft as a test. For simplicity we used only the vertical component transmitter and all three orthogonal receivers at the 5m offset. These data were fit in stages. We first applied a layered inverse code to fit the vertical component data (ZZ). Using this as a starting model we fit the null component data to a 3D-resistivity distribution. The final solution was then checked against all data. This procedure, although somewhat laborious, was found to be more effective in the long run. Our attempts to fit all data simultaneously produced poor data fits or unreasonable models.

Even for this limited depth interval the 3D inversion was a lengthy process. Each inverse model required 2-5 days for convergence. In addition the results were dependent on the weighting of data, the starting model and the noise level and calibration correction of collected data. The results were that numerous runs were made over a two-month period to produce the model shown below.

In Figure 5.2-2 we show the 3D model derived from inverting the Geo-BILT data in the 1400-1800 ft interval. The final 3D model is consistent with the logs and the geology, and the data fit is adequate. The main feature of the model is a somewhat hemispherically shaped, low resistivity body extending southwards and westward from the borehole. This zone seems confined within 25 ft of the well at depths from 1660 to 1740 ft.

We can learn two things from this model. First, the range of influence of the 5 m offset sensor is probably about 8m (25 ft), which is about the radius of the anomalous mass. This limit probably also influences the shape of the body. Secondly, the low resistivity zone is predominantly south and west of the injector which is consistent with flow from a northeastern trending fracture zone at the injector where the leading edge of the flow is quite close to the observation well.

The 3D and 2D results are quite similar. They both indicate that that some injected water is flowing past OB-C1 but the majority of the saltwater is south and west of OB-C1. Both data sets confirm that the flood is confined predominantly to a few layers mostly towards the bottom of the reservoir.

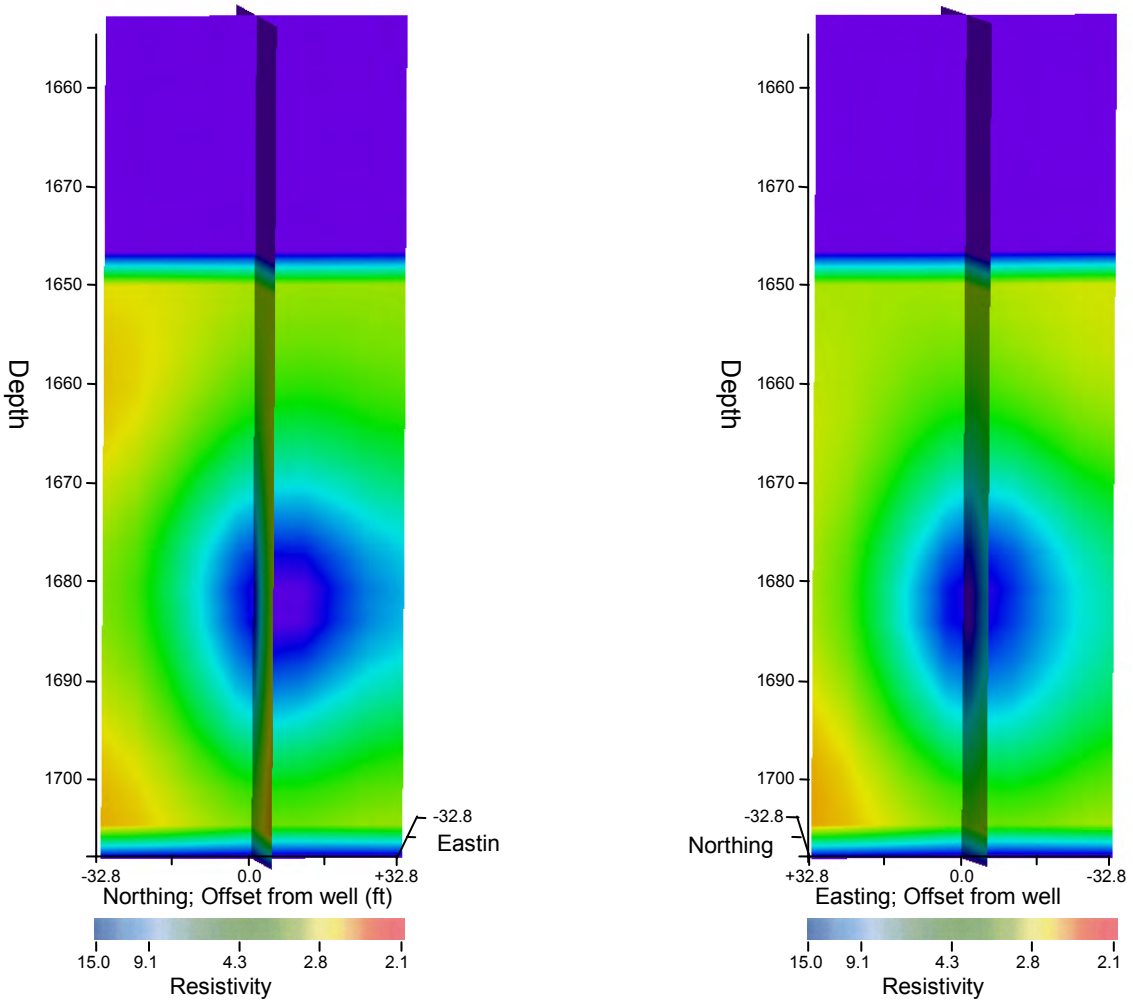

Figure. 5.2-2. Geo-BILT 3D inversion: 6 kHz and 5 m transmitter-receiver separation.

5.3 CROSSWELL ELECTROMAGNETIC IMAGING

Barry Kirkendall and Jeff Roberts
Lawrence Livermore National Laboratory

Lawrence Livermore National Laboratory (LLNL) conducted research in three different areas; using electromagnetic induction to image between observation wells OB-C1 and OB-C2, using passive electromagnetic monitoring during hydrofracture periods to attempt to locate active fractures developing in the ground, and electrical resistivity and injection measurements on core samples from the CO_2 field to attempt to improve interpretation of the electromagnetic induction images.

Crosswell EM Imaging:

LLNL analyzed multiple-frequency (2.0, 4.0, and 6.0 kHz) in October 2001 in a cross-borehole electromagnetic (EM) induction survey between OB-C1 and OB-C2. Figure 5.3-1 shows the inversion results for the 4.0 kHz source frequency. The focus on multiple frequency data is to develop quantitative interpretive methods instead of the traditional "hand-waving" method, understand the error in the images to a higher degree, and provide a stronger link to the laboratory core data that are continuing. The top figure (A) in Figure 5.3-1 is the baseline, or pre-injection, image, while the middle (B) and bottom (C) images were acquired in April 2001 and October 2001, respectively. These images show trends, such as the higher resistivity band at 1670 feet depth. This feature appears to have an increasingly lower resistivity over time, possibly due to the CO_2 flooding. Another feature, the body at 1720 – 1780 feet appears to show a decrease in resistivity from August 2000 until April 2001 and then a slight increase from April 2001 until October 2001. We are currently looking into the cause of this reverse shift and have no explanation in the present. The final aspect we are looking into regarding the time-lapse imaging is a new method to show the change over time. Currently, each image is separately processed and inverted to produce a two-dimensional image and these are the images compared. A new methodology is to subtract the two data sets, multiply them by a reasonable forward model (in the case of the baseline data) or use the previous image as a forward model (in the case of subsequent datasets) and invert that difference. In this manner we expect to eliminate artifacts from the inversion and produce images. Work in this area has been progressing and LLNL expects to submit a peer reviewed paper in April of this year.

Passive EM:

In June 2001 passive electromagnetic data was collected in OB-9 (1100ft. southwest of the CO_2 pilot) during a hydrofracture at 1650 feet. depth. An EM induction receiver antenna with an accelerometer attached to the inside of the antenna with epoxy was placed at 1550 feet. depth for 45 minutes during a hydrofracture of a nearby producer 9-10G. The EM and accelerometer data (Figure 5.3-4 A-D) were initially high pass filtered to prevent aliasing before digitization and then streamed to a PC running LABVIEW and recorded at a 30 kHz sample rate. In this accelerometer analysis, a Kalman filter was applied to the time series that was then integrated to produce velocity data, and can then be compared to seismometer data. The focus of this investigation is to determine if the

EM signal arrives at an earlier time than the accelerometer data. The seismoelectric effect is the physical description that states that seismic waves, produced by a hydrofracture event, are converted into EM waves at discontinuities within the ground. These EM waves, measured by the EM induction receiver antenna, will travel much faster than the seismic waves, measured by the accelerometer. If we can distinguish the EM component from the seismic component, we would be able to advance this experiment to include multiple receivers and attempt to locate the fracture. Initial views of the data suggest that for an event as pictured in Figure 5.3-4, the EM data is arriving a millisecond earlier than the seismic waves, although we are in an investigation to determine the errors in the integration and filtering to ascertain the relative position of each signal. Research efforts in this area are ongoing in collaboration with Schlumberger-Cambridge Research and Massachusetts Institute of Technology.

Laboratory Measurements:
Estimates of formation factor and the associated electrical conductivity were calculated by formation evaluation in the laboratory using core samples of the Blue and Brown Etchegoin formation. Figure 5.3-3 shows the results of laboratory petrophysical measurements performed on three samples from the Etchegoin Formation. The formation factor was measured at room temperature using a confining pressurized apparatus with a specific pore pressure while the pore fluid used was a NaCl solution with varying fluid conductivity from which the estimates of formation factor and surface conductivity were calculated. Permeability was also measured by inducing flow using a pressurized gradient.

Interpretation of Results:
The 4.0 kHz images, 5.3-1B and 5.3-1C, shown below clearly indicate an increase of resistivity at a depth interval of 1700 feet and 1770 feet, which suggests, based on laboratory measurements that CO_2 is invading this interval. Figure 5.3-2 suggests that oil has a higher resistivity than CO_2. LLNL is currently working to attain volumetric analysis on the oil and CO_2 components using a joint laboratory and field analysis. The conductive brine plume (dark blue) between 1800 feet and 1820 feet on next to OB-C2 (right side of image) also is decreasing in time, indicating that the conductive fluid is being removed from the system. The top and bottom areas of the image also indicate change, but these areas have an increased error due to a lesser amount of data sampling, and should not be interpreted as quantitatively. LLNL has acquired similar data for other frequencies (2.0 and 6.0 kHz) and is in the process of inverting the multiple frequency data simultaneously to achieve a better fit. At the present, the 2.0 kHz data is inverted to produce a starting model for the higher, and more accurate, frequencies. In the above section, it was noted that permeability measurements were taken directly. LLNL is currently involved in also extracting permeability information from the electromagnetic data using a characteristic length parameter (Lambda parameter) technique developed at LLNL.

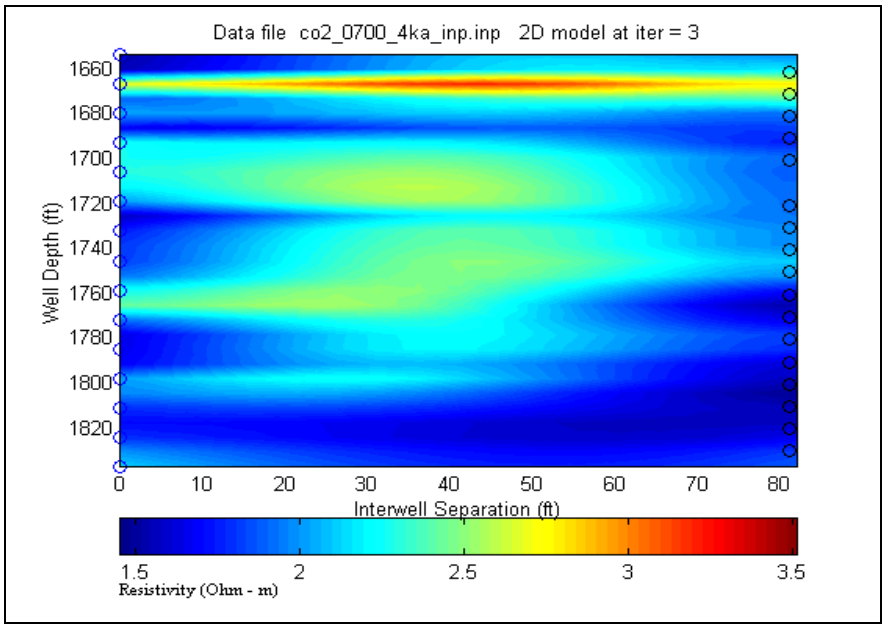

Figure 5.3-1A. 4.0 kHz source frequency images of CO_2 (OB-C1, OB-C2) pilot at Lost Hills, CA. Image (A) is a pre-injection baseline acquired in August 2000, images (B) and (C) were acquired in April 2001 and October 2001 respectively.

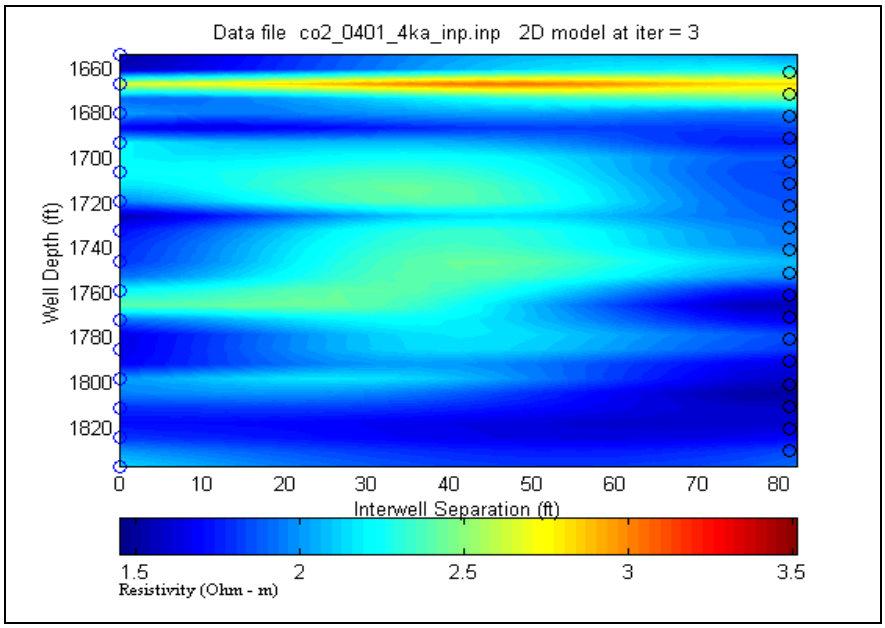

Figure 5.3-1B. 4.0 kHz source frequency images of CO_2 (OB-C1, OB-C2) pilot at Lost Hills, CA. Image (B) was acquired in April 2001.

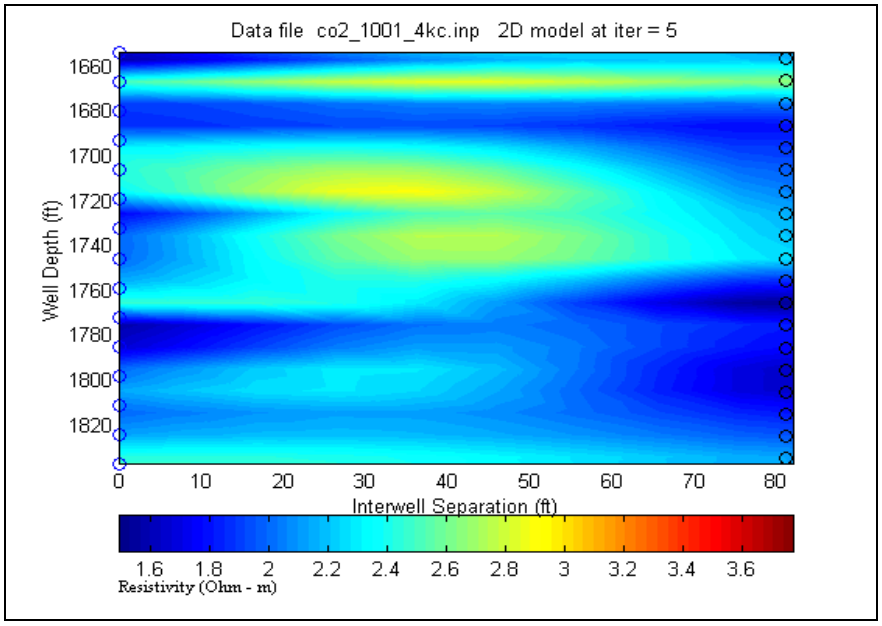

Figure 5.3-1C. 4.0 kHz source frequency images of CO_2 (OB-C1, OB-C2) pilot at Lost Hills, CA. Image (C) was acquired in October 2001.

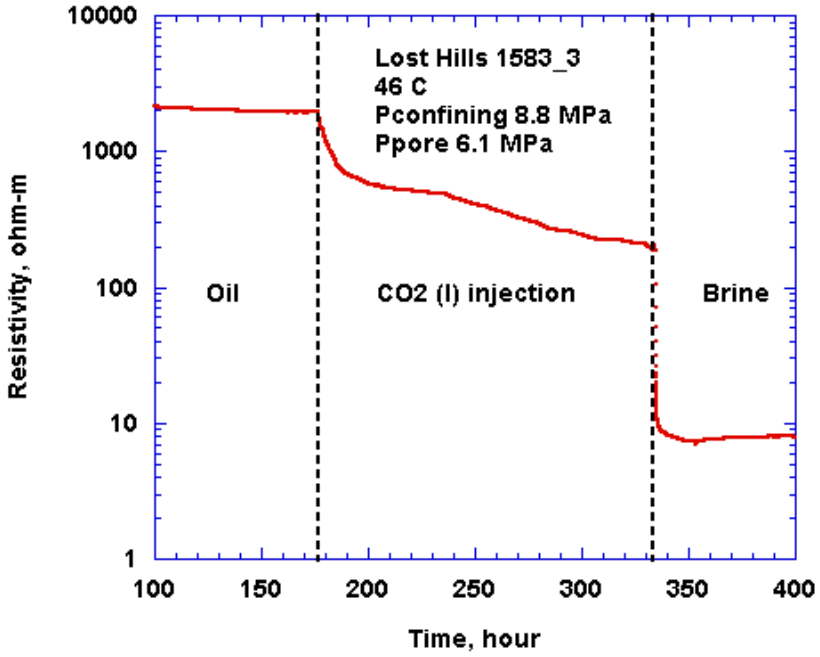

Figure 5.3-2. Laboratory core injection suggests decreasing resistivity during CO_2 injection process. This plot, acquired in the laboratory, suggests quantitative values for the resistivity of core samples while saturated with either CO_2 or oil. The temperature and pressure of this sample are equivalent to reservoir conditions. In this plot, oil has a higher resistivity than CO_2.

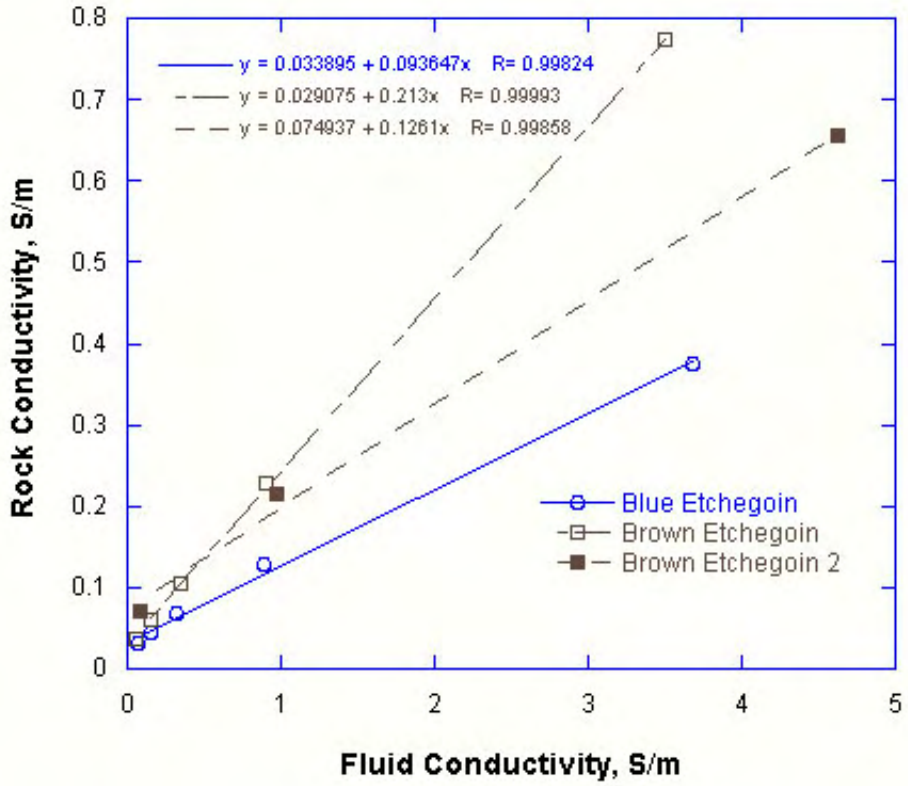

Figure 5.3-3 Laboratory petrophysical measurements were performed on three samples from the Etchegoin Formation. The formation factor F was measured at room temperature using a confining pressuring of 100 psi and a pore pressure of ~50 psi. The pore fluid was a NaCl solution with varying fluid conductivity (from 9 microS/cm to 65 mS/cm). This permitted both an estimate of F and surface conductivity. Permeability was also measured by inducing flow using a pressure gradient between 2 and 50 psi.

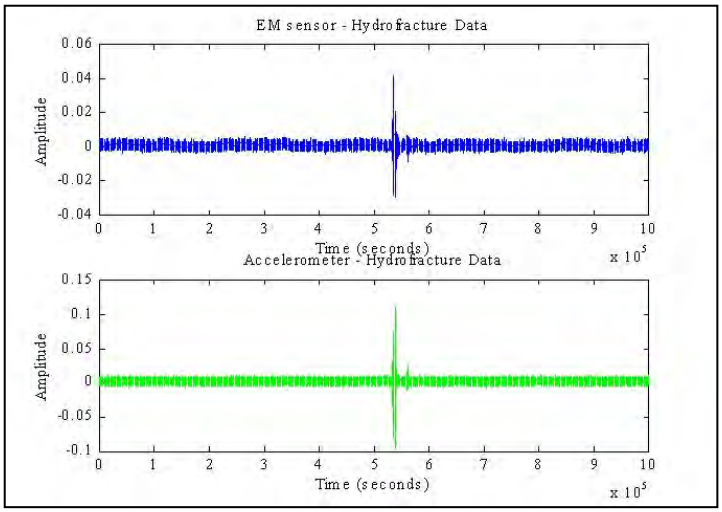

Figure 5.3-4A. For the experiment described in the summary, time series plots of velocity (from the accelerometer) and electromagnetic (EM) induction data. In picture (A), 33 seconds is displayed with increasing resolution in subsequent plots; 3.3 seconds in (B), 1.5 seconds in (C), and 0.36 seconds in (D). In all plots, the EM induction data is on top and the accelerometer data is below. The focus on this data is to determine if the EM signal arrives at an earlier time than the seismic signal recorded by the accelerometer.

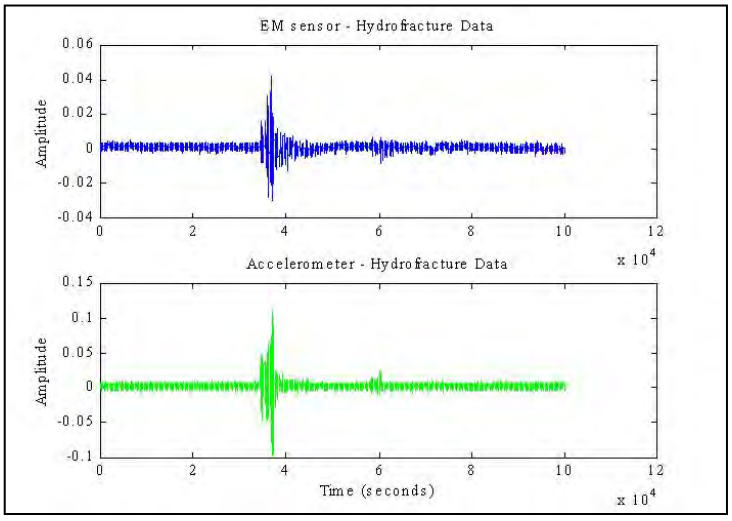

Figure 5.3-4B. Time series plots of velocity (from the accelerometer) and electromagnetic (EM) induction data. 3.3 seconds is displayed.

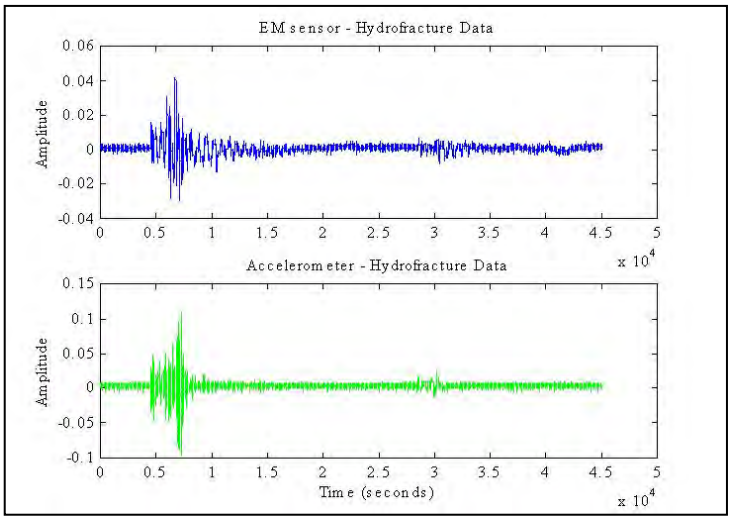

Figure 5.3-4C. Time series plots of velocity (from the accelerometer) and electromagnetic (EM) induction data. 1.5 seconds is displayed.

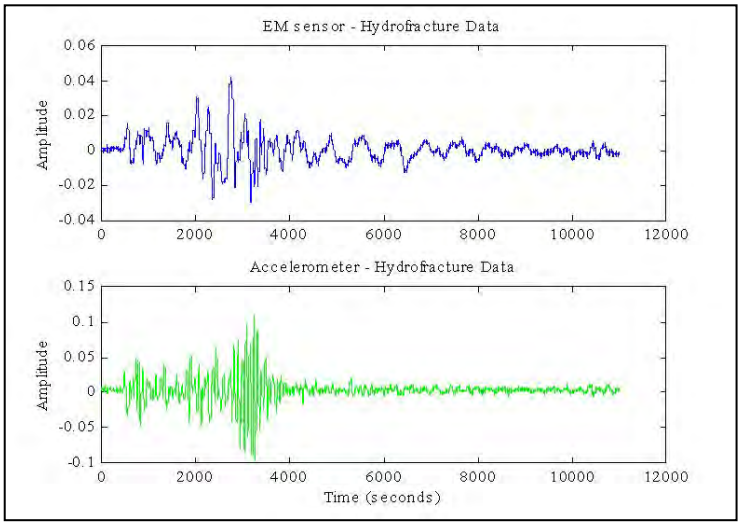

Figure 5.3-4D. Time series plots of velocity (from the accelerometer) and electromagnetic (EM) induction data. 0.36 seconds is displayed.

5.4 MONITORING SULFUR AND HYDROCARBON CHEMISTRY OF LOST HILLS OILS DURING CO_2 FLOODING

Rong J. Hwang
ChevronTexaco Energy Research and Technology Company
Michael F. Morea
ChevronTexaco Exploration and Production Company

SUMMARY AND CONCLUSIONS:

Geochemical characterization has been conducted on produced oils that were sampled periodically from selected producing wells located in the CO_2 flood pilot area of the Lost Hills field. The objective is to determine if the formation of solids, specifically elemental sulfur, has been induced by CO_2 injection to the reservoir. The analytical results of the recent oil samples (second set) taken in December 2000, January 2001 and November 2001 are comparable to those of the earlier samples (first set) taken in August 2000 shortly before the start of CO_2 injection. Little changes in bulk properties of the oils including API gravity, total sulfur %, and asphaltene % indicate that there are no significant changes in oil chemistry caused by CO_2 injection for over one year.

Elemental sulfur was absent in all the oils produced from wells in the pilot area prior to CO_2 injection. No elemental sulfur was found in the second or third sets of oil samples either. Thus, CO_2 injection has so far not caused formation of elemental sulfur. The results indicate that the oils in the pilot area, based on bulk properties, have remained virtually unchanged after CO_2 injection for over one year months. This suggests the interaction between oil and CO_2 in the reservoir has been fairly weak.

However, the oil from one of the monitoring wells, 11-8D, has experienced some measurable changes in molecular properties (more sensitive indicators), hydrocarbon and sulfur fingerprints, suggesting a significant interaction between this oil and CO_2, and proximity of this well to the CO_2 flow in the reservoir.

INTRODUCTION:

Enhanced oil recovery processes involving reservoir injection of gases, such as light hydrocarbons and CO_2, are known to often induce organic deposits that plug rock pores and thus reduce rock permeability (Shelton and Yarborough, 1977; Monger and Fu 1987) and well injectivity. The deposition of organic solids, mostly asphaltic components of crude oils, can lead to reduction in oil recovery and hence operational profits. In addition to asphaltics, heavy hydrocarbons can also segregate from the oil phase and precipitate in the reservoir, contributing to solid deposition (Hwang and Ortiz, 1998). Less known is CO_2 flooding may cause formation of elemental sulfur in the reservoir that enhances the deposition of solids (Hwang and Ortiz, 1998; Mathis, 1998). Elemental sulfur is insoluble in water and has limited solubility in oil. It would greatly contribute to the reduction of rock permeability once it is formed in the reservoir.

As a part of the overall monitoring plan, the oil chemistry monitoring during CO_2 flood could likely provide insightful information for understanding and managing the CO_2

flood process. The objectives of monitoring oil chemistry include (1) evaluating the impact of CO_2 flood on in-reservoir asphaltene precipitation, and (2) determining if elemental sulfur is formed in the reservoir during CO_2 flood. The results of oil geochemistry monitoring would provide the basis for the planning on remediation or mitigation. Further, defining the spatial and temporal changes in oil composition in the study would provide the clue on the flow direction of injected CO_2 in the reservoir, facilitating reservoir management and injection strategy for the CO_2 flood process.

Samples and Methods:

The sampling plan was to take oil samples about quarterly from well heads of selected producers in the CO_2 pilot area during the lifetime of the CO_2 flood for geochemical characterization. The first set of samples was taken in August 2000, prior to CO_2 injection (Table 5.4-1). These samples would provide the baseline data. Two oil samples of the second set (wells 12-7 and 12-8D) were taken in December 2000, about three month after the start of CO_2 injection. The sample from the third well, 11-8D, was not taken until January 2001. The sampling delay was caused by the sand production problem associated with the 11-8D well. Another set of samples (11-8D, 12-7, and 12-8D) was taken in November 2001.

Bulk properties such as API gravity and wt % asphaltenes were determined by standard geochemical procedures. Wt % sulfur of the oils was measured by ASTM method, D2622, using X-ray. Gas chromatography-atomic emission detector (GC-AED) was used to determine the elemental sulfur content of the oils. Gas chromatography was performed with an HP5890A Series II chromatograph equipped with HP7673A autosampler and HP 5921A atomic emission detector. The chromatograph was fitted a 15m x 0.25 mm DB-1 capillary column. Helium was used as carrier gas. After injection the column oven temperature was programmed from 50 to 300 °C at 3.5 °C/min. The sulfur emission line at 181 nm was used for detecting sulfur compounds and the carbon emission line at 179 nm for detecting hydrocarbons. The samples were also analyzed by GC-AED for sulfur and hydrocarbon fingerprints to profile sulfur and hydrocarbon species.

RESULTS AND DISCUSSION

Bulk Properties:

The bulk compositions of two sets of the oils produced at different times from 3 wells located in the pilot CO_2 flood area of Lost Hills are listed in Table 5.4-1. The analytical results of the recent oil samples (second set) taken in December 2000, January 2001 and November 2001 are comparable to those of the earlier samples (first set) taken in August, 2000 shortly before the start of CO_2 injection. Little changes in bulk properties of the oils including API gravity, total sulfur %, and asphaltene % indicate these is no significant change in oil chemistry caused by CO_2 injection for over one year.

Elemental sulfur was not detected in the pre-CO_2 flood oil samples (first set) indicating elemental sulfur is absent in the oils or present in the trace level (< 10 ppm) not detected by the instrument. No elemental sulfur was found in the second or third sets of oil samples either. Thus, CO_2 injection has so far not caused formation of elemental sulfur.

The results indicate that the oils have remained virtually unchanged after CO_2 injection for over one year.

The observations suggest that injected CO_2 has not had significant interaction with the reservoir oil resulting in little changes in physicochemical properties of the oil. This is contrary to the results of an earlier study of the McElroy CO_2 flood. In the McElory field, CO_2 injection caused an increase in oil API gravity and reduction in asphaltics and heavy hydrocarbon content within three months of CO_2 injection (Hwang and Ortiz, 1998). The differences in oil responses to CO_2 flood between the Lost Hills and McElory may lie in differences in reservoir conditions and oil properties. Alternatively, no contact between injected CO_2 and oil in the reservoir would account for little change in Lost Hills oil. However tracer and production data show CO_2 has been in contact with these wells.

Molecular Properties:
Molecular properties of the oils such as hydrocarbon fingerprints (composition) derived from gas chromatographic analysis are generally more sensitive to the changes (perturbation) in recovery processes than bulk properties. To detect the early impact of the CO_2 flood on oil chemistry, the oils were analyzed by gas chromatograph-atomic emission detector (GC-AED) to monitor the changes, if any, in composition of hydrocarbon and sulfur species. Gas chromatograms of the oils are shown in Figures 5.4-1-6.

Hydrocarbon Fingerprints:
The oils produced from the three monitoring wells are badly biodegraded. Paraffinic hydrocarbons and isoprenoids are absent in all the samples indicating the oils have undergone significant biodegradation in the reservoir. Hydrocarbons of the oils mainly consist of naphthenics and aromatics that are more resistant to biodegradation than paraffins and isoprenoids. Distributions of these hydrocarbons (hydrocarbon profiles) in the oils are illustrated in Figure 5.4-1 showing the dominance of light hydrocarbons ($\leq$ C10) despite the very moderate API gravity of the oils. The intermediate (C11~ C25) and heavy (> C25) hydrocarbons are relatively low in abundance. These hydrocarbon distributions remain pretty much the same for all the oils produced from monitoring wells even after CO_2 injection for three months (Figure 5.4-1). It appears no heavy hydrocarbons have dropped out from the oil phase in the Lost Hills reservoirs despite CO_2 injection. The observation is again consistent with that no strong interaction between the reservoir oil and injected CO_2 has occurred.

However, close examinations of chromatograms for detailed comparison of hydrocarbon fingerprints of oils produced before and after the start of CO_2 injection have revealed a slightly different story on the effect of CO_2 flood so far on oil chemistry. While it is true that hydrocarbon fingerprint remains virtually unchanged for some oils, it shows significant changes for the oil from well 11-8D (Figure 5.4-2). Hydrocarbon peak ratios selected for grouping to show similarity or dissimilarity in composition among the oils are listed in Table 5.4-2. The peak ratios that are chosen to maximize the differences among the oils are the basis for multi-variant statistic analysis, yielding the cluster diagram. Figure 5.4-3 shows the most dissimilar oil is the January 2001 sample from well 11-8D that clusters apart from the oils from other wells but also from the early

sample of the same well. For wells 12-7D and 12-8D, the oils sampled before and after the start of CO_2 group together, respectively. The results suggest that the well 11-8D has probably seen more CO_2 than other wells implying the well is located closer to pathways of CO_2 flow.

Quantitatively, the magnitude of compositional differences between the oils sampled before and after the start of CO_2 flood from well 11-8D is very significant and has an average difference of ~ 12 % for 9 ratios (Table 5.4-2). Analytical precision of the chromatographic analysis presented in peak ratios is generally 3 % or less. Thus, peak ratio differences of 5 **%** or more represent real compositional differences among the oils.

In comparison, the oils from other two wells, 12-7D and 12-8D, have little changes (≤ ~ 1 %) since the start of CO2 injection.

Sulfur Fingerprinting:

Oils in the offshore California and San Joaquin Valley sourced from the Monterey Formation and its equivalent shale are known rich in sulfur. With different physicochemical properties, sulfur compounds and their distribution in the oils have potential to enhance hydrocarbon based oil grouping for characterizing reservoirs and monitoring production processes.

Sulfur fingerprints of the oils, illustrated in Figure 5.4-5, are characterized by high abundances of well resolved C2-, C3-, and C4- alkyl substituted benzothiophenes although the parent compound, benzothiophene, is low in abundance. Moderate amounts of dibenzothiophene and its alkyl derivatives are also present. High abundances in benzothiophenes relative to dibenzothiophenes indicate the oils are low in thermal maturity. An increase in thermal maturity generally results in a decrease in abundances of benzothiophenes relative to those of dibenzothiophenes (Ho et al., 1974). All the oils display a huge hump of unresolved complex mixtures (UCM) of heavy organic sulfur compounds that are dominated by compounds heavier than C2-dibenzothiophenes, consistent with low maturity of the oils.

Unlike hydrocarbons, sulfur compounds in the Lost Hills oils have not suffered from biodegradation related depletion due to their higher resistance to biodegradation. Sulfur fingerprints can thus possibly provide information that may not be available from studying hydrocarbon composition. The oils from the three monitoring wells were analyzed for sulfur fingerprints, as shown in Figures 5.4-5, 6, and 7. Comparing sulfur fingerprints of the oils produced before and after the start of CO_2 flood, they are highly similar for the oils from well 12-7 and significantly different for the oils from 11-8D (Figures 5.4-5 and 6), which are consistent with the observations on hydrocarbon fingerprints of the oils. For the oils from well 12-8D, sulfur fingerprints show subtle changes while hydrocarbon fingerprints exhibit little changes (Figure 4.4-7).

Sulfur peak ratios selected for grouping to show similarity or dissimilarity in composition among the oils are listed in Table 5.4-3. Cluster analysis of the sulfur data yielded an oil

grouping (Figure 5.4-8) similar to that based on hydrocarbons with one exception. The oils from well 12-8D do not group as closely because of larger differences seen in sulfur fingerprints than those indicated by hydrocarbon fingerprints. Inconsistency in grouping 12-8D oils suggests the CO_2 effect on this well is very marginal. The magnitude of composition differences between the produced oils from well 12-8D has an average difference of ~ 6 % again suggesting the oil in this well has been slightly perturbed by CO_2 injection (Table 5.4-3).

REFERENCES:

Ho, T.Y., Rogers, M. A., Drushel, H. V., and Koons, C. B. (1974) Evolution of sulfur compounds in crude oils. AAPG Bull., 58, 2338-2348.

Hwang, R. J. and Ortiz, J. (1998) Effect of CO_2 flood on geochemistry of McElroy oil. In *Advances in Organic Geochemistry* 1997 (Edited by Horsfield B., Radke M., Schaefer R. G., and Wilkes H.), 485-503.

Mathis, L (1998) Deposition of elemental sulfur during CO_2 flood in the Goldsmith Field, personal communication.

Monger, T. G. and Fu, J. C. (1987) "The Nature of CO_2-Induced Organic Deposition", Society of Petroleum Engineers, SPE 16713.

Shelton, J. L. and Yarborough, L. (1977) "Multiple Phase Behavior in Porous Media During CO_2 or Rich-gas Flooding", Journal of Petroleum Technology, 1171-1178.

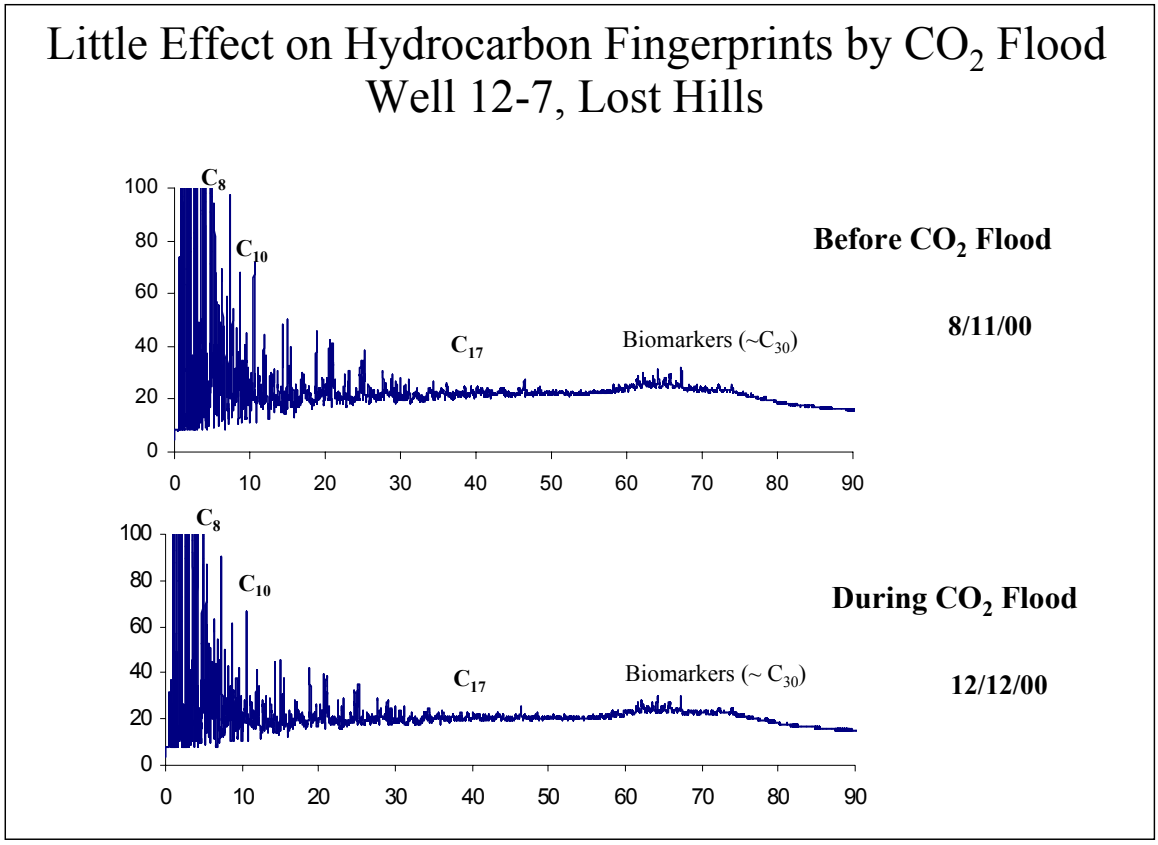

Figure 5.4-1. Hydrocarbon fingerprints are highly similar for the oils from well 12-7D, produced before and after the start of CO_2 flooding.

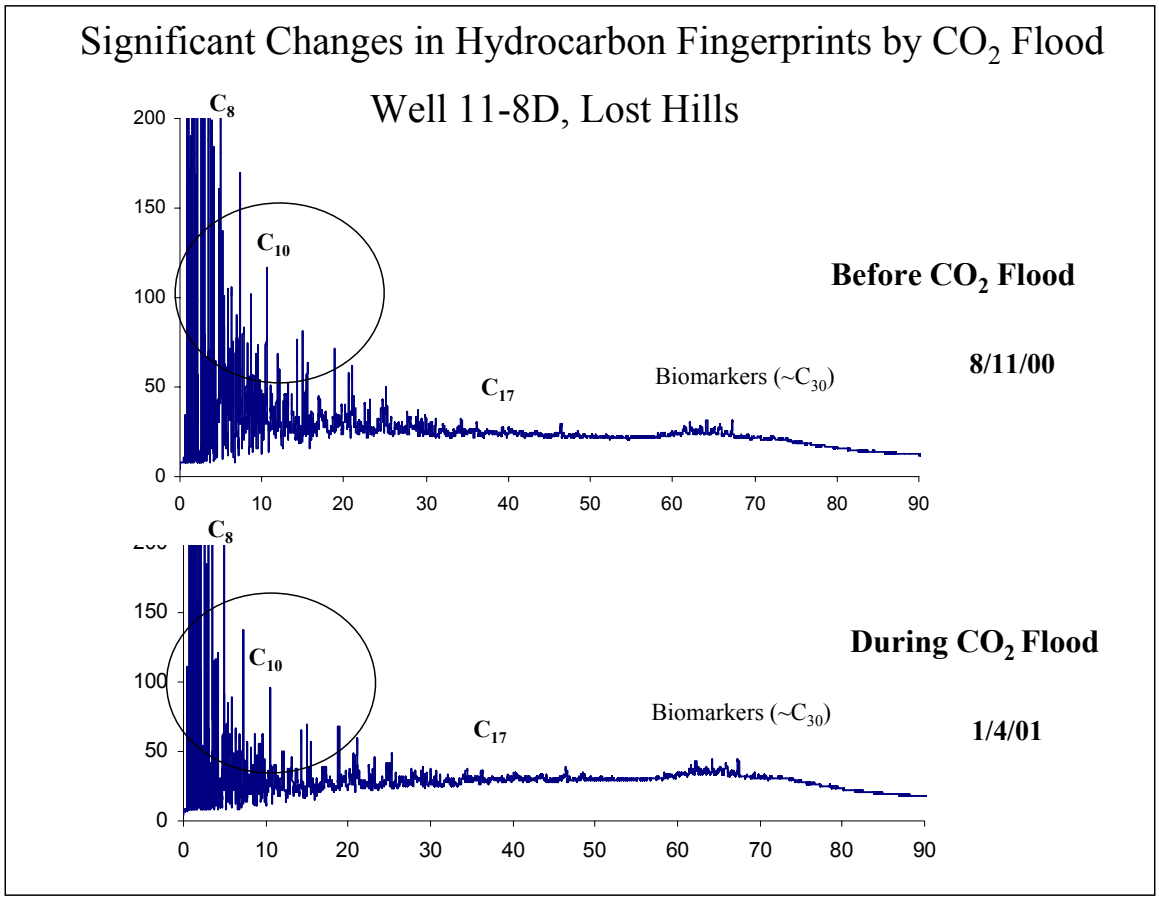

Figure 5.4-2. Hydrocarbon fingerprints are significantly different in the light ends for the oils from well 11-8D, produced before and after the start of CO_2 flooding.

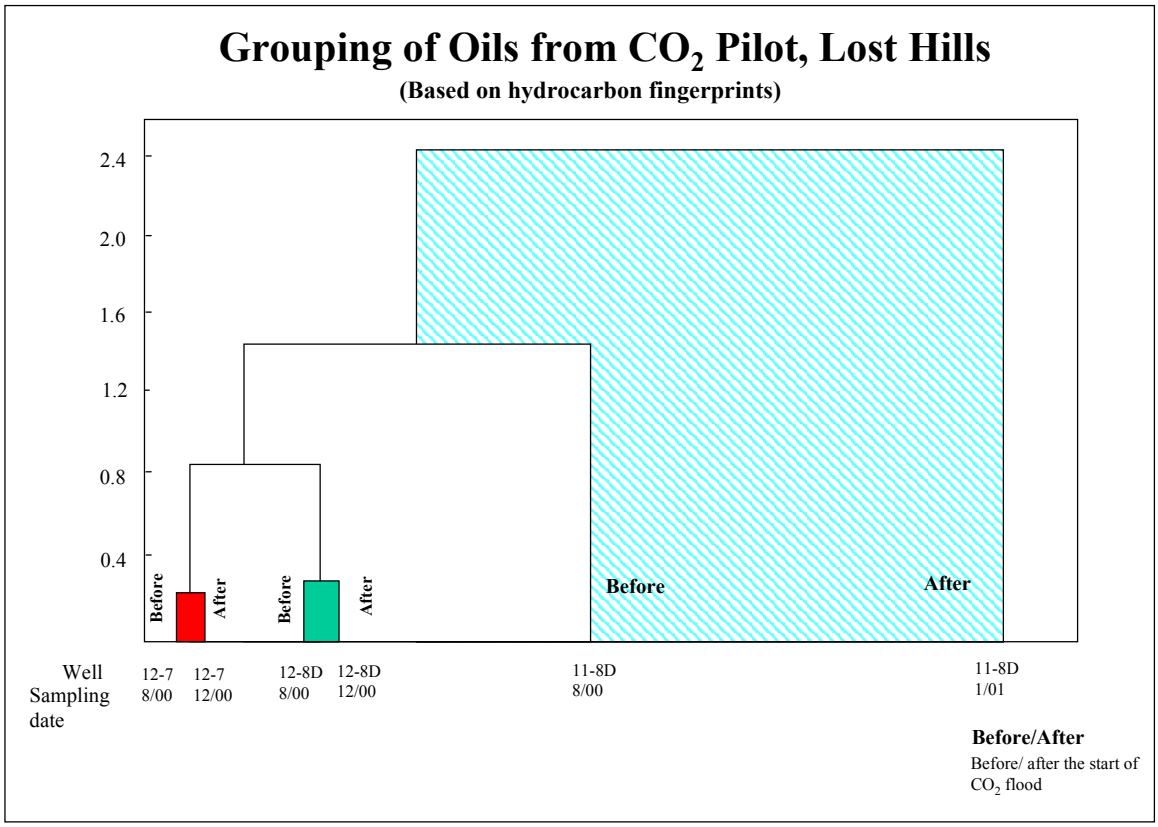

Figure 5.4-3. Cluster analysis showing well 11-8D has the most significant changes in hydrocarbon fingerprint after the start of CO_2 flooding.

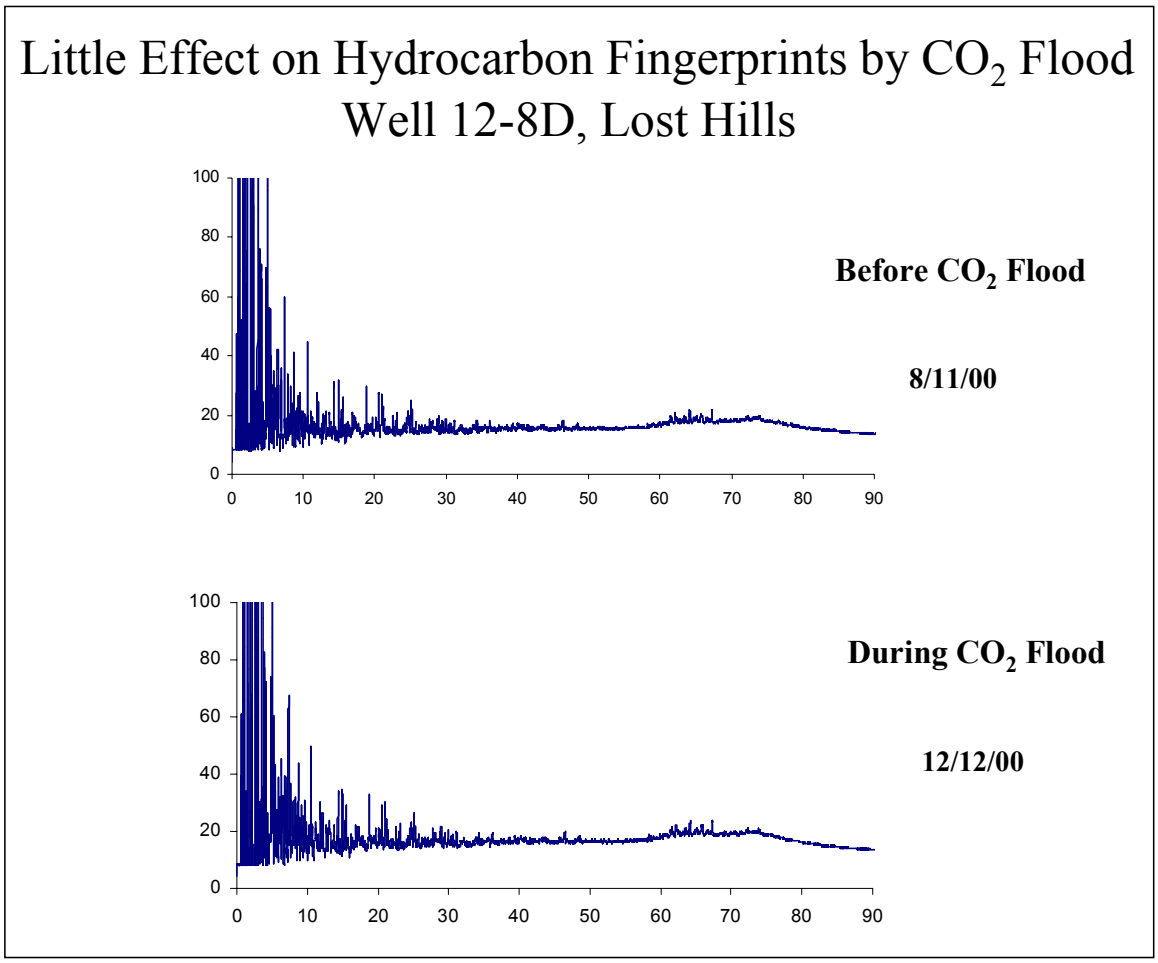

Figure 5.4-4. Hydrocarbon fingerprints are similar for the oils from well 12-8D, produced before and after the start of CO_2 flooding.

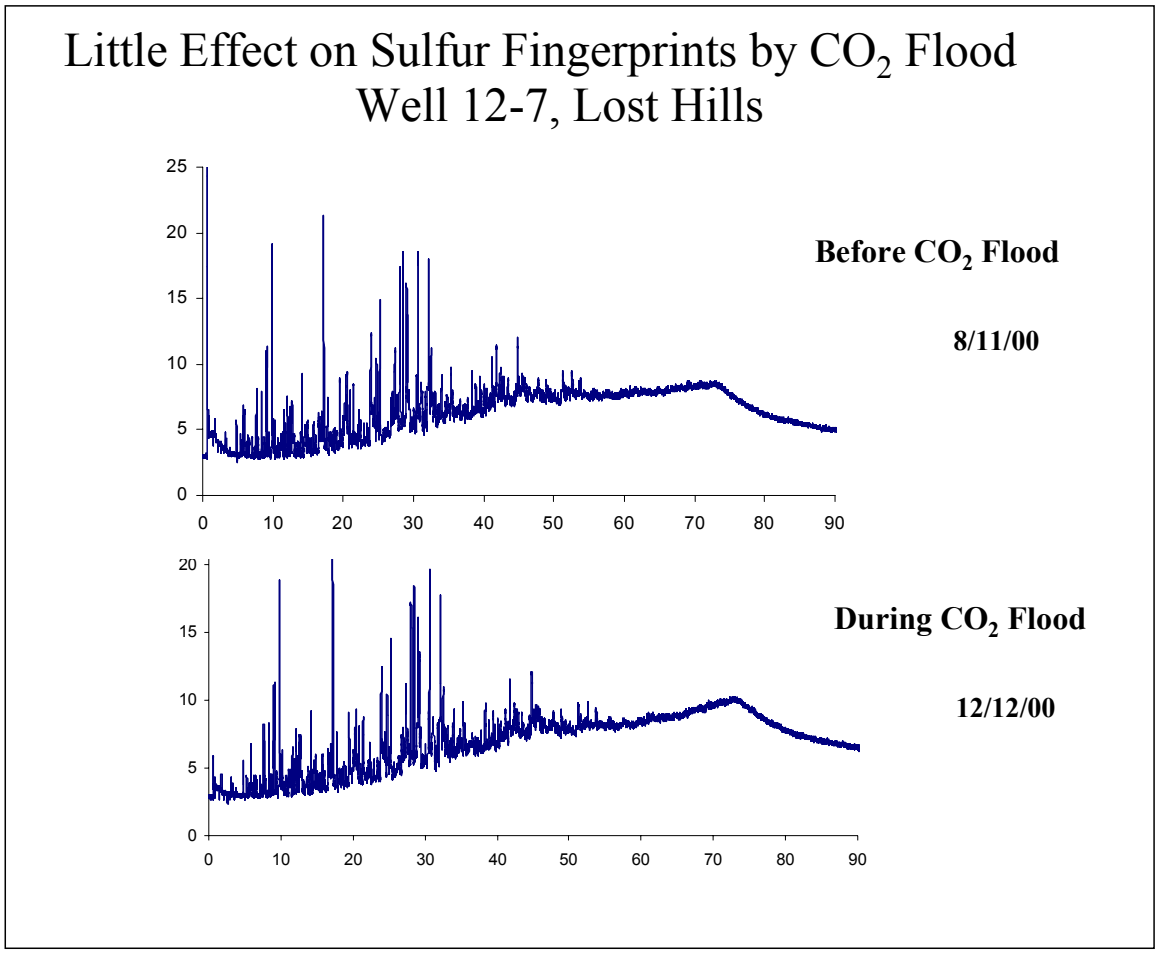

Figure 5.4-5. Sulfur fingerprints are highly similar for the oils from well 12-7, produced before and after the start of CO_2 flooding.

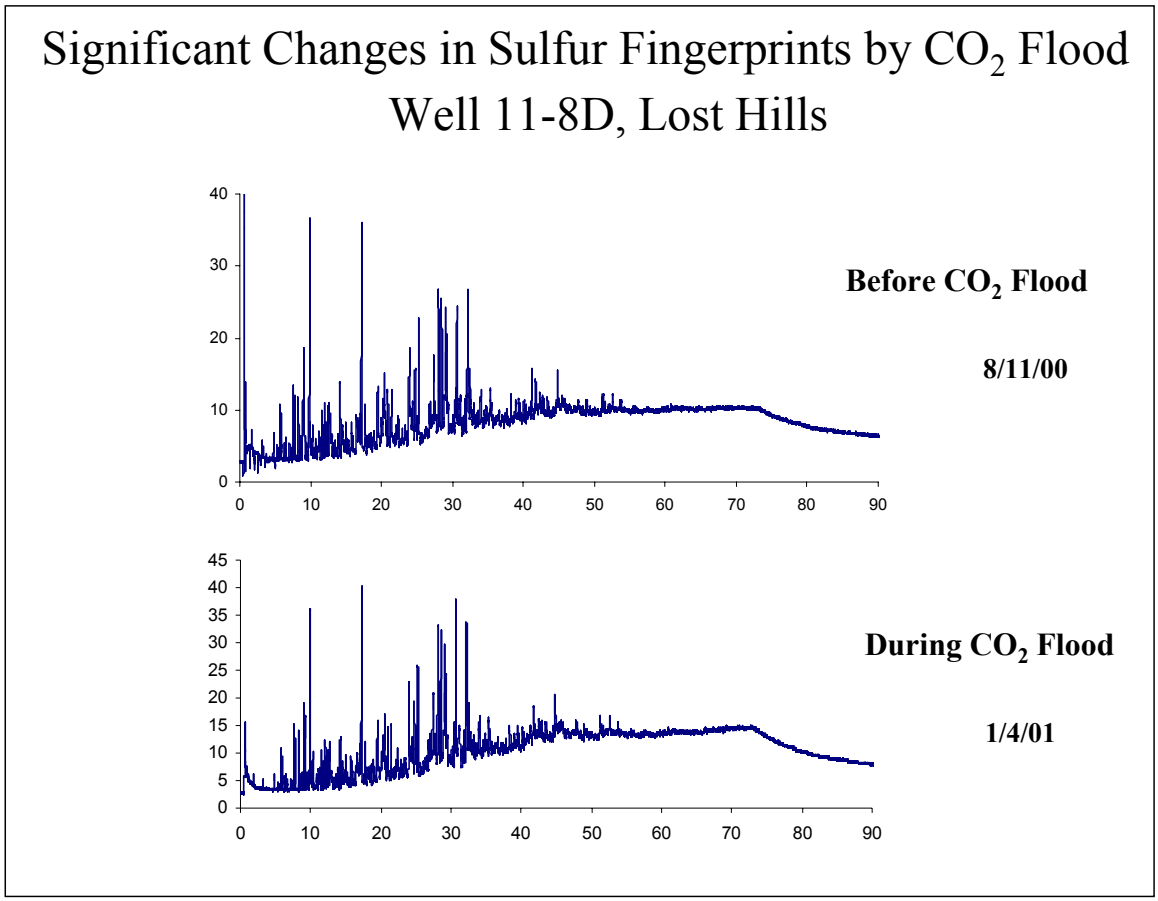

Figure 5.4-6. Sulfur fingerprints are significantly different for the oils from well 11-8D, produced before and after the start of CO_2 flooding.

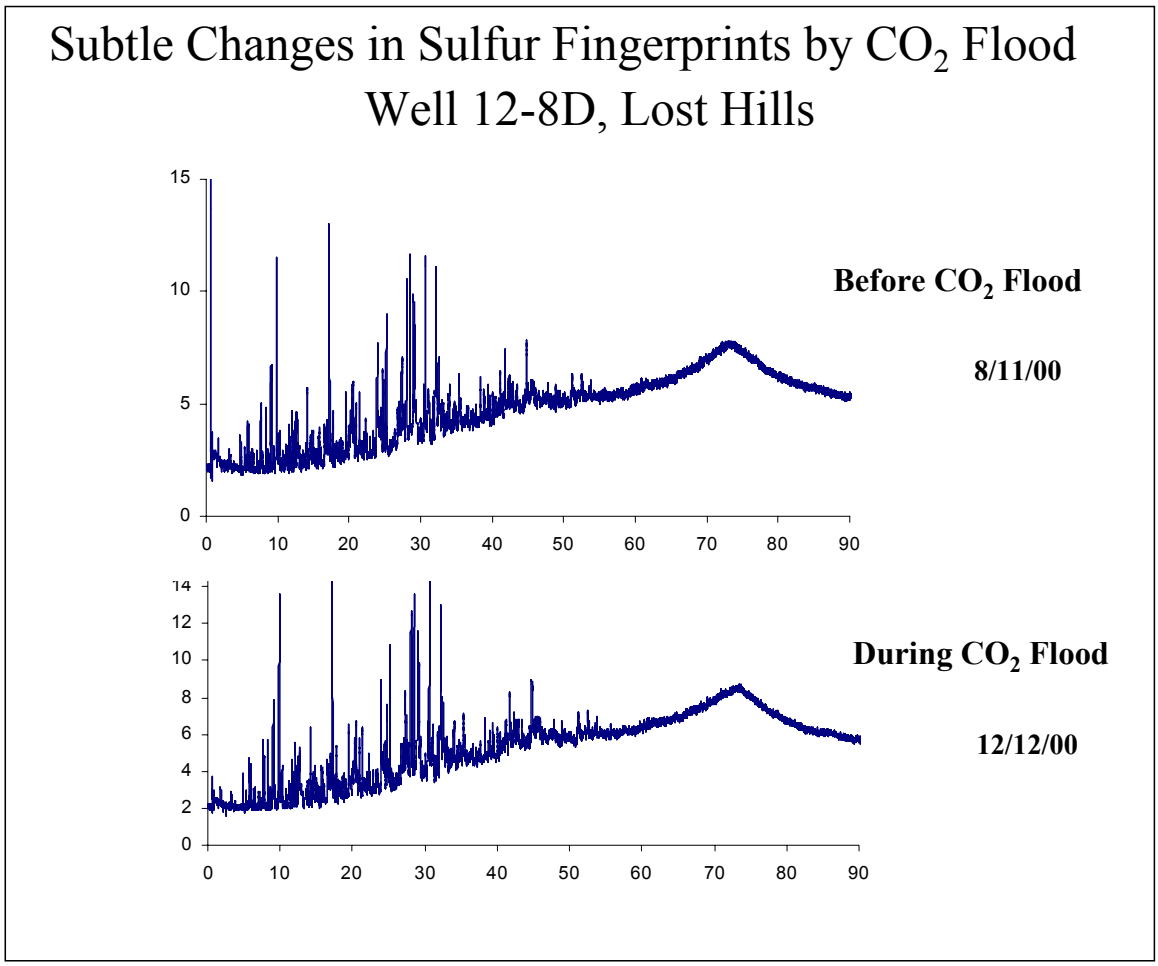

Figure 5.4-7. Sulfur fingerprints are slightly different for the oils from well 12-8D, produced before and after the start of CO_2 flooding.

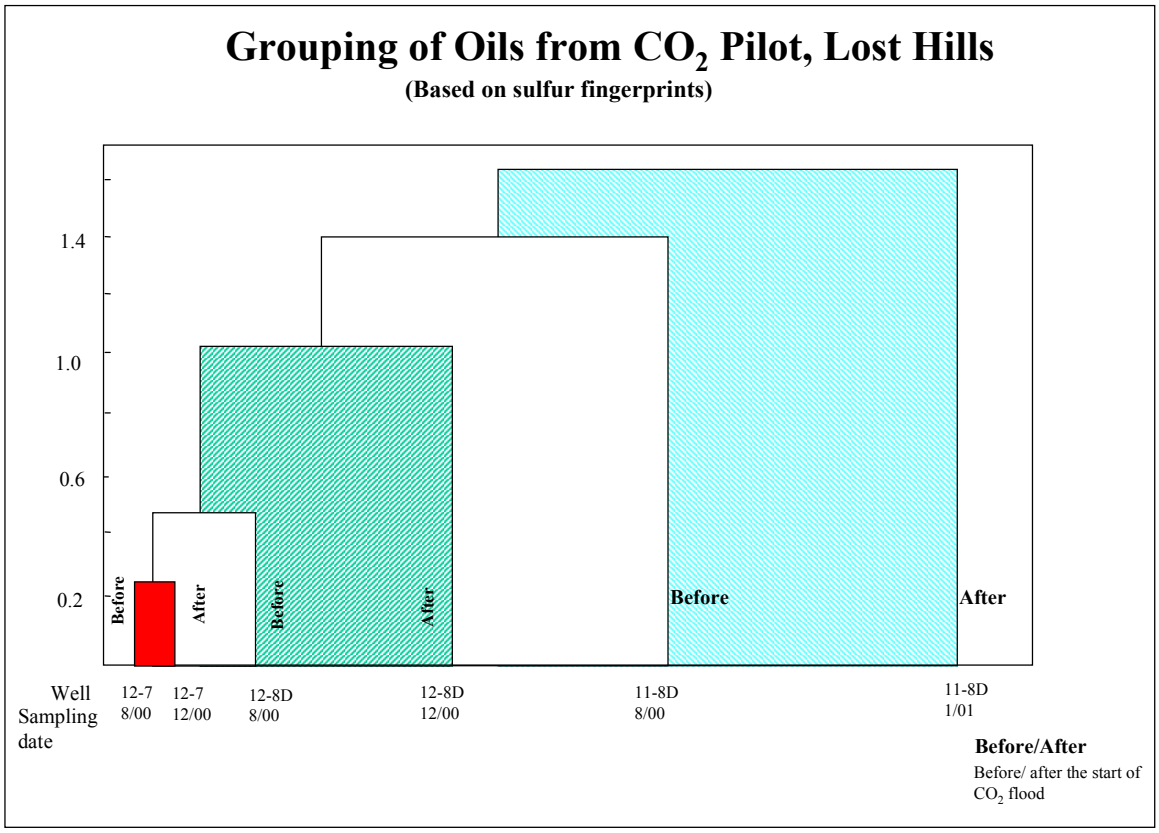

Figure 5.4-8. Cluster analysis showing the most significant changes for well 11-8D and moderate changes for well 12-8D in sulfur fingerprint after the start of CO_2 flood.

Table 5.4-1. Analysis of oils from CO_2 pilot area.

Table 1 Analyses of oils from Lost Hills (Pilot CO2 Flood)

CRC	Well	Sampling		API	Total Sulfur	Asphaltenes	Elemental
		Date	Time	Gravity	%	%	Sulfur
57422-1	11-8D	8/11/2000	9:45 AM	21.8	1.10	3.2	ND
57423-1	12-7	8/11/2000	11:00 AM	23.6	1.03	4.3	ND
57424-1	12-8D	8/11/2000	10:00 AM	23.1	1.00	3.3	ND
57422-2	11-8D	1/4/2001	7:40 AM	21.2	1.23	3.8	ND
57423-2	12-7	12/12/2000		23.7	0.94	3.1	ND
57424-2	12-8D	12/12/2000		22.4	1.04	2.7	ND
57422-3	11-8D	11/16/2001	9:20am	20.8	0.94	3.0	ND
57423-3	12-7	11/16/2001	9:00am	24.1	0.96	4.5	ND
57424-3	12-8D	11/16/2001	9:35am	22.8	1.04	3.2	ND

Wt % of Crude oils

ND, not detected; detection limit 10 ppm (GC-AED).

Table 5.4-2. Selected hydrocarbon peak ratios of oils from CO_2 pilot area.

CRC	Well	Sampling	Hydrocarbon Peak Ratios									
		Date	86/ 89	101/ 98	82/ 77	119/ 122	149/ 146	99/ 94	75/ 74	242/ 241	68/ 72	Avg. % Diff.
57422-1	11-8D	8/11/2000	2.066	1.28	1.067	2.399	0.972	2.096	1.167	1.14	0.73	
57422-2	11-8D	1/4/2001	2.556	1.341	1.156	2.828	1.082	2.685	1.414	1.281	0.729	
% Diff.			19.2%	4.5%	7.7%	15.2%	10.2%	21.9%	17.5%	11.0%	0.1%	11.9%
57423-1	12-7	8/11/2000	1.668	1.212	0.932	2.216	0.955	1.742	0.97	0.945	0.695	
57423-2	12-7	12/12/2000	1.665	1.211	0.928	2.202	0.957	1.754	0.969	0.952	0.695	
% Diff.			0.2%	0.1%	0.4%	0.6%	0.2%	0.7%	0.1%	0.7%	0.0%	0.3%
57424-1	12-8D	8/11/2000	1.719	1.191	0.92	2.213	0.971	1.822	0.992	1.068	0.732	
57424-2	12-8D	12/12/2000	1.726	1.192	0.92	2.212	0.967	1.859	1.027	1.039	0.74	
% Diff.			0.4%	0.1%	0.0%	0.0%	0.4%	2.0%	3.4%	2.8%	1.1%	1.1%

Table 5.4-3. Selected sulfur peak ratios of Lost Hills oils from the CO_2 pilot area.

CRC	Well	Sampling	Sulfur Peak Ratios										
		Date	135/ 130	64/ 67	125/ 123	136/ 140	92/ 96	65/ 66	208/ 205	116/ 119	57/ 56	183/ 185	Avg. % Diff.
57422-1	11-8D	8/11/2000	0.424	1.055	0.7	1.165	0.653	0.959	0.74	1.665	0.865	0.217	
57422-2	11-8D	1/4/2001	0.536	1.012	0.721	1.156	0.709	1.188	0.682	1.828	0.79	0.251	
% Diff.			20.9%	4.2%	2.9%	0.8%	7.9%	19.3%	8.5%	8.9%	9.5%	13.5%	9.6%
57423-1	12-7	8/11/2000	0.458	0.84	0.647	1.038	0.665	0.955	0.64	1.711	0.769	0.223	
57423-2	12-7	12/12/2000	0.461	0.841	0.641	1.002	0.661	0.995	0.645	1.71	0.762	0.225	
% Diff.			0.7%	0.1%	0.9%	3.6%	0.6%	4.0%	0.8%	0.1%	0.9%	0.9%	1.3%
57424-1	12-8D	8/11/2000	0.46	0.854	0.641	0.997	0.67	0.99	0.626	1.659	0.784	0.21	
57424-2	12-8D	12/12/2000	0.472	0.999	0.721	0.821	0.695	1.069	0.622	1.72	0.782	0.212	
% Diff.			2.5%	14.5%	11.1%	21.4%	3.6%	7.4%	0.6%	3.5%	0.3%	0.9%	6.6%

5.5 Stable Isotope Measurements of Gases from Lost Hills CO_2 Pilot

David R. Cole
Oak Ridge National Laboratory

Gas chromatograph-combustion-isotope ratio mass spectrometry (GC-C-IRMS) was used to characterize the isotopic and gas chemistry of gases from the Lost Hills CO_2 pilot (Figure 5.5-1). Carbon and oxygen isotopes were measured in the injection CO_2 (sampled 8/11/00), CO_2 from pre-injection "reservoir" gases (wells 11-8D, 12-8D, and 12-7 sampled 8/11/00), and the return CO_2 sampled in wells 11-8D (sampled 1/4/01; 12/20/01), 12-8D (sampled 12/6/00; 12/20/01), 12-7 (sampled 12/6/00; 12/20/01), 11-7B (sampled 12/20/01), 11-9J (sampled 12/20/01), and 12-8C (sampled 12/20/01). Carbon isotopes have also been measured in C_1-C_6 hydrocarbon gases. The initial injection CO_2 had a $\delta^{13}C$ (PDB) value of –30.1 ‰ and a $\delta^{18}O$ (VSMOW) value of –1.12 ‰. Gases sampled prior to injection were dominated by CH_4 with lesser amounts of CO_2 and subordinate amounts of C_2-C_6. The $\delta^{13}C$ (PDB) values for CH_4 in pre-injection and all return gases were very similar, ranging from –36 to –42 ‰, with an average of –40.4‰ (± 1.5‰ 1 σ).

The $\delta^{13}C$ (PDB) values for pre-injection CO_2 ranged from 15.6 to 18.5 ‰ whereas the return CO_2 gases from the first sampling effort (12/6/00 and 1/4/01) exhibited a narrow range of values, -27.5 to –29.9 ‰. Chemically, return gases from this first sampling effort were very rich in CO_2 and clearly have carbon isotope values very close to the injection CO_2. Interestingly, the percentages of injection CO_2 estimated from the isotopic data (using –30.1 ‰ as the injectate end member and 16.8 as the average "reservoir" gas end member) do not agree exactly with similar estimates based on gas chemistry (Figure 5.5-1). In all cases for this first sampling effort, the isotopic mixing model over-estimates the amount of injectate CO_2 compared to the gas chemistry model by 6 to 14 %. Assuming that the gas chemistry is a better measure of mixing, this means the isotopic values are somewhat more negative (by a few per mil) than simple binary mixing would predict. Pathways that might explain this include (1) loss of CO_2 to an aqueous phase, and/or (2) oxidation of hydrocarbons (CH_4, oil) to CO_2 either inorganically or microbially. The minor differences in predicted mixing percentages based on the isotope and chemical models indicate that these exchange mechanisms made only a minor contribution to the overall carbon isotope budget in the Lost Hills gases immediately after the first main CO_2 injection episode (terminated due to well sanding problems).

This is not true, however, for the gases sampled from all wells on 12/20/01 (Figure 5.5-1). Gas chemistries indicate that the amount of injectate CO_2 was less dominant than the previous sampling at the end of 2000. The data show a clear trend on the ternary plot of CO_2-CH4-Σ C_2-C_6 where samples collected on 12/20/01 fall on a line connecting the "reservoir" gases with gases collected at the end of 2000. Gases with the most amount of injectate CO_2 include 11-9J, 12-8C and 12-7 with $\delta^{13}C$ values of –20.5, -19.2 and –17.7 ‰, respectively. The remaining wells (11-8D, 12-8D, and 11-7B) have $\delta^{13}C$ values of –16, -10.3 and –1.9 ‰, respectively. Use of the same kinds of simple isotopic and chemical mixing models for these results indicates that the isotopic model over-estimates

the percentage of injectate CO_2 by between 8 and 20%. CO_2 injected since the sanding problem of 12/00 was carried out as two distinct pulses, one lasting from March to early May 2001 and a second lasting from September to November 2001 (personal communication, Mike Morea, ChevronTexaco).

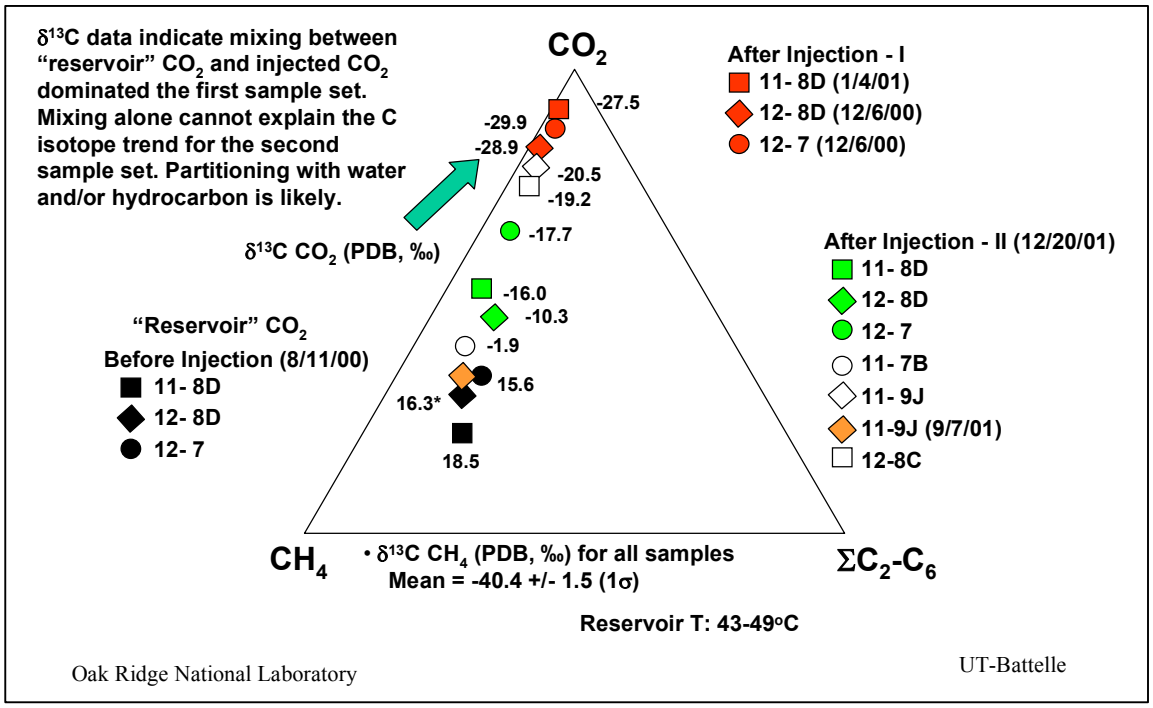

Figure 5.5-1. Chemical and carbon isotope data for wells sampled at Lost Hills, CA. The injection CO_2 had a $\delta^{13}C$ value of -30.1‰ and $\delta^{18}O$ value of -1.12 ‰.

Interspersed between these two CO_2 injection pulses was a period of water injection, which was also continued after the last CO_2 pulse in December 2001. The isotopic and chemical data indicate that this complex injection did not lead to a greater influx of CO_2 to the return wells, and in fact seems to indicate that the CO_2 may have had sufficient time to interact more extensively with water and/or hydrocarbons in the reservoir.

The $\delta^{18}O$ compositions of the pre-injection CO_2 ranged from about 16 to 24 ‰ (average ~20.9‰), whereas the return CO_2 gases from the first sampling effort were somewhat more enriched, ranging from approximately 29 to 34 ‰. Since these samples are dominated by injectate CO_2 (78-90%), this constitutes nearly a ~30‰ increase in $\delta^{18}O$ from the injection value of –1.1 ‰. Simple mixing of an isotopically light injectate and the heavy "reservoir" CO_2 cannot explain the even heavier $\delta^{18}O$ values measured in the three return wells. It is likely that the enrichment in ^{18}O is due to kinetically fast exchange of CO_2 with water encountered during migration. The oxygen isotope fractionation between CO_2 and water is ~37 ‰ at 45°C (a reasonable estimate of the subsurface reservoir temperature), so applying this number to the oxygen values measured for the return CO_2 yields $\delta^{18}O$ values for water of between –3 and –7 ‰. These values are generally consistent with numbers reported for ground waters in this part of California. The interaction of CO_2 with the water in the reservoir is also

consistent with the carbon isotope data that suggest possible loss of CO_2 to the aqueous phase as one mechanism to produce isotopic values somewhat more negative than the chemical mixing models predict.

5.6 Injection Profile Monitoring Results

Michael Morea
ChevronTexaco Exploration and Production Company

Injection profiles were run in all four injectors to determine if there was any change in vertical conformance of CO_2. An "excellent" profile would be one that had CO_2 exiting all the perforations in equal amounts. A "poor" injection profile would be one that had uneven distribution or portions of the wellbore receiving no CO_2. While injection profiles indicate where CO_2 is exiting the wellbore, the profiles do not show how far it migrates into the reservoir or the path it may take once in the reservoir.

Figures 5.6-1 through 4 show the injection profiles for the four injectors in the CO_2 pilot. The figures illustrate the following curve tracks, starting from the left: (1) percent water injection (0-50%, in blue); percent CO_2 injection (0-50%, pink); (2) completion interval; (3) percent clay, silt/sand, biogenic silica (0-100%); (4) depth and markers; and (5) deep resistivity (1-10 ohm-m). The leftmost water injection profile represents the pre-CO_2 injection baseline survey. The most recent profiles are on the right side of the injection profile track. Wells 12-7W and 12-8W (Figures 5.6-1 and 2) are hydraulically propped fractured with more extensive, evenly (linear) spaced wellbore perforations, whereas wells 11-8WR and 11-8WAR (Figures 5.6-3 and 4) are hydraulically propped fractured with limited (clustered) perforations.

12-7W has the best injection profile (Figure 5.6-1). This well was part of the CO_2 injection test that was performed in 1999 prior to the pilot. 12-7W clearly shows that CO_2 was providing better vertical coverage than water early in the project but has deteriorated over time. Also CO_2 has a slight preference for the sandy diatomite (higher permeability). The poorer injection profiles in the other wells (Figures 5.6 2-4) could be due to many reasons, such as blocked perforations, preference for lower pressure zones, or poor hydraulic fractures. Wells 12-8W (Figure 5.6-2) and 11-8WR (Figure 5.6-3) have poor injection profiles with most of the CO_2 exiting the upper perforations. 11-8WR has 65% of the CO_2 exiting out of the top perforations.

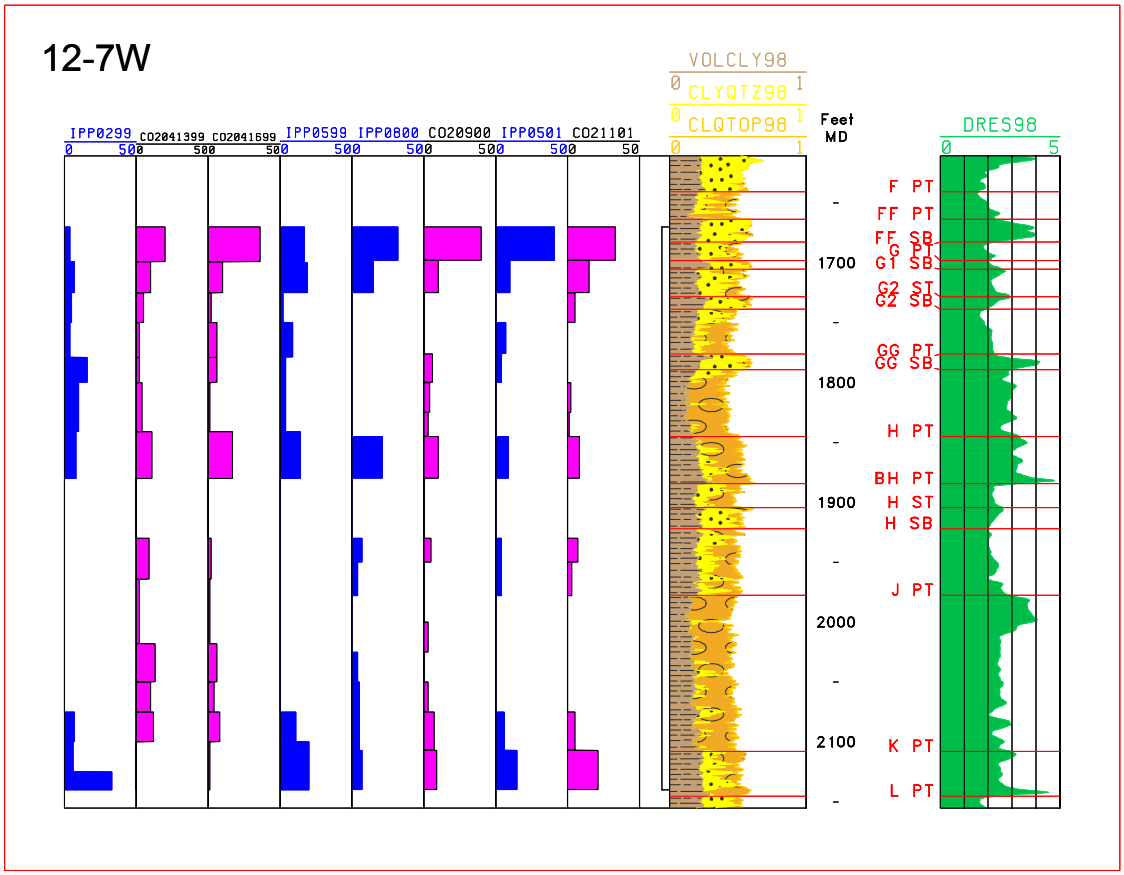

Figure 5.6-1. Injectivity profiles of 12-7W. Profiles were run in February 1999 (H_2O), April 1999 (CO_2 low rate), April 1999 (CO_2 high rate), May 1999 (H_2O), August 2000 (H_2O), September 2000 (CO_2), May 2001 (H_2O), and November 2001 (CO_2). 12-7W was the injector used in the 1999 injectivity test. Initial CO_2 profiles show fairly good vertical coverage, whereas the latest profile indicates a slight decrease in coverage. Profiles show injected water and CO_2 to have a slight preference for the sandy diatomites. This is the best profile of all 4 pilot injectors. See text for description of log curves.

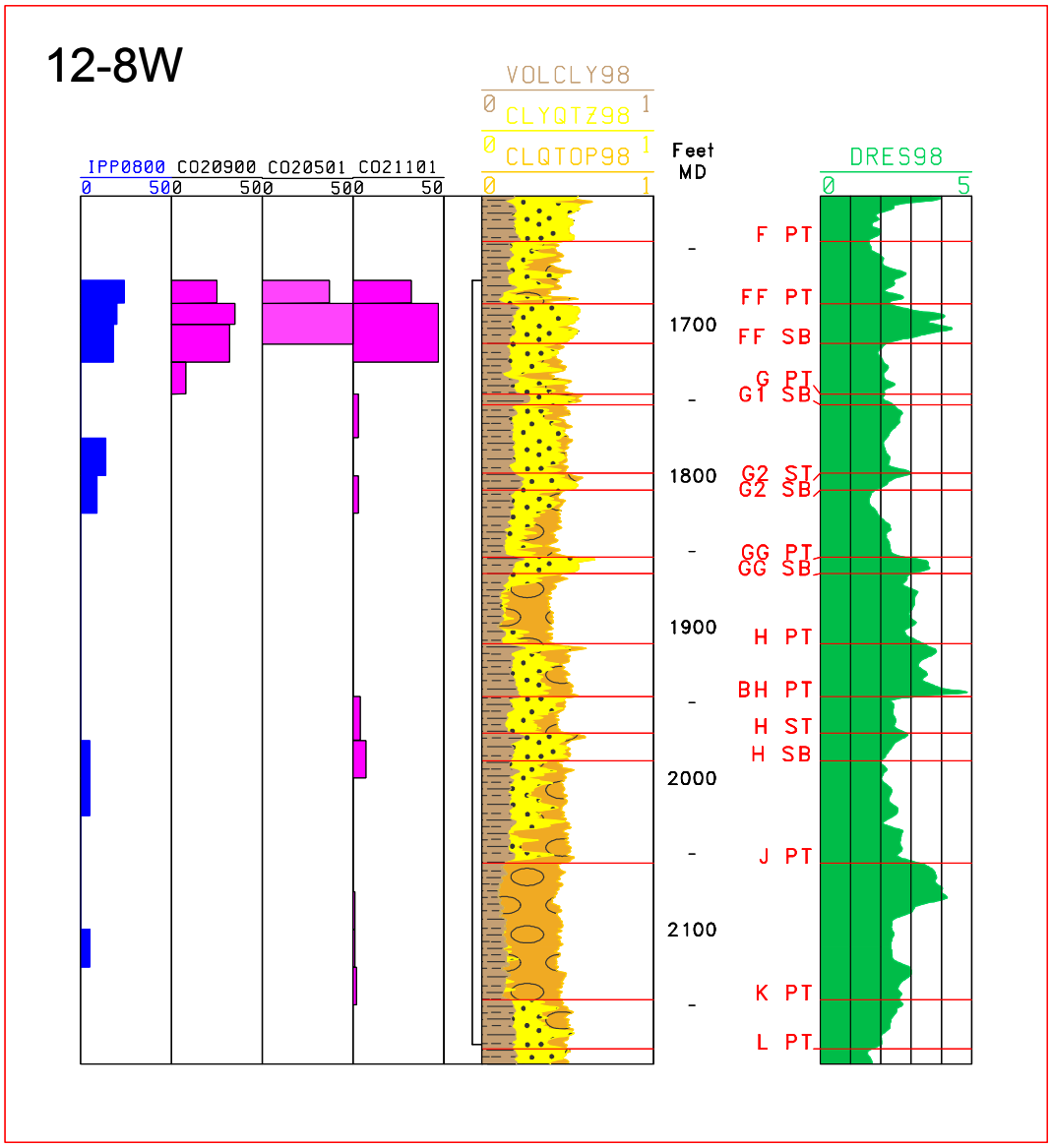

Figure 5.6-2. Injectivity profiles of 12-8W. Profiles were run in August 2000 (H_2O), September 2000 (CO_2), May 2001 (CO_2), and November 2001 (CO_2). 12-8W has a poor profile that shows most of the CO_2 exiting the upper perforations were there is lower reservoir pressure. While most of the CO_2 is entering sandy diatomites, some is also entering lower permeability diatomite. See text for description of log curves.

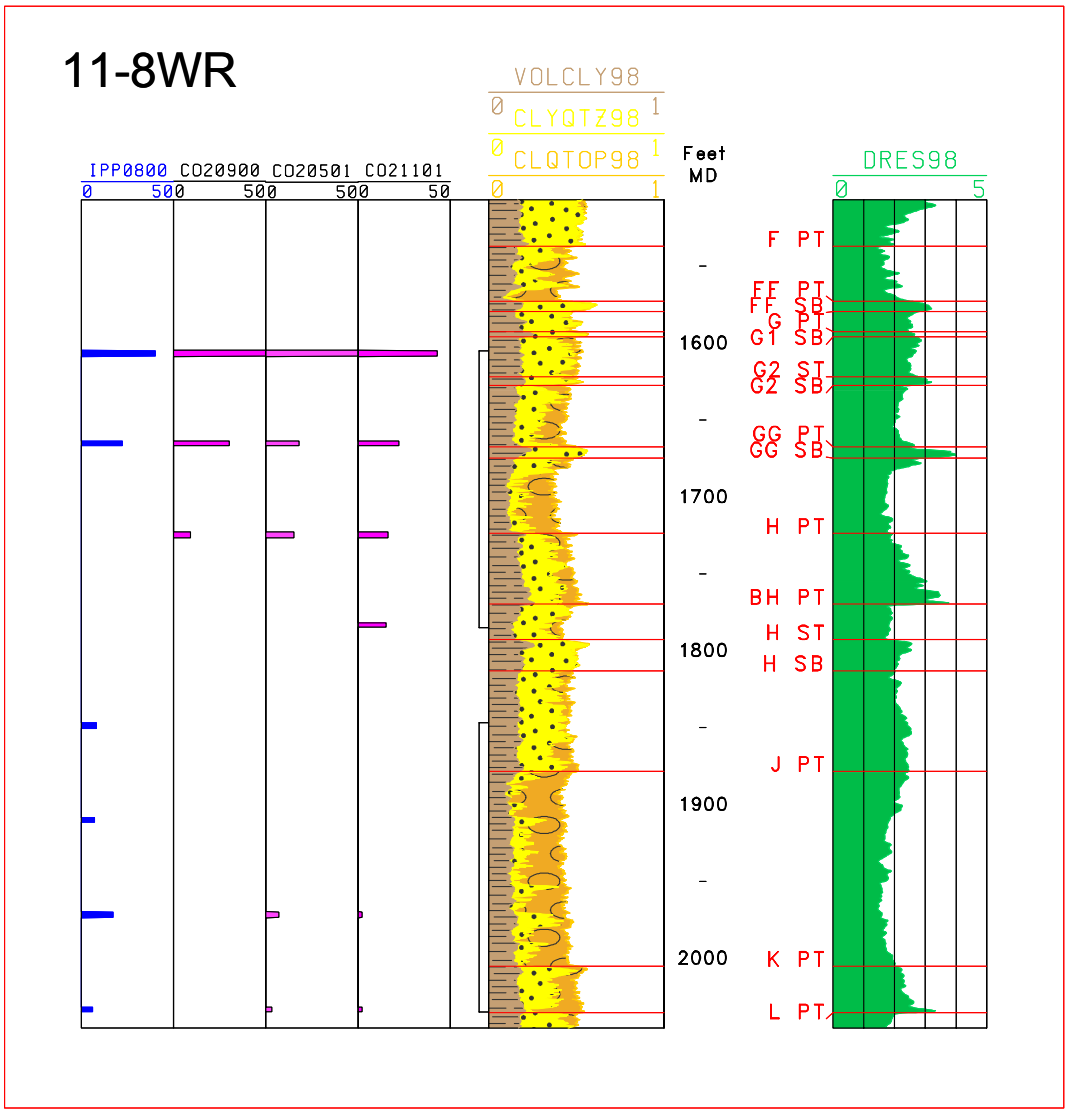

Figure 5.6-3. Injectivity profiles of 11-8WR. Profiles were run in August 2000 (H_2O), September 2000 (CO_2), May 2001 (CO_2), and November 2001 (CO_2). 11-8WR has most of the CO_2 exiting out of the top perforations. See text for description of log curves.

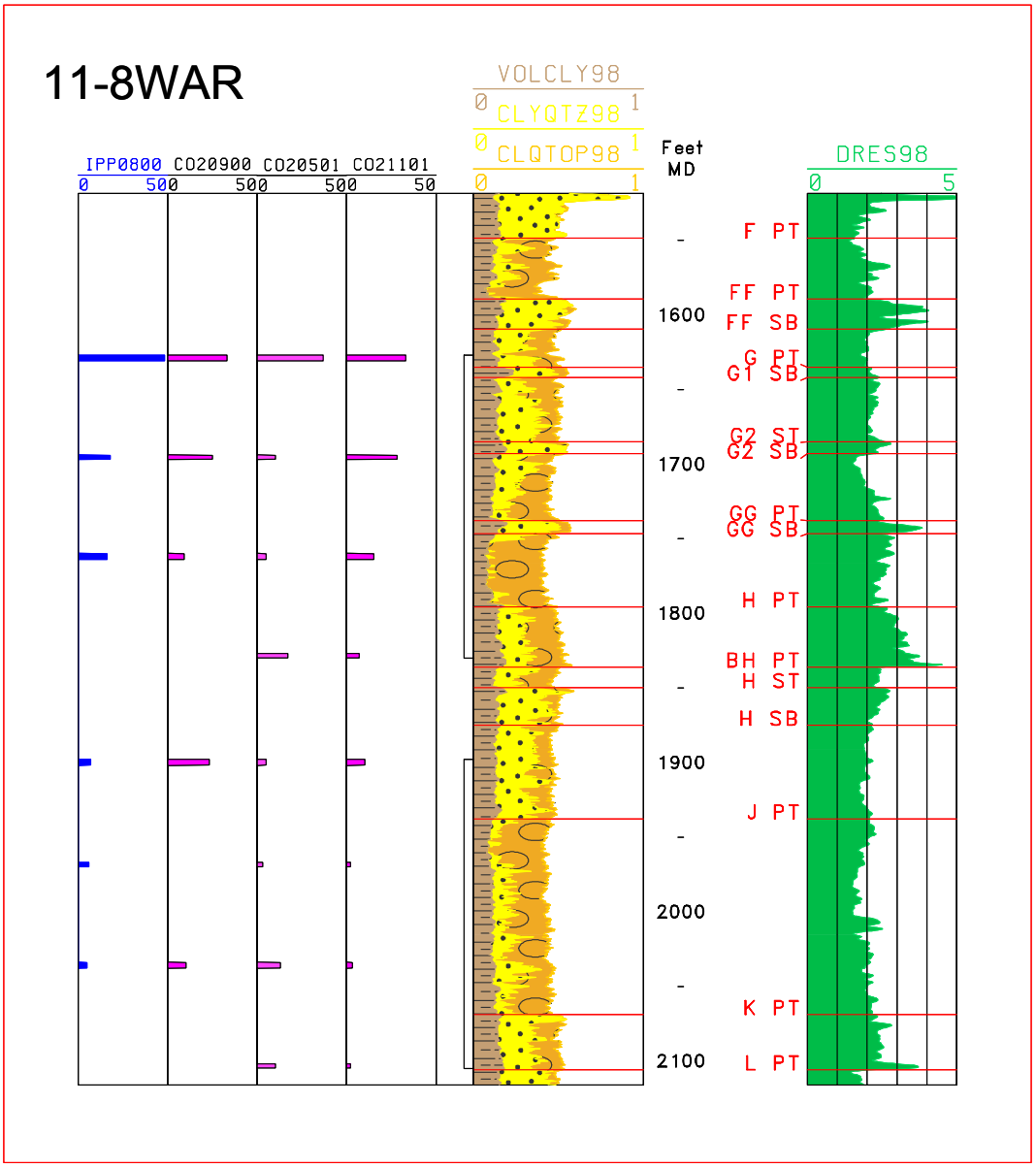

Figure 5.6-4. Injectivity profiles of 11-8WAR. Profiles were run in August 2000 (H_2O), September 2000 (CO_2), May 2001 (CO_2), and November 2001. Like 11-8WR, 11-8WAR was clustered perforated and hydraulically fractured in two stages but shows a better profile. It also is more comparable to the baseline water injection survey. See text for description of log curves.

5.7 Cased Hole Monitor Logging

Michael F. Morea
ChevronTexaco Exploration and Production Company

Gamma ray/resistivity/neutron logs were run in fiberglass-cased, observation wells OB-C1 and OB-C2 in November 2001 to monitor hydrocarbon saturation changes over time. Baseline logs were originally acquired prior to CO_2 start-up in September 2000, and then re-acquired in December 2000. Both observation wells are less than 50 feet from CO_2 injector 11-8WR (Figure 5.7-1). The CO_2 injection interval extends from the FF marker to the L marker (~1500 to 2050 feet). However, the producing interval extends from the C marker to 150 ft. below the L marker (Figure 5.7-2).

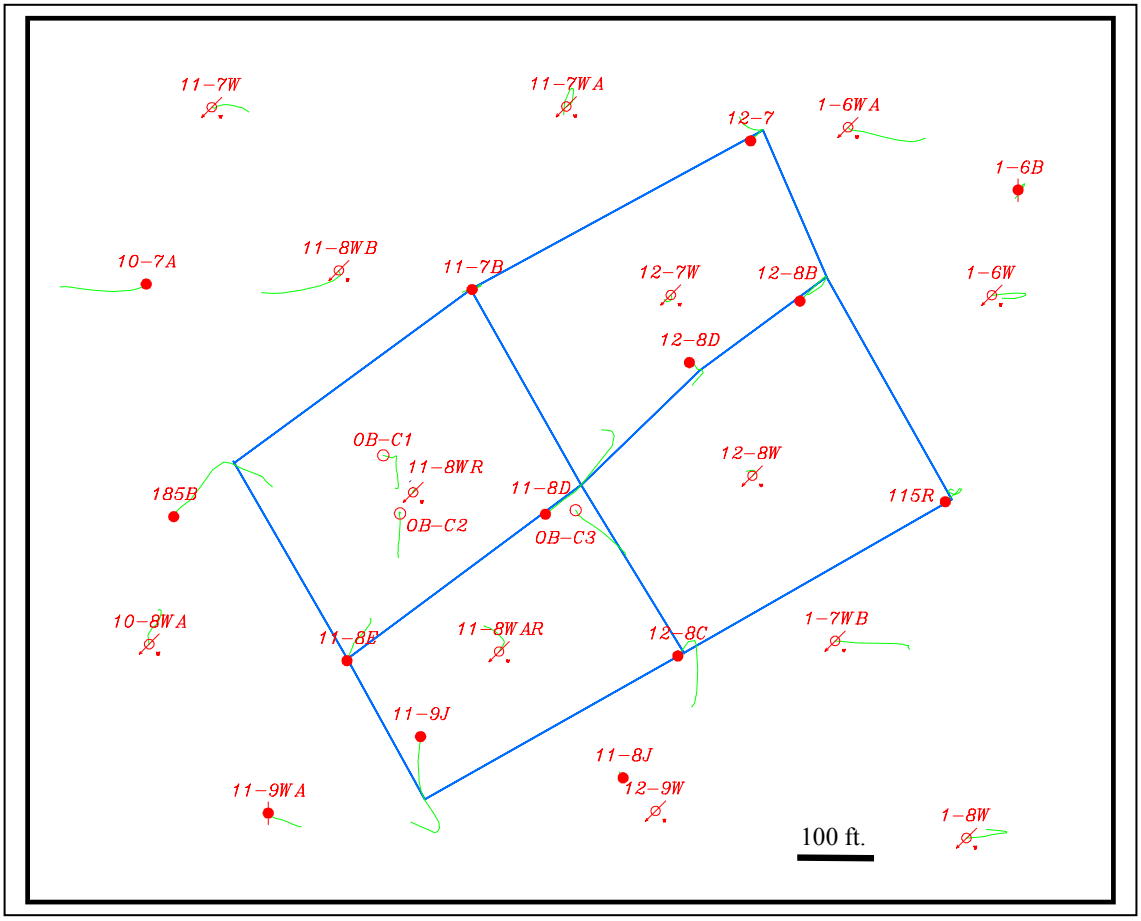

Figure 5.7-1. CO_2 pilot map and location of observation wells OB-C1, OB-C2, and injector 11-8WR.

Figures 5.7-3 and 4 are log plots illustrating the changes in log response over time in the two observation wells, OB-C1 and OB-C2. The tracks are, from left to right:

1. Gamma ray – baseline (pre-September 2000), December 2000, and November 2001
2. Deep resistivity – baseline (pre-September 2000), December 2000, and November 2001
3. Neutron/density – baseline (pre-September 2000)
4. Baseline saturation (pre-September 2000) – water, oil, gas
5. Lithologic components – clay, sand, biogenic silica (opal-A)
6. Resistivity difference log – baseline (pre-September 2000) and December 2000
7. Resistivity difference log – December 2000 and November 2001
8. Cumulative resistivity difference log – baseline (pre-September 2000) and November 2001
9. Hydrocarbon saturation – baseline and November 2001

Tracks 6 – 8 show the difference measured between an earlier logging run and a later one. Thus the curve values to the left of the centerline indicate a decrease in resistivity over time, and those changes to the right of the centerline indicate an increase in resistivity over time. The scale for tracks 6 – 8 is –1.0 to +1.0 ohm-m. The scale for track 9 is 0 – 0.75 hydrocarbon saturation units.

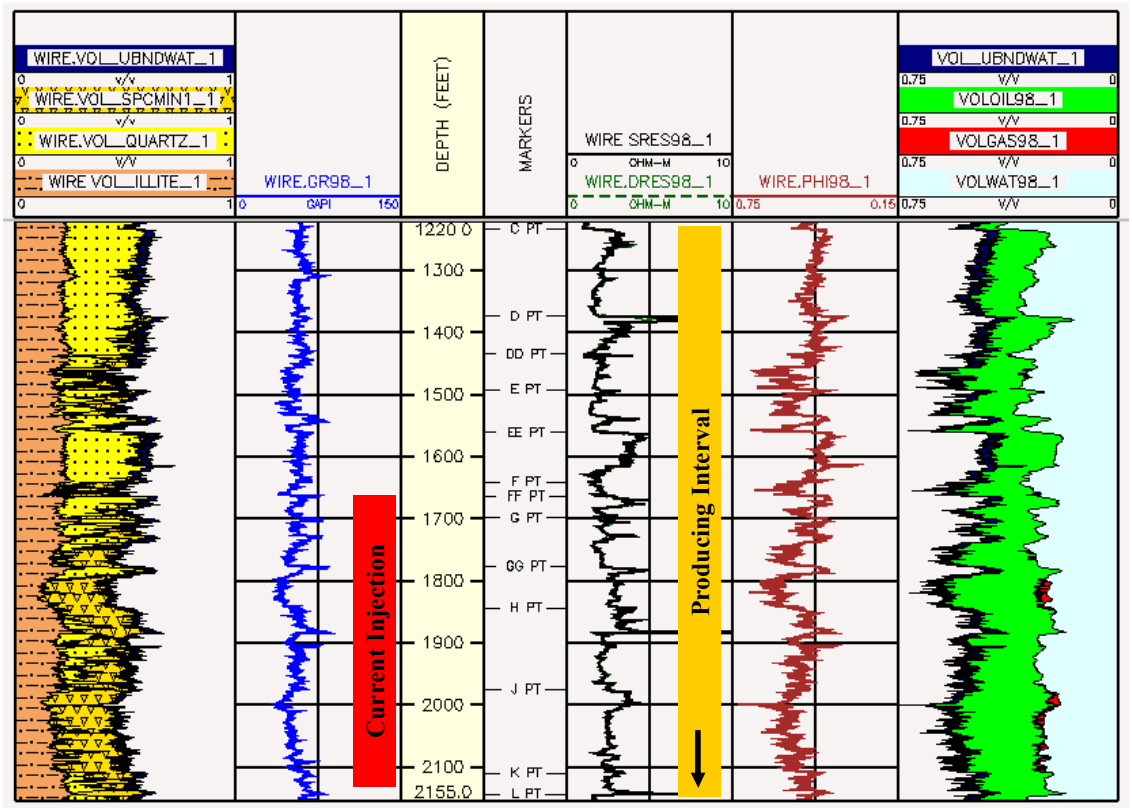

Figure 5.7-2. Comparison of the injection interval (FF Pt. – L Pt.) with the producing interval (C – L Pt.).

Observation well OB-C1 (Figure 5.7-3) shows a noticeable decrease in hydrocarbon saturation at depths 1180 – 1260 ft. (C interval; sandy diatomite) and at 1670 – 1725 ft. (GG interval; clean

diatomites). All the rest of the diatomite reservoir in OB-C1 shows no change or shows an increase in hydrocarbon saturation.

Observation well OB-C2 (Figure 5.7-4) shows a noticeable decrease in hydrocarbon saturation at depths 1390 – 1600 ft. (E – G interval; clayey and sandy diatomites) and at 1930 – 2035 ft. (J – L interval; clean and clayey diatomites). All the rest of the diatomite reservoir in OB-C2 shows no change or shows a slight decrease in hydrocarbon saturation.

Figures 5.7-3 and 4 show that there are both increases and decreases of resistivity and hydrocarbon saturation in the two observation wells over time. These changes are not limited only to the higher permeability lithologies (sandy diatomites). A decrease in resistivity and hydrocarbon saturation indicates CO_2 is flushing oil from the reservoir near the observation wells. Increase in hydrocarbon saturation is interpreted as the result of oil being banked toward the observation wells. The logs show CO_2 migrating in discrete beds of 5 feet or less in thickness, and CO_2 has reached OB-C2 first. Also it appears that CO_2 is migrating above the injection interval as evidenced by hydrocarbon saturation changes in that part of the reservoir. This could be the result of CO_2 channeling through fractures in the reservoir near the injector.

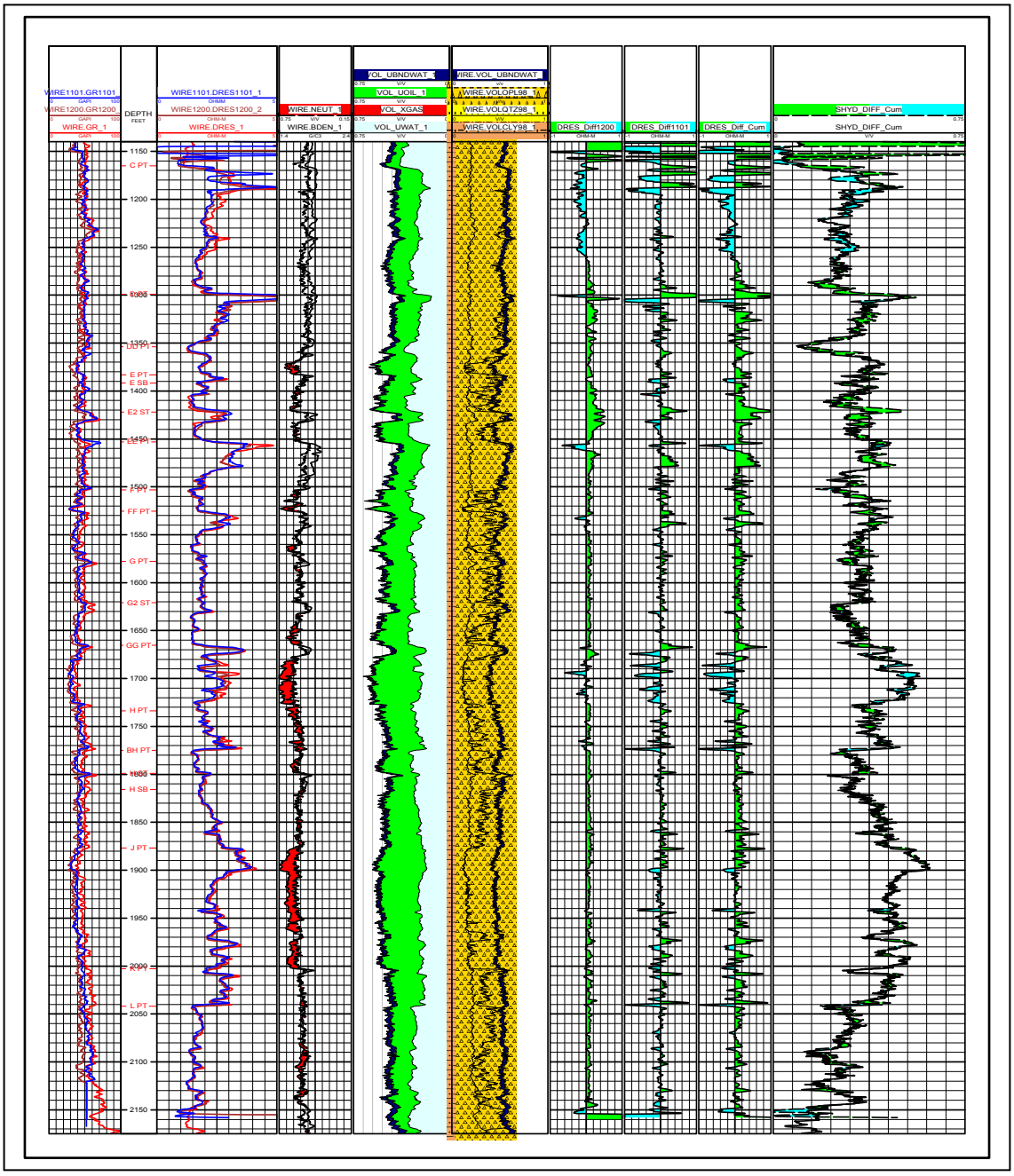

Figure 5.7-3. Reservoir monitoring logging of fiberglass-cased OB-C1.

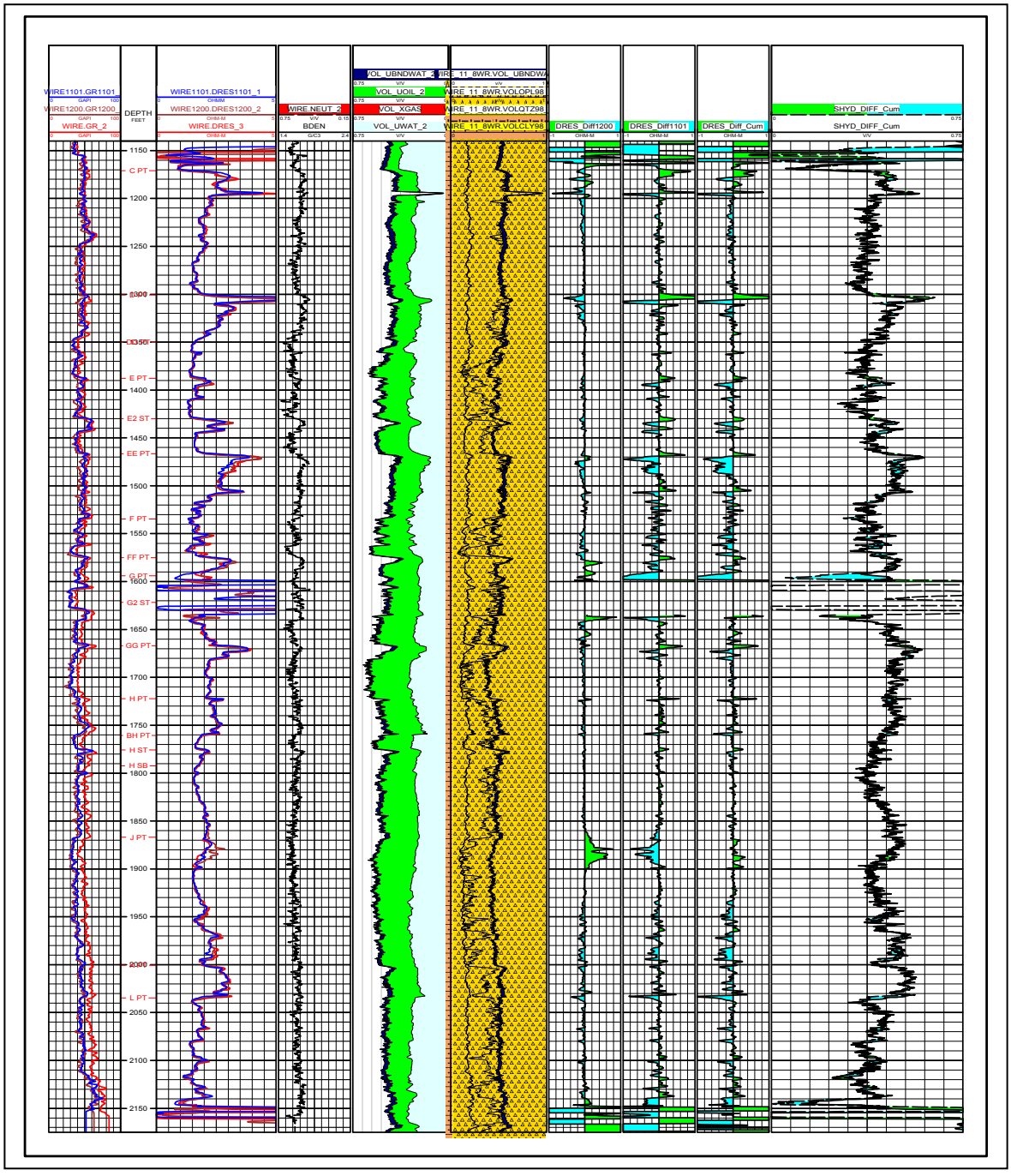

Figure 5.7-4. Reservoir monitoring logging of fiberglass-cased OB-C2. The interval 1600 – 1635 feet has a steel patch in the casing.

5.8 Cross Well Seismic Studies

Roland Gritto
Lawrence Berkeley National Laboratory

A series of time-lapse seismic cross well and single well experiments were conducted to monitor the injection of CO_2 into a hydrofracture zone, based on P- and S-wave data. A high-frequency piezo-electric P-wave source and an orbital-vibrator S-wave source were used to generate waves that were recorded by hydrophones as well as three-component geophones. During the first phase the set of seismic experiments were conducted after the injection of water into the hydrofracture zone. The set of seismic experiments were repeated after a time period of 7 months during which CO_2 was injected into the hydrofractured zone. The questions to be answered ranged from the detectibility of the geologic structure in the diatomite reservoir to the detectibility of CO_2 within the hydrofracture. Furthermore it was intended to determine which experiment (cross well or single well) is best suited to resolve these features.

During the injection experiment, the P-wave velocities exhibited relatively low values between 1700-1900 m/s, which decreased to 1600-1800 m/s during the post-injection phase (-5%). The analysis of the pre-injection S-wave data revealed slow S-wave velocities between 600-800 m/s, while the post-injection data revealed velocities between 500-700 m/s (-6%). These velocity estimates produced high Poisson ratios between 0.36 and 0.46 for this highly porous (~ 50%) material. Differencing post- and pre-injection data revealed an increase in Poisson Ratio of up to 5%. Both velocity and Poisson estimates indicate the dissolution of CO_2 in the liquid phase of the reservoir accompanied by a pore-pressure increase.

The single well data supported the findings of the cross well experiments. P- and S-wave velocities as well as Poisson ratios were comparable to the estimates of the cross well data.

The cross well experiment did not detect the presence of the hydrofracture but appeared to be sensitive to overall changes in the reservoir and possibly the presence of a fault. In contrast, the single well reflection data revealed an arrival that could indicate the presence of the hydrofracture between the source and receiver wells, while it did not detect the presence of the fault, possibly due to out of plane reflections.

5.9 Fluid Saturation and Pressure Prediction in a Multi-Component Reservoir by Combined Seismic and Electromagnetic Imaging

G. Michael Hoversten, Roland Gritto, and Tom Daley
Lawrence Berkeley National Laboratory
John Washbourne
TomoSeis Inc.

Summary:
The quantitative estimation of changes in water saturation (S_w) and effective pressure (P) in terms of changes in compressional and shear impedance is becoming routine in the interpretations of time-lapse surface seismic data. However, when the number of reservoir constituents increases to include in situ gas and injected CO_2 there are too many parameters to be determined from seismic velocities or impedances alone. In such situations the incorporation of electromagnetic (EM) images of the change of electrical conductivity (σ) provides essential independent information. The purpose of this study was to demonstrate a methodology for jointly interpreting cross well seismic and EM data in conjunction with detailed constitutive relations between geophysical and reservoir parameters to quantitatively predict changes in P, S_w, gas saturation (S_g) and gas/oil ratio (R_g) in a reservoir undergoing CO_2 flood.

Introduction:
Crosswell seismic and EM technology has been developed over the past two decades to provide high spatial resolution images of the compressional velocity (V_p), shear velocity (V_s) and the σ of the inter-well region. The majority of effort, as measured by the topics of published and presented work, has concentrated on developing and improving algorithms for estimating the geophysical parameters themselves. In most reported applications the output from a survey is a cross section of V_p, V_s or σ or the time-lapse change (Δ) of these parameters, which is discussed in terms of its implications for the distribution and/or Δ of the reservoir parameter of interest. These interpretations are qualitative and can be in error when more than one reservoir parameter effects the geophysical parameter.

Simple regression fits between V_p and S_w, for example, can be used to convert from geophysical to reservoir parameters. This approach can be used successfully in relatively simple environments with a minimum of fluid components. However, in many settings the geophysical parameters depend on many reservoir parameters that are variable in both space and time. In particular ϕ, P, S_w and S_g strongly influence V_p. σ can generally be described as a function of ϕ, S_w and fluid σ (Archie, 1942). As we will show in a multi-component fluid reservoir the spatial distribution of the time-lapse change in geophysical parameters, such as V_p, can vary significantly from the spatial distribution of the time-lapse change in a desired reservoir parameter such as S_g. This is due to the geophysical parameters dependence on other parameters such as P and S_w that must be sorted out before a picture of any single reservoir parameter can be obtained.

The objective of the work described in this paper is to demonstrate a methodology of combining time-lapse changes in σ, V_p and V_s with a detailed rock properties model to produce quantitative estimates of the change in fluid saturations (including oil, water and gas) and reservoir pressure.

Experiment Description:
Crosswell seismic and EM measurements were conducted in the Lost Hills oil field in southern California during a CO_2 injection pilot study conducted by Chevron USA Production Co. The pressure and temperature of the reservoir make this an immiscible flood; CO_2 is in the gas phase within the reservoir. The experiment took place in a portion of the field that had been undergoing water flood since 1995. Figure 5.9-1 shows the placement of relevant wells and estimated hydraulic fracture locations.

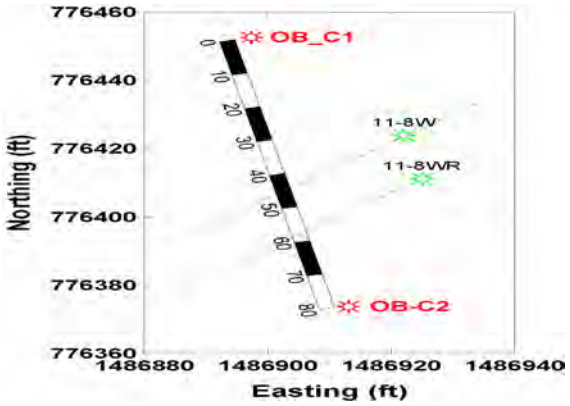

Figure 5.9-1: Plan view of observation wells OB-C1 and OB-C2 with old water injector 11-8W and new CO_2 injector 11-8WR. Estimated hydraulic fracture locations are shown as black lines.

The observation wells, OB-C1 and OB-C2, were drilled for the pilot and fiberglass cased to allow the use of crosswell EM. The nearby CO_2 injector (11-8WR) is located just 20 feet out of the crosswell-imaging plane. The injection wells are hydraulically fractured to increase injectivity into the low permeability Diatomite reservoir. In some cases down hole pressures were increased above the lithostatic pressure, which may have induced fracturing above the desired injection interval. If the fracture did indeed extend above the desired interval there is a high probability that much of the injected CO_2 will not sweep its intended target but will move in the higher section.

The base line crosswell seismic and EM surveys were conducted in September 2000 just prior to the beginning of CO_2 injection. Two seismic sources were used; a piezoelectric V_p source and an orbital vibrator V_s source with maximum frequency contents of 2000 and 350 Hz respectively. A repeat seismic survey was conducted in late May 2001 with the repeat EM survey conducted in early July 2001.

A Rock Properties Model:

The reservoir parameters that have a dominant affect on the geophysical parameters are ϕ, P, S_w and S_g. Effective pressure, P, is equal to lithostatic minus pore pressure (P_{pore}). So as P_{pore} increases, P will decrease. Pressure has a significant effect in Lost Hills since this is a shallow reservoir in soft rock. We sought constituative relations between geophysical and reservoir parameters (rock properties model) that would be able to predict observed V_p, density and σ from observed P, ϕ, S_w and S_g. Laboratory measurements of the dry frame moduli and grain density of the diatomite reservoir rock were unavailable so Hertz-Mindlin theory with the modified Hashin-Strikman lower bound (Hashin & Shtrikman, 1963) was used to model the dry frame moduli of the reservoir rock. Fluid substitution in the dry frame is modeled by Gassmann's equation. The bulk modului and densities of gas, live oil and brine as well as the gas/oil ratio (R_g) are modeled using relations published by Betzel and Wang (1992). The bulk σ of the reservoir rock is modeled using Archie's (1942) relationship.

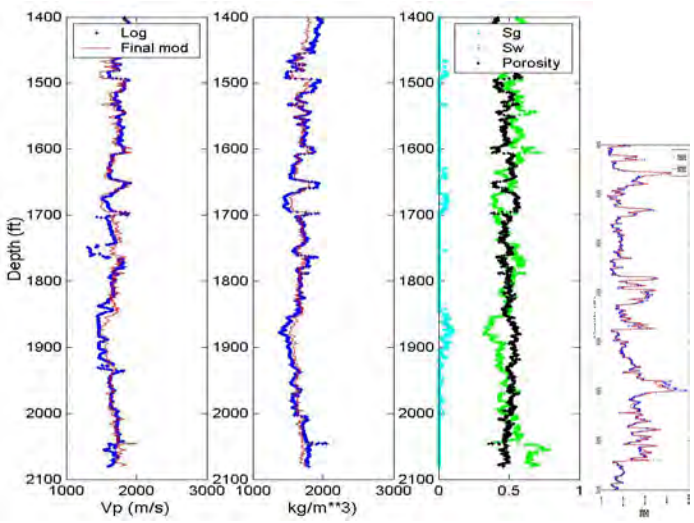

Figure 5.9-2: Rock properties model uses logged porosity (black), water saturation (green) and gas saturation (light blue) as inputs in a multi-parameter simplex regression to predict the V_p (left panel), density (second from left panel) and electrical resistivity (right panel). Measured V_p, density and resistivity are shown in blue, model predicted values shown in red.

A simplex algorithm was used to solve for the model parameters that would minimize the combined miss-fit between observed V_p and density logs and the model predictions given the ϕ, S_w and S_g logs. Because the wells did not have full logging suites a nearby well with a full suite of logs was used. The results of this minimization along with the Archie's law fit to the OB-C1 σ log are shown in Figure 5.9-2.

The pressure prediction capability of the model was validated by comparison to measurements made by Wang (2001) on core samples of diatomite from the Lost Hills field. Figure 5.9-3 presents the measured data recast as ΔV_p as a function of ΔP about a reference pressure of 4.7 MPa, the effective pressure in the reservoir at the start of CO_2 injection.

For expected decreases in pressure in the range 0 to 2.5 MPa from the initial pressure the model predictions are within a few percent of the lab measurements for vertical V_p.

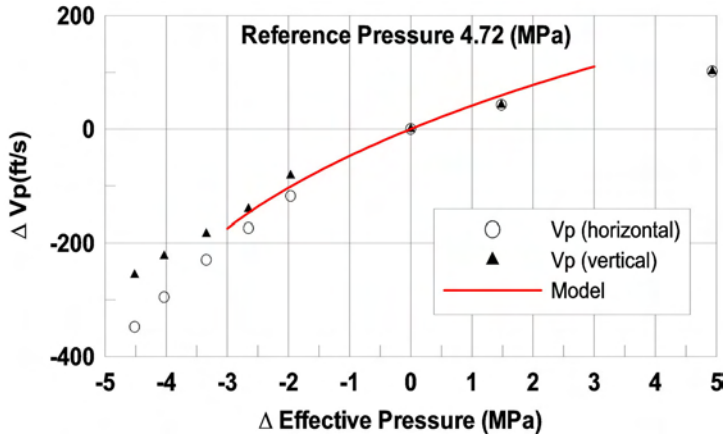

Figure 5.9-3: Predicted V_p change as a function of change in effective pressure compared to laboratory measurements on Lost Hills diatomite core samples.

The rock properties model is used to calculate changes in V_p, V_s and σ as functions of changes in P, S_w, S_g and S_{CO2} when certain reference values of P, ϕ, S_w and S_g are assumed. Figure 5.9-4 shows ΔV_p and ΔV_s as functions of ΔP and ΔS_w about a reference point (reservoir just prior to CO_2 injection) where S_w, S_g, ϕ and P and equal 0.5, 0.0, 0.5 and 4.7 (MPa) respectively. Relations between ΔV_p and ΔV_s and ΔP and ΔS_w such as illustrated in Figure 4 form the basis of 4D seismic ΔP and ΔS_w prediction. However, when S_g is non-zero as shown in Figure 5.9-5, the orientation and magnitude of contours of constant ΔV_p change dramatically. ΔV_s is only slightly effected (through density) by the presence of gas. Without additional information ΔV_p and ΔV_s are insufficient to predict ΔP, ΔS_w and ΔS_g. EM data provides an independent estimate of ΔS_w. σ is a much simpler function of reservoir parameters than is the velocity and can be described by Archie's law (Archie, 1942). Assuming ϕ is constant $\Delta\sigma$ is only a function of ΔS_w and Δ pore σ. Since water flood has been in effect for over 6 years we assume that the pore fluid water has reached equilibrium between injected and native water and fluid σ does not change. Therefore, conductivity changes are interpreted solely in terms of water saturation changes.

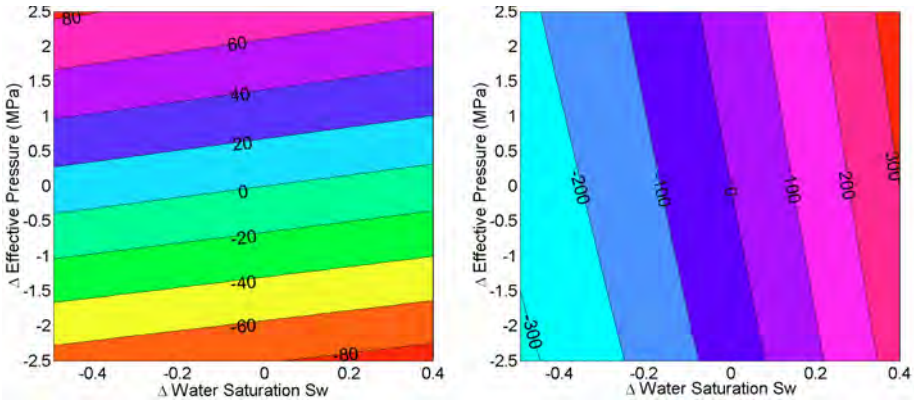

Figure 5.9-4: ΔV_s (left panel) and ΔV_p (right panel) vs. ΔP and ΔS_w about a reference S_w, S_g, ϕ and P of 0.5, 0.0, 0.5 and 4.7 MPa.

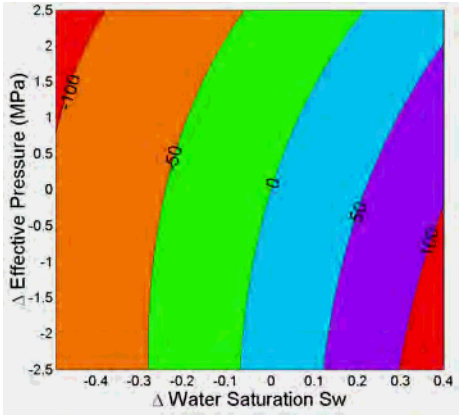

Figure 5.9-5: ΔV_p at Sg=0.05

Integrated Time-Lapse Geophysical Images:

The strategy we adopted to maximize the spatial correlation between V_p, V_s and σ images was to begin with the EM were the most a priori information existed and then use the σ images to produce starting V_p models followed by producing starting V_s models from the final V_p models. We chose to use a conjugate gradient algorithm (Jackson & Tweeton 1996) because the final model is sensitive to the initial model and is perturbed from the starting values only as much as needed to fit the observed data.

The EM inversion (Newman, 1995) for the data at initial conditions was started from a model built by laterally interpolating the σ logs between the OB-C1 and OB-C2 wells. The EM inverse σ model at initial conditions was then used as the starting model for the inversion of the July 2001 EM data. Differencing these inversions provides the $\Delta\sigma$ shown in Figure 5.9-6c. There is a high degree of correlation between the 11-8WR permeability log and the areas where the largest decrease in σ occur. The correlation between high permeability and large changes in S_w, and thus σ, is expected. Also, the largest σ changes occur more in alignment with the estimated location of the old water injection fracture than with the much newer CO_2 fracture. This is not

surprising when we consider that the water injection was ongoing for more that 6 years and thus likely produced a high permeability damage zone that is a better conduit to flow than the very new CO_2 fracture.

Next the pre and post CO_2 σ models were converted to V_p, these were then used as initial models in the inversion of the V_p travel time data to produce the change in V_p shown in Figure 5.9-6b. In addition to V_p changes occurring in the vicinity of the estimated water injection fracture there are decreases in V_p that align with the mapped fault. Since there are little σ changes associated with the fault we interpret this to mean that pressure changes are occurring along the fault zone without significant changes in water saturation.

The V_p sections were converted to V_s using a V_p/V_s ratio derived from the rock properties model and used as starting models for the V_s travel time inversions resulting in the ΔV_s section shown in Figure 5.9-6a. The ΔV_s section is smoother than either the $\Delta\sigma$ or ΔV_p sections due in part to the lower frequency content in the shear wave data. The ΔV_s section is also smoother because Vs is relatively insensitive to ΔS_w that has high spatial variability but very sensitive to ΔP that has much lower spatial variability. Even with the smoother spatial changes in the V_s data we see correlation with the V_p and σ changes. In particular the zone along the fault shows a decrease in V_s, lending support to our interpretation that pressure is changing along the fault zone.

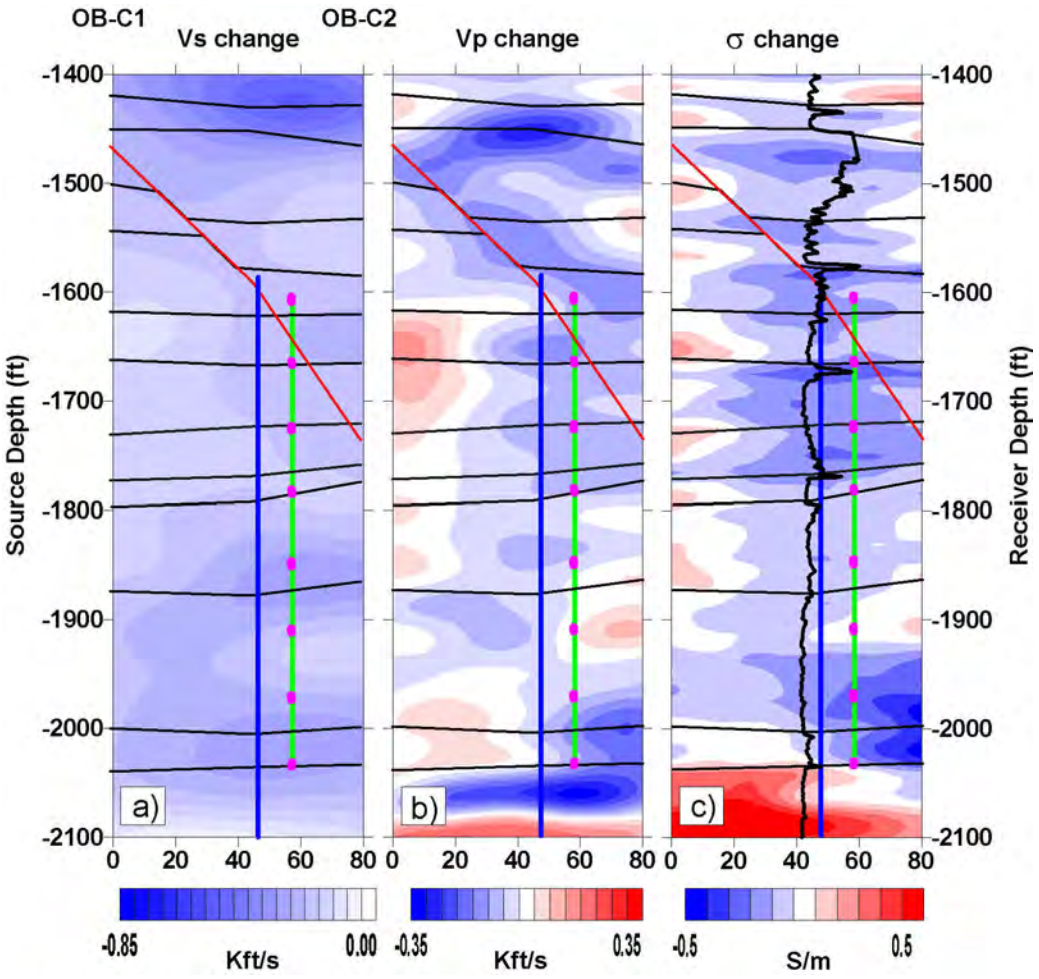

Figure 5.9-6: Time-lapse changes in a) V_s, b) V_p and c) σ. Major unit boundaries are shown as black horizontal lines, estimated location of previous water injection fracture is shown as vertical blue line (x=45ft), estimated location of the CO_2 injection fracture is shown as a vertical green line (x=60ft), perforation intervals for CO_2 injection are shown as magenta dots, location of a fault zone is shown as the red diagonal line. The permeability log from the CO_2 injection well 11-8WR is shown in black on panel c.

Predicting Changes in Reservoir Parameters:

First the $\Delta\sigma$ image was used to predict ΔS_w assuming that ϕ and fluid σ did not change. The predicted ΔS_w was used with the observed ΔV_s and the relation illustrated in Figure 5.9-4a to predict ΔP. The predicted ΔS_w and ΔP were then used to calculate the ΔV_p that would be due to ΔS_w and ΔP alone assuming $S_g=0$. Over the majority of the image plane ΔS_w and ΔP are negative thus producing a negative ΔV_p. The difference between the observed and calculated ΔV_p (ΔV_R) was generated. We expect the CO_2 to decrease V_p in excess of the effects of ΔS_w and ΔP alone. There are two mechanisms for CO_2 to decrease V_p; 1) through decreasing the bulk modulus of the oil by increasing the gas/oil ratio and 2) by increasing S_g through introduction of

free CO_2. Either of these mechanisms would produce a negative ΔV_R. On the other hand, if ΔV_R is positive this indicates that ΔV_p calculated from ΔS_w and ΔP assuming S_g=0 is too large. The presence of initial gas will produce this effect, as seen in Figure 5.9-5 where the presence of gas reduces the decrease in V_p associated with a given ΔS_w and ΔP.

The OB-C1 log shows the presence of gas over certain intervals within the reservoir. Therefore a two-step process was used to calculate ΔV_R. The first pass used S_g=0 as described. Next, sections of the image where ΔV_R was positive were recalculated assuming S_g = 0.05 (the average non-zero S_g in the reservoir interval). After the second pass calculation of ΔV_R much of the areas that had $+\Delta V_R$ after pass one became negative. The final ΔV_R was converted to ΔR_g and ΔS_g where both CO_2 and hydrocarbon gas are considered.

This final step requires assumptions about the partitioning of $-\Delta V_R$. First we assumed that the $+\Delta P_{pore}$ caused by injection would drive as much of the initial S_g into the oil as possible. Next we assume a partitioning between the $+\Delta R_g$ and $+\Delta S_{CO2}$ effects on ΔV_R. We chose to allow the maximum increase in CO_2 R_g for the given $+\Delta P_{pore}$. $-\Delta V_R$ was converted to $+\Delta R_g$ up to the maximum R_g for the final P_{pore} and T. If the $+\Delta R_g$ did not completely account for the $-\Delta V_R$, then ΔS_{CO2} was calculated to account for the rest. Figure 5.9-7 shows the calculated ΔR_g and ΔS_g generated from the geophysical parameter changes shown in Figure 5.9-6. As has been stated these calculations are based on differences calculated about reference values of P, ϕ, S_w and S_g. The sensitivity of the ΔR_g and ΔS_g predictions to the reference parameters has been studies and shows that the calculations are relatively insensitive to the reference ϕ and S_w values. The calculations are most sensitive to the reference P. P from a history matched flow simulation model at the beginning of CO_2 injection was used as a reference to produce the results shown in Figure 5.9-7. The effect of the reference pressure can be seen above 1600 ft where there is a large $+\Delta S_g$ and relatively low $+\Delta R_g$. This is due to the relatively low initial P_{pore} in this region, which reduces the amount of gas (CO_2 or hydrocarbon) that can dissolve in the oil as P_{pore} increases. The effect of changing the reference P to a constant, such as the average before injection, is to cause a larger $+\Delta R_g$ and a smaller $+\Delta S_g$ in the upper section. The effect of the reference pressure below 1600ft is negligible.

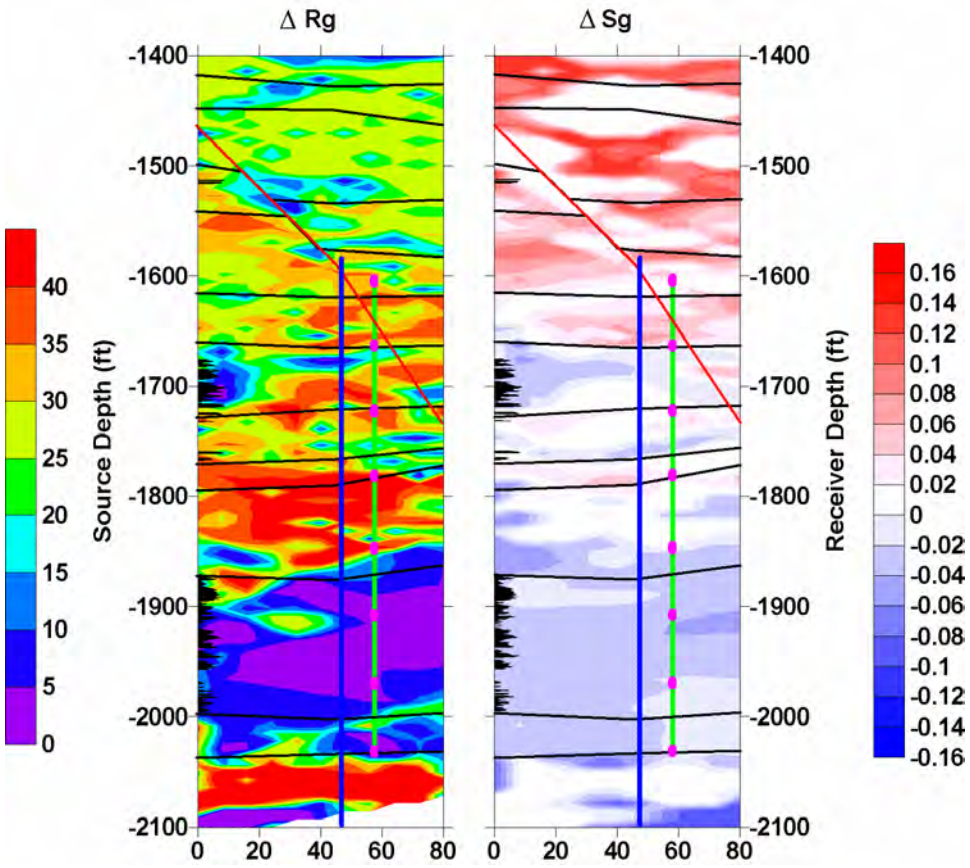

Figure 5.9-7: Predicted ΔR_g (left side) and ΔS_g (right side). Initial OB-C1 gas log in black on left side. See Figure 6 caption for figure overlays.

There is a strong correlation between the areas with initial gas, as indicated by the gas log (left side of Figure 5.9-7), and areas with high $-\Delta S_g$ and low $+\Delta R_g$. This is consistent with the initial gas in place being driven into the oil with $+\Delta P_{pore}$ thus reducing the amount of CO_2 that can be dissolved in the oil. In addition, the images of ΔS_g and ΔR_g have a much higher spatial correlation with unit boundaries and the fault zone than do the individual time-lapse geophysical images. This is a benefit of partitioning the geophysical changes by first removing the effects of ΔP and ΔS_w.

Conclusions:

We have demonstrated that by combining seismically derived ΔV_p and ΔV_s with EM derived $\Delta\sigma$ estimates of ΔP, ΔS_w ΔS_g and ΔR_g can be made in a complex reservoir containing oil, water, hydrocarbon gas and introduced CO_2. The resulting predicted ΔS_g and ΔR_g are better correlated with logged unit boundaries than are any of the Δ geophysical parameter images. The predicted ΔS_g and ΔR_g images indicate that a significant portion of the injected CO_2 is filling the upper portions of the section above the intended injection interval. These conclusions are validated by CO_2 injectivity measurements made in the 11-8WR well.

While the methodology outlined in this paper relies on many assumptions that were required because the project was not designed to use this methodology in future applications these could be substantially reduced by design. In particular, the most benefit could be drawn from repeat logging of the wells with a full suite of logs. This would provide control points for the ΔP, ΔS_w, ΔS_g, ΔV_p, ΔV_s and $\Delta\sigma$ all of which would serve to greatly constrain the problem. In addition, having full log suites would enable much better control of the geophysical inverse solutions through superior starting models.

References:

Archie, G. E., 1942, The electrical resistivity log as an aid in determining some reservoir characteristics. Trans. Am. Inst. Mech. Eng., 146, 54-62.

Betzel, M. and Wang, Z., 1992, Seismic properties of pore fluids, Geophys., 57, 1396-1408.

Hashin, Z., and Shtrikman, S., 1963, A variational approach to the elastic behavior of multiphse materials, J. Mech. Phys. Solids, 11, 127 – 140.

Newman, G. A., 1995, Crosswell electromagnetic inversion using integral and differential Equations: Geophysics, **60**, 899-911.

Jackson, M. J. and Tweeton, D. R., 1996, 3DTOM: Three-Dimensional Geophysical Tomography, US Dept. of the Interior, Bureau of Mines, Report of Investigation 9617.

Wang, Z., 2001 Personal Communication.

5.10 CORROSION MONITORING

John F. Cooney
ChevronTexaco Exploration and Production Company

Overview:
A corrosion monitoring program was implemented to determine the impact of produced CO_2, in higher concentrations, on our existing facilities. It would have helped us determine what facilities and flow lines would be needed to be replaced or upgraded, due to CO_2 corrosion, if the pilot is successful. If excessive corrosion was detected, we would have attempted to mitigate it utilizing chemicals. If necessary, some flow lines and facilities would have been replaced. Mitigation measures would also have been scaled up to evaluate facility costs (capital and operating expenditures) for full-field CO_2 development.

General Description of the Corrosion Monitoring Program:
The intent of the corrosion monitoring program is to determine the impact of produced CO_2, in higher concentrations, on our existing facilities. It will help us determine what facilities and flowlines would need to be replaced or upgraded, due to CO_2 corrosion, if the pilot is successful. If excessive corrosion is detected, we will attempt to mitigate it utilizing chemicals. If necessary, some flowlines and facilities will be replaced. Mitigation measures will be scaled up to evaluate facility costs (capital and operating expenditures) for full-field CO_2 development.

Benchmarking

Producing Wells & Flowlines:
Baseline iron and hardness samples were taken on each of the 10 producing wells in the CO_2 flood every day from August 14, 2000 to August 18, 2000. The corrosion rate was also measured prior to commencing CO_2 injection. In addition, a total water analysis was also run on each producing well.

Production Facilities:
Corrosion rates were monitored on the pool lines leaving the CO_2 gauge setting, and on the main pool line coming from an adjacent production facility.

Continuos Monitoring:
Iron loss and hardness at each well are being monitored weekly. Corrosion coupons are measured every two weeks. If and when breakthrough occurs at a well, a LPR probe (resistivity probe that correlates to corrosion rate) is installed to replace the corrosion coupon in order to monitor corrosion rate in a shorter time frame. The oil/water pool line leaving the gauge setting is being continuously monitored with a LPR probe. In December 2000 and January 2001, LPR probes were added to the wells that have seen a significant amount of CO_2 tracer. New data from these LPR probes will not be compiled until March 2001.

Results for Well Flowline Corrosion:
For the first few months of the pilot, only well 11-8E had a LPR probe (due to their high cost). The orange line in Figure 5.10-1 shows these LPR readings. Corrosion coupons were being utilized to monitor the other 9 wells. Even though the monitoring shows signs of increased corrosion, the increase is not significant enough to require chemical or facility changes for protection.

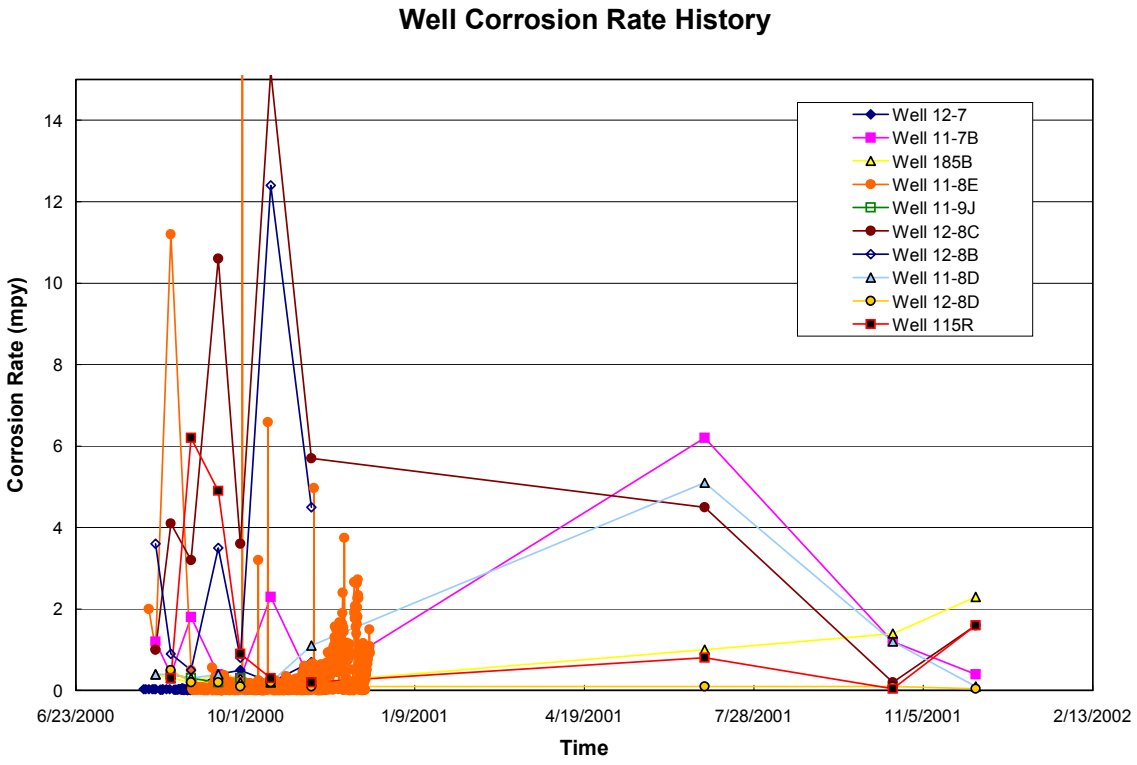

Figure 5.10-1: Well Corrosion Rate History Chart

LPR Probe Results:
The LPR readings at 11-8E correlated very well to breakthrough of CO_2 in this producing well. Readings started to climb slightly only a few weeks after CO_2 injection started (early September 2000). The LPR readings increased significantly in November 2000, which is also when we started to measure significant CO_2 production from this well.

Corrosion Coupons:
Data from corrosion coupons has a large amount of error. As you can see from Figure 5.10-1 above (the Well Corrosion Rate History Chart), it is very difficult to draw any conclusions. Of the wells that saw a large CO_2 flow rate increase (12-8D, 11-8D, and 12-7) only 11-8D showed any signs of flowline corrosion increases. This happens to be the center producer. The uncertainty in the corrosion coupons resulted in another 4 LPR probes being installed on producers that are starting to see CO_2 breakthrough.

Iron Loss Counts from Wells:
Iron loss counts are an indication of how much iron loss is occurring in the well. There have been no measurable changes in the iron loss counts for the producing wells in the pilot.

Production Line / Facility Corrosion:

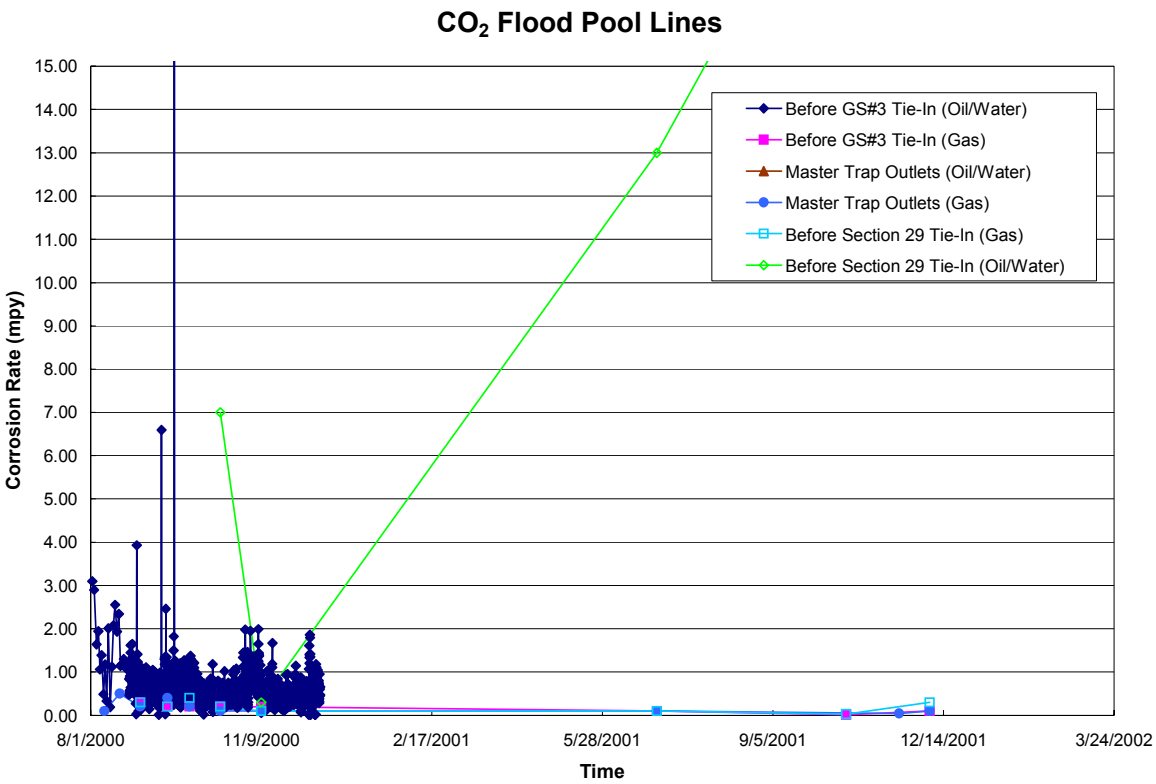

Figure 5.10-2: Production Lines/Facilities Corrosion Rate History Chart

Conclusions:
Changes in the LPR probe, dark blue line in Figure 5.10-2, do not correlate to changes in CO_2 concentrations. The data from the corrosion coupons has too much error to detect the subtle changes. Since very little of the CO2 volume injected was produced back, very little associated corrosion was detected. Corrosion monitoring was significantly scaled back in 2002 because of the low CO_2 production rates.

5.11 Summary of CO_2 Pilot Monitoring Activities

Michael F. Morea
ChevronTexaco Exploration and Production Company

An extensive program was carried out to monitor the CO_2 pilot using a combination of routine and new, experimental methods. Some of the monitoring results are highlighted below:

- Image log data showed that the natural fracture network had fracture azimuths that differed from the typical induced hydraulic azimuth direction. These observations are consistent with other image log data in the field. Natural fractures, while not prevalent, do play a role in distributing injection fluid through the reservoir.
- CO_2 injection tracers showed that a small amount of tracer traveled quickly through the natural fractures, faults and induced hydraulic fractures. This phenomenon has also been observed in water injection tracer tests in the 1.25 and 0.625 acre pilots in other areas of the field.
- Produced water salinity studies in the CO_2 pilot area also show that injection fluids move quickly through a natural fracture network (Zhou et al., 2002).
- Oil geochemistry surveys showed no increase in sulfur or asphaltenes due to CO_2 injection.
- Corrosion was not an issue during the life of the project.
- Injection rate was not an issue during the life of the project.
- Pressure could not be monitored due to an error during perforating the long and short strings of the pressure observation well (OB-C3).
- CO_2 injection profiles showed both good and poor vertical coverage, with the poor coverage mainly going out the top perforations. Similar variability can also be seen in water injection profiles through the waterflood.
- Cased hole, fiberglass observation well logging showed that minor changes in resistivity occurred in the J-L (clean diatomite), GG-BH (mixed) and D-FF (sandy and mixed) intervals. However the largest change occurred in the C (sandy) interval which is over 200 ft. above the injection interval.
- Baseline EM data (pre-CO_2) showed water injection to have mainly been confined to the GG-BH and J-K intervals. Post CO_2 injection EM surveys could not detect any additional change unfortunately due to the low volume of CO_2 injected during the pilot.
- Combined crosswell seismic and EM interpretation indicated that CO_2 moved above and out of zone along a fault/hydraulic fracture plane.
- Even though numerous remedial attempts were made, the sanding of producers was a major problem that could not reasonably be overcome. The sanding problem was the result of CO_2 finding its way through the natural and hydraulic fracture network and causing "frac" sand to enter the wellbores of most of the producers in the pilot.
- CO_2 did manage to adversely effect (spike in gas production/sanding) other wells outside the 10-acre pilot.

Overall, the monitoring program was very effective except for measuring pressure. Through the life of the pilot, CO_2 behaved similarly to injected water (waterflood) in that a larger portion of

CO_2 traveled through the fracture network and only a small portion entered into the low permeability diatomite.

Reference:

Zhou, D., Kamath, J., Friedmann, F., and Morea, M., 2002, Identifying Key Recovery Mechanisms in a Diatomite Waterflood, Society of Petroleum Engineers, no. 751

SECTION 6
PILOT COSTS

6.1 Pilot Cost Summary:

The pilot was completed without fully expending the funds appropriated by ChevronTexaco and the DOE. Most of the remaining funds were intended for continued purchase of CO_2, which is no longer necessary. Facility abandonment costs are the only remaining expenditures.

Some of the funds originally slated for CO_2 purchases were utilized to repair the wells that had sanding problems. Table 6.1-1 summarizes planned vs. actual expenditures. Total costs are shown which is approximately 50% DOE and 50% ChevronTexaco.

Table 6.1-1. Lost Hills CO_2 Pilot – Planned vs. Actual Expenditures.

Scope Description	Phase 3 Report Amount	Appropriated Amount	Actual Expenditures as of 12/31/02	Over / (Under) AFE Amount
CAPITAL				
Injectivity Test	$496,000	$415,396	$355,749	-$59,647
Project Management and Reporting	$50,000	$120,000	$9,229	-$110,771
Facility Designs	$80,000	$81,867	$100,209	$18,342
New Wells (Producers, Injectors, & Observation)	$1,600,000	$1,397,005	$1,329,105	-$67,900
CO2 Injection Facilities Installation	$858,000	$567,100	$402,038	-$165,062
Gauge Setting Installation	$825,000	$807,850	$660,823	-$147,027
Monitoring	$428,000	$428,000	$218,149	-$209,851
Engineering for CO2 **Project** Phase 2	$250,000	$0	$0	$0
CAPEX Totals:	**$4,587,000**	**$3,817,218**	**$3,075,303**	**-$741,915**
EXPENSE				
CO2 Supply CO2 & Equip. Rental)	$2,832,000	$1,810,836	$1,395,930	-$414,906
Existing Well Upgrades	$280,000	$327,760	$268,742	-$59,018
Sand Remediation	$0	$304,000	$505,048	$201,048
Expense Totals:	**$3,112,000**	**$2,442,596**	**$2,169,720**	**-$272,876**
Project Totals:	**$7,699,000**	**$6,259,814**	**$5,245,023**	**-$1,014,791**
ChevronTexaco Share	$4,962,000	$3,473,645	$2,888,227	-$585,418
DOE Share	$2,737,000	$2,786,170	$2,356,796	-$429,373

SECTION 7

CONCLUSIONS AND LESSONS LEARNED

7.1 Technical Conclusions

The following conclusions have been arrived after operating and monitoring the CO_2 pilot for two years, including two simulation studies:

1. The tracer and salinity survey data suggest the producers are highly connected with the injectors.
2. Simulations show that the existence of higher flow channels in the reservoir play an adverse role on the performance of Lost Hills CO_2 pilot. Most of injected CO_2 flows through the high flow channels and only a small portion of the injected CO_2 invades the reservoir formation. Because of low viscosity, CO_2 prefers the high permeability zones, which has been waterflooded before the WAG started. The combination of the high flow channels and the poor sweep efficiency contributes to the poor performance observed in the pilot.
3. It appears CO_2 is capable of increasing oil recovery from the diatomite.
4. CO_2 is very good at finding the proverbial "path of least resistance" and by-passing matrix oil.
5. CO_2 predominantly flows through the induced hydraulic fractures, connects with the natural fractures, faults, and channels through a very small portion of the reservoir carrying high-velocity sand. The sand-laden CO2 finds holes already in place due to subsidence-related well failures and exacerbates the sanding problems and can even lead to catastrophic tubing failure.

7.2 Operational Lessons Learned

A *Lessons Learned* session was conducted on January 16, 2003. We were fortunate in that just about all key players involved with the pilot attended. The most noteworthy lessons that were captured are summarized below:

Things That Went Well

- **Safety:**
  There were zero incidents associated with the Pilot. Some elements of the safety plan that contributed to this success were: Detailed traffic plan for CO_2 deliveries, Awareness of the hazards of CO_2 and training by supplier (BOC) on handling, CO_2 evacuation drill conducted by Operations, Operator from Rangely CO_2 Operations (Reed Chernenko) was assigned to the pilot, and Facilities designed and Operated with CO_2 hazards in mind.

- **Partnerships and Technology**:
  Strong partnerships formed and fostered with the DOE and National Labs resulted in shared pilot risk and advancement of monitoring technologies.

- **Commitment by Operations to the Pilot:**
  Operations supported and implemented the effort 100%. Operations attributed this to the fact that they understood the significant potential of CO_2 flooding, if the pilot were successful. Frequent problem solving (i.e. producer sanding problems) meetings between the Project Team and Operations was also cited as a contributor.

- **Networking and Applying Best Practices:** The pilot was operated very successfully in spite of the fact that Engineers and Operators at Lost Hills are very unfamiliar with the process of CO_2 flooding. This success was attributed to the fact that the Project Team made several visits to CO_2 flood operations and established a network of contacts. Lessons learned from CO_2 floods/pilots in West Texas and Rangely Colorado were captured and applied.

What Could Have Been Improved?

- **Facility Design:**
  The CO_2 tank level telemetry system that communicated the amount of product onsite, to BOC (in Pennsylvania) was problematic. Power surges and inadequate phone lines were identified as the root causes. Infrastructure upgrades or alternative communication methods (wireless?) were discussed as possible solutions.

- **Schedule Contingency**:
  Inadequate contingency was built into the schedule. Two elements of the project contributed to the start-up delay. These elements could easily be part of other pilots and should be taken into consideration:

  1. Allow sufficient time to establish reliable/accurate baseline information (i.e. oil/water/gas production from producers). This is especially true if you are relying on new, pilot dedicated equipment (new CO_2 gauging facilities), to establish the baseline.

  2. Build in extra contingency for processes that involve new technology or are new to the personnel that will be designing and operating the process. The need for new technology/processes schedule contingency is well known, but seldom applied as it should be.

SECTION 8
TECHNOLOGY TRANSFER

8.1 TECHNOLOGY TRANSFER

Aydin, A., 1997, Fault Control on Hydrocarbon Migration and Fluid Flow in Neogene Basins and Related Reservoirs of Central and Coastal California, USA: An Overview, in, Pollard, D. D. and Aydin, A. eds., Proceedings of the Rock Fracture Project Workshop, Stanford University, Stanford, CA.

Aydin, A., Dholakia, S. K., Antonellini, M., and Lore, J., 1996, Fault Control on Hydrocarbon Migration in Neogene Basins in Central and Coastal California, USA, Faulting, Fault Sealing and Fluid Flow in Hydrocarbon Reservoirs, Conference, University of Leeds.

Bilodeau, B. J., and Smith, S. C., 1997, Session Chairmen for Reservoir Characterization and Improving Recovery in Monterey-type Siliceous Shales, Pacific Section AAPG/SEPM Annual Convention, Bakersfield, CA.

Bilodeau, B. J., Smith, S. C., and Julander, D. R., 1997, Comprehensive Reservoir Characterization Using Open-Hole Wireline Logs, Core, and Downhole Video, Buena Vista Hills Field, California, Pacific Section AAPG/SEPM Annual Convention, Bakersfield, CA.

Britton, A.W., Smith, J. L., and Chapman, D., 1997, Continuous Permeability and Porosity Determinations in the Chevron 653Z-26B Well, Buena Vista Field, Kern County, CA, Pacific Section AAPG/SEPM Annual Convention, Bakersfield, CA.

Britton, A. W., and Morea, M. F., 1998, Acoustic Anisotropy Measurements in the Siliceous Shale, 653Z-26B Well, Buena Vista Hills Field, California, AAPG Annual Convention, Salt Lake City, UT.

Campagna, D. J., Amos, J. F., and Mamula, N., 1998, Influence of Structure, Reservoir Compartments, and Natural Fractures on Oil and Gas Production in the Southern San Joaquin Basin, California, AAPG Annual Convention, Salt Lake City, UT.

Carpenter, A. B., and Moore, T. S., 1997, Origin of Boron-Rich Pore Water in the Monterey Formation, San Joaquin Valley, CA, Pacific Section AAPG/SEPM Annual Convention, Bakersfield, CA.

Cole, D.R., Horita, J., M. C. van Soest, M.C., Kennedy, B.M., Morea, M.F., 2003, Gas Chemistry and Isotope Monitoring during the Lost Hills, CA, CO_2 Injection Test, 2nd Annual Carbon Sequestration Conference, Alexandria, VA.

Daley, T.M., Majer, E.L., Gritto, R., Benson, S.M., 2000, Borehole Seismic Monitoring of CO_2 Injection in a Diatomite Reservoir, AGU, EOS, v. 81, n. 48.

Decker, D. and Bilodeau, B. J., 1997, Antrim Shale Resource and Reservoir Characterization as an Analog for Diffusion Controlled Gas Production from the Monterey Formation Pacific Section AAPG/SEPM Annual Convention, Bakersfield, CA.

Dholakia, S. K., 1995, An Integrative Study of Fractures and In Situ Stress in the Antelope Shale, Monterey Formation, Stanford Rock Fracture Project, Stanford University, Stanford, CA.

Dholakia, S. K., 1996, Outcrop to Reservoir: Importance of Faulting to Hydrocarbon Migration in the Monterey Formation, CA, Stanford Rock Fracture Project, Stanford University, Stanford, CA.

Dholakia, S. K., Aydin, A. Pollard, D. D., and Zoback, M. D., 1995, Relationship between Hydrocarbon Transport and Shearing Deformation in the Antelope Shale, Monterey Formation, San Joaquin Valley, California, GSA Annual Convention.

Dholakia, S. K., Aydin, A., Pollard, D. D., and Zoback, M. D., 1996, Hydrocarbon Transport and Shearing Processes in the Antelope Shale, Monterey Formation, San Joaquin Valley, California, AAPG Annual Convention San Diego, CA.

Dholakia, S. K., Aydin, A., Pollard, D. D., and Zoback, M. D., 1998, Development of Fault-controlled Hydrocarbon Pathways in the Monterey Formation, California, AAPG Bulletin, v. 82, no. 8, p. 1551-1574.

Dholakia, S. K., Aydin, A., Pollard, D. D., Zoback, M. D., and Barton, C., 1996, Integration of Geological and Borehole Image Data for the Interpretation of Conductive Structural Inhomogeneities in the Monterey Formation, California, Geological Application of Borehole Imaging Conference, Houston, TX.

Dholakia, S. K., Aydin, A, Pollard, D. D., Zoback, M. D., Barton, C., and Bilodeau, B. J., 1997, Integration of Surface Geology and Borehole Geophysics for Reservoir Characterization in the Monterey Siliceous Shales for the Purpose of Facilitating Improved Recovery Designs, Pacific Section AAPG/SEPM Annual Convention, Bakersfield, CA.

Dholakia, S. K., Aydin, A., Zoback, M. D., and Pollard, D. D., 1995, Plan for an Integrative Study of Fractures and In Situ Stress in the Antelope Shale, Monterey Formation, Stanford Rock & Borehole Geophysics Project Annual Report, Stanford University, Stanford, CA.

Dholakia, S. K., Lore, J., Brankman, C. M., and Roznovsky, T., 1996, Fault Control on Hydrocarbon Migration in the Monterey Formation, CA, Proceedings of the Stanford Rock Fracture Project Field Workshop, Stanford University, Stanford, CA.

Dholakia, S. K., Zoback, M. D., and Aydin, A., 1996, Stress State, Shearing Deformation and Implications for Hydrocarbon Transport in the Monterey Formation, California, Stanford Rock & Borehole Geophysics Project Annual Report, Stanford University, Stanford, CA.

Dholakia, S. K., Zoback, M. D., Barton, C., Aydin, A. and Pollard, D. D., Active Faults and Hydrocarbon Migration and Production in the Monterey Formation, California, Geophysics (in prep).

Fargo, D., 1997, Advanced Coring and Wellsite Handling Add Pizazz to Buena Vista Hills Core, Pacific Section AAPG/SEPM Annual Convention, Bakersfield, CA.

Fargo, D., 1997, Advanced Coring and Wellsite Case Study of Chevron/DOE Well 653Z-26B, Core Technology Meeting, Anchorage, AK.

Fargo, D., 1997, Case Study: Chevron/DOE Buena Vista Field Core Project, Technology Meeting, AERA Energy, Bakersfield, CA.

Gritto, R., Daley,T.M., and Myer, R.L., submitted, Joint Cross Well and Single Well Seismic Studies of CO_2 Injection in an Oil Reservoir, Geophysical Prospecting.

Hackert, C.L., Parra, J.O., Brown, R.I., and Collier, H.A., 2001, Characterization of Dispersion, Attenuation, and Anisotropy at the Buena Vista Hills Field, California, Geophysics, v. 66.

Hoversten, G.M., 2001, Crosswell Seismic and Electromagnetic Monitoring of CO_2 Injection, SEG Development and Production Forum, Taos, N.M.

Hoversten, G. M., Majer, E. L., Daley, T. M., 2001, Crosswell Seismic and Electromagnetic Monitoring Methods of CO_2 Sequestration, 2001 AAPG Annual Convention, Denver, CO (June 3-6).

Jacobs, J. L., 1997, Characterization and Formation of En Echelon Fracture Arrays in the Monterey Formation, California. In, Pollard, D. D. and Aydin, A., eds., Proceedings of the Rock Fracture Project Workshop, Stanford University, Stanford, CA.

Jacobs, J.L., 1999, Characterization and Formation of Veins and Associated Structures in Siliceous Shales and their Impact on Hydrocarbon Flow, M.S. Thesis, Stanford University.

Kirkendall, B., and Roberts, J., 2001, Cross-Borehole Electromagnetic Imaging of a CO_2 site: An Integrated Field and Laboratory Study, First National Conference on Carbon Sequestration, Washington D.C. (May 14 – 17).

Kirkendall, B. and Roberts, J., 2001, Reservoir Management of Sequestrated CO_2 using Borehole Electromagnetic Tomographic Imaging, 2001 International Gas Research Conference, Amsterdam, The Netherlands (November 5 – 8).

Kuuskraa, V., 1997, Incorporating Reservoir Characterization into Optimized Production of Siliceous Shales and Other Gas Bearing Shales, Pacific Section AAPG/SEPM Annual Convention, Bakersfield, CA.

Langan, R. T., 1997, Crosswell Reflection Imaging in the San Joaquin Valley: Buena Vista Hills, Society of Exploration Geophysicists, Development and Production Forum, Vail, CO.

Langan, R. T., 1997, Crosswell Seismology, Where We've Been and Where We're Going, Producers Executive Committee, Gas Research Institute, Chicago, IL.

Langan, R. T., 1997, Crosswell Imaging in West Texas and the San Joaquin Valley, Geosciences Department, Princeton University, Princeton, NJ.

Langan, R. T., Julander, D. R., Morea, M. F., Addington, C. M., and Lazaratos, S. K., 1998, Crosswell Seismic Imaging in the Buena Vista Hills, San Joaquin Valley: A Case Study, Annual International Meeting, Society of Exploration Geophysicists, New Orleans, LA.

Langan, R.T., Julander, D.R., Morea, M.F., Addington, C.M., and Lazaratos, S.K., 2000, Crosswell Seismic Imaging in the Buena Vista Hills, San Joaquin Valley: A Case History, Pacific Section Convention, AAPG, Long Beach.

Lee, K.H., Kim, H.J., Tseng, H.W., and Wilt, M., 2001, Electromagnetic Methods for Geothermal Exploration, Annual Meeting Geothermal Resources Council, San Diego (August 26-29).

Majer, E. L., Daley, T. M., Gritto, R., Korneev, V., and Li, G., 2001, Application of Crosswell and Single Well Seismic Methods for Mapping CO_2 Movement, GSA Cordilleran Section Annual Meeting, Universal City, CA, Paper 3514.

Mamula, N., and Campagna, D. J., 1997, Determination of Reservoir Compartmentalization Using Mesoscopic Scale Fracture Analysis in the Buena Vista Hills Area of the Southern San Joaquin Valley, CA, Pacific Section AAPG/SEPM Annual Convention, Bakersfield, CA.

Montgomery, S.L., Morea, M.F., Perri, P.R., and Emanuele, M.A., 2000, New Effort to Evaluate EOR Possibilities in Monterey Formation, San Joaquin Basin, Oil and Gas Journal, September 25.

Montgomery, S.L., Morea, M.F., 2001, Antelope Shale (Monterey Formation), Buena Vista Hills Field: Advanced Reservoir Characterization to Evaluate CO_2 Injection for Enhanced Recovery, AAPG Bulletin, v. 85, n. 4.

Morea, M. F., 1997, Advanced Reservoir Characterization in the Antelope Shale to Establish the Viability of CO_2 Enhanced Oil Recovery in California's Monterey Formation Siliceous Shales, Oil Technology and Gas Environmental Program Review Meeting, Houston, TX.

Morea, M. F., 1998, Advanced Reservoir Characterization in the Antelope Shale to Establish the Viability of CO_2 Enhanced Oil Recovery in California's Monterey Formation Siliceous Shales, DOE/BC/14938-8, (DE98000484), 1997 Annual Report, National Petroleum Technology Office, US Department of Energy, Tulsa, OK.

Morea, M. F., 1999, Advanced Reservoir Characterization in the Antelope Shale to Establish the Viability of CO_2 Enhanced Oil Recovery in California's Monterey Formation Siliceous Shales, DOE/BC/14938-12, (OSTI ID: 5127), 1998 Annual Report, National Petroleum Technology Office, US Department of Energy, Tulsa, OK.

Morea, M. F., Julander, D. R., Zalan, T. A., and Beeson, D. C., 1998, Advanced Reservoir Characterization of the Siliceous Shale, Buena Vista Hills, California, Pacific Section AAPG Convention, Ventura, CA.

Morea, M. F., Zalan, T. A., and Jacobs, J. L., 1997, Buena Vista Hills Reservoir Characterization Study, Chevron/DOE Class III Reservoir Project. In, Advances in Reservoir Description Techniques as Applied to California Oil and Gas Fields Workshop, Pacific Section AAPG/SEPM Annual Convention, Bakersfield, CA.

Morea, M. F., Zalan, T. A., Julander, D. R., Beeson, D. C., and Britton, A. W., 1998, Advanced Reservoir Characterization of the Siliceous Shale, Buena Vista Hills, California: Integration of Geological, Geochemical, and Petrophysical Data, AAPG Annual Convention, Salt Lake City, UT.

Morea, M. F., and Zalan, T. A., in press, Chapter 3, Buena Vista Hills Field, California, Borehole Imaging, DOE/AAPG Advanced Logging Volume, Tulsa, OK.

Morea, M. F., and Zalan, T. A., in press, Chapter 4, Buena Vista Hills Field, California, Advanced Logging Tools, DOE/AAPG Advanced Logging Volume, Tulsa, OK.

Morea, M.F. and Perri, P.R., Results from a CO_2 Pilot in the Belridge Diatomite, Lost Hills, California, 2003, AAPG Annual Convention, Salt Lake City, UT.

Parra, J.O. and Hackert,C.L., 2002, Wave Attenuation Attributes as Flow Unit Indicators, The Leading Edge.

Parra, J.O., Hackert, C.L., Brown, R.I., and Collier, H.A., 1998, Estimation of Components of Elastic Scattering and Intrinsic Attenuation via Well Control at the Buena Vista Hills Field, 68th Ann. Internat. Mtg., Soc. Expl. Geophys.

Parra, J.O., C.L. Hackert, and P.C. Xu, 2002, Characterization of Fractured Low Q Zones at the Buena Vista Hills Reservoir, California, Geophysics. v. 76.

Perri, P. R., 2000, Advanced Reservoir Characterization in the Antelope Shale to Establish the Viability of CO_2 Enhanced Oil Recovery in California's Monterey Formation Siliceous Shales, DOE/BC/14938-12, (OSTI ID: 5127), 1999 Annual Report, National Petroleum Technology Office, US Department of Energy, Tulsa, OK.

Perri, P. R., 2001, Advanced Reservoir Characterization in the Antelope Shale to Establish the Viability of CO_2 Enhanced Oil Recovery in California's Monterey Formation Siliceous Shales, DOE/BC/14938-12, (OSTI ID: 5127), 2000 Annual Report, National Petroleum Technology Office, US Department of Energy, Tulsa, OK.

Perri, P. R., 2002, Advanced Reservoir Characterization in the Antelope Shale to Establish the Viability of CO_2 Enhanced Oil Recovery in California's Monterey Formation Siliceous Shales, DOE/BC/14938-12, (OSTI ID: 5127), 2001 Annual Report, National Petroleum Technology Office, US Department of Energy, Tulsa, OK.

Perri, P.R., Emanuele, M.A., Morea, M.F., and Fong, W.S., 2000, Lost Hills CO_2 Pilot: Evaluation, Design, Injectivity Test Results, and Implementation, Western Regional Meeting, SPE, Long Beach, n. 62526.

Perri, P.R., Emanuele, M.A., Morea, M.F., and Fong, W.S., "Lost Hills CO_2 Pilot: Evaluation, Design, Implementation and Early Results," Sixth Annual Permian Basin CO_2 Flood Conference, Midland, TX, December 6, 2000.

Tang, R. W., Zhou, D., Beeson, D. C., Ulrich, R. L., and Morea, M. F., 1998, Immiscible CO_2 Floods in Low Permeability Reservoirs, International Energy Agency, Collaborative Project on Enhanced Oil Recovery, 19th Workshop and Symposium, Carmel, CA.

Toronyi, R. M., 1997, Advanced Reservoir Characterization in the Antelope Shale to Establish the Viability of CO_2 Enhanced Oil Recovery in California's Monterey Formation Siliceous Shales, DOE/BC/14938-7, (DE98000460), 1997 Annual Report, National Petroleum Technology Office, US Department of Energy, Tulsa, OK.

Wang, G. Y., 1997, 3-D Attenuation Imaging, Annual International Meeting, Society of Exploration Geophysicists, Dallas, TX.

Wang, G. Y., Harris, J. M., Magalhaes, C. G., Julander, D. R., and Morea, M. F., 1998, Buena Vista Hills 3-D Attenuation and Velocity Tomography, Annual International Meeting, Society of Exploration Geophysicists, New Orleans, LA.

Wilt, M., Zhang, P., Morea, M., Julander, D., Mock, P., 2001, Using Crosswell Electromagnetics to Map Water Saturation and Formation Structure at Lost Hills, SPE Western Regional Meeting, n. 68802.

Wilt, M., Mallan, R., Kasamyer, P., and Kirkendall, B., 2002, 3D Extended Logging for Geothermal Resources: Field Trials with the GEO-BUILT System, Proceedings, 27th Workshop on Geothermal Reservoir Engineering, Stanford University, Stanford, CA, SGP-TR-171.

Zalan, T. A., Morea, M. F., Julander, D. R., and Denoo, S. A., 1998, Applying Integrated Formation Evaluation to Advanced Reservoir Characterization in California's Monterey

Formation Siliceous Shales, DOE/BDM OK/ PTTC Class Project Logging Workshop, Advanced Applications of Wireline Logging for Improved Oil Recovery, Denver, CO.

Zalan, T. A., Morea, M. F., Julander, D. R., and Denoo, S. A., 1998, Integrated Formation Evaluation in California's Monterey Formation Siliceous Shales, Buena Vista Hills Field, California, 1998, SPE Western Regional Meeting, Gems Session, Bakersfield, CA.

Zalan, T. A., Morea, M. F., Julander, D. R., and Denoo, S. A., 1998, Applying Integrated Formation Evaluation to Advanced Reservoir Characterization in California's Monterey Formation Siliceous Shales, Society of Professional Well Log Analysts, 39th Annual Logging Symposium, Keystone, CO.

Zoback, M. D., Barton, C., Finkbeiner, T., and Dholakia, S. K., 1996, Evidence for Fluid Flow along Critically-Stressed Faults in Crystalline and Sedimentary Rock, Faulting, Fault Sealing and Fluid Flow in Hydrocarbon Reservoirs, Abstracts, Conference, University of Leeds.

Data from this project has been given to Southwest Research Institute, San Antonio, TX and included in their project:

Parra, J. O., Characterization of Fracture Reservoirs using Static and Dynamic Data: From Sonic and 3D Seismic to Permeability Distribution, BDM Subcontract No. G4S51-731, and Prime Contract No. DE-AC22-94PC91008.